

# COLLECTED PAPERS

ON

## COHERENT QUANTUM OPTICS AND TECHNOLOGY

### Volume 6

August 1990—July 1991

Associate Professor  
Motoichi OHTSU

TOKYO INSTITUTE OF TECHNOLOGY

THE GRADUATE SCHOOL AT NAGATSUTA

4259 Nagatsuta, Midori-ku, Yokohama,

Kanagawa 227, JAPAN

各位殿

拝啓 時下ますますご清祥のこととお慶び申し上げます。

さて、このたび、前回に引き続きまして、最近の私どもの発表論文をまとめましたので、ここにお送り致します。よろしくご査収下されば幸いです。

尚、従来の私たちの研究の進展に伴い、現在はコヒーレントなレーザを積極的に応用することを試みております。このような背景をもとに論文集の題名を変更致しました。いずれも未熟な論文ばかりですので、ご意見、ご批評をお待ちしております。今後ともご指導ご鞭撻のほどお願い申し上げます。

敬具

平成3年8月

東京工業大学 総合理工学研究科

大津 元一

## PREFACE

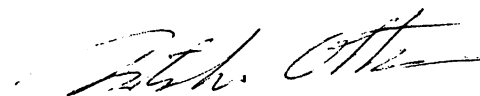
This is a research review by Assoc. Prof. M. Ohtsu, Tokyo Institute of Technology (, formerly " Collected Papers on Coherent Opto-Electronics" ). Since several improvements on the coherence properties of my lasers have been achieved ( , e.g., the half-linewidth of a semiconductor laser field spectral profile has been reduced to 7-Hz ), applications of these lasers to several advanced systems have been started. Based on this direction of researches, the title of this research review is changed to "Collected Papers on Coherent Quantum Optics and Technology" in order to include the topics of these application systems. It contains copies of technical papers published during August 1990 - July 1991.

Research subjects on lasers and optical detection systems, being covered in this volume, are; (1) realization of highly coherent lasers, (2) realization of a Peta-Hz-class coherent optical sweep generators, and (3) highly accurate optical frequency counting systems. In relation to the subject (3), a study on optical properties of a High- $T_c$  oxide superconductor film has also begun recently in order to use it as a highly sensitive and wideband photo-detector. Furthermore, frequency control of a semiconductor laser-pumped YAG laser has begun in April 1991 for gravitational wave detection. The results of these studies will be reported in the forthcoming volumes.

With the help of the results of these researches, studies on several advanced application systems have been carried out. Among

them, technical transfers of "A Passive Ring Cavity-type Fiber Gyroscope" and "A Semiconductor Laser-Pumped Rubidium Atomic Clock" to the industry have been starting from this year, sponsored by Research Development Corporation of Japan ( JRDC ) in order to develop commercially available systems. Research subjects on the application systems being covered in this volume are; (1) semiconductor Laser-pumped rubidium beam atomic clocks to achieve a very high frequency accuracy, and (2) photon scanning tunneling microscopes ( PSTM ) to be used as a super-resolution optical microscope and as a processor for micro-devices, bio-medical system, and so forth. Results of the studies on the applications of the PSTM for manipulating atoms and photons will be reported in the forthcoming volumes.

August 1991



Motoichi OHTSU

\* Back numbers of the collected papers are still available on your request.

## MEMBERS

### Associate Professor

Motoichi OHTSU ( Dr. Eng. )

### Research Associate

Ken'ichi NAKAGAWA ( Dr. Sci. )

### Graduate Students ( Doctor Candidates )

Hiroyuki FURUTA ( M. Eng. )<sup>a)</sup> ( - 03/1991 )

Chul-Ho SHIN ( M. Eng. )<sup>b)</sup> ( - 03/1991 )

Hideo KUSUZAWA ( M. Eng. ) ( - 03/1991 )

Shudong JIANG ( M. Eng. )

Morihiro KOUROGI ( M. Eng. )

Mituru MUSHA ( M. Eng. ) ( 04/1991 - )

Togar PANGARIBUAN ( M. Eng. ) ( 04/1991 - )

Weizhi WANG ( M. Eng. ) ( 04/1991 - )

### Graduate Students ( Master Course )

Hiromasa SUZUKI ( B. Eng. )<sup>c)</sup> ( - 03/1991 )

Mitsuhiro TESHIMA ( B. Eng. )<sup>d)</sup> ( - 03/1991 )

Naoyuki TOMITA ( B. Eng. )<sup>e)</sup> ( - 03/1991 )

Yoshihi FUJIE ( B. Eng. )

Yasumasa KIKUNAGA ( B. Eng. )

Keiji YAMAMOTO ( B. Eng. )

Yoshinari AWAJI ( B. Eng. ) ( 04/1991 - )

Madoka KAWAI ( B. Eng. ) ( 04/1991 - )

Yukitaka SHIMIZU ( B. Eng. ) ( 04/1991 - )

Yasunobu TODA ( B. Eng. ) ( 04/1991 - )

#### Undergraduate Students

Hideo OCHI<sup>f)</sup> ( - 03/1991 )

Kouji TAKADA<sup>g)</sup> ( - 03/1991 )

Kazunobu YAMADA

Mikio KOZUMA ( 04/1991 - )

Shyuji SAYAMA ( 04/1991 - )

Takeshi YAMASHITA ( 04/1991 - )

#### Research Students

Toru IMAI<sup>h)</sup>

Jun KAWAKAMI<sup>i)</sup>

Tadanori SENOH<sup>j)</sup> ( - 03/1991 )

Naoto KITABAYASHI<sup>k)</sup> ( 04/1991 - )

#### Visiting Scientists

Hisao OHSAWA<sup>l)</sup> ( 04/1991 - )

Bambang WIDIYATMOKO<sup>m)</sup>

( 03/1991 - 04/1991 )

Alexander Sergeevich ZIBROV<sup>n)</sup> ( 07/1991 - )

Alexander Michailovich AKULSHIN<sup>n)</sup> ( 07/1991 - )

Hirokazu HORI<sup>o)</sup> ( 07/1991 - )

#### Secretaries

Yuko YABE

Kaoru OGURA

- a) Presently with Science and Technical Research Lab., NHK ( Japan Broadcasting Corp. )
- b) Presently with National Mokpo Merchant Marine College, Mokpo, Korea
- c) Presently Toyota Corp.
- d) Presently with NTT Corp.
- e) Presently with Nissan Corp.
- f) Presently with Pioneer Corp.
- g) Presently with Graduate School, Tokyo Inst. Technology
- h) Permanent affiliation : Tokyo Aircraft Instrument Co. Ltd., Tokyo, Japan
- i) Permanent affiliation : NIKON Co. Ltd., Kanagawa, Japan
- j) Permanent affiliation : Central Research Lab., Asahi Glass Co. Ltd., Kanagawa, Japan
- k) Permanent affiliation : Research Lab., Nihon Musen Co., Ltd., Saitama, Japan
- l) Permanent affiliation : Research Lab., NIKON Co. Ltd., Tokyo, Japan
- m) Permanent affiliation : R & D Center for Appl. Phys., LIPI, Serpong, Indonesia
- n) Permanent affiliation : P.N. Lebedev Physical Inst. of USSR, Moscow, USSR
- o) Permanent affiliation : Faculty of Engineering, Yamanashi Univ.

## LIST OF PAPERS

### [I] IMPROVEMENTS IN COHERENCE OF LASERS

#### (a) Journal Papers

[1] M. Ohtsu, H. Suzuki, K. Nemoto and Y. Teramachi, "Narrow-Linewidth Tunable Visible InGaAlP Laser, Application to Spectral Measurements of Lithium, and Power Amplification", Jpn. J. Appl. Phys., Vol. 29, No.8, August 1990, pp.L1463-L1465

[ pp.1 - 3 ]

[2] K. Kuboki and M. Ohtsu, "An Allan Variance Real-Time Processing System for Frequency Stability Measurements of Semiconductor Lasers", IEEE Trans. on Instrum. and Meas., Vol.39, No.4, August 1990, pp.637-641

[ pp.4 - 8 ]

[3] C.-H. Shin, "Improved Allan variance real-time processing system to measure frequency tracking error of heterodyne optical phase-locked loops", Electron. Lett., Vol.26, No.19, 13th Sept. 1990, pp.1571-1572

[ pp.9 - 10 ]

[4] M. Ohtsu, I. Koshiishi and Y. Teramachi, "A Semiconductor Laser as a Stable Phase Conjugate Mirror for Linewidth Reduction of Another Semiconductor Laser", Jpn. J. Appl. Phys., Vol.29, No.11, Nov. 1990, pp.L2060-L2062

[ pp.11 - 13 ]

[5] C.-H. Shin and M. Ohtsu, "Stable semiconductor laser with a 7-Hz linewidth by an optical-electrical double-feedback



technique", Opt. Lett., Vol.15, No.24, 15th Dec. 1990, pp.1455-1457

[ pp.14 - 16 ]

[6] M. Kourogi and M. Ohtsu, "Novel optical frequency discriminator for FM noise reduction of semiconductor lasers", Opt. Commun., Vol. 81, No.3, 4, 15th Feb. 1991, pp.204-208

[ pp.17 - 21 ]

[7] M. Kourogi, C.-H. Shin and M. Ohtsu, "A 134 MHz Bandwidth Homodyne Optical Phase-Locked-Loop of Semiconductor Laser Diodes", IEEE Photonics Technol. Lett., Vol.3, No.3, March 1991, pp.270-272

[ pp.22 - 24 ]

[8] M. Kourogi, C.-H. Shin and M. Ohtsu, "A 250 Hz Spectral Linewidth 1.5  $\mu$ m MQW-DFB Laser Diode with Negative-Electrical-Feedback", IEEE Photonics Technol. Lett., Vol.3, No.6, June 1991, pp.496-498

[ pp.25 - 27 ]

[9] M. Ohtsu and C.-H. Shin, "Measurements of frequency fluctuations and field spectral linewidths of lasers", Optronics, No.104, Aug. 1990, pp.56 - 62 ( Review paper, in Japanese )

[ pp.28 - 34 ]

[10] K. Nakagawa, "Ultra-high Coherent Laser", KOGAKU ( Jpn. J. of Optics: A publication of the Opt. Soc. of Jpn. ), Vol. 19, No.10, Oct. 1990, pp.642-649 ( Review paper, in Japanese )

[ pp.35 - 42 ]

[11] K. Nakagawa and M. Ohtsu, "Ultra Stable Laser", The Astronomical Herald, Vol.84, No.4, April 1991, pp.125-126 (

Review Paper, in Japanese )

[ pp.43 - 44 ]

[12] M. Ohtsu and K. Nakagawa, "Spectroscopy by Semiconductor Lasers", Chapter 5 of **Coherence, Amplification, and Quantum Effects in Semiconductor Lasers**, Edited by Y. Yamamoto, John Wiley & Sons, Inc., New York, 1991, pp.137-190

[ pp.45 - 98 ]

[13] C.-H. Shin, "Measurement of frequency fluctuations in ultra-high coherent lasers", OYO BUTURI ( A monthly publication of the Jpn Soc. of Appl. Phys. ), Vol. 60, No.6, June 1991, pp.602-603 ( Review paper, in Japanese )

[ pp.99 - 100 ]

(b) International Conferences

[1] M. Ohtsu, "Frequency Stabilization of Diode Lasers", Conference Digest of IEEE/LEOS Summer Topical Meeting on New Semiconductor Laser Devices and Applications, August 1-3, 1990, Monterey CA, paper number SCW1, pp.9-10 ( Invited )

[ pp.101 - 102 ]

[2] C.-H. Shin and M. Ohtsu, "Very Precise Phase/Frequency Control of Confocal Fabry-Perot Cavity Coupled Semiconductor Laser", Conference Digest of IEEE/LEOS Summer Topical Meeting on New Semiconductor Laser Devices and Applications, August 1-3, 1990, Monterey CA, paper number SCW3, pp.12-13

[ pp.103 - 104 ]

[3] M. Ohtsu, "IR to UV coherent optical sweep generator by

semiconductor lasers", Abstracts of XXIII General Assembly of the International Union of Radio Science ( URSI ), August 28 - Sept. 5, 1990, Prague, Czechoslovakia, Vol.2, p.495 ( Invited )

[ p.105 ]

[4] M. Ohtsu, "Frequency control of semiconductor lasers and its applications", Conference Digest of Jpn - US Seminar on Quantum Electronic Manipulation of Atoms and Fields, Sept. 3-7, 1990, Hiei-san, Kyoto, p.451 ( Invited )

[ p.106 ]

[5] M. Ohtsu, "Coherent Quantum Optics and Technology", Abstracts of The 2nd International Forum on the Frontier of Telecommunications Technology", Oct. 23-24, 1990, Tokyo, paper number (2)-1-2 ( Invited )

[ p.107 ]

[6] M. Ohtsu, C.-H. Shin, H. Furuta, M. Kouroggi, H. Kusuzawa, S. Jiang and K. Nakagawa, "7-Hz-linewidth diode lasers, wideband optical phase locking, and applications", Technical Digest of Conference on Quantum Electronics and Laser Science ( QELS'91 ), May 12-17, 1991, Baltimore, MA, paper number QThL1, pp.242-243 ( Invited )

[ pp.108 - 109 ]

[7] T. Senoh, Y. Fujino, Y. Tanabe, M. Ohtsu and K. Nakagawa, "Direct modulation of stable blue radiation from frequency-doubled GaAlAs laser diode by using EO effect in  $\text{KNbO}_3$  nonlinear crystal", Technical Digest of Conference on Lasers and Electro-Optics ( CLEO'91 ), May 12-17, 1991, Baltimore, MA, paper number CWA6, pp.220-221

[ pp.110 - 111 ]

[8] M. Kouroggi and M. Ohtsu, "Genuine optical frequency discriminator with wide recovery range and high gain for FM noise reduction of semiconductor lasers", Technical Digest of Conference on Lasers and Electro-Optics ( CLEO'91 ), May 12 - 17, 1991, Baltimore, MA, paper number CThF4, pp.380-381

[ pp.112 - 113 ]

[9] M. Kouroggi, K. Nakagawa, C.-H. Shin, M. Teshima and M. Ohtsu, "Accurate frequency measurement system for 1.5-um wavelength laser diodes", Technical Digest of Conference on Lasers and Electro-Optics ( CLEO'91 ), May 12 - 17, 1991, Baltimore, MA, paper number CThR57, pp.490-491

[ pp.114 - 115 ]

[10] K. Nakagawa, M. Ohtsu, C.-H. Shin and M. Kouroggi, "Semiconductor lasers for highly coherent optical sweep generator", Abstracts and Summary of Tenth International Conference on Laser Spectroscopy, June 17-21, 1991, Font-Romeu, France, paper number E38 ( Invited ) ( Summary will be published by Springer-Verlag )

[ pp.116 - 122 ]

[11] M. Ohtsu, C.-H. Shin and M. Kouroggi, "Overview of Coherent Lightwave Communication", Conference Proceedings of International Microwave Conference/Brazil ( SBMO 91 ), July 22-25, 1991, Rio de Janeiro, Brazil, paper number 03.4, pp.498-502 ( Invited )

[ pp.123 - 127 ]

### [III] APPLICATION TO ATOMIC CLOCKS

(a) Journal Papers

[1] H. Furuta, H. Suzuki and M. Ohtsu, "Observation of Ramsey-Type Resonant Fringe Using a Cylindrical Microwave Cavity for a Diode Laser-Pumped Rb Beam Atomic Clock", Jpn. J. Appl. Phys., Vol.30, No.3, March 1991, pp.596-602

[ pp.128 - 134 ]

**[III] APPLICATION TO PHOTON SCANNING TUNNELING MICROSCOPE**

(a) Journal Papers

[1] M. Ohtsu, "Photon Scanning Tunneling Microscope", SHOKUBAI (CATALYST: A publication of the Catalysis Society of Japan ), Vol.32, No.8, Dec. 1990, pp.548-550 ( Review paper, in Japanese )

[ pp.135 - 137 ]

[2] S. Jiang, N. Tomita and M. Ohtsu, "Photon Scanning Tunneling Microscope", KOGAKU ( Jpn. J. Optics: A publication of the Opt. Soc. of Jpn. ), Vol. 20, No. 3, March 1991, pp.134-141 ( Review paper, in Japanese )

[ pp.138 - 145 ]

[3] M. Ohtsu, "Trends on Photon Scanning Tunneling Microscope", O plus E, No.138, May 1991, pp.90-97 ( Review paper, in Japanese )

[ pp.146 - 153 ]

(b) International Conferences

[1] S. Jiang, N. Tomita, K. Nakagawa and M. Ohtsu, "Super-

resolution photon scanning tunneling microscope using diode lasers", Technical Digest of Conference on Lasers and Electro-Optics, May 12-17, 1991, Baltimore, MA, paper number CTh05, pp.420-421

[ pp.154 - 155 ]

#### **[IV] Books**

[1] M. Ohtsu, **COHERENT QUANTUM OPTICS AND TECHNOLOGY**, ASAKURA-SHOTEN Publishers, Tokyo, Nov. 1990 ( in Japanese )

#### **[V] AWARDS**

[1] M. Ohtsu and K. Nakagawa: Award from The Japanese Society of Applied Physics ( to the review paper entitled, "Frequency Control of Semiconductor Lasers and Its Applications" by M. Ohtsu and K. Nakagawa, OYO BUTURI, Vol.58, No.10, Oct. 1990, pp.1428-1444, ( in Japanese ) ) Sept. 26, 1990

[2] C.-H. Shin: The Best Ph.D Thesis Award from Teshima Foundation, March 1991

#### **[VI] PRESENTED PH.D. THESES**

[1] H. FURUTA, "Semiconductor Laser-Pumped Rubidium Beam Atomic Clock", January 1991 ( in Japanese ).

[2] C.-H. SHIN, "Optical Phase-Locking of Semiconductor Lasers", January 1991.

## Narrow-Linewidth Tunable Visible InGaAlP Laser, Application to Spectral Measurements of Lithium, and Power Amplification

Motoichi OHTSU, Hiromasa SUZUKI, Kouhichi NEMOTO<sup>†</sup>  
 and Yasuaki TERAMACHI<sup>††</sup>

*Graduate School at Nagatsuta, Tokyo Institute of Technology,  
 4259 Nagatsuta, Midori-ku, Yokohama, Kanagawa 227*

<sup>†</sup>*Komae Research Laboratory, Central Research Institute of Electric Power Industry,  
 11-1, Iwato Kita, 2, Komae-shi, Tokyo 201*

<sup>††</sup>*Department of Information Engineering, University of Industrial Technology,  
 1960 Aihara, Sagamihara, Kanagawa 229*

(Received June 8, 1990; accepted for publication July 5, 1990)

Coarse and fine tuning of a 3.3 THz sweep range for an optically stabilized InGaAlP laser were realized for the first time by varying the angle of an external grating surface and the length of an external confocal Fabry-Perot cavity while maintaining the narrow linewidth of less than 50 kHz. Optogalvanic spectral shapes of D<sub>1</sub> and D<sub>2</sub> lines in Li vapor were measured by this laser, and the spectral splitting due to D.C. Stark effect was clearly observed. The laser power was amplified 25 dB by a dye solution which was optically pumped by the second harmonics of a pulsed YAG laser.

**KEYWORDS:** InGaAlP laser, linewidth reduction, frequency tuning, optogalvanic spectroscopy, power amplification

Linewidth reduction, frequency tuning, and high output power have been required for visible InGaAlP lasers (wavelength of 600~700 nm)<sup>1,2)</sup> for applications in analytical spectroscopy,<sup>3)</sup> precise optical measurements, and fundamental quantum optics. However, our preliminary measurements showed that their field spectral linewidths were as wide as 200 MHz, which were not able to satisfy requirements in the above-mentioned applications. Although the output power as high as 300 mW has already been realized by a multimode broad-area InGaAlP laser device,<sup>4)</sup> the typical output power of commercially available InGaAlP lasers is lower than 10 mW. The present letter demonstrates for the first time the experimental results of three new trials. They are (1) the linewidth reduction and frequency tuning by the simultaneous optical feedback from an external confocal Fabry-Perot (CFP) cavity<sup>5)</sup> and from an external diffraction grating, (2) optogalvanic spectroscopy of Li vapor to confirm the applicability of this improved InGaAlP laser to spectroscopy, and (3) power amplification by a dye solution which is pumped by the second harmonics of a pulsed YAG laser to improve the sensitivity and efficiency of the application systems described above.

Figure 1(a) shows the experimental setup for linewidth reduction and frequency tuning. A Toshiba TOLD9211-type InGaAlP laser was used without any AR coating. Its maximum output power, wavelength, and field spectral linewidth were measured as 4 mW, 670 nm, and 200 MHz, respectively, at room temperature. Temperature fluctuations of the laser heat sink were reduced to less than 1 mK. Although the negative electrical feedback shows an extremely high gain and high stability for the linewidth reduction,<sup>6)</sup> the present study employed the optical feedback for a simpler frequency tuning. The CFP cavity had two mirrors of 99.5% reflectivity and the free

spectral range of 1.5 GHz. The number of grooves and the blaze wavelength of the external grating were 900 lines/mm and 600 nm, respectively. The separations between the laser and the CFP cavity, and the grating were 20 cm and 17 cm, respectively. The laser and all the op-

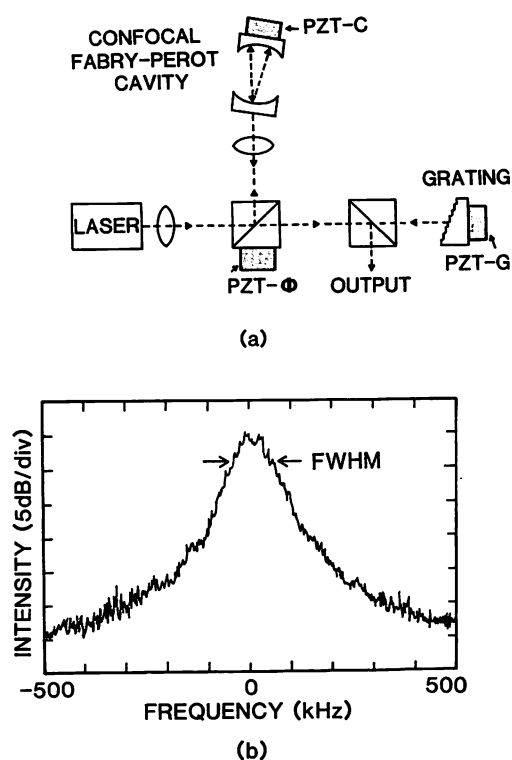


Fig. 1. (a) Experimental setup for linewidth reduction and frequency tuning. PZT: Piezoelectric transducer. (b) Field spectral profile of the signal from the delayed self-homodyne system. FWHM: Full width at half maximum.

tical components were fixed on a super Invar plate to reduce thermal drift. Preliminary linewidth reduction was carried out by optical feedback of the first-order diffracted light from the external grating. A scanning Fabry-Perot (SFP) interferometer (Spectra-Physics, model 470-3, finesse=60 at the 670-nm wavelength, free spectral range=2 GHz) was used to measure the preliminarily reduced linewidth. Coarse frequency tuning was carried out by varying the angle of the grating surface in cooperation with sweeping the temperature of the laser heat sink. The tuning of the narrower frequency range was carried out by a piezoelectric transducer PZT-G. The value of the coarse tuning range was measured by a grating monochromator. Further linewidth reduction was carried out by simultaneous optical feedback from the CFP cavity, where stable optical feedback was maintained by controlling the PZT- $\phi$ . The reduced linewidth was measured by a delayed self-homodyne method<sup>7)</sup> using a 2-km long optical fiber. The resolution of the linewidth measurement was 50 kHz. The fine frequency tuning was carried out by sweeping the CFP cavity length by a PZT-C. The SFP interferometer described above was also used to measure the fine-tuned frequency range.

A coarse tuning range of 3.3 THz was obtained by simultaneous sweeps of the grating surface angle and the heat sink temperature for 10°C ~ 20°C, and the field spectral linewidth was reduced to 60 MHz. The external cavity modes composed of the laser facets and grating were observed; however, the powers of these side modes were reduced to lower than 1/40 of the main mode by simultaneous optical feedback from the CFP cavity. Figure 1(b) shows the field spectral profile of the delayed self-homodyne signal. Its full width at half maximum (FWHM) was exactly the same as the resolution of the delayed self-homodyne system. This means that the true value of the laser FWHM was less than 50 kHz, from which it was confirmed that the laser FWHM was reduced to less than  $2.5 \times 10^{-4}$  times that of the free-running laser. To the authors' knowledge, such a narrow linewidth has not been documented so far. It was also confirmed that the fine tuning was realized for the first time by sweeping the PZT-C while maintaining this narrow linewidth; i.e., precise and wide-band frequency tuning was realized by combining the fine tuning with the above-mentioned coarse tuning. It can thus be claimed that this narrow-linewidth and wide-band tunable visible laser is used instead of dye lasers for applications to various precise optical measurements.

To confirm this applicability, optogalvanic spectroscopy of Li vapor was carried out by using a hollow cathode lamp (Hamamatsu Photonics, L233-3NB), in which a cathode containing Li atoms was used and a Ne gas of 7 Torr pressure was filled. Figure 2 shows the spectral profiles of the D<sub>1</sub> and D<sub>2</sub> lines of Li vapor measured by the lock-in detection of the changes in the discharge current by irradiating the chopped laser power to the lamp. Their wavelengths have been known as 670.791 nm and 670.776 nm, respectively.<sup>8)</sup> The curves A, B, and C correspond to the discharge currents of 4, 7, and 10 mA, respectively. They confirmed that the measurements were carried out by a very high signal-to-noise ratio. Spectral

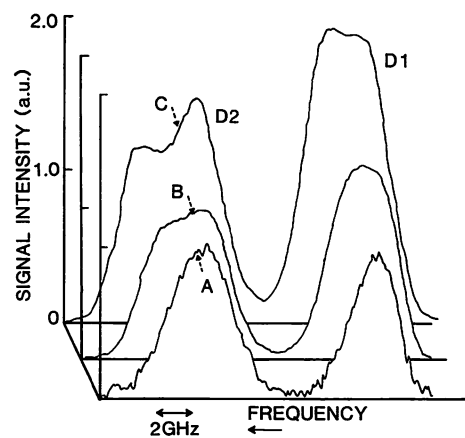


Fig. 2. Optogalvanic spectral shapes of D<sub>1</sub> and D<sub>2</sub> lines in Li vapor. The discharge current for the hollow cathode lamp was 4 (A), 7 (B), and 10 (C) mA.

splitting on curves B and C, which was due to the D.C. Stark effect of the hyperfine energy levels in the ground and excited states, can be clearly seen by increasing the discharge current. For example, the separation between the two peaks on the D<sub>2</sub> line of curve C was measured as about 3.0 GHz. Quantitative comparison with the calculated and measured magnitude of the D.C. Stark shift has not yet been completed because the magnitude depended strongly on the complicated D.C. electric field and the optical path in the hollow cathode. However, it can be claimed by these measurements that the present laser could be used as a reliable coherent and tunable light source for sensitive laser spectroscopy.

For some applications such as the laser isotope separation, high-power-pulsed laser lights have been required.<sup>9)</sup> To confirm the feasibility of the present laser for such applications by pulse power amplification, the laser power was amplified by using a dye solution which was optically pumped by the second harmonics (SH) of a pulsed YAG laser (Spectra Physics DCR-10(A)). Figure 3(a) shows an experimental setup. A dye (Spectra Physics LDS698) was dissolved into ethanol with a density of 225 mg/l, and was filled into a quartz glass cell. The optical path length of the InGaAlP laser in the dye cell was 10 mm. A SH pulse had the 350-mJ energy and the 10-ns pulse width. The pulse repetition rate was 0.2 Hz. The SH was focused onto the dye cell by a cylindrical lens of 60-mm focal length. Pinholes, lenses, and a grating monochromator (resolution of several angstroms) were used to reduce the amplified spontaneous emission (ASE) power incident on the photodetector (Si-APD). The output pulse waveforms from the sensitivity-calibrated Si-APD were observed by a digital storage oscilloscope.

Figure 3(b) shows an example of observed waveforms. The amplification gain was defined by  $I_1/I_2$ , where  $I_1$  and  $I_2$  are the peak power of the amplified InGaAlP laser waveform and the CW InGaAlP laser power incident into the dye cell, respectively. (The  $I_2$  is not shown in this figure because its value was too small to be illustrated.) As the first step, the value of  $I_2$  was measured, and then the peak power  $I_3$  of the pulsed ASE was measured by blocking the InGaAlP laser light in front of the dye cell.



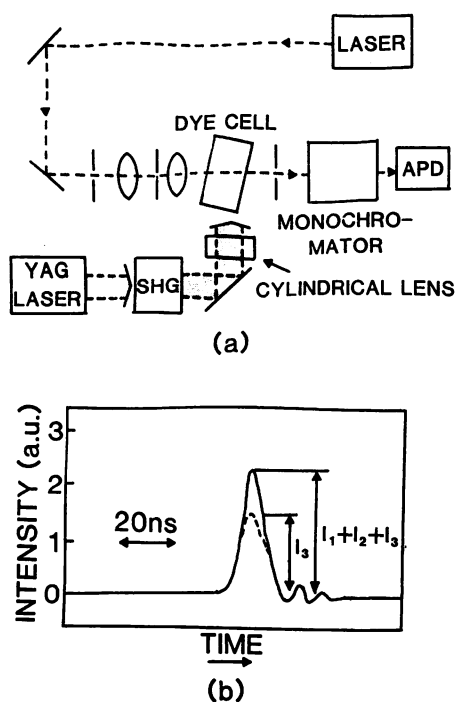


Fig. 3. (a) Experimental setup for InGaAlP laser power amplification by a dye solution which was pumped by the second harmonics of a pulsed YAG laser. SHG: Second harmonics generator. (b) Oscilloscope traces of the signal from the APD in (a).  $I_1$ : The peak power of the amplified InGaAlP laser.  $I_2$ : The CW power of the InGaAlP laser incident into the dye cell, which was too low to be illustrated in this figure.  $I_3$ : The peak power of the amplified spontaneous emission from the optically pumped dye solution.

As the second step, the value of  $I_1 + I_2 + I_3$  was measured. The amplification gain was calculated by these values to obtain  $I_1/I_2 = 25$  dB within the maximum available value of  $I_2$  ( $\leq 0.5$  mW). The maximum available power  $I_2$  was lower than the original output power from the free-run-

ing InGaAlP laser because the power has been attenuated by the beam splitters, mirrors, and pinholes in Figs. 1(a) and 3(a). The amplification gain could be large enough so as to be used as a pulsed light source to improve the sensitivity and efficiency of several analytical spectroscopy systems.

In summary, the linewidth of the InGaAlP laser was reduced to less than 50 kHz, i.e., less than  $2.5 \times 10^{-4}$  times that of the free-running laser, by the optical feedback. Frequency tuning was realized for 3.3 THz sweep range while maintaining the narrow linewidth. Spectral splitting due to the D.C. Stark effect of optogalvanic spectral shapes of  $D_1$  and  $D_2$  lines in Li vapor was observed. The laser power was amplified 25 dB by a dye solution which was optically pumped by the second harmonics of a pulsed YAG laser.

The authors are indebted to H. Sasada of Keio Univ. for providing a hollow cathode lamp and to K. Nakagawa and S.-H. Shin of their research group for valuable discussions.

#### References

- 1) M. Ishikawa, Y. Ohba, Y. Watanabe, H. Sugawara, M. Yamamoto and G. Hatakoshi: *Trans. IECE Jpn.* **E69** (1986) 382.
- 2) S. Kawata, H. Fujii, K. Kobayashi, A. Gomyo, I. Hino and T. Suzuki: *Electron. Lett.* **23** (1987) 1327.
- 3) J. Lawrenz, A. Obrebski and K. Niemax: *Anal. Chem.* **59** (1987) 1232.
- 4) K. Itaya, G. Hatakoshi, Y. Watanabe, M. Ishikawa and Y. Uematsu: *Electron. Lett.* **26** (1990) 214.
- 5) B. Dahmani, L. Hollberg and R. Drullinger: *Opt. Lett.* **12** (1987) 876.
- 6) M. Ohtsu, M. Murata and M. Kourogi: *IEEE J. Quantum Electron.* **26** (1990) 231.
- 7) T. Okoshi, K. Kikuchi and A. Nakayama: *Electron. Lett.* **16** (1980) 630.
- 8) J. Vanier and C. Audoin: *The Quantum Physics of Atomic Frequency Standards* (Adam Hilger, Bristol, 1989) Vol. 1, Chap. 4.
- 9) J. I. Davis: *IEEE Trans. Nucl. Sci.* **NS-30** (1983) 24.

# An Allan Variance Real-Time Processing System for Frequency Stability Measurements of Semiconductor Lasers

K. KUBOKI AND M. OHTSU, MEMBER, IEEE

**Abstract**—A real-time frequency stability measurement system for semiconductor lasers was developed. Since the frequency of the input signal is successively measured without clearing the counter, the Allan variance can be accurately measured by following its definition. Measurements of the Allan variance made with this system are more accurate than those made with conventional instruments. The Allan variance may be measured for integration times  $\tau$  from 1  $\mu$ s to 10 000 s, and the number  $N$  of measured frequencies averaged over the integration time  $\tau$  can be arbitrarily selected up to  $N = 707$  for each integration time. The highest measurable frequency was 90 MHz. It was demonstrated experimentally that this system can be used for measurements of the frequency stability of semiconductor lasers.

## I. INTRODUCTION

TEMPORAL coherence of semiconductor lasers needs to be improved when they are used for coherent optical communications, and coherent optical measurements. To accomplish this, several groups have been using frequency stabilization [1], [2] and linewidth reduction of the field spectrum [2]–[4]. They have also been developing a heterodyne frequency-locked loop (HFLL) [5] between semiconductor lasers by using frequency offset locking methods [6]. In order to evaluate the performance of the HFLL, measurements of the frequency stability of the heterodyne signal were required. For longer integration times and an increased number of measurements, frequency stability needs to be efficiently evaluated. A frequency and time interval analyzer HP5371A (Hewlett-Packard) [7] is commercially available for measuring frequency stability. Its fundamental functions are continuous counting and recording of the time of signal zero-crossings. In other words, it measures the relation between time and frequency. Frequency stability measurement does not require the determination of the heterodyne frequency but only the measurement of relative frequency change. The HP5371A can measure the frequency stability for integration times up to 8 s. In the present paper, the authors developed a real-time frequency stability measurement system, i.e., the Allan variance real-time processing system

(ARPS) which is quite simple and can measure frequency stability for integration times from 1  $\mu$ s to 10 000 s.

## II. HARDWARE OF THE ARPS

The ARPS calculates the square root of the Allan variance as a measure of the frequency stability of semiconductor lasers. The Allan variance is calculated [8] by

$$\sigma_y^2(\tau) = \frac{1}{2(N-1)} \sum_{i=1}^{N-1} (f_{i+1} - f_i)^2 / f_0^2 \quad (1)$$

where  $f_i$  is a signal frequency averaged over the integration time  $\tau$ ,  $N$  is the number of averaged frequencies ( $f_i$ ), and  $f_0$  is the nominal frequency of the oscillator that is being evaluated. The averaged frequency  $f_i$  can be obtained by

$$f_i = (C_{i+1} - C_i) / \tau \quad (2)$$

where  $C_i$  is the number of TTL pulses obtained from positive-going zero crossings of the sinusoidal analog input signal in the time interval  $\tau$  (s). The timing chart is shown in Fig. 1. It should be noted that the definition of the Allan variance requires zero deadtime between successive measurements of  $C_i$  [8]. The deadtime of this system is sufficiently small compared to  $\tau$ . If these measurements were to contain significant deadtime, the Allan variance could diverge as it does when the fluctuations are caused by flicker noise, random walk, etc. [9].

The block diagram of the ARPS is shown in Fig. 2. The ARPS is composed of a counter, a memory, and a personal computer (PC). Since high-speed-type TTL integrated circuits are used in the counter and memory, the maximum measurable frequency of the input signal is as high as 90 MHz. The number of TTL pulses, that is converted from the sinusoidal analog input signal, is continuously counted by a 32-bit synchronous binary counter without clearing the counted value. Thus there is no deadtime in counting the pulse number. The output signal from the counter is transferred to a 32-bit latch. This latch is followed by two 16-bit buffers, and these buffers are connected to the data terminals of a 4-kbyte static RAM. Since this RAM is a 16-bit  $\times$  2048 device, output signals from the 32-bit latch are divided into the upper 16-bit and the lower 16-bits. The values of these divided bits are stored in this RAM and the shortest measurable integra-

Manuscript received February 4, 1989; revised February 26, 1990.

The authors are with the Tokyo Institute of Technology, the Graduate School at Nagatsuta, 4259 Nagatsuta, Midori-ku, Yokohama, Kanagawa 227, Japan.

IEEE Log Number 9036026.

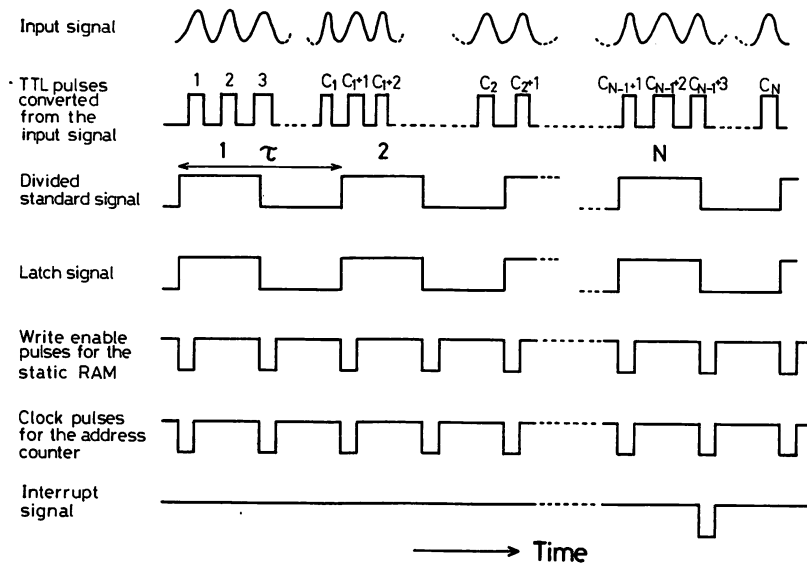


Fig. 1. Timing chart of the TTL pulses used in the ARPS.  $C_i$  is a number of the input TTL pulses coming into the counter within the time interval  $\tau$ , where  $\tau$  represents the integration time of the Allan variance measurement. The time interval between adjacent pulses of the divided standard signal determines  $\tau$ .

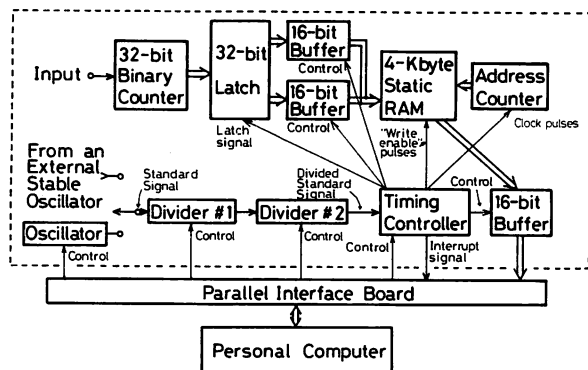


Fig. 2. Block diagram of the ARPS. The block surrounded by the broken lines represents the counter and memory.

tion time of frequency stability is determined by its access speed. Because of the capacity of the RAM, the maximum value of  $N$  in (1) can be fixed at 707, which is large enough to measure the Allan variance accurately. An address counter is connected to the address terminals of the static RAM to up-count the stored address. Furthermore, a 16-bit buffer is also connected to the data terminals of the RAM to transfer the counted signal stored in the RAM to the PC.

A standard TTL pulse signal is generated from an oscillator for timing control and for fixing the value of the integration time  $\tau$ . Its repetition frequency is 1 MHz, and the frequency accuracy and stability are  $10^{-4}$  and  $10^{-5}$ /year, respectively. Two dividers are connected in series to the next stage of the oscillator. The frequency of the standard signal can be divided by anything from 1 to  $10^{10}$  by these dividers, where the division ratio is selected by the control signals applied to the dividers from the PC. Thus the frequency is varied between 1 MHz and 0.0001 Hz, and this varies the range of  $\tau$  between 1  $\mu$ s and 10 000

s. An external standard TTL pulse signal of 1 MHz frequency can also be used instead of the signal from the oscillator. The Allan variance can be measured with higher precision if the external standard signal is derived from a more stable oscillator. If an external standard signal with a frequency lower than 1 MHz is supplied, the frequency stability for  $\tau \geq 10\,000$  s can be measured. In this case, the longest measurable integration time is given by  $f_{\text{ext}}^{-1} \times 10^{10}$  (s), where  $f_{\text{ext}}$  (Hz) is the frequency of the external standard signal. Control signals in the timing controller for the latch, the static RAM, the address counter, and the buffers can be generated by using the output signal from this oscillator or they can be generated from the oscillator in the PC.

The PC used in the ARPS was a PC-9801Vm (NEC). A parallel interface board with two programmable peripheral interface IC's was added to the PC. This board was used to exchange the signals between the PC and the block of the counter and memory.

### III. OPERATION OF THE ARPS

Fig. 1 shows a timing chart of the pulses used in the ARPS. The ARPS begins measuring the values of  $f_i$  without any manual operation when the oscillator starts generating the standard signal. The "start/stop" command to the standard signal is controlled by a program of the PC, and the time interval between adjacent pulses of the standard signal is fixed to be the same as the integration time  $\tau$  for calculating the Allan variance. The 32-bit counted values of  $C_i$  are latched at every  $\tau$  (s). The output signals from the latch are divided into two 16 bits, and sent to the two 16-bit buffers. To store these two 16-bit counted values into the static RAM, the timing controller generates two "write enable" pulses and two clock pulses for the static RAM and for the address counter, respectively. This

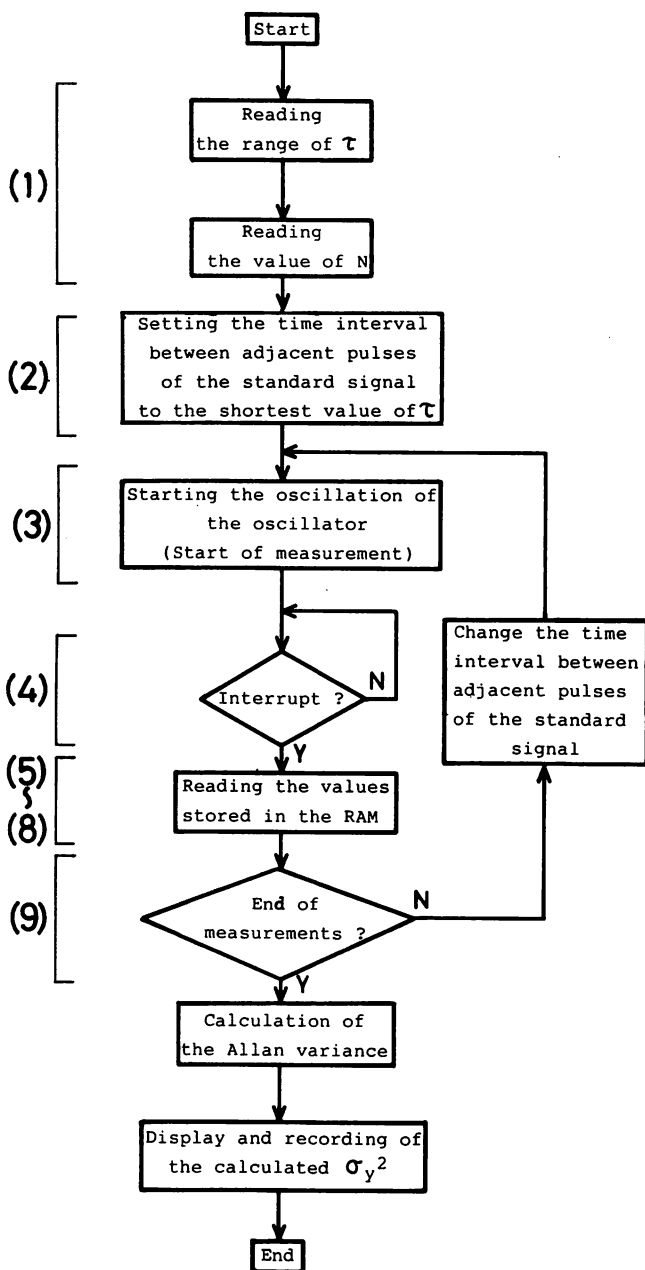


Fig. 3. Flowchart of the program of the ARPS. Each number given next to the block corresponds to sequence number described in the paper.

occurs at each rising edge of the standard signal pulse from the oscillator.

Fig. 3 shows a flowchart of the computer program for the ARPS. Functions of this program are reading the values of the parameters  $\tau$  and  $N$ , initializing the counter and memory, reading the value stored in the RAM, and calculating the Allan variance. The operating procedures of the computer program are summarized as follows.

1) As soon as the input of a range of  $\tau$  and  $N$  for each  $\tau$  is finished, all the flip-flops used in the timing controller and the address counter are cleared.

2) The time interval between adjacent pulses of the standard signal is fixed to the value of the shortest integration time, and an initial value of the address counter is fixed to  $(2048 - 2 \times N)$ .

3) After initializing by 1) and 2), the oscillator begins generating the standard signal. Data acquisition is then carried out automatically.

4) After the static RAM stores the values of  $C_i$  for  $N$  times (i.e., when the value of the address counter reaches 2048), an interrupt signal is sent from the block of the counter and memory to the PC.

5) When the interrupt signal is received by the PC, the program stops generating the standard signal from the oscillator, clears all flip-flops, and again fixes the value of the address counter to  $(2048 - 2 \times N)$ .

6) The program carries out an IN read command through the parallel interface board. The values stored in the memory cells at address numbers  $(2048 - 2 \times N)$  and  $(2048 - 2 \times N + 1)$  in the static RAM are read by the PC. The TTL level of the input-output read signal (IOR signal) of the PC is changed from high to low to high in sequence by the IN command.

7) By using the IOR signal, the timing controller sends two more clock pulses to the address counter. Then, the values stored in the memory cells at address numbers  $(2048 - 2 \times N + 2)$  and  $(2048 - 2 \times N + 3)$  in the static RAM are read by the PC by a second execution of the IN command.

8) When the program carries out the IN command  $N$  times, all values stored in the RAM are read into the PC.

9) If there are any other integration times  $\tau$  for measuring the Allan variance, the time interval between adjacent pulses of the standard signal is fixed to the next  $\tau$  and the procedures of 2)–8) are repeated.

The Allan variance is then calculated by using 1) and 2), and the measured values of  $C_i$  obtained by the procedures of 2)–9).

#### IV. EVALUATION OF PERFORMANCES OF THE ARPS AND THE EXAMPLES OF MEASUREMENTS

Fig. 4 shows a range of values of the square root of the Allan variance which can be measured by the ARPS. On the vertical axis, the values of the squared root of the Allan variance are normalized to the nominal optical frequency  $f_0$  (375 T · Hz) of a semiconductor laser of 0.8- $\mu\text{m}$  wavelength. The range of integration times for which the Allan variance could be measured was from 1  $\mu\text{s}$  to 10 000 s. Since the value of  $C_i$  was measured by the TTL counter in the ARPS, a roundoff error of  $\pm 1$  count may occur. Because of this count error, the lower limit of the measurable range of the square root of the Allan variance is expressed as

$$\sigma_y(\tau)_{\text{lower limit}} = f_0^{-1} \cdot \tau^{-1}. \quad (3)$$

Line A in Fig. 4 represents the value of (3). The upper limit of the measurable range is determined by the response speed (line B) of the TTL counter used in the ARPS and by the maximum number of pulses countable (line C) by the counter ( $2^{32} = 4.3 \times 10^9$  counts). Curve D represents a calculated value of normalized frequency fluctuations caused by the spontaneous emission of 0.8  $\mu\text{m}$  semiconductor lasers whose typical optical output

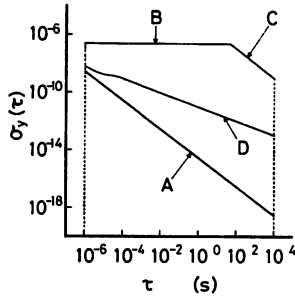


Fig. 4. The range of values of the Allan variance which can be measured by the ARPS. The vertical axis represents the square root of the Allan variance, which is normalized to the optical frequency of a semiconductor laser of  $0.8 \mu\text{m}$  wavelength. Curve *A*: Lower limit caused by  $\pm 1$  count error. Curve *B*: Upper limit determined by the response speed of the TTL counter used in the ARPS. Curve *C*: Upper limit determined by the maximum number of pulses countable by the counter ( $2^{32} = 4.3 \times 10^9$  counts). Curve *D*: The calculated value of the frequency stability of  $0.8 \mu\text{m}$  AlGaAs lasers determined by the magnitude of spontaneous emission [11].

power is 3 mW [10]. Since curve *D* lies within the range surrounded by the lines *A*, *B*, and *C*, we conclude that the frequency stability of semiconductor lasers can be measured by the ARPS.

To check the operation of the ARPS, a test signal was prepared by dithering the output of a frequency synthesizer to give

$$f(t) = f_0 + (\Delta f/2) \sin(2\pi f_m t) \quad (4)$$

where  $f_0$  is the center or nominal frequency,  $\Delta f$  is the peak-to-peak value of the frequency deviation, and  $f_m$  is the modulation frequency. Prior to the measurement by the ARPS, the Allan variance of frequency fluctuations of this controlled dithered test signal was calculated. The power spectral density of frequency fluctuations can be derived from (4), and expressed as

$$S_y(f) = \frac{\Delta f^2}{8f_0^2} \delta(f - f_0) \quad (5)$$

where the suffix  $y$  represents the frequency fluctuations normalized to  $f_0$ , and  $\delta(f - f_0)$  is a delta function. The relation between the Allan variance and the power spectral density of frequency fluctuations is given by [10], [11]

$$\sigma_y^2(\tau) = 2 \int_0^\infty S_y(f) \frac{\sin^4(\pi f \tau)}{(\pi f \tau)^2} df. \quad (6)$$

The Allan variance for (4) can be calculated from (5) and (6) to give

$$\sigma_y^2(\tau) = \left( \frac{\Delta f \cdot \sin^2(\pi f_m \tau)}{2 \cdot f_0 \cdot \pi f_m \tau} \right)^2. \quad (7)$$

Fig. 5 shows the values of the square root of the Allan variance calculated by (7) as well as the values measured by the ARPS. The values of  $f_m$ ,  $\Delta f$ , and  $f_0$  in (4) and (7) were fixed to 12.3 kHz, 12 MHz, and 22 MHz, respectively. The good agreement of the two results in this figure confirms the accurate operation of the ARPS.

By using the ARPS, the frequency stability of two semiconductor lasers (CSP-type, Hitachi, HL8312E,  $0.83$

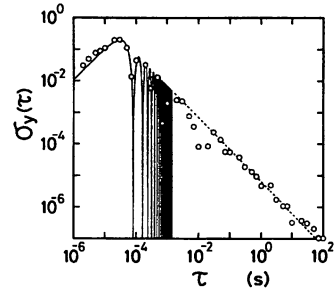


Fig. 5. Results of the operation test of the ARPS by using an artificially dithered signal. The solid curve and broken line represent calculated values, where the broken line is an envelope of the sinusoidally oscillating solid curve. Open circles represent measured values. The values of modulation frequency  $f_m$ , frequency deviation  $\Delta f$ , and nominal frequency  $f_0$  were fixed to 12.3 kHz, 12 MHz, and 22 MHz, respectively.

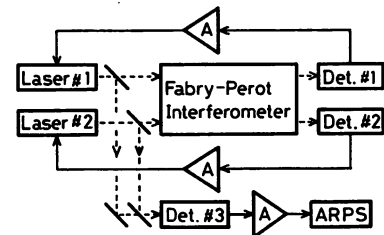


Fig. 6. Experimental setup for the frequency stability measurement of two semiconductor lasers whose frequencies were stabilized independently by using a Fabry-Perot interferometer as a common frequency reference.

$\mu\text{m}$  wavelength) was measured. Fig. 6 shows the experimental setup. The frequencies of both lasers were independently stabilized by using a linear portion of a slope of the resonance curve of a Fabry-Perot interferometer as a common frequency reference. The Fabry-Perot interferometer was made using a cylindrical rod of fused silica with dielectric multilayer films coated on both ends. The reflectivity of these films was 90%. The free spectral range of this interferometer was 3.45 GHz. The Allan variance  $\sigma_{yM}^2(\tau)$  of residual frequency fluctuations of the heterodyne signal between the two lasers was measured by the ARPS. The average of the heterodyne signal was 200 MHz, and this frequency was divided by 5 before it was applied to the ARPS. Fig. 7 shows the results of this measurement. In this figure, the square root of the Allan variance  $\sigma_{yM}^2(\tau)$  of the residual frequency fluctuations  $\delta f$  was represented by normalizing to the nominal optical frequency  $f_0$ , i.e.,  $y = \delta f/f_0$ . Curves *A* and *B* represent the values under free-running and feedback conditions, respectively. Since the bandwidth of the feedback loop was 20 kHz, the value of curve *B* was smaller than that of curve *A* for the range of  $\tau \geq 50 \mu\text{s}$ . The minimum of curve *B* was  $1.5 \times 10^{-10}$  at  $\tau = 2$  s, which corresponds to frequency fluctuations of 54 kHz.

The frequency stability of the heterodyne signal in a HPLL was also measured. Fig. 8 shows an experimental setup for this measurement. Detailed explanations of this system has been given elsewhere [12]. The master laser frequency was stabilized by the method shown in Fig. 6, and its frequency stability was approximated by curve *B* in Fig. 7. The frequency of the heterodyne signal between

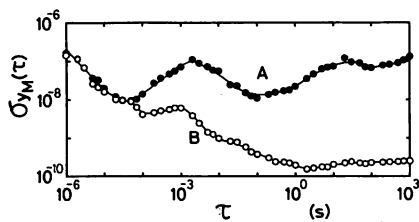


Fig. 7. Frequency stability of the semiconductor lasers measured by using the ARPS.  $\sigma_{yM}^2(\tau)$  represents the square root of the Allan variance of the residual frequency fluctuations of the heterodyne signal between two semiconductor lasers, which was normalized to the nominal optical frequency. Curves *A* and *B* represent the values under free-running and feedback conditions, respectively.

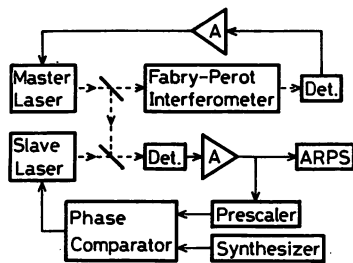


Fig. 8. Experimental setup of HFLL.

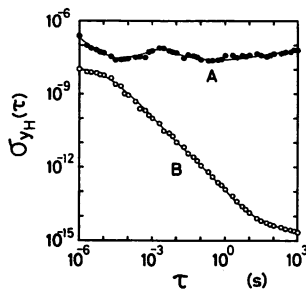


Fig. 9. Frequency stability of the heterodyne signal between the master and the slave lasers by using the ARPS.  $\sigma_{yM}^2(\tau)$  represents the square root of the Allan variance of the residual frequency fluctuations of the heterodyne signal, which was normalized to the optical frequency. Curves *A* and *B* represent the values under free-running and feedback conditions, respectively.

the master and the slave lasers was locked to that of a stable microwave synthesizer so that the slave laser frequency accurately tracked the master laser frequency. The frequency of the heterodyne signal was 30 MHz. The Allan variance  $\sigma_{yM}^2(\tau)$  of the residual frequency fluctuations of the heterodyne signal was measured by the ARPS to evaluate the performance of this system quantitatively. Fig. 9 shows the results of this measurement. This figure shows relative frequency fluctuations between master and locked slave lasers. These results are also expressed by the square root of the Allan variance  $\sigma_{yM}^2(\tau)$  of the residual frequency fluctuations  $\delta f$  normalized to the nominal optical frequency  $f_0$  ( $y = \delta f/f_0$ ). Curves *A* and *B* represent the values under free-running and feedback conditions, respectively. Since this system has a bandwidth wider than 1 MHz, the value of curve *B* is lower than that of curve *A* at  $\tau \geq 1 \mu\text{s}$ . The minimum of curve *B* was 2.2

$\times 10^{-15}$  at  $\tau = 1000$  s, which corresponds to relative frequency fluctuations as low as 0.8 Hz.

## V. CONCLUSION

An Allan variance ARPS was developed for frequency stability measurements of semiconductor lasers. The performance of this system is summarized as follows.

1) Since the number  $C_i$  of the input TTL pulses in this system can be read without clearing the counter and there was no deadtime in measurements, and the Allan variance can be accurately measured.

2) The square root of the Allan variance can be measured for integration times from 1  $\mu\text{s}$  to 10 000 s.

3) The maximum number of data of values of the averaged frequency  $f_i$  measurable by this system is 707.

4) The highest measurable frequency of the signal is 90 MHz.

The result of measurements of the frequency stability of two semiconductor lasers by the ARPS gives a minimum  $\sigma_{yM}^2(\tau)$  of  $1.5 \times 10^{-10}$  at  $\tau = 2$  s. This corresponds to frequency fluctuations of  $\pm 54$  kHz. Measurements of the frequency stability of the heterodyne signal in the heterodyne frequency locked loop gave a minimum  $\sigma_{yM}^2(\tau)$  of  $2.2 \times 10^{-15}$  at  $\tau = 1000$  s. This corresponds to frequency fluctuations between the locked laser and the master laser of about 0.8 Hz.

## ACKNOWLEDGMENT

The authors thank Dr. Y. Saburi, S. Kodato, S. Kinugawa, and T. Saito (Anritsu Co.), and T. Kato (Tokyo Institute of Technology) for their technical support.

## REFERENCES

- [1] M. Ohtsu, "Realization of ultrahigh coherence in semiconductor lasers by negative electrical feedback," *J. Lightwave Technol.*, vol. 6, pp. 245-256, 1988.
- [2] B. Dahmani, L. Hollberg, and R. Drullinger, "Frequency stabilization of semiconductor lasers by resonant optical feedback," *Opt. Lett.*, vol. 12, pp. 876-878, 1987.
- [3] N. A. Olsson and J. P. van der Ziel, "Performance characteristics of 1.5  $\mu\text{m}$  external cavity semiconductor lasers for coherent optical communication," *IEEE J. Lightwave Technol.*, vol. 5, pp. 510-515, 1987.
- [4] M. Ohtsu and N. Tabuchi, "Electrical feedback and its network analysis for linewidth reduction of a semiconductor laser," *J. Lightwave Technol.*, vol. 6, pp. 357-369, 1988.
- [5] R. L. Barger and J. L. Hall, "Pressure shift and broadening of methane line at 3.39  $\mu$  studied by laser-saturated molecular absorption," *Phys. Rev. Letts.*, vol. 22, no. 1, pp. 4-8, 1969.
- [6] K. Kuboki and M. Ohtsu, "Frequency offset locking of AlGaAs semiconductor lasers," *IEEE J. Quantum Electron.*, vol. QE-23, pp. 388-394, 1987.
- [7] D. Chu, "Phase digitizing sharpens timing measurements," *IEEE Spectrum*, pp. 28-32, July 1988.
- [8] D. W. Allan, "Statistics of atomic frequency standards," *Proc. IEEE*, vol. 54, pp. 221-230, 1966.
- [9] P. Kartaschoff, *Frequency and Time*. London, England: Academic, 1978.
- [10] L. S. Cutler and C. L. Searle, "Some aspects of the theory and measurement of frequency fluctuations in frequency standards," *Proc. IEEE*, vol. 54, pp. 136-154, 1966.
- [11] M. Ohtsu, H. Fukada, T. Tako, and H. Tsuchida, "Estimation of the ultimate frequency stability of semiconductor lasers," *Japan. J. Appl. Phys.*, vol. 22, pp. 1157-1166, 1983.
- [12] K. Kuboki and M. Ohtsu, "A synthesized method to improve coherence in semiconductor lasers by electrical feedback," *IEEE J. Quantum Electron.*, vol. 25, pp. 2084-2090, 1989.

## IMPROVED ALLAN VARIANCE REAL-TIME PROCESSING SYSTEM TO MEASURE FREQUENCY TRACKING ERROR OF HETERODYNE OPTICAL PHASE-LOCKED LOOPS

*Indexing terms: Optical communications, Phase-locked loops*

The performance of an Allan variance measuring system was drastically improved by employing time interval analysis incorporating a beat frequency method. It was used to evaluate the performance of a heterodyne optical phase-locked loop with a very low optical frequency tracking error of 0.4 mHz at the integration time of 70 s. Advantages of the system are precise measurement for highly stable frequency sources with good reproducibility and simple structure.

Allan variance is a popular and important measure of the frequency stability of frequency sources.<sup>1,2</sup> It can also be used to evaluate the performance of phase-locked loops in the time domain.<sup>3</sup> To measure the stability of the optical frequency of stabilised semiconductor laser diodes (LD) and the frequency offset-locked heterodyne signal between two LDs, we have proposed and demonstrated an Allan variance real-time processing system (ARPS),<sup>4</sup> which employed the direct frequency counting method. In this system, the frequency of the source under measurement is down-converted to a countable frequency of the ARPS by a photo-diode and/or a double balanced mixer (DBM) or frequency dividers. The performance of the ARPS was high enough to measure the frequency stabilities of LDs under stabilised and free-running conditions. Its resolution was limited by one count ambiguity during a sampling period, which means that the ARPS cannot resolve the frequency fluctuations smaller than 1 Hz in a sampling period. To overcome this restriction, we have developed a novel ARPS employing the time interval analysis method. The optical frequency tracking performance of a heterodyne optical phase-locked loop with the phase error of 0.14 rad could be successfully evaluated by this novel system.

Fig. 1 shows the new ARPS. The frequency under test  $\nu_0$  is down-converted to a lower frequency so that the final beat frequency  $\nu_B \ll \nu_{TB}$ , where  $\nu_{TB}$  is the frequency of the time

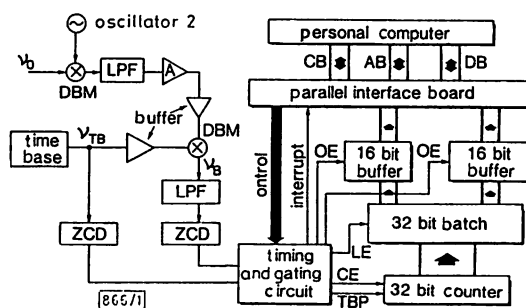


Fig. 1 Novel Allan variance real-time processing system

DBM: double balanced mixer  
 LPF: low pass filter  
 ZCD: zero crossing detector  
 TBP: pulse generated by time base signal  
 CE: count enable  
 LE: latch enable  
 OE: output enable  
 CB: control bus  
 AB: address bus  
 DB: data bus

base. Then the sinusoidal signals with the frequencies of  $\nu_{TB}$  and  $\nu_B$  are converted to TTL level digital signals by zero crossing detectors (ZCD), which are high speed voltage comparators. The number of pulses generated by the time base signal is continuously counted by a 32 bit counter, which consisted of four 8-bit TTL counters. Each digital signal corresponding to  $\nu_B$  generates two timing pulses at the same time, i.e., one is the interrupt signal to the personal computer and the other is the latch enable signal to the 32-bit data latch. From these timing signal, the 32-bit data latch latches the value of the 32-bit non-stop counter, and the computer reads the latched value through two 16-bit data buffers and a parallel interface board as soon as it receives the interrupt signal. By this operation, the computer can collect the number of pulses corresponding to the frequency of the time base during each period of  $\nu_B$  without any dead time for measurement. The integration time,  $\tau$ , can be determined by  $m/\nu_B$ , where  $m$  is a positive integer selected by the software program. The minimum measurable integration time is  $1/\nu_B$ . The maximum distinguishable counting value is  $2^{32}$  because the value of the counter is zero when the number of counters reaches  $2^{32}$ . The condition of  $2^{32}/(\tau\nu_{TB}) > 1$  is therefore required. Timing and gating circuits, the counter, the data latch and the data buffer were constructed using commercial TTL logic ICs. The maximum operating frequency of the system was about 30 MHz. The total required sample number  $N$  for each  $\tau$  to be measured can be selected using software, and the Allan variance  $\sigma_y^2(\tau)$  can be calculated using the collected data and the equation

$$\sigma_y^2(\tau) = \left(\frac{\nu_B}{\nu_0}\right)^2 \left(\frac{1}{\tau\nu_{TB}}\right)^2 \left[ \frac{1}{N-1} \sum_{k=1}^{N-1} \frac{(\nu_{k+1} - \nu_k)^2}{2} \right] \quad (1)$$

where  $\nu_k$  is the collected data for the  $k$ th sampling period. Frequency stabilities of the oscillators 1 and 2 used for the time base and the frequency down conversion of  $\nu_0$  have to be higher than that of the device under test. If we ignore the effects on the measurement of instabilities in the oscillators 1 and 2, the measurement limit is determined by one count ambiguity of the time base signal during a sampling period and is given by

$$\sigma_{y \min}^2(\tau) = \left(\frac{\nu_B}{\nu_0}\right)^2 \left(\frac{1}{\tau\nu_{TB}}\right)^2 \quad (2)$$

Considering that the measurement limit of the previous ARPS was given by  $(1/\tau\nu_0)^2$ ,<sup>4</sup> the measurement limit of the new ARPS is improved by a factor of  $(\nu_{TB}/\nu_B)^2$ . The Allan variance of a higher stable frequency source can be measured by increasing this factor.

Precise frequency tracking between two LDs could be achieved by a heterodyne optical phase-locked loop (OPLL),<sup>5</sup> on which experiments have been carried out using two confocal Fabry-Perot cavity coupled LDs with spectral linewidths less than 10 kHz and wavelengths of 0.83  $\mu\text{m}$ . The optical frequency tracking error of the heterodyne OPLL was measured by the new ARPS. A measured result is shown by the closed circles (B) in Fig. 2, where  $\nu_0$  was the optical frequency of the LDs used in the OPLL experiment. The broken curve A and the solid line C in Fig. 2 are the theoretical measurement limits for the previous ARPS and the new ARPS, respectively. In this measurement,  $\nu_{TB}$  and  $\nu_B$  were 5 MHz and 1 kHz, respectively. The line C was determined with these values and eqn. 2. From the measurements we find that the minimum optical frequency tracking error was 0.4 mHz at  $\tau = 70$  s, which is the lowest value among the published data. Such a stable phase-locked laser heterodyne signal could not be evaluated in the time domain with the previous ARPS as can be seen by comparing the experimental result B with the curve A in Fig. 2. To confirm the reproducibility of the measurement, the Allan variance of a signal was repeatedly measured more than 10 times, and the results showed very good reproducibility.

In summary, a novel Allan variance real-time processing system with high performance and simple structure was made with commercial TTL logic ICs, a popular 16-bit personal computer and some analogue circuits. This system could be

applied to evaluate a heterodyne optical phase-locked loop with a very low optical frequency tracking error. This system

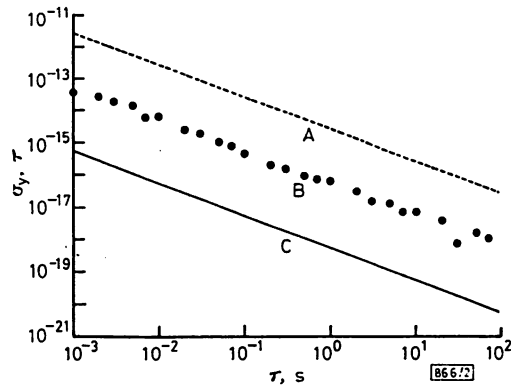


Fig. 2 Square root of Allan variance against integration time

- A: measurement limit of the previous ARPS employing the direct frequency counting method
- B: measured results of a stably phase-locked laser heterodyne signal to show an example
- C: measurement limit of the new ARPS when  $\nu_B = 1$  kHz and  $\nu_{TB} = 5$  MHz

can also be applied to measure the frequency stability of a highly stable microwave oscillator.

The authors thank Mr. Budi Pardono of the Indonesian Institute of Science for technical assistance and also thank Dr. K. Kuboki of Hitachi, Ltd, and Dr. M. Hashimoto of Sony, Ltd., for their fruitful discussions on the design of this new system.

C.-H. SHIN  
M. OHTSU

26th July 1990

Graduate School at Nagatsuta  
Tokyo Institute of Technology  
4259 Nagatsuta, Midori-ku  
Yokohama 227, Japan

#### References

- 1 ALLAN, D. W.: 'Statistics of atomic frequency standards', *Proc. IEEE*, 1966, 54, pp. 221-230
- 2 BARNES, J. A., CHI, A. R., CUTLER, L. S., HEALEY, D. J., LEESON, D. B., MCGUINIGAL, T. E., MULLEN, JR., J. A., SMITH, W. L., SYDNOR, R. L., VESSOT, R. F. C., and WINKLER, G. M. R.: 'Characterization of frequency stability', *IEEE Trans.*, 1971, IM-20, pp. 105-120
- 3 LINDSEY, W. C., and CHIE, C. M.: 'Performance measures for phase-locked loops—A tutorial', *IEEE Trans.*, 1982, COM-30, pp. 2224-2227
- 4 KUBOKI, K., and OHTSU, M.: 'An Allan variance real-time processing system for frequency stability measurements of semiconductor lasers', *IEEE Trans.*, 1990, IM-39, (8), in press.
- 5 SHIN, C.-H., and OHTSU, M.: 'Heterodyne optical phase-locked loop by confocal Fabry-Perot cavity coupled AlGaAs lasers', *IEEE Photon. Technol. Lett.*, 1990, 2, pp. 297-300



## A Semiconductor Laser as a Stable Phase Conjugate Mirror for Linewidth Reduction of Another Semiconductor Laser

Motoichi OHTSU, Isao KOSHIISHI and Yasuaki TERAMACHI<sup>†</sup>

Graduate School at Nagatsuta, Tokyo Institute of Technology,  
 4259 Nagatsuta, Midori-ku, Yokohama, Kanagawa 227

<sup>†</sup>Department of Information Engineering, University of Industrial Technology,  
 1960 Aihara, Sagamihara, Kanagawa 229

(Received August 27, 1990; accepted for publication October 11, 1990)

An AlGaAs laser was used as a phase conjugate mirror. Reflectivities as high as  $10^3$  and bandwidth as wide as 1.9 GHz were observed. The linewidth of a second AlGaAs laser was reduced to 1/5 times that of its free-running value by optical feedback of the phase conjugate wave generated by the first laser. The reduced linewidth was independent of the separation between the two lasers, and was maintained in a stable manner for over two hours.

**KEYWORDS:** AlGaAs laser, phase conjugate wave, four-wave mixing, linewidth reduction, optical feedback

Linewidth reductions of semiconductor lasers (SL's) have been carried out by electrical and optical feedback to meet requirements for various applications. By negative electrical feedback, a linewidth of 560 Hz has been obtained by using a reproducible and optimal design for a stable feedback circuit.<sup>1)</sup> For the optical feedback, a diffraction grating and a Fabry-Perot interferometer were used as an external reflector to reduce the linewidth to several tens of kHz<sup>2-4)</sup> Although the optical feedback system structures are simple, they have the problem of instability induced by the phase change of the light fed back from the reflector. In this connection, stable optical feedback is expected by utilizing a phase conjugate wave (PCW) since it does not require optical path length control because of the self-aligning nature of a phase conjugate mirror (PCM). Although this type of feedback has been demonstrated by using a BaTiO<sub>3</sub> as a PCM, jumps between the external cavity modes were observed, and furthermore, the build-up time of the PCW was too long for this application due to the slow response time of the BaTiO<sub>3</sub>.<sup>5)</sup>

The SL is an efficient device to generate a PCW<sup>6)</sup> by four-wave mixing (FWM)<sup>7-9)</sup> because of its large third-order nonlinear susceptibility  $\chi^{(3)}$ , fast response time, and a high laser power density in the active waveguide which is used as the pump power.<sup>6)</sup> In this letter, as an active application utilizing the above-mentioned property of the SL as a PCM, stable linewidth reduction of a SL is reported for the first time by the optical feedback of PCW generated in another SL.

Two 833 nm wavelength AlGaAs SL's (Hitachi, HL8312E) were used without any AR coatings, whose heat sink temperatures were controlled at 25°C to within 1 mK fluctuations. The inset of Fig. 1 shows the experimental setup used to measure the property of nearly degenerate FWM process in a SL. Part of the laser beam was slightly frequency-shifted ( $\delta\nu=80$  MHz) by an acousto-optic modulator, and was used as a probe beam by injection into the SL. The frequency of the incident probe beam is, therefore,  $\nu_0+\delta\nu$ , where  $\nu_0$  is the frequency emitted from the SL. By this injection, the PCW

of the frequency  $\nu_0-\delta\nu$  generated from the SL was observed by a scanning Fabry-Perot interferometer (FP in this figure). The main part of this figure shows the dependence of the reflectivity of the PCM (the ratio between the PCW power  $P_c$  and the probe power  $P_{in}$  irradiated to the SL) on the normalized bias level  $I/I_{th}-1$  ( $I$  and  $I_{th}$  are the injection current and its threshold value, respectively). This figure shows that the reflectivity decreased with increasing  $P_{in}$ , which agreed with the results presented by Fig. 3(b) of ref. 6. Although it may be expected that the reflectivity increased with increasing

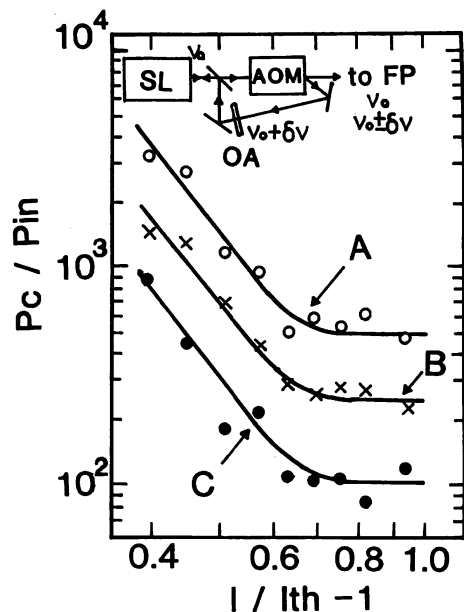


Fig. 1. A relation between the reflectivity of the PCM and the normalized bias level. The inset represents the experimental setup. SL: semiconductor laser. FP: scanning Fabry-Perot interferometer. OA: optical attenuator used to keep the probe power at a constant value when the injection current was varied for the measurement.  $\nu_0$ : laser frequency. The probe powers  $P_{in}$  irradiated to the SL were -41 dBm (A), -36 dBm (B), and -31 dBm (C). An acousto-optic modulator (AOM) was used to fix the detuning between the pump and probe beams to  $\delta\nu=80$  MHz.

$I/I_{th}-1$  because the pump power is proportional to  $I/I_{th}-1$ , it is seen from this figure that it decreased with increasing  $I/I_{th}-1$ . This decrease was attributed to the decreases in the corrugation depth of the index grating. The origin of this grating generation can be interpreted as follows: the carrier density  $N$  cannot reach its threshold value  $N_{th}$  even though  $I \geq I_{th}$  because of the contribution of the spontaneous emission to the laser oscillation.<sup>10</sup> By increasing the value of  $I/I_{th}$ ,  $N_{th}-N$  gradually decreases, which means that the corrugation depth of the grating decreases by increasing the bias level. It can be interpreted that the reflectivity decreased by increasing  $I/I_{th}-1$  because the contribution from the decrease of the corrugation depth was larger than that from the increase of the pump power. Although the decrease in the reflectivity has been briefly pointed out in ref. 7, it was, to the authors' knowledge, quantitatively demonstrated for the first time by the present work. In the range of  $I/I_{th}-1 > 0.7$  in this figure, the reflectivity took a constant value, whose cause may also be a large contribution from the decrease of the corrugation depth. However, no accurate theoretical model to explain the dependence of the reflectivity on the bias level has appeared. Development of this theoretical model remains a problem to be solved.

Figure 2(a) shows an experimental setup to measure the dependence of the PCM reflectivity on the detuning between the probe and pump beams. The output from a SL1 was used as a probe beam and was injected colinearly into the active waveguide of a SL2 (a PCM device). Figure 2(b) shows the measured results when the probe powers  $P_{in}$  irradiated to the SL2 were  $-32$  and  $-25$  dBm, and  $I/I_{th}-1=0.53$  for the SL2. The curves A and B are the Lorentzian which were least-square-fitted to the measured values. Their full widths at half maximum

(FWHM) were 390 MHz and 1.9 GHz, respectively. The FWHM increased with increasing  $P_{in}$ , which agreed with the theoretical prediction by Fig. 4 of ref. 11. The PCW powers at the peak of these curves were estimated as 2.6 and  $-2.9$  dBm, respectively, which were sufficiently high for application to the optical feedback. For reducing the phase fluctuations and linewidth of the SL1 by optical feedback of the PCW, the response time of the PCM should be sufficiently fast in order to follow temporal variations of the fluctuating phase. Since the bandwidth of the PCM (as wide as 1.9 GHz in Fig. 2(b)) was much wider than the free-running linewidth of the SL1, it can be expected that the linewidth of the SL1 be reduced. It should be noted that the essential property of the PCM required for the linewidth reduction is the sufficiently broad bandwidth.

Next, the linewidth reduction of the SL was carried out by utilizing the PCW for the optical feedback method. The experimental setup for the optical feedback was almost the same as that shown by Fig. 2(a). However, the optical isolator was removed, and the optical axis of the probe beam was aligned slightly off-axis to that of the pump beam. A high finesse ( $=20,000$ ) scanning Fabry-Perot interferometer 1 (FP1) was used to observe the field spectral profile of the SL1. Its free spectral range was 6 GHz. A scanning Fabry-Perot interferometer 2 (FP2) was used to monitor the detuning between the pump and probe beams.

The experimental condition was optimized based on the following criteria: (1) The bias level of the SL2 was adjusted low enough to get a high efficiency of the PCW generation. (2) The value of  $P_{in}$  was adjusted low enough to avoid the injection locking of the SL2 to the probe beam. (3) A lens L with a long focal length (46 mm) was placed in front of the SL2 so that the probe beam was focused onto the SL2 and the pump beam emitted from the SL2 was well diverged. Two apertures ( $A_1$  and  $A_2$ ) were placed to block most of this divergent beam. As a result, the emitted pump power irradiated to the SL1 was reduced to  $-45$  dBm.

Numerical values of the optimized experimental parameters were:  $I/I_{th}-1=0.93$  and  $0.53$  for the SL1 and SL2, respectively. The probe power  $P_{in}$  incident to the SL2 was  $-20$  dBm. The off-axis angle was  $5.2 \times 10^{-3}$  degrees. The PCW power reaching the SL1 was  $-18$  dBm, which was estimated by extrapolating the results of Fig. 1 to  $P_{in} = -20$  dBm and by considering the losses of the optical elements between the two SL's. Measured field spectral profiles of the SL1 are shown by Fig. 3(a), where the solid and broken curves are for the optical feedback and the free-running conditions, respectively. By the optical feedback, the FWHM of the field spectrum  $\Delta\nu$  was reduced to 1/5 times that of the free-running laser.

It was confirmed by the four measurements listed below that this linewidth reduction was not due to a conventional optical feedback from an external reflector: (1) To confirm the independence of the reduced linewidth on the separation between the two lasers, the separation was varied by a piezoelectric transducer (PZT) on which a beam splitter 2 (BS2) in Fig. 2(a) was mounted. Figure

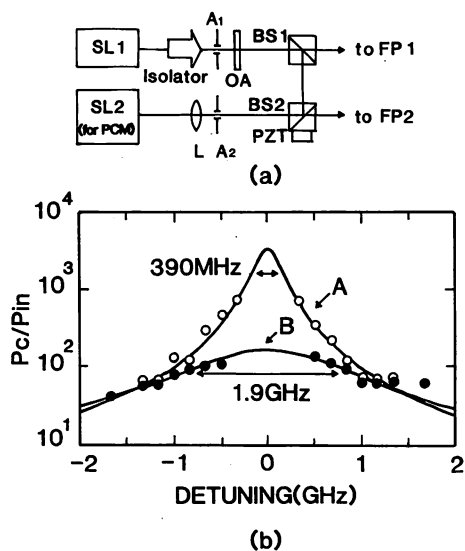


Fig. 2. (a) An experimental setup to measure the relation between the reflectivity of the PCM and the detuning between the pump and probe beams. OA: optical attenuator. L: lens with a focal length of 46 mm.  $A_1$  and  $A_2$ : apertures. (b) Measured results. Open and closed circles are for  $P_{in} = -32$  and  $-25$  dBm, respectively. The curves A and B are the Lorentzian, which were least-square-fitted to the experimental results.

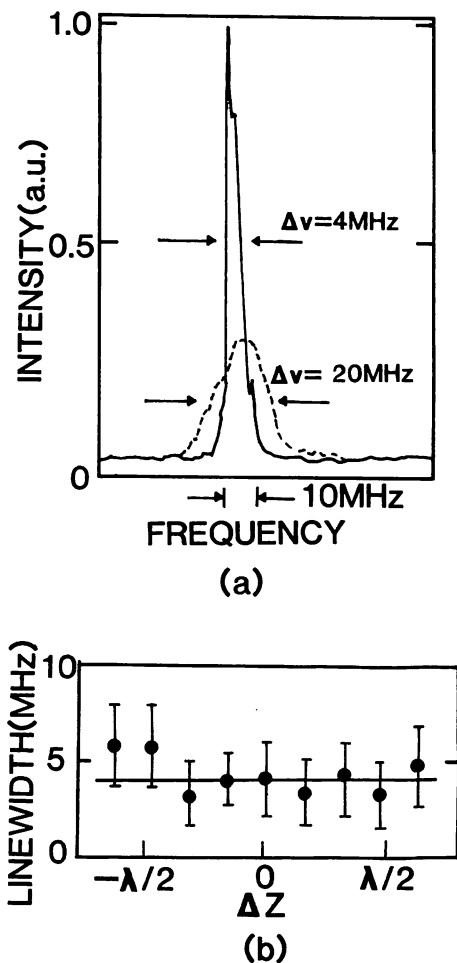


Fig. 3. (a) The field spectral profile measured by a scanning Fabry-Perot interferometer 1 (FP1). The solid and broken curves represent the results under optical feedback and free-running conditions, respectively. (b) A relation between the FWHM of the SL1 and  $\Delta z$ , where  $\Delta z$  is the variation of separation between two SL's.  $\lambda$ : laser wavelength.

3(b) shows the results and confirms that the reduced linewidth was independent of the variation  $\Delta z$  of the separation. (2) The measurements using the FP1 showed that no additional external cavity modes of the SL1 appeared within the measurement dynamic range of 21 dB. Furthermore, no instabilities such as mode jump between the external cavity modes were observed. (3) The reduced linewidth was maintained in a stable manner for over two hours without any servocontrol loops. (4) When the SL2 was replaced by an Al-coated mirror to inject the same amount of the light power into the SL1 as that by the experimental conditions given above, the linewidth could

not be accurately measured by the FP1 because the SL1 exhibited oscillation instabilities due to conventional optical feedback. To maintain the stable linewidth reduction for over two hours, the frequency difference between the SL1 and SL2 under free-running conditions must be less than the bandwidth of the PCM given by Fig. 2(b). However, since the temperature fluctuations of the two SL's were maintained within 1 mK, it was confirmed that the frequency difference should be kept lower than 60 MHz. This value satisfies the requirement presented above.

It was also experimentally confirmed that injection locking did not occur when the off-axis angle was as large as  $5.2 \times 10^{-3}$  degrees and the injection power from the SL2 was lower than  $-25$  dBm. It could be said that the present system using a SL as the PCM is more advantageous than that using photo-refractive materials or atomic vapors because the two SL's may be integrated together with passive channel waveguides on a common semiconductor substrate.

In conclusion, it was demonstrated that a SL could be used as an effective and stable PCM. The linewidth of one SL was reduced to 1/5 by the optical feedback of the PCW generated from another SL. The reduced linewidth was independent of the separation between the two SL's, and was maintained in a stable manner for over two hours.

The authors are indebted to K. Nemoto of the Central Research Institute of Electric Power Industry for his valuable comments. The assistance of and discussions with K. Nakagawa, C.-H. Shin, and H. Suzuki of the authors' research group are gratefully acknowledged.

## References

- 1) M. Ohtsu, M. Murata and M. Kourogi: IEEE J. Quantum Electron. **26** (1990) 231.
- 2) N. A. Olsson and J. P. van der Ziel: IEEE J. Lightwave Technol. **LT-5** (1987) 510.
- 3) R. Wyatt and W. J. Devlin: Electron. Lett. **19** (1983) 110.
- 4) B. Dahmani, L. Hollberg and R. Drullinger: Opt. Lett. **12** (1987) 876.
- 5) K. Vahala, K. Kyuma, A. Yariv, S. Kwong, M. Cronin-Golomb and K. Y. Lau: Appl. Phys. Lett. **49** (1986) 1563.
- 6) H. Nakajima and R. Frey: IEEE J. Quantum Electron. **QE-22** (1986) 1349.
- 7) N. Zhang, Y. Nitta, H. Ito and H. Inaba: Proc. XVI-th Int. Quantum Electronics Conference, 1988, Tokyo (IEE of Japan, Tokyo, 1988) p. 276.
- 8) M. Lecente, J. G. Fujimoto and G. M. Carter: Appl. Phys. Lett. **53** (1988) 1897.
- 9) K. Inoue, T. Mukai and T. Saitoh: Appl. Phys. Lett. **51** (1987) 1051.
- 10) Y. Suematsu: Oyo Buturi **50** (1981) 748 [in Japanese].
- 11) G. P. Agrawal: J. Opt. Soc. Am. B **5** (1987) 147.

# Stable semiconductor laser with a 7-Hz linewidth by an optical–electrical double-feedback technique

Chul-Ho Shin and Motoichi Ohtsu

Graduate School at Nagatsuta, Tokyo Institute of Technology, 4259 Nagatsuta, Midori-ku, Yokohama, 227 Japan

Received July 6, 1990; accepted October 2, 1990

A semiconductor laser with a linewidth of 7 Hz locking to a supercavity was achieved by using an optical–electrical double-feedback technique. The emitted power concentration within the stabilized field spectrum was 81%. The minimum value of the square root of the Allan variance for the frequency stability was  $2.4 \times 10^{-14}$  at the integration time of 70 msec.

Semiconductor lasers with ultranarrow linewidths are attractive and indispensable for applications to ultra-high-resolution laser spectroscopy, quantum optics, and the semiconductor-laser-based frequency chain<sup>1</sup> to measure Rydberg's constant precisely and as a master laser for injection locking and the frequency-offset-locked optical frequency sweep generator. The confocal Fabry–Perot cavity-coupled semiconductor laser diode (CFP-LD) shows wideband frequency noise suppression characteristics with a narrow linewidth of less than 10 kHz.<sup>2–5</sup> The FM characteristics of the CFP-LD have been reported.<sup>6</sup> We have carried out the experiment on the heterodyne optical phase-locked loop using two AlGaAs CFP-LD's, which showed a phase error of  $8.1^\circ$ , a frequency tracking error between the two lasers of 0.4 mHz at an integration time of 70 sec, and a noise bandwidth of approximately 1 MHz.<sup>7</sup> We also carried out the experiment on the homodyne optical phase-locked loop using these lasers and had a phase error of  $2.6^\circ$  and a noise bandwidth of 1.3 MHz.<sup>8</sup> From the results of Refs. 7 and 8, it could be expected that the linewidth of the CFP-LD can be narrowed to a subhertz level if its frequency is locked to a stable reference with a control bandwidth of the order of 1 MHz.

In this connection, we tried to frequency stabilize a semiconductor laser with the optical–electrical double-feedback method by simultaneously using the optical feedback from an external cavity (CFP-LD) and the electrical negative feedback from the reflection mode of a high-finesse stable optical cavity. The laser diode (LD) used in this experiment was a commercially available channelled-substrate-planar-type AlGaAs laser (Hitachi HL8314E) with a wavelength of 830 nm. The linewidth of this laser was 15 MHz at the bias level of 1.5 times its threshold value, which was measured by heterodyning with a 10-kHz-linewidth CFP-LD. It was mounted on the temperature-controlled copper block, whose temperature fluctuation was suppressed to within 1 mK. Before we used the electrical negative feedback scheme, this laser was optically stabilized with an optical feedback scheme similar to that of Dahmani *et al.*<sup>2</sup> (Fig. 1). The free spectral range and the finesse of the external CFP cavity were 1.5 GHz and 75, respectively. The wide control bandwidth of

the order of 1 MHz could be secured by using two control routes, the external cavity length and the injection current for lower-frequency ( $<5$  kHz) and higher-frequency components, respectively. The frequency tuning coefficients of the CFP-LD were 31 MHz/mA and 80 MHz/V for the injection current control and the external cavity length control, respectively.<sup>6,7</sup>

Figure 2 shows the FM noise suppression ratio (NSR) of the CFP-LD measured by using the reflection mode of another CFP cavity, which is not indicated in the figure. The NSR was  $-39$  dB at a Fourier frequency range of less than 5 MHz. Since the linewidth reduction ratio is approximately equal to the NSR,<sup>5</sup> the reduced linewidth with the optical feedback was estimated to be 1.9 kHz. However, the measured linewidth of the CFP-LD by heterodyning with another CFP-LD was  $\sim 10$  kHz. The difference between these values stems mainly from the effects of acoustics, mechanical vibrations, and temperature variations, by which the length of the CFP cavity and the optical feedback phase are changed and/or affected. Therefore, to achieve a narrow linewidth, it is necessary to suppress FM noise at a Fourier frequency of less than  $\sim 1$  MHz in a stable manner with a high NSR. To this end, the electrical negative feedback technique<sup>9</sup> is a good solution, so as to lock the oscillating frequency of the LD to a stable frequency reference.

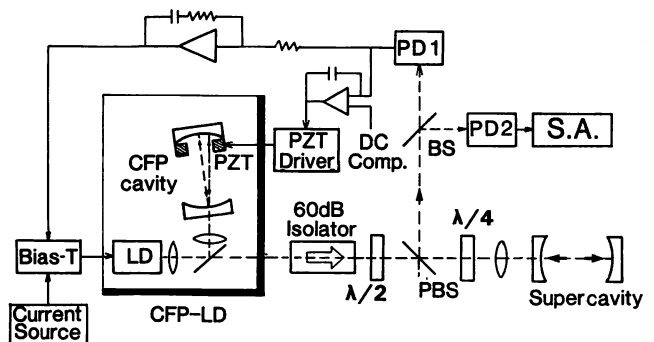


Fig. 1. Experimental setup. PBS, polarization beam splitter; BS, beam splitter; DC Comp., dc compensation; PZT, piezoelectric transducer; S.A., spectrum analyzer.

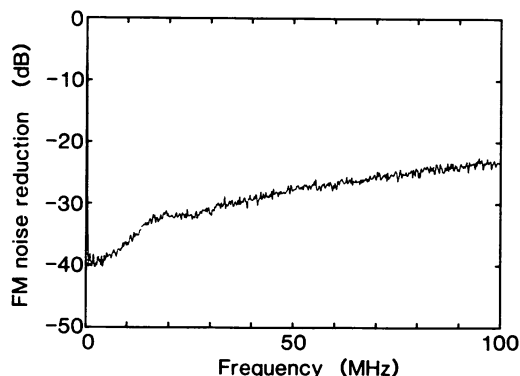


Fig. 2. Power spectral density of frequency noise suppression ratio of the CFP-LD that was normalized to that of the free-running laser.

The most important factor for FM noise suppression in achieving a narrow linewidth is the stable frequency reference. As the frequency reference for this purpose, we employed a hermetically sealed and temperature-controlled commercial supercavity (Newport SR-140) with a finesse of  $\sim 34,500$  at  $0.83 \mu\text{m}$  and a free spectral range of 6 GHz; thus the half-linewidth of the cavity is  $\Delta\nu_c = 174 \text{ kHz}$ . Figure 1 shows the experimental setup for linewidth narrowing of the CFP-LD by the electrical negative feedback scheme. The FM noise of the CFP-LD was demodulated by the reflection mode<sup>9</sup> of the supercavity, and then the demodulated signal was negatively fed back to the CFP-LD through the injection current and the CFP cavity length controls. For this control, an optical power  $P_C$  of 0.67 mW detected by photodiode PD1 was used. The optical power for noise measurement  $P_{\text{mon}}$  was 0.62 mW, which was detected by photodiode PD2. When the frequency of the CFP-LD is locked to the center of the slope of the reflection mode resonance spectral profile, the detection gain of the suppressed FM noise is  $K_{\text{PD}} = \eta_C P_{\text{mon}} R r / \Delta\nu_c$  (V/Hz), where  $\eta_C$  is the efficiency of the reflection mode (in our case, 0.64),  $R$  (A/W) is the responsivity of the photodiode, and  $r$  is the load resistor of the photodiode. This relationship was used to determine the measured FM noise level. The values of  $R$  and  $r$  of photodiode PD2 were 0.58 A/W and  $50 \Omega$ , respectively. The optical isolation ratio between the CFP-LD and the supercavity was larger than 80 dB. If optical feedback power from the supercavity is high, the mode competition between the CFP cavity and the supercavity modes by double optical feedback may occur, and output light from the LD may become unstable by a mode-hopping phenomenon. Therefore, rigid optical isolation and optical axis alignment are required for using the electrical negative feedback scheme to avoid influence by optical feedback from the supercavity.

In comparing curve B with curve A in Fig. 3(a), the FM noise power spectral density  $S$  of the CFP-LD is suppressed by  $\sim 50 \text{ dB}$  by the electrical negative feedback scheme, in which curve A was obtained by the lower gain and narrower bandwidth control. The data for the Fourier frequency  $f$  greater than a few kilohertz are, therefore, those for the uncontrolled CFP-LD. This means that the linewidth of the CFP-LD was

narrowed to the order of 100 mHz. The measured power spectral density of  $f$  greater than several tens of kilohertz in curve A shows approximately  $-24 \text{ dB/decade}$  mainly by the FM noise discrimination characteristics of the reflection mode of a Fabry-Perot interferometer, which is  $-20 \text{ dB/decade}$  for  $f \geq \Delta\nu_c/2$ . To confirm the FM noise suppression in the range of  $f < 100 \text{ Hz}$ , FM noise was measured by a fast-Fourier-transform spectrum analyzer as shown by Fig. 3(b). From Fig. 3 it can be seen that FM noise was suppressed to a level of less than  $1/\pi$  ( $\text{Hz}^2/\text{Hz}$ ) in the range of  $10 \text{ Hz} \leq f \leq 1.5 \text{ MHz}$ , except for the 50-Hz power supply line frequency and its higher harmonics. This noise level corresponds to the linewidth of the Lorentzian field power spectral profile of  $\Delta\nu_{\text{LD}} = 1 \text{ Hz}$  because  $\Delta\nu_{\text{LD}} = \pi S$ . The short-term frequency stability of the controlled laser was therefore considerably high. To confirm the frequency stability in the time domain, the Allan variance  $\sigma_y^2(\tau)$  was calculated by using the data of Fig. 3 and the equation  $\sigma_y^2(\tau) = 2 \int_0^\infty df S(f) \sin^4(\pi f \tau) / (\pi f \tau)^2$ ,<sup>10</sup> where  $\tau$  is the integration time. The calculated result is shown in Fig. 4, in which the measured results for the free-running laser and the CFP-LD are also shown. The minimum of  $\sigma_y(\tau)$  was  $2.4 \times 10^{-14}$  at  $\tau = 70 \text{ msec}$ , from which it can be confirmed that the short-term stability of the LD was drastically improved by the present scheme.

Power concentration in the field spectral profile of the stabilized CFP-LD within the control bandwidth

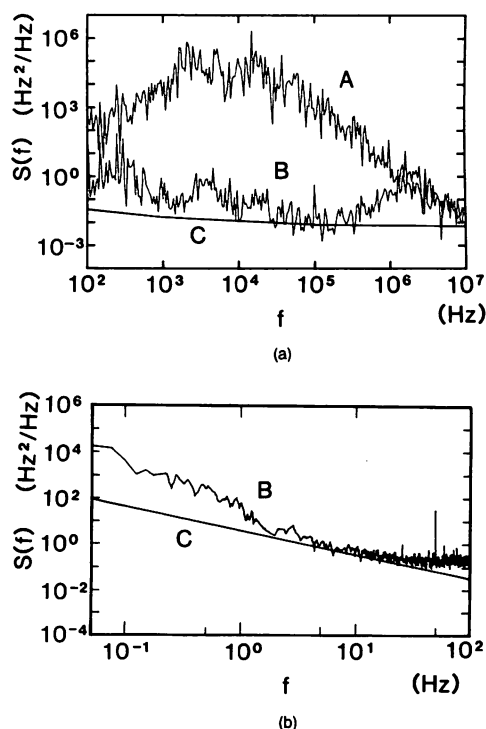


Fig. 3. Electrically controlled power spectral densities of FM noise for the CFP-LD. The field spectral linewidth of the noncontrolled CFP-LD was less than 10 kHz. Solid curves C indicate the FM noise detection limit imposed by the intensity-modulated noise level of the CFP-LD. (a) Results for a lower gain and narrower bandwidth (curve A) and a higher gain and wider bandwidth (curve B) controls measured by an rf spectrum analyzer. (b) Extension of curve B in (a) for a lower Fourier frequency range measured by a fast-Fourier-transform spectrum analyzer.

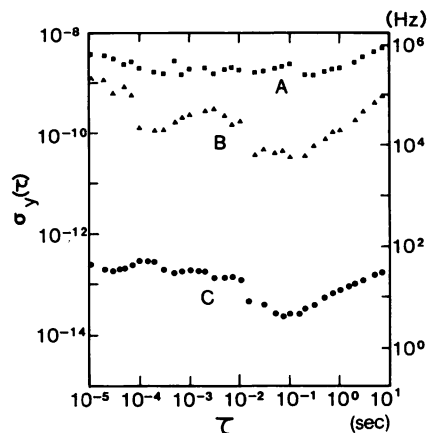


Fig. 4. Square root of the Allan variance. Curves A and B are the measured results for the free-running laser and the CFP-LD, respectively. Curve C is the calculated results for the CFP-LD electrically locked to a supercavity by using curves B of Figs. 3(a) and 3(b). The left scale of the y axis is normalized to the nominal optical frequency.

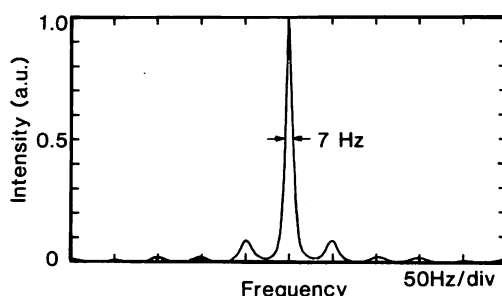


Fig. 5. Calculated field spectral profile of the stabilized CFP-LD, in which curves B of Figs. 3(a) and 3(b) were used.

was estimated. To this end, the total residual phase noise outside the bandwidth must be estimated, where it is convenient to use the relation of the total phase noise variance  $\Delta\phi_{\text{rms}}^2 = \int_{f_{\text{BW}}}^{\infty} [S(f)/f^2] df$  (in  $\text{rad}^2$ ). Here  $f_{\text{BW}}$  represents the Fourier frequency corresponding to the bandwidth to be considered. Introducing the concept of the power spectrum modulated by broadly distributed random phase noise, the power concentration within  $|\nu - \nu_0| \leq f_{\text{BW}}$  is then  $100|J_0(\beta)|^2$  (%), where  $\nu_0$  and  $\nu$  are the center frequency of the laser and the offset frequency from  $\nu_0$ , respectively, and the modulation index  $\beta = \sqrt{2}\Delta\phi_{\text{rms}}$ . In our case,  $\Delta\phi_{\text{rms}}^2$  was  $\sim 0.02 \text{ rad}^2$  with  $f_{\text{BW}} = 1.5 \text{ MHz}$ , i.e.,  $\beta = 0.2$ , thus the concentrated power within  $|\nu - \nu_0| \leq f_{\text{BW}}$  is estimated to be 98%. However, the concentrated power is further frequency modulated by the 50-Hz power supply line frequency and its harmonic frequencies, as can be seen in Fig. 3. The modulation index was  $\sim 0.6$ , which was estimated from the calculated field spectral shape of the stabilized CFP-LD, as shown in Fig. 5. The calculation procedure of the field spectral profile from the measured FM noise has been described in detail.<sup>9</sup> The linewidth of the calculated field spectral profile was 7 Hz with a resolution bandwidth of 2 Hz,

which is to our knowledge the lowest published value. The modulation index of 0.6 means that the power concentration was 83% of the concentrated power within the controlled bandwidth. Therefore 81% of the total power emitted from the laser was actually concentrated on the controlled field spectrum.

To find the limiting factor of the FM noise suppression, intensity-modulated noise of the LD was measured as shown by curves C in Figs. 3(a) and 3(b). In comparing these curves with curves B, the suppressed FM noise level almost reached the level limited by the intensity-modulated noise. The shot-noise-limited detection of the FM noise power spectral density by the optical power of 0.62 mW was  $6.6 \times 10^{-5} \text{ Hz}^2/\text{Hz}$ , which can be calculated by the equation expressing the shot-noise-limited linewidth for the present scheme,  $\Delta\nu_{\text{sh}} = 2\pi e\Delta\nu_C^2/(\eta C^2 P_{\text{mon}} R)$  (Hz). The major problem to be solved is, therefore, the intensity-modulated noise of semiconductor lasers, which is widely distributed in the frequency range up to the relaxation oscillation frequency of the laser device itself. To solve the problem and achieve further reduction of FM noise, a balanced detector consisting of two photodiodes<sup>11</sup> has to be employed in detecting FM noise-discriminated signals.

In summary, a commercially available AlGaAs laser was frequency stabilized to the power spectral density of FM noise lower than  $1/\pi$  ( $\text{Hz}^2/\text{Hz}$ ) in the Fourier frequency range from 10 Hz to 1.5 MHz by employing an optical-electrical double-feedback method. The minimum of  $\sigma_y(\tau)$  was  $2.4 \times 10^{-14}$  at  $\tau = 70$  msec. The linewidth was estimated to be 7 Hz.

## References

1. H. R. Telle, D. Meschede, and T. W. Hänsch, *Opt. Lett.* **15**, 532 (1990).
2. B. Dahmani, L. Hollberg, and R. Drullinger, *Opt. Lett.* **12**, 876 (1987).
3. Ph. Laurent, A. Clairon, and Ch. Breant, *IEEE J. Quantum Electron.* **25**, 1131 (1989).
4. H. Li and H. R. Telle, *IEEE J. Quantum Electron.* **25**, 257 (1989).
5. C. H. Shin, M. Tehsima, M. Ohtsu, T. Imai, J. Yoshida, and K. Nishide, in *Digest of Seventh Integrated Optics and Optical Fiber Communication Conference* (Institute of Electronics, Information and Communication Engineers, Tokyo, 1989), paper 21D4-5.
6. C. H. Shin, M. Tehsima, M. Ohtsu, T. Imai, J. Yoshida, and K. Nishide, *IEEE Photon. Technol. Lett.* **2**, 167 (1990).
7. C. H. Shin and M. Ohtsu, *IEEE Photon. Technol. Lett.* **2**, 297 (1990).
8. C. H. Shin and M. Ohtsu, in *Digest of Third Optoelectronics Conference* (Institute of Electronics, Information and Communication Engineers, Tokyo, 1990), paper 12C3-3.
9. M. Ohtsu, M. Murata, and M. Kourogi, *IEEE J. Quantum Electron.* **26**, 231 (1990).
10. J. A. Barnes, A. R. Chi, L. S. Cutler, D. J. Healey, D. B. Leeson, T. E. McGunigal, J. A. Mullen, Jr., W. L. Smith, R. F. C. Vessot, and M. R. Winkler, *IEEE Trans. Instrum. Meas.* **IM-20**, 105 (1971).
11. H. Y. Yuen and V. W. S. Chan, *Opt. Lett.* **8**, 177 (1983).

# Novel optical frequency discriminator for FM noise reduction of semiconductor lasers

Motonobu Kourogi and Motoichi Ohtsu

*Graduate School at Nagatsuta, Tokyo Institute of Technology, 4259 Nagatsuta, Midori-ku, Yokohama, 227, Japan*

Received 24 July 1990

A compact and highly-reliable optical frequency discriminator is proposed for the FM noise reduction of semiconductor lasers. This discriminator provides the error signal for locking laser frequency to the center of a resonant spectral profile of a Fabry-Perot interferometer (FPI) without any modulation techniques. The gain of this discriminator is 10 dB larger than that of other discriminators using the slope of a resonant profile of a FPI. The phase delay of the discriminator is only  $90^\circ$ . For the high-gain and fast electrical negative feedback loop, these properties are superior to those of the others. To demonstrate the feasibility of this discriminator, the spectral linewidth of a semiconductor laser was reduced from 6 MHz to 250 kHz.

## 1. Introduction

The development of highly-coherent semiconductor lasers is very important for several applications such as the resonator-type fiber gyroscope [1], the high-resolution laser spectroscopy, the optical pumping for atomic clocks [2,3], cooling of atoms [4], and coherent optical communication systems. For this purpose, by using optical feedback and electrical negative feedback techniques of refs. [5,6], and references cited therein, the line widths of semiconductor lasers were reduced to several kHz and sub-kHz, respectively.

When the slope of resonant profile of a Fabry-Perot interferometer (FPI) is used as an optical frequency discriminator (OFD) without any modulation techniques [6], there are, however, four problems to be solved. (i) The laser frequency cannot be locked just to the center of a resonant spectral profile of the FPI. (ii) The minimum FM noise reduction level is limited by the IM noise of the laser. (iii) The recovery range, which is defined by the automatic re-locking range after larger accidental frequency jumps, is very narrow. (iv) It is difficult to keep the laser frequency locking to the reference even when the laser frequency is modulated. In this letter, we propose a novel OFD to overcome these four problems. The operating principle is similar to the OFD, which has

been proposed by T.W. Hänsch et al. [7]. The present OFD has a simple structure, i.e. a FPI with an intra-cavity polarization rotor or wave plate, and provides the error signal for locking laser frequency to the center of a resonant spectral profile of the FPI. Three kinds of practical schemes for this OFD have also been demonstrated.

## 2. Principle of the proposed optical frequency discriminator

Fig. 1 shows a schematic explanation of the proposed OFD. Either of a traveling wave-type resonator (ring-resonator) and a standing wave-type resonator can be employed alternatively, as shown by (a) and (b) in fig. 1. These two kinds of setup are operated under the same principle. Available optical power for fig. 1 (a), which can be used to detect the FM noise discrimination signals, is higher than that for fig. 1 (b). When the ring-resonator is used, all incident power can be used to detect the error signals. On the other hand, when the standing wave-type resonator is used, a quarter of the incident laser power to the OFD is utilized to detect the error signals, because of the loss of the laser power at the non-polarized beam splitter (NPBS) installed in front of the resonator. This is only a difference between two

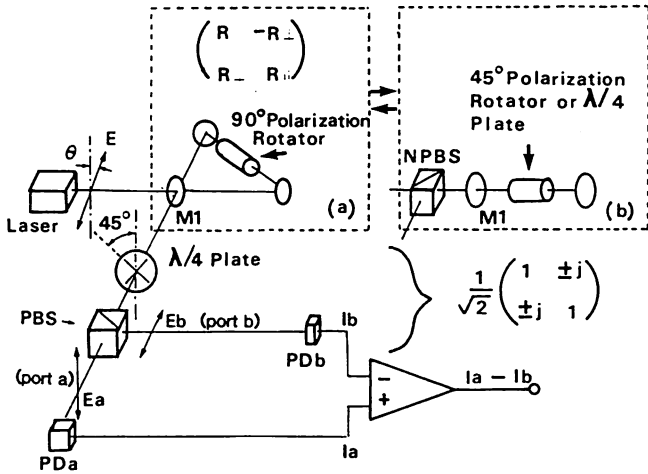


Fig. 1. Present optical frequency discriminator for FM noise reduction. (a) A traveling type resonator. (b) A standing wave type resonator.

setups. The advantages of the setup in fig. 1(b) are that it can be designed compactly, and the effect of the phase shift of the laser beam at the cavity mirrors can be ignored to design it.

To explain and analyze the operation of these OFD, let us consider mainly the setup illustrated in fig. 1(a). In this setup, linearly polarized light from a single mode laser is input onto the ring-resonator in which a 90° polarization rotator is installed. (In the resonator of fig. 1(b), a 45° polarization rotator or a λ/4 plate is used to achieve 90° polarization rotation for the round trip beams.) The output light of the ring-resonator is sent into the analyzer assembly consisting of a λ/4 plate and the polarization beam splitter (PBS). The axis of the λ/4 plate is rotated by 45° relative to the axis of the PBS output port a. The light intensities  $I_a$  and  $I_b$  at the two output ports of the PBS are monitored by the two photodetectors  $PD_a$  and  $PD_b$ . The electric field vector of the linearly polarized incident beam of the laser onto the ring-resonator has an angle  $\theta$  with the polarization axis of the PBS output port a. In order to calculate the amplitude of the output light of the PBS, we defined that the light is decomposed into the two orthogonal components parallel and perpendicular to the polarization axis of the PBS output port a. By using the Jones matrix similar to that employed in ref. [7], the field amplitudes of the reflected beam after passing through the λ/4 plate and PBS, can be expressed as

$$\begin{pmatrix} E_a \\ E_b \end{pmatrix} = \frac{1}{\sqrt{2}} \begin{pmatrix} 1 & \pm i \\ \pm i & 1 \end{pmatrix} \begin{pmatrix} R_{\parallel} & -R_{\perp} \\ R_{\perp} & R_{\parallel} \end{pmatrix} \begin{pmatrix} E \cos \theta \\ E \sin \theta \end{pmatrix}. \tag{1}$$

In the right hand side of this equation, the first matrix represents the λ/4 plate, the second one represents the ring-resonator in which a 90° polarization rotator is located, and the third one is the incident laser beam. In the second matrix,  $R_{\parallel}$  and  $R_{\perp}$  are the complex amplitude reflectivity of the electric field components which are parallel and perpendicular to the axis resonator, respectively.  $R_{\parallel}$  and  $R_{\perp}$  can be expressed as

$$R_{\parallel} = \sqrt{r - lt} \exp(i2\delta) / \{ \sqrt{r} [1 - l \exp(i2\delta)] \}, \tag{2a}$$

$$R_{\perp} = \sqrt{lt} \exp(i\delta) / \{ \sqrt{r} [1 - l \exp(i2\delta)] \}, \tag{2b}$$

where  $r$  and  $t$  are the power reflectivity and the transmittivity of the input mirror M1, respectively.  $l$  ( $=r\alpha$ ) is the round trip power attenuation in the resonator, which determines the cavity finesse  $F$  ( $=\pi\sqrt{l}/(1-l)$ ),  $\alpha$  is the power attenuation of the 90° polarization rotator located in the resonator.  $\delta$  is  $\pi\nu/\text{FSR}$ , and the free spectral range (FSR) is  $c/(2nL)$ , where  $L$  is a length of the ring-resonator,  $\nu$  is the laser frequency. The corresponding intensities at the two output ports are  $I_{a,b} = c\epsilon |E_{a,b}|^2/2$ , where  $\epsilon$  is the dielectric constant. By using this relation and eqs. (1), (2), the output signal from the differential amplifier yields

$$I_a - I_b = 2(r+l)\sqrt{lt} \sin \delta / \{ r [ (1-l)^2 + 4l \sin^2 \delta ] \} I, \tag{3}$$

where  $I$  ( $=c\epsilon |E|^2/2$ ) is the intensity of the incident laser beam. It should be noted that this expression is independent of  $\theta$  in the case when the Faraday rotator was used as a 90° polarization rotator. This independence is an advantage of the present OFD comparing with that of ref. [7], in which a Brewster plate or a linear polarizer is used inside the reference cavity to provide a signal similar to that of the proposed OFD. The  $I_a - I_b$  of eq. (3) is illustrated in fig. 2(a) as a function of  $\nu$ . The laser frequency is locked to the position represented by point P in this figure. This point is the center of a resonant spectral profile of the FPI, and the contribution of the laser IM noise to the frequency discrimination is suppressed by the differential amplifier. As shown in fig. 2(a), the re-



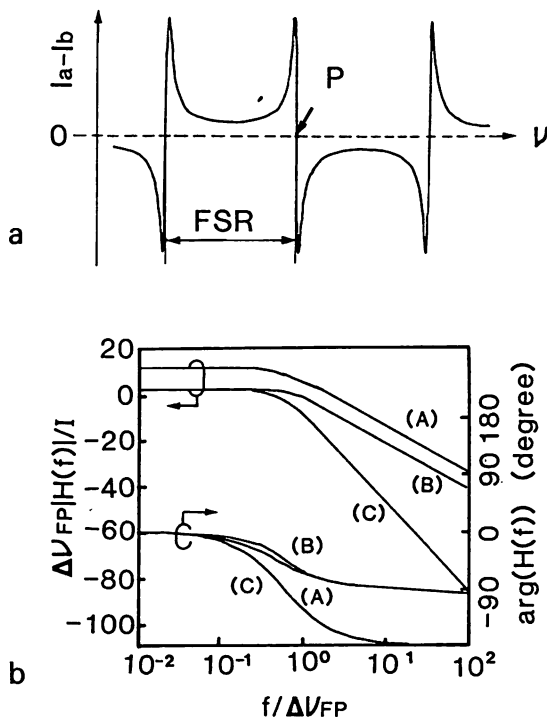


Fig. 2. Calculated results. (a) Resonant profile of the present discriminator. (b) Transfer functions of the present optical frequency discriminator (curve A), the reflection mode of a Fabry-Perot interferometer (curve B), and the transmitted mode of a Fabry-Perot interferometer (curve C).

covery range of the OFD is  $\pm 1 \times \text{FSR}$ , because it combines a couple of wings reaching to  $\pm 1 \times \text{FSR}$  from the point P.

The transfer function of an OFD using slopes of resonant profiles normalized with the intensity of the incident laser beam is calculated as

$$h(X(\nu), f) = [X^*(\nu_0)X(\nu_0 + f) - X(\nu_0)X^*(\nu_0 - f)]/f, \quad (4)$$

where  $X$  is a complex amplitude transmittivity of an OFD.  $X^*$  is the complex conjugate of  $X$ .  $\nu_0$  is the locked center frequency of the laser, and  $f$  is Fourier frequency. With eqs. (1), (2), and (4), the transfer function of the present OFD using the two output ports of the PBS is calculated as

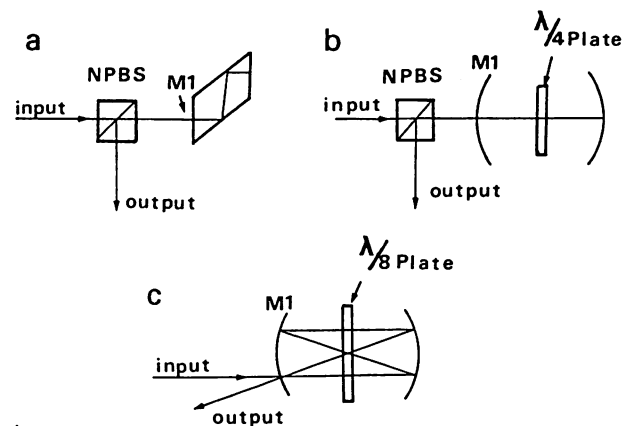
$$H(f) = [h(E_a(\nu)/E(\nu), f) - h(E_b(\nu)/E(\nu), f)] I. \quad (5)$$

The transfer functions of the present OFD, and of the other OFD using slopes of resonant profiles of transmitted mode (T-mode) and reflection mode (R-

mode) of a FPI, are plotted in fig. 2(b) as curves A, B, and C, respectively. The functions are normalized to  $I$  and the linewidth of the cavity  $\Delta\nu_{\text{FP}} (= \text{FSR}/F)$ . The gain of curve A is 10 dB larger than those of others, and shows  $90^\circ$  phase delay at  $f \rightarrow \infty$ , the same as the case of curve B. These properties mean that the performances of the present OFD are superior to those of others when it is employed in the fast and high-gain electrical negative feedback loop for laser FM noise reduction.

### 3. Experiment and discussion

Three kinds of resonators were constructed as examples of the proposed OFD as shown by figs. 3(a),



d

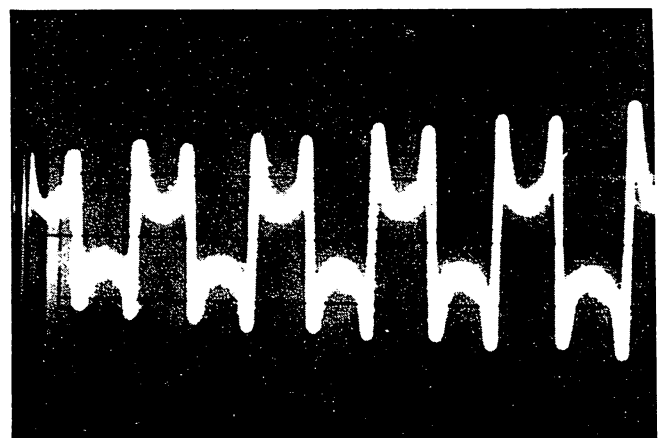


Fig. 3. Various examples for the present optical frequency discriminators (a) Fresnel rhomb  $\lambda/4$  plate with both ends high reflection coated. (b) A confocal reference cavity off-axis with an intracavity  $\lambda/4$  plate. (c) A confocal reference cavity off-axis with an intracavity  $\lambda/8$  plate. (d) Signal obtained by the setup of (a) ( $r=0.95, F=7, \text{FSR}=1.7 \text{ GHz}$ ). A similar signal could be also obtained by (b) and (c).

(b), and (c), where a Fresnel rhomb  $\lambda/4$  plate with reflection film coated on both ends, a confocal reference cavity on-axis with an intra-cavity  $\lambda/4$  plate, and an off-axis confocal cavity with an intra-cavity  $\lambda/8$  plate, were used respectively. The setups shown in figs. 3(a) and (b) are operated under the principle of the standing wave-type resonator shown in fig. 1(b), and the setup shown in fig. 3(c) is equivalent to the traveling type resonator shown in fig. 1(a). As an example, fig. 3(d) shows the signal obtained by the setup of fig. 3(a), where  $r=0.95$ ,  $F=7$  and  $\text{FSR}=1.7$  GHz. The finesse is rather low, owing to poor optical quality of the Fresnel rhomb  $\lambda/4$  plate. However, this setup has advantages, which the system can be compact and solid. When we used a mirror  $r=0.95$  and  $\text{FSR}=1.5$  GHz in fig. 3(b),  $F$  was increased up to 25. When we used a mirror  $r=0.95$  and  $\text{FSR}=750$  MHz in fig. 3(c),  $F$  was 12.

As the first experiment, we measured the reliability of the center frequency stabilization of the semiconductor laser under frequency modulated condition. An AlGaAs laser of  $0.83$   $\mu\text{m}$  wavelength (CSP-type, Hitachi HL8314E) was used at room temperature. The center frequency of the field spectrum of the laser was locked to the present OFD (of the type shown in fig. 3(a),  $F=7$ ,  $\text{FSR}=1.7$  GHz) with control bandwidth of  $100$  Hz, and then the laser frequency was directly modulated (modulation frequency range is between  $1$  kHz and  $100$  kHz) to measure the maximum frequency deviation to maintain the laser frequency under locked condition. As a result, the maximum frequency deviation was  $3.6$  GHz, which is roughly equal to  $2 \times \text{FSR}$ . On the other hand, in case of using a slope of the resonant profile of the FPI (T-mode,  $F=7$ ,  $\text{FSR}=1.7$  GHz), the maximum frequency deviation was only  $240$  MHz, which is roughly equal to the  $\Delta\nu_{\text{FP}}$ . Thus the maximum frequency deviation in case of using the present OFD is  $2 \times F$  times as large as that in case of using the slope of a resonant profile of the same FPI.

As the second experiment, the FM noise of the semiconductor laser was reduced by the electrical negative feedback control using the present OFD shown in fig. 3(b) ( $\text{FSR}=1.5$  GHz,  $F=25$ ) to demonstrate the feasibility of the present OFD. The circuit of the feedback loop was designed by the same method described in ref. [6]. Fig. 4 shows the power spectral density of the suppressed FM noise which

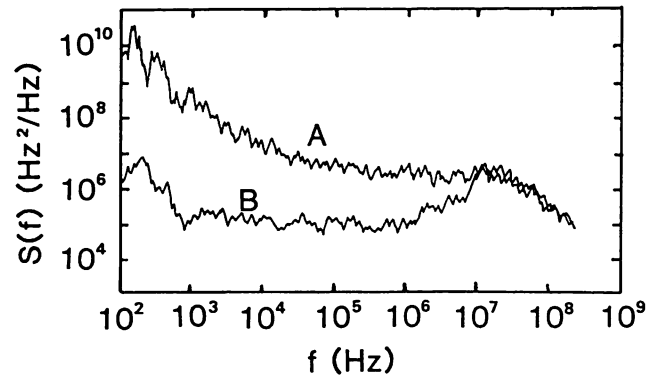


Fig. 4. Power spectral density of the FM noise, which was measured by another Fabry-Perot interferometer. (a) Under free-running condition. (b) Under frequency controlled condition.

was measured by another FPI. Curves A and B represent the results for free-running and frequency controlled condition, respectively. The maximum reduction was  $30$  dB at  $f=1$  kHz. The control bandwidth was  $10$  MHz. The spectral linewidth of the laser, which was measured by a self-delayed homodyne method using a  $2$  km optical fiber, was reduced from  $6$  MHz to  $250$  kHz by this control.

If we use the present OFD, for example the setup shown in fig. 3(b), it is possible to simultaneously apply the optical feedback [5] and the electrical negative feedback methods by using one cavity, because the locking points of these methods are the same. If this method is used, one can simultaneously utilize the advantageous performances of the electrical and optical feedback method, such as very wideband frequency control, very high FM noise reduction, and high center frequency stability. If the OFD as shown in fig. 1(a) is made with ring-fiber FPI, it will be able to be used for a resonant type gyroscope, and some other kinds of fiber sensors.

#### 4. Summary

A novel optical frequency discriminator for FM noise reduction of semiconductor lasers was proposed. The properties of the discriminator are superior to those of the discriminators which use the slope of a resonant profile of a FPI, especially when it is employed in the fast and high-gain negative electrical feedback loop. The gain of the discriminator is

10 dB larger than those of the others. Its phase delay is only  $90^\circ$ . The four problems of discriminators using the slope of a resonant profile of a FPI, which is pointed out in the introduction, were overcome. (i) The laser frequency is locked just to the center of the resonant spectral profile of a FPI. (ii) The contribution of the IM noise of the laser to the frequency discrimination can be suppressed. (iii) The recovery range is  $\pm 1 \times \text{FSR}$  from the locked position. (iv) The maximum frequency deviation is  $2 \times \text{FSR}$ . To demonstrate the feasibility of this discriminator, the spectral linewidth of a semiconductor laser was reduced from 6 MHz to 250 kHz.

#### Acknowledgement

The authors are thankful to C.H. Shin, K. Naka-

gawa and A. Kiyohara for stimulating discussions.

#### References

- [1] M. Ohtsu and S. Araki, *Appl. Optics* 26 (1987) 464.
- [2] M. Hashimoto and M. Ohtsu, *IEEE J. Quant. Electron.* QE-23 (1987) 446.
- [3] J.L. Picque, *Metrologia* 13 (1977) 115.
- [4] D. Sesko, C.G. Fan and C.E. Wieman, *J. Opt. Soc. Am. B* 5 (1988) 1225.
- [5] C.H. Shin, M. Teshima, M. Ohtsu, T. Imai, J. Yoshida and K. Nishide, *IEEE Photon. Technol. Lett.* 2 (1990) 167.
- [6] M. Ohtsu, M. Murata and M. Kourogi, *IEEE J. Quant. Electron.* QE-26 (1990) 231.
- [7] T.W. Hänsch and B. Couillaud, *Optics Comm.* 35 (1980) 441.

# A 134 MHz Bandwidth Homodyne Optical Phase-Locked-Loop of Semiconductor Laser Diodes

Motonobu Kourogi, Chul-Ho Shin, and Motoichi Ohtsu, *Senior Member, IEEE*

**Abstract**—Experiments on homodyne phase-locking of 7.5 MHz spectral linewidth semiconductor laser diodes were carried out. A very fast speed optical phase-locked loop (OPLL) with a 134 MHz bandwidth has been achieved with a phase error variance of 0.15 rad<sup>2</sup>. The total phase-locked power was 86% of output of the slave laser. Slow speed OPLL's with the electrically frequency stabilized semiconductor laser diodes are also demonstrated for the first time.

## I. INTRODUCTION

THE optical phase-locked-loop (OPLL) [1]–[5] of semiconductor laser diodes (LD) is an important technique in the fields of coherent optical-sensing, frequency synthesis, communications, etc. The LD's have high-FM efficiency and their wavelength can easily be changed. However, their coherences are not high enough for applications to coherent lightwave systems. In order to realize a high-quality phase-locking of LD's, one of the following two methods should be employed.

One is the improvement of the coherence of LD's, which is employed in an OPLL. This is indispensable for a narrow bandwidth OPLL. In this connection, LD's controlled by the optical feedback methods, i.e., external cavity LD's (ECL), have been used [1]–[4]. The negative electrical feedback method can be used to improve the coherence of the LD's [6], and even the ECL [7]. By using this method, narrower spectral linewidth than that by optical feedback could be obtained. This method is superior to optical feedback in respects of reproducibility and stability. It might be expected that the OPLL using the LD's stabilized by the negative electrical feedback method (NEFL) can be used in the field of coherent optical sensing which is employed in low Fourier frequency range. In this letter, the experiments of the homodyne OPLL using NEFL's are reported for the first time.

Another method to achieve high-quality phase-locking is to realize a very fast OPLL. When the free-running LD (the slave laser) is locked to a highly coherent master laser using a wide bandwidth ( $\gg$  linewidth of the slave laser) OPLL, the high coherence of the master laser is transferred to the slave laser. Thus, this method can also be used to power amplification of a highly coherent laser. For the same purpose, injection locking techniques have been used [8]. In case of the injection locking technique, however, it is difficult to fully suppress the slower changes of phase errors with a high gain because of in optical path length by acoustics, mechanical vibrations, etc. Further-

more, it requires relatively high power of the master laser. To compensate the slower phase error fluctuations, the OPLL must be introduced additionally to the injection locking system. On the other hand, a wide bandwidth OPLL can be used for this purpose with a low power master laser. The LD's can be directly used as current controlled oscillators in a wide bandwidth OPLL because of their frequency modulation capability up to the GHz range. So far the bandwidth of the fastest OPLL (in this letter, the bandwidth represents a maximum Fourier frequency, the phase noise within which could be controlled by the loop) to the authors' knowledge, was only about 8 MHz, which was 1.1 times the linewidth of the slave laser [5]. This bandwidth is not enough for the above-mentioned purpose. In this letter, the experimental result of homodyne OPLL with 134 MHz bandwidth is reported.

## II. OPLL OF ELECTRICALLY STABILIZED LD'S

As the first experiment, we start by describing the slow speed OPLL with the NEFL's. The block diagram of the experimental setup for OPLL is shown in Fig. 1. The laser beams from the master and slave lasers were mixed at the beam splitter, and the two mixed laser beams were detected by p-i-n photodetectors *A* and *B* (PD.A and PD.B). The phase error signal from PD.A was fed back to the slave laser. The power spectral density (PSD) of the phase error signal detected by PD.B was monitored by an RF spectrum analyzer. The estimated PSD of the phase error was calculated by

$$S_{\phi}(f) = \frac{S_{fm}(f) + S_{fs}(f)}{|jf + MH(f)|^2} \quad (1)$$

where  $S_{fm}(f)$  and  $S_{fs}(f)$  were the PSD of the FM noise of the master laser and the unlocked slave laser, respectively.  $M$  is a gain factor which was determined by the optical power incident into the PD.A and the sensitivity of the PD.A.  $H(f)$  is the transfer function of the slave laser. The value of  $M$  was adjusted by an optical attenuator shown in Fig. 1.

LD's used in this experiment were CSP-type LD's of 830 nm wavelength (Hitachi HL8314 for the master laser, HL8312 for the slave laser), and the linewidths of these LD's under free-running condition were 7.5 MHz, which were measured by the self-delayed homodyne method using a 2 km long optical fiber.

The principle of the frequency stabilizations in the NEFL's used in the master and slave lasers was basically same as that shown as in [6]. We used Fabry-Perot interferometers (FPI) (finesse 15, FSR = 1.5 GHz) for the NEFL's. Spectral linewidths of the NEFL's were 150 kHz. A block diagram of the slave laser using NEFL is shown in Fig. 2. In order to control the phase of the NEFL, we used the direct modulation of the laser injection current and the modulation of the length of the FPI, to which the frequency of the slave laser was locked. The

Manuscript received November 13, 1990; revised December 21, 1990.

M. Kourogi and M. Ohtsu are with the Graduate School at Nagatsuta, Tokyo Institute of Technology, 4259 Nagatsuta, Midori-ku, Yokohama, Kanagawa 227, Japan.

C.-H. Shin was with the Graduate School at Nagatsuta, Tokyo Institute of Technology. He is now with National Mokpo Merchant Marine College, Mokpo, Chun-Nam, Republic of Korea.

IEEE Log Number 9143128.

phase error signal was added to the error signal for the FM noise reduction of the NEFL at the point *A* in Fig. 2. A integrator was used for the modulation of the length of the FPI. This method, thus, constituted an active loop filter. In this case, the transfer function of the slave laser of Fig. 2 was simply calculated as

$$H(f) = \frac{1 + 1/jfT}{H_p H_d} \quad (2)$$

where  $H_p$  [mA/W] and  $H_d$  [W/Hz] were transfer functions of the photodetector and the FPI. In this experiment,  $H_p$  and  $H_d$  have constant values, and  $1/H_p H_d$  was 38 MHz/mA.  $T$  ( $= 0.5$  ms) is a time constant of the integrator.

The measured result of PSD of the phase error of the slow speed OPLL is shown in Fig. 3. Here the curves (a) and (b) are for unlocked conditions with free-running lasers and with NEFL's, respectively. These were calculated by using (1) with  $M = 0$  and the values of FM noise PSD of the master and slave lasers, which were measured by using a FPI. As seen from difference between curves (a) and (b), the phase noise of NEFL's were reduced in the range of  $f < 10$  MHz. Curves (c) and (d) show the results under phase-locking conditions with lower and higher gains, respectively. The bandwidth of OPLL's for curves (c) and (d) can be seen as 500 kHz and 10 MHz, respectively.

Curves (e) and (f) represent the calculated results corresponding to the curves (c) and (d), respectively, by (1), (2), and curve (b). They show good agreements with each other. The estimated phase error variances  $\sigma_\phi^2$  for curves (c) and (d) were 0.8 and 0.5  $\text{rad}^2$ , respectively. These larger values of  $\sigma_\phi^2$  are mainly attributed to the residual phase noises of the NEFL's because of their insufficient FM noise reduction. This is the first demonstration of OPLL by using electrically stabilized LD's.

### III. WIDEBAND OPLL

As the second experiment, we tried to demonstrate a very fast OPLL using an NEFL for the master laser and a free-running LD for the slave laser. Although the estimated loop delay time ( $T_d$ ) of the OPLL system considering the length of the loop was 0.3 ns, the measured  $T_d$  of the OPLL system by the network analyzer was 1 ns. This difference was attributed to the group delay time of the photodetector and the LD in the loop. The transfer function of the slave laser system was expressed by

$$H(f) = \frac{g_1 + jg_2 f / g_3}{1 + jf / g_3} \exp(-j2\pi f T_d) \quad (3)$$

where  $g_1 = 1.4$  GHz,  $g_2 = 250$  MHz, and  $g_3 = 280$  kHz; these parameters were estimated by the method described in [6].

The measured PSD's of the phase error are shown in Fig. 4. Curves (a) and (b) are the measured results under unlocked and phase-locked conditions, respectively. As being seen by the difference between the curves (a) and (b), the bandwidth of the OPLL was 134 MHz. This is the first experimental result to demonstrate an extremely fast OPLL with a bandwidth wider than 100 MHz, which is, to the authors knowledge, the fastest OPLL among the values reported so far. Curves (c) and (d) with broken lines are the calculated results corresponding to those for curves (a) and (b). The estimated phase error variance for the curve (b) was 0.15  $\text{rad}^2$ . The total power  $P_{\text{phase locked}}$  of the slave laser phase-locked to the master laser was 86%, which was estimated by using the relation given in [7]

$$P_{\text{phase locked}} = |J_0(\beta)|^2 \quad (4)$$

where  $\beta = \sqrt{2} \sigma_\phi$  and  $J_0(\cdot)$  is the 0th order Bessel function.

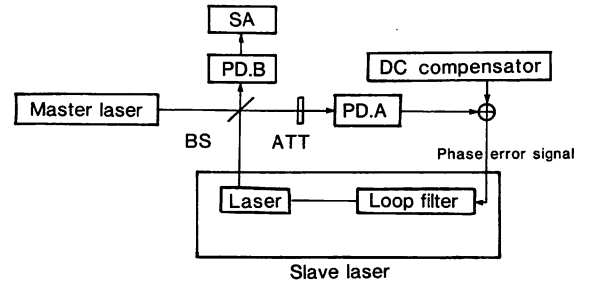


Fig. 1. The block diagram of the experimental setup for OPLL's. BS: beam splitter. PD.A and PD.B: p-i-n photodetectors. SA: spectrum analyzer. ATT: optical attenuator.

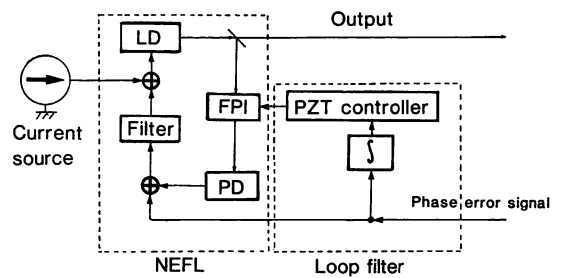


Fig. 2. A block diagram of the slave laser for the OPLL by two NEFL's.

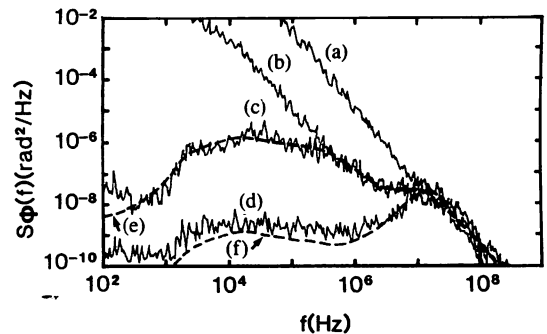


Fig. 3. Power spectral density  $S_\phi(f)$  of the phase error for the OPLL by two NEFL's. Curves (a) and (b) are for unlocked conditions with free-running lasers and with NEFL's. Curves (c) and (d) show the results under phase-locking conditions with lower and higher gains. Curves (e) and (f) are the calculated result, which correspond to curves (c) and (d), respectively.

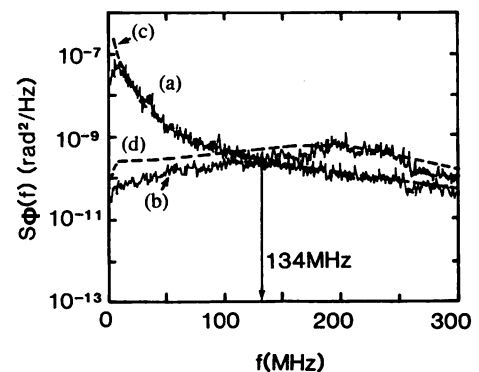


Fig. 4. Power spectral density  $S_\phi(f)$  of the phase error for the OPLL by a NEFL and a free-running laser. Curves (a) and (b) are the measured results under unlocked and phase-locked conditions, respectively. Curves (c) and (d) are the calculated results, which correspond to curves (a) and (b), respectively.

By using a simple first-order loop approximation [9], the average time  $T_{AV}$  between cycle slips of curves (c) and (d) in Fig. 3 and Curve (b) in Fig. 4 were  $1.6 \times 10^{-5}$ s,  $3.3 \times 10^{-6}$ s and  $2.3 \times 10^{-3}$ s, respectively. Wideband OPLL is therefore effective to reduce cycle slips. However, this performance is still poor. The value of  $T_{AV}$  can be increased by decreasing values of phase error and the loop noise bandwidth. To further reduce the probability of cycle slips, it is therefore required to suppress phase error by increasing the loop bandwidth or, more effectively, by employing LD's, the FM noise of which is reduced with a wideband, then the loop bandwidth can also be narrowed.

#### IV. SUMMARY

We summarize the above experimental results. Using NEFL's as master and slave lasers, of which the spectral linewidth were narrowed from 7.5 MHz to 150 kHz, phase-locking was successfully achieved. The bandwidths of optical phase-locking were between 500 kHz and 10 MHz. The estimated phase error variances were between  $0.8 \text{ rad}^2$  and  $0.5 \text{ rad}^2$ , respectively. This is the first report of OPLL using NEFL's. A free running LD was phase-locked to a highly coherent master laser with a very fast OPLL. This is the first experimental result to demonstrate an extremely wideband OPLL with a 134 MHz bandwidth. The estimated phase error variance was  $0.15 \text{ rad}^2$ , then the total phase-locked power of the slave laser was 86%.

#### ACKNOWLEDGMENT

The authors thank Dr. K. Nakagawa of their institute for stimulating discussion.

#### REFERENCES

- [1] R. C. Steele, "Optical phase-locked loop using semiconductor laser diodes," *Electron. Lett.*, vol. 19, no. 2, pp. 69-71, 1983.
- [2] D. J. Malyon, D. W. Smith, and R. Wyatt, "Semiconductor laser homodyne phase-locked loop," *Electron. Lett.*, vol. 22, no. 8, pp. 421-422, 1986.
- [3] J. M. Kahn, "1 Gbits/s PSK homodyne transmission system using phase-locked semiconductor lasers," *IEEE Photon. Technol. Lett.*, vol. 1, pp. 340-342, Oct. 1989.
- [4] C. H. Shin and M. Ohtsu, "Heterodyne optical phase-locked loop by confocal Fabry-Perot cavity coupled AlGaAs lasers," *IEEE Photon. Technol. Lett.*, vol. 2, pp. 297-300, Apr. 1990.
- [5] G. Wenke and S. Saito, "Phase locking of semiconductor lasers using homodyne detection and negative electrical feedback," *Japan J. Appl. Phys.*, vol. 24, no. 12, pp. L908-L910, 1985.
- [6] M. Ohtsu, M. Murata, and M. Kouroggi, "FM noise reduction and subkilohertz linewidth of an AlGaAs laser by negative electrical feedback," *IEEE J. Quantum Electron.*, vol. 26, no. 2, pp. 231-241, 1990.
- [7] C. H. Shin and M. Ohtsu, "Stable semiconductor laser with a 7-Hz linewidth by an optical-electrical double-feedback technique," *Opt. Lett.*, vol. 15, Dec. 1, 1990.
- [8] C. N. Man and A. Brillat, "Injection locking of argon-ion lasers," *Opt. Lett.*, vol. 9, no. 8, pp. 333-334, 1984.
- [9] F. M. Gardner, *Phaselock techniques*. 2nd ed. New York: Wiley, 1979.

# A 250 Hz Spectral Linewidth 1.5 $\mu\text{m}$ MQW-DFB Laser Diode with Negative-Electrical-Feedback

Motonobu Kourogi, Chul-Ho Shin, and Motoichi Ohtsu, *Senior Member, IEEE*

**Abstract**—A 1.5  $\mu\text{m}$  corrugation-pitch-modulated MQW-DFB laser diode (LD) with multielectrodes was frequency stabilized by using the negative electrical feedback technique. The FM response of the LD was precisely measured and used for the feedback loop design. The FM noise of the LD was reduced and reached  $10 \text{ Hz}^2/\text{Hz}$  at  $1 \text{ kHz} \leq f \leq 10 \text{ kHz}$  where  $f$  is the Fourier frequency, and the resulting spectral linewidth was 250 Hz, which was mainly limited by the IM noise in the lower Fourier frequency range. The controlled power concentration ratio was 99%.

## I. INTRODUCTION

THE development of narrow spectral linewidth laser diodes (LD) is an important topic in the fields of precise optical measurements, high-resolution laser spectroscopy, and coherent optical communication systems. Recently, we have proposed a novel frequency measurement system for a 1.5  $\mu\text{m}$  wavelength region [1]. For this system, a 1.5  $\mu\text{m}$  LD with a narrow spectral linewidth, e.g., as narrow as subkilohertz is desirable and sometimes indispensable in achieving very high resolution and accuracy of the measurement.

Techniques for optical feedback and negative electrical feedback (NEF) have been used for reducing the FM noise of LD's. It is known that the optical feedback technique has wide-band noise suppression characteristics. On the other hand, it has been demonstrated that the NEF technique is superior to the optical feedback technique with respect to reproducibility and stability [2]. Furthermore, LD's with NEF can achieve lower FM noise in a low-Fourier-frequency region and narrower spectral linewidth than that with optical feedback because the NEF technique can realize a larger feedback gain. Spectral linewidths [full width at half maximum (FWHM)] of 560 Hz [3] and 7 Hz [4] have been realized by using a double NEF technique and by an optical-electrical double-feedback technique, respectively.

In order to achieve LD's with a narrow spectral linewidth and high controlled power concentration ratio, the noise suppression bandwidth should be wider than the spectral

linewidth of the free-running LD. In this case, improved DFB-LD's by introducing a multiquantum well, a long-cavity structure, and so on, is very attractive for applying the NEF technique because of their submegahertz free-running spectral linewidth, e.g., 170 kHz, as reported in [5]. The flat FM response is also desirable to realize NEF with a wider bandwidth, and such LD's have been achieved by using multielectrodes [6], [7]. The narrow free-running spectral linewidths allow us to use a high-resolution Fabry-Perot interferometer (FPI) as an optical frequency discriminator for the NEF without any double-feedback techniques. It should be noted that it has a further advantage, i.e., the degree of freedom for the feedback loop design can be increased due to the decrease of the required noise suppression bandwidth. Although in [8] the linewidth of a multielectrode DFB laser had been reduced by using the NEF technique, the reported linewidth was 95 kHz. This spectral linewidth was probably limited by a lower resolution, i.e., a larger linewidth of the reference FPI and a lower feedback gain.

In this letter, we report experimental results on FM noise reduction of a corrugation-pitch-modulated MQW-DFB LD with multielectrodes [5], which shows the flat FM characteristics and a submegahertz free-running spectral linewidth. To realize a subkilohertz linewidth, we used a higher resolution FPI, and we ensured high feedback gain by improving the NEF with carefully designed loop filter.

## II. EXPERIMENTS

Fig. 1 shows the experimental setup of the FM noise reduction by NEF. The electrode of the LD was divided into three parts ( $E.1$ ,  $E.2$ , and  $E.3$  as shown in this figure). The total injection current ( $I = I_1 + I_2 + I_3$ ) was fixed to 70 mA ( $3.5I_{th}$ ), at which the output power was 7 mW. After a laser beam passed through a 60 dB optical isolator and a  $\lambda/2$  wave plate, it was divided into two beams by a polarization beam splitter. One beam passed through a Faraday rotator and was used for FM noise discrimination by using an FPI. The other beam was detected by  $D.3$  ( $D.1$ - $D.3$  are InGaAs p-i-n photodiodes with a 3 dB gain bandwidth of 700 MHz and a responsivity  $R$  of 1 A/W), and it was used for the measurement of the IM noise of the LD. The laser beam reflected from the FPI (reflection mode: RM) was detected by  $D.1$ , and it was used for the NEF by applying it to  $E.1$  after removing the dc offset and filtering by the PI controller. The laser beam transmitted through the FPI (transmission mode:

Manuscript received March 5, 1991; revised April 3, 1991.

M. Kourogi and M. Ohtsu are with the Graduate School at Nagatsuta, Tokyo Institute of Technology, 4259 Nagatsuta, Midori-ku, Yokohama, Kanagawa 227, Japan.

C. H. Shin was with the Graduate School at Nagatsuta, Tokyo Institute of Technology, 4259 Nagatsuta, Midori-ku, Yokohama, Kanagawa 227, Japan. He is now with the National Mokpo Merchant Marine College, Mokpo, Chun-Nam, Republic of Korea.

IEEE Log Number 9100951.

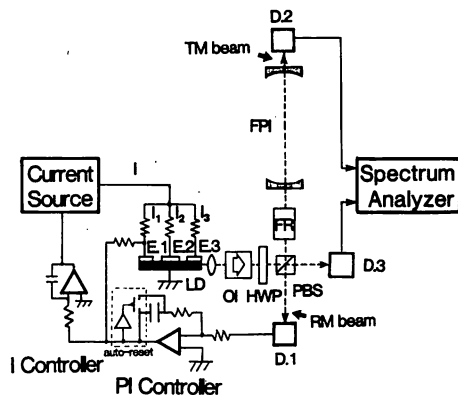


Fig. 1. Experimental setup for FM noise reduction by negative electrical feedback of MQW-DFB LD with multielectrodes. LD: MQW-DFB LD. PBS: polarization beam splitter. D.1-D.3 InGaAs p-i-n photodiodes. OI: optical isolator. FR: Faraday rotator. FPI: Fabry-Perot interferometer. HWP:  $\lambda/2$  wave plate. I controller: integral controller. PI controller: proportional and integral controller.

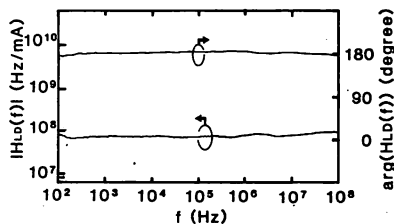


Fig. 2. Transfer function  $H_{LD}(f)$  of the FM response by modulating the injection current  $I_1$  of Fig. 1.

TM) was detected by D.2, and it was used for the measurement of FM noise.

A nonconfocal configuration was employed for the reference FPI in order to suppress the degenerated transverse resonance modes. The linewidth (FWHM)  $\Delta\nu_{FP}$  of the FPI was 2 MHz, and the efficiency  $\eta_c$  of the RM was 0.4. The input laser power  $P$  to the FPI was 2.4 mW. The slope of the resonant spectral profile of the RM was used as an optical frequency discriminator because the RM is superior to the TM to realize a wide-band NEF loop for FM noise reduction [3]. The transfer function  $H_{FP}(f)$  of the RM can be approximated as that of a first-order lag filter with a 3 dB gain bandwidth of  $\Delta\nu_{FP}/2$ , i.e.,  $H_{FP}(f) = K\eta_c PR / (\Delta\nu_{FP} + j2f)$  where  $K = 1.2$ , i.e., the slope of the resonant spectral profile of the FPI to which the laser frequency is locked, where the average photocurrent of the D.1 under NEF was 1.7 mA.

The transfer function of the laser FM response  $H_{LD}(f)$  is shown by Fig. 2, which was measured by modulating the injection current  $I_1$  of E.1. It is seen from this figure that  $|H_{LD}(f)|$  and  $\arg(H_{LD}(f))$  took a constant value of 70 MHz/mA and  $-180^\circ$  for a Fourier frequency range as wide as  $100 \text{ Hz} \leq f \leq 100 \text{ MHz}$ . These performances of  $H_{LD}(f)$  were enough to meet the requirement for the design of the present NEF loop. The FM response by using the other electrodes E.2 and E.3 showed similar performances. The only difference from that of E.1 was that the transfer function of the FM response of E.2 showed a higher efficiency of 560 MHz/mA.

In order to design the loop filter, the loop delay time should be known. The estimated loop delay time  $\tau$  was 5 ns because the loop length was 1.5 m.

The loop filter was designed by using  $H_{FP}(f)$ ,  $H_{LD}(f)$ , and  $\tau$  evaluated above. Since the free-running laser shows low FM noise and a useful FM response, several specific NEF loop filter designs were possible, e.g., using the operational amplifier in order for further drastic reduction of the FM noise. The PI control scheme was used to realize high gain at a low Fourier frequency and a wide bandwidth up to the range of the 3 dB cutoff frequency of the FPI, i.e.,  $\Delta\nu_{FP}/2$ . The transfer function of the PI controller  $H_{PI}(f)$  was  $0.5 \cdot (1 + 5 \cdot 10^5/jf)$  mA/mA, which was tailored to reduce the power spectrum density of the free-running FM noise as much as possible. (If an NEF loop design must be optimized, two parameters of the PI controller should be calculated from a performance criterion, e.g., the phase error variance, and so on.) In the open-loop transfer function  $G(f) = H_{FP}(f)H_{LD}(f)H_{PI}(f) \exp(-j2\pi f\tau)$ , the gain crossover frequency and the gain margin were estimated as 20 MHz and 8 dB, respectively. An auto-reset circuit was introduced into the PI controller, as shown by Fig. 1, in order that the NEF loop can recover to its controlled condition even if the laser frequency is out of lock by an accidental large surge signal. In order to avoid the drift of the current dividing ratio of E.1, E.2, and E.3, an additional I controller was used to slowly control the current source.

The TM beam was used to measure the FM noise magnitude under an NEF condition. The contribution of the laser IM noise was 7 dB lower than that from using the RM beam due to the lower efficiency of the FPI. The FM noise thus could be measured even when the FM noise was reduced to the value limited by the laser IM noise of the RM beam. The FM noise under a free-running condition was measured by another FPI with a  $\Delta\nu_{FP}$  of 200 MHz to get a wider dynamic range of RM noise measurement.

### III. RESULTS AND DISCUSSIONS

The experimental results are shown in Fig. 3(a) where curves A and B are the power spectral densities of the FM noise  $S_{FM}(f)$  for the free-running and NEF conditions, respectively. The 0 dB noise suppression bandwidth was 12 MHz, as can be seen by a comparison of curves A and B. It is worth mentioning that this bandwidth was 12 times larger than the bandwidth of the FPI, i.e.,  $\Delta\nu_{FP}/2$ . Curves C and D are the measured magnitudes of the IM noise contribution under NEF and free-running conditions, respectively. The difference between curves C and D indicates an increase of the IM noise by the NEF, as has been reported by [2]. Curves B and C show that the FM noise was successfully reduced to the value limited by the IM noise level for  $f \leq 10$  kHz. The FM noise was as low as  $10 \text{ Hz}^2/\text{Hz}$  at  $1 \text{ kHz} \leq f \leq 10 \text{ kHz}$ . Curves A and B in Fig. 3(b) show the calculated spectral profile by using the measured results of curve A in the range of  $100 \text{ kHz} \leq f$  and curve B in the range of  $50 \text{ Hz} \leq f$ , and [3, eq. (1)]. The FWHM of curve B of Fig. 3(b) is 250 Hz, while that of curve A is 680 kHz. This is, to the authors' knowledge, the first report of realizing a subkilo-



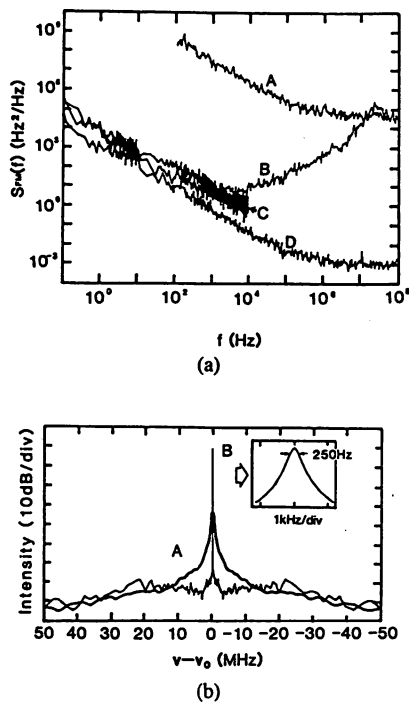


Fig. 3. (a) Power spectral density  $S_{FM}(f)$  of the FM noise. Curves *A* and *B* are for the free-running and under feedback conditions, respectively. Curves *C* and *D* show the laser IM noise effects under feedback and free-running conditions, respectively. (b) Calculated spectral profile. Curves *A* and *B* are the calculated results by using curves *A* and *B*, respectively, in (a). The inset is the spectral profile shown by magnifying the scale of the axis of abscissa, from which the linewidth is measured to be 250 Hz.

hertz spectral linewidth 1.5  $\mu\text{m}$  LD. From curve *B*, it was calculated that the controlled power concentration ratio [3] within this NEF bandwidth was as high as 99%, which means that the total sideband power at  $12 \text{ MHz} \leq |\nu - \nu_0|$  was only 1%, where  $\nu_0$  is a center frequency of the LD.

For a further reduction of FM noise, the effect of the IM noise at a lower Fourier frequency range, i.e.,  $f \leq 1 \text{ MHz}$ , must be rejected from the discriminated signal of the FM noise, as seen in Fig. 3(a). This IM noise effect can be reduced by the techniques of [9]–[11], by which the laser frequency can be locked to the center of a resonant frequency of the FPI. The methods of [10], [11] can perfectly reduce the effect of IM noise in theory. If the technique of FM spectroscopy [9] is used for the NEF with an FM frequency higher than 10 MHz, it is expected that the FM noise can be reduced down to the  $1 \times 10^{-3} \text{ Hz}^2/\text{Hz}$  level, because curve *D* in Fig. 3(a) took a constant value of  $1 \times 10^{-3} \text{ Hz}^2/\text{Hz}$  in the range of  $10 \text{ MHz} \leq f$ . This FM noise level corresponds to a spectral linewidth of 3 mHz.

In order to realize a wider control bandwidth, the loop delay time should be reduced. Following [12], it is expected that a bandwidth over 134 MHz is possible.

#### IV. SUMMARY

A 1.5  $\mu\text{m}$  corrugation-pitch-modulated MQW-DFB laser diode with multielectrodes was frequency stabilized by using the negative electrical feedback technique. By this control, FM noise of the LD was reduced to  $10 \text{ Hz}^2/\text{Hz}$  at  $1 \text{ kHz} \leq f \leq 10 \text{ kHz}$ , which was limited by the effect of the IM noise. The spectral linewidth was reduced to 250 Hz, which is the minimum value for 1.5  $\mu\text{m}$  LD among the values reported so far. The controlled power concentration ratio in the NEF bandwidth was as high as 99%. It is expected that further FM noise reduction down to  $1 \times 10^{-3} \text{ Hz}^2/\text{Hz}$  corresponding to a 3 mHz spectral linewidth can be realized by employing the technique of FM spectroscopy.

#### ACKNOWLEDGMENT

The authors thank Dr. K. Nakagawa, Tokyo Institute of Technology, for stimulating discussions, and Dr. N. Chinone and M. Okai, Central Research Laboratory, Hitachi, Ltd., for supplying the DFB LD's and for their helpful discussions.

#### REFERENCES

- [1] M. Kourogi, N. Nakagawa, C. H. Shin, M. Teshima, and M. Ohtsu, "Proposal of an accurate frequency measurement system for 1.5  $\mu\text{m}$  wavelength laser diodes," presented at CLEO'91, 1991, paper CThR57.
- [2] M. Ohtsu and N. Tabuchi, "Electrical feedback and its network analysis for linewidth reduction of a semiconductor laser," *J. Lightwave Technol.*, vol. 5, pp. 357–369, Mar. 1988.
- [3] M. Ohtsu, M. Murata, and M. Kourogi, "FM noise reduction and subkilohertz linewidth of an AlGaAs laser by negative electrical feedback," *IEEE J. Quantum Electron.*, vol. 26, pp. 231–241, Feb. 1990.
- [4] C. H. Shin and M. Ohtsu, "Stable semiconductor laser with a 7-Hz linewidth by an optical-electrical double-feedback technique," *Opt. Lett.*, vol. 15, no. 24, pp. 1455–1457, 1990.
- [5] M. Okai, T. Tsuchiya, K. Uomi, N. Chinone, and T. Harada, "Corrugation-pitch-modulated MQW-DFB laser with narrow spectral linewidth (170 kHz)," *IEEE Photon. Technol. Lett.*, vol. 2, pp. 529–530, Aug. 1990.
- [6] Y. Yoshikuni and G. Motodugi, "Multielectrode distributed feedback laser and chirping suppressed amplitude modulation," *J. Lightwave Technol.*, vol. LT-5, pp. 516–522, Apr. 1987.
- [7] O. Ishida and H. Toba, "Multielectrode DBR laser diode for wide bandwidth flat FM response," *Electron. Lett.*, vol. 25, no. 11, pp. 703–704, 1989.
- [8] H. Yasaka, Y. Yoshiuni, Y. Nakano, and K. Oe, "Optical frequency stabilization and linewidth reduction of a multielectrode DFB laser with current feedback," *Electron. Lett.*, vol. 23, no. 21, pp. 1161–1162, 1987.
- [9] W. Lentz, "High frequency heterodyne spectroscopy with current-modulated diode lasers," *IEEE J. Quantum Electron.*, vol. QE-20, pp. 1045–1050, Sept. 1984.
- [10] M. Kourogi and M. Ohtsu, "Novel optical frequency discriminator for FM noise reduction of semiconductor laser," *Opt. Commun.*, vol. 81, no. 3, 4, pp. 204–208, 1991.
- [11] T. W. Hänsch and B. Couillaud, "Laser frequency stabilization by polarization spectroscopy of a reflecting reference cavity," *Opt. Commun.*, vol. 35, no. 3, pp. 441–444, 1980.
- [12] M. Kourogi, C. H. Shin, and M. Ohtsu, "A 134 MHz bandwidth homodyne optical phase-locked loop of semiconductor lasers," *IEEE Photon. Technol. Lett.*, vol. 3, Mar. 1991.

# レーザの周波数揺らぎ， スペクトル線幅計測

東京工業大学  
大津 元一  
申 哲浩

## 1. ま え が き

光通信，光計測システム用光源としてのレーザ，特に半導体レーザのFM雑音特性の評価，測定は重要性を増している。特に，最近の半導体レーザは素子構造の改良により，スペクトル線幅1 MHz以下のものが実現している<sup>1,2)</sup>。従って，これらの高品質素子の性能評価のためにもFM雑音のパワースペクトル密度，アラン分散，スペクトル線幅の測定は必須である。本稿ではその原理，方法，例について記す。

## 2. 揺らぎの尺度

周波数揺らぎの瞬時値を $\delta\nu(t)$ ，公称周波数値を $\nu_0$ とすると，相対周波数揺らぎは

$$y(t) = \delta\nu(t) / \nu_0 \quad (1)$$

なる無次元量である。本稿ではこの揺らぎの特性を表す尺度の例としてパワースペクトル密度，アラン(Allan)分散，スペクトル線幅について記す。

$y(t)$  の自己相関関数は

$$R(\tau) = \langle y(t) \cdot y(t + \tau) \rangle \\ \equiv \lim_{T \rightarrow \infty} \frac{1}{T} \int_{-T/2}^{T/2} y(t) y(t + \tau) dt \quad (2)$$

で定義され，そのフーリエ変換

$$S(f) = 4 \int_0^{\infty} R(\tau) \cos(2\pi f\tau) d\tau, \quad (1/\text{Hz}) \quad (3)$$

が $y(t)$  の片側パワースペクトル密度である。これはフーリエ周波数 $f$ のまわりの単位フーリエ周波数幅あたりの揺らぎ振幅を公称周波数で規格化した値の2乗を与える。

パワースペクトル密度がフーリエ周波数領域での尺度であるのに対し，アラン分散は時間領域での尺度である。まず，測定時間(積分時間) $\tau$ にわたり測定した $y(t)$ の値を $\bar{y}_k$ とし，これによりアラン分散を

$$\sigma^2(\tau) = \left\langle \frac{(\bar{y}_{k+1} - \bar{y}_k)^2}{2} \right\rangle \\ \equiv \lim_{N \rightarrow \infty} \frac{1}{N-1} \sum_{k=1}^{N-1} \frac{(\bar{y}_{k+1} - \bar{y}_k)^2}{2} \quad (4)$$

で定義する。これは $S(f)$ を用いると

$$\sigma^2(\tau) = 2 \int_0^{\infty} S(f) \frac{\sin^4(\pi f\tau)}{(\pi f\tau)^2} df \quad (5)$$

により求められる。 $S(f)$ と $\sigma^2(\tau)$ との変換例を表1に示す。3. 節で詳しく述べられるF/V変換器により検出されるFM雑音のパワースペクトル密度 $S_f(f)$ は単位が $\text{Hz}^2/\text{Hz}$ で， $S(f)$ との間には

$$S_f(f) = \nu_0^2 \cdot S(f) \quad (6)$$

の関係が成り立つ。

レーザ光の発振スペクトル形状は

$$I(\nu - \nu_0) = 4 \cdot \text{Re} \left[ \int_0^{\infty} \exp[i2\pi(\nu_0 - \nu)\tau] \right]$$

表1 片側パワースペクトル密度とアラン分散との関係の例

片側パワースペクトル密度 $S(f)$	アラン分散 $\sigma^2(\tau)$
$h_2 \cdot f^2$ (*) ( $2\pi f_h \cdot \tau \gg 1$ )	$h_2 \cdot \frac{3f_h}{(2\pi)^2} \tau^{-2}$
$h_1 \cdot f^1$ (*) ( $2\pi f_h \cdot \tau \gg 1$ )	$h_1 \frac{1}{(2\pi)^2} \left[ \frac{9}{2} + 3\ln(2\pi f_h \tau) - \ln 2 \right] \cdot \tau^{-2}$
$h_0 \cdot f^0$	$\frac{1}{2} h_0 \cdot \tau^{-1}$
$h_{-1} \cdot f^{-1}$	$(2\ln 2) h_{-1} \tau^0$
$h_{-2} \cdot f^{-2}$	$\frac{(2\pi)^2}{6} h_{-2} \tau^1$

(\*) 遮断周波数  $f_h$  の高域遮断フィルタを使用して測定

$$2(\pi\nu_0\tau)^2 \int_0^\infty S(f) \frac{\sin^2(\pi f\tau)}{(\pi f\tau)^2} df | d\tau \quad (7)$$

により与えられる。Reは [ ] 内の複素数の実部を表す。もし  $S(f)$  が一定値  $S_0$  をとる (すなわち白色雑音) の場合、 $I(\nu - \nu_0)$  は図1のようにローレンツ形

$$I(\nu - \nu_0) \propto \frac{1}{(\nu - \nu_0)^2 + (\Delta\nu/2)^2} \quad (8)$$

となり、その半値全幅  $\Delta\nu$  は  $\pi\nu_0^2 S_0$  となる。これをスペクトル線幅と称する。また、光の全電力のうち  $|\nu - \nu_0| \leq \Delta\nu/2$  の周波数範囲に入る割合は50%である。これをパワー集中度と考へ、スペクトル線幅と併せて、周波数揺らぎの高フーリエ周波数成分の少なさを表す尺度と考えることができる。

半導体レーザの周波数揺らぎの基本的要因は自然放出光揺らぎである。低フーリエ周波数領域では白色雑音とみなすと、スペクトル線幅は

$$\Delta\nu = \frac{h\nu_0}{8\pi P_0} \left( \frac{c}{nL} \right)^2 (\alpha_i L + \ln \frac{1}{R}) (\ln \frac{1}{R}) (1 + \alpha^2) \quad (9)$$

で与えられる。ここで、 $h$  はプランクの定数、 $P_0$  は出力パワー、 $c$  は真空中の光速、 $n$  は共振器中媒質の屈折率、 $L$  は共振器長、 $\alpha_i$  は共振器内部損失、 $R$  は共振器端面反射率、である。さらに、 $\alpha$  は線幅増大係数と呼ばれ、自然放出光揺らぎによって誘起されたキャリア密度揺らぎによる影響の大きさを表す。 $\alpha$  はおよそ2~9の値をとる。(9)式は半導体レーザのために修正されたシャウロウ・タウンズの公式と呼ばれる。 $\alpha = 0$  の場合が

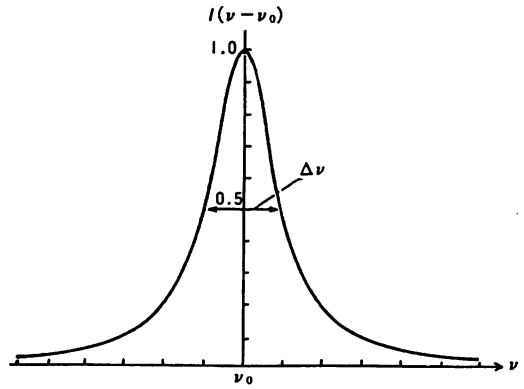


図1 ローレンツ形の発振スペクトル形状

シャウロウ・タウンズの公式に対応し、レーザ光がコヒーレント状態にあるときの揺らぎの大きさを表す。すなわち、フリーランニング・レーザの量子雑音限界である。ただし、一般にはレーザの周波数揺らぎのパワースペクトル密度は一定値ではなく、フーリエ周波数  $f$  に依存した値をとる。さらに、周波数制御された半導体レーザの  $S(f)$  は低フーリエ周波数領域で減少する。従って、スペクトル線幅は精度の高い尺度ではない。

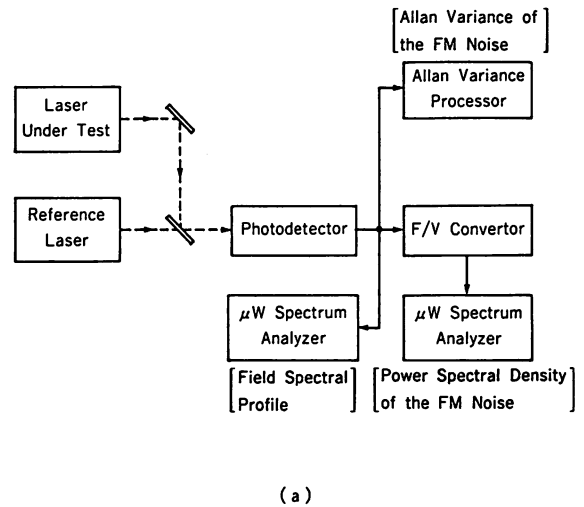
以上の尺度を比較すると、パワースペクトル密度が最も高い尺度である。アラン分散は(4)式のように  $\bar{y}_{k+1}$  と  $\bar{y}_k$  との順序を入れ替えても同じ値をとる。すなわち時間の順序性が失われているので注意が必要である。

### 3. 測定法

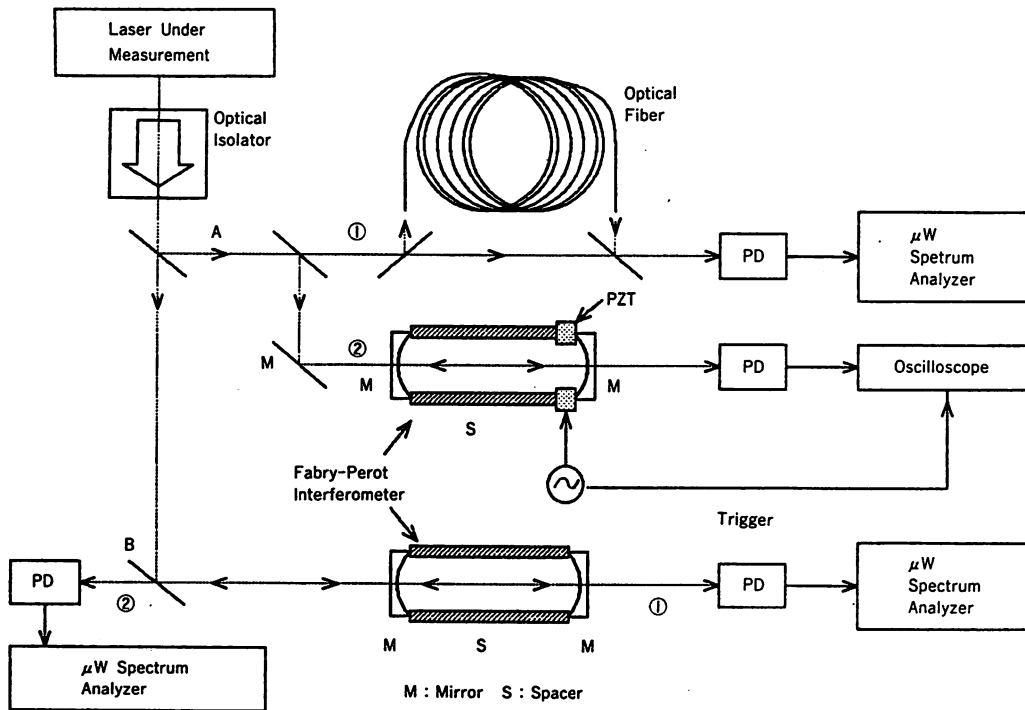
光は100THz以上の超高周波数をもつので、これに対応する検出器はない。そこで、ヘテロダイン法を利用する。その測定原理を図2(a)に示す。被測定レーザに比べ十分にFM雑音の小さなレーザを基準レーザとし、2乗検波特性を有する光検出器で両レーザのヘテロダイン信号を測定する。それをF/V変換器に通し、その出力信号をマイクロ波スペクトラム・アナライザに加えれば、FM雑音のパワースペクトル密度が測定される。また、

この光検出器出力信号をゲート開時間  $\tau$  の周波数カウンタに加え、計算機により(4)式に従って計算すればアラン分散が計算できる。一方、光検出器出力信号そのものをマイクロ波スペクトラム・アナライザに加えれば、ヘテロダイン信号のスペクトル形状、すなわち、(7)式の値が測定される。基準レーザが無い場合には2台の互いに無相関なレーザのヘテロダイン信号を使うことにより、両者の揺らぎの和の値を測定できる。

被測定レーザのみの場合、この測定法を図2(b)に示す。スペクトル形状はA-①のように光ファイバを使う方法と、A-②のように掃引形ファブリ・ペロー干渉計を使う方法とがある。まず、A-①を説明する。レーザの光を2つに分け、一方を長い光ファイバを通して遅延させた後、2つの光を再合成する。このとき、両者の光の揺らぎはもはや無相関とみなされるので、再合成に使



(a)



(b)

図2 FM雑音の測定原理

(a) 基準レーザがある場合 (b) 基準レーザがない場合

った光検出器の出力をマイクロ波スペクトラム・アナライザに加えれば、被測定レーザのスペクトルの2倍の線幅をもつスペクトル形状が観測される。これは遅延自己ホモダイン法と呼ばれる<sup>3)</sup>。この測定の分解能は遅延後の無相関性が破れることに起因するので、ファイバの長さ $L_f$ に反比例し、 $c/2n_fL_f$ である。ここで $n_f$ はファイバの屈折率である。分けられた2つのレーザ光の一方を音響光学変調器で周波数シフトさせ測定するヘテロダイン法もある。A-②の場合にはレーザ光をファブリ・ペロー干渉計に入射させ、干渉計の長さを掃引すると光検出器で検出された干渉計透過光の強度変化によりスペクトルの形状が測定できる。測定分解能は干渉計の共振曲線の幅によって決まる。

被測定用のレーザのみの場合、FM雑音のパワースペクトル密度の測定のためには、図2(a)中の光検出器の後に電気的F/V変換器を使うかわりに、図2(b)に示したように、光検出器の前に、光学的F/V変換器を設置する場合がある。これにはファブリ・ペロー干渉計の透過モード(図2(b)のB-①)と反射モード(図2(b)のB-②)、マイケルソン干渉計、原子、分子の吸収線、などを使う。この内、ファブリ・ペロー干渉計は装置の簡便さ、高S/N、高い短期周波数安定度、の利点があるので最もよく利用される。この場合、検出帯域幅は干渉計の共振曲線の線幅の1/2であり、その帯域より高いフーリエ周波数では透過モードで-40dB/dec、反射モードでは-20dB/dec、の割合で検出感度が落ちる。一方、検出感度は干渉計の共振曲線の線幅が狭いほど高い。従って、検出感度と帯域幅とはトレードオフの関係にある。最近ではフィネス10,000以上のファブリ・ペロー干渉計、すなわちスーパーキャビティが市販されている。この場合、光のIM雑音が測定感度を制限する場合があるので、高精度測定には光バランス検出器を使う必要がある。最近では、ファブリ・ペロー干渉計とマッハ・ツェンダ干渉計とを組み合わせ、ファブリ・ペロー干渉計よりも感度と帯域の優れた光学的F/V変換器が考案されている<sup>4)</sup>。ただし、これらの光学的F/V変換器を使う場合、F/V変換器の固有周波数へのレーザ周波数追従度を測っていることになるので、固有周波数の揺らぎが小さく安定なF/V変換器を使うことが重要である。以上

により測定されたFM雑音のパワースペクトル密度と(5)~(7)式とを利用するとアラン分散、スペクトル形状が求められる。

#### 4. 測定装置

3. 節の測定に使うための装置として、従来よりあるマイクロ波スペクトラム・アナライザ、さらにFFTアナライザなどを低周波スペクトラム・アナライザとして使う必要がある。これらの測定の分解能はスペクトラム・アナライザ用のフィルタ帯域により決まる。アラン分散測定装置としては周波数カウンタのゲート閉時間が開時間にくらべ十分小さいことが必須で、これを満たす測定器としてHP5372Aがある。さらに精密な専用測定装置として、アラン分散実時間測定装置<sup>5)</sup>、さらにその性能を向上させたもの<sup>6)</sup>が開発されている。後者のシステムを図3に示す。測定精度は基準マイクロ波発振器の周波数安定度によって決まるが、この安定度が十分高い場合には測定限界は

$$\sigma^2(\tau) = (\nu_i / \nu_m \nu_0 \tau)^2 \quad (10)$$

で与えられる。ここで、 $\nu_i$ は入力信号周波数、 $\nu_m$ は基準マイクロ波周波数である。測定可能最小積分時間は $1/\nu_i$  (s) である。

遅延自己ホモダイン法のための光の分岐、再合成のた

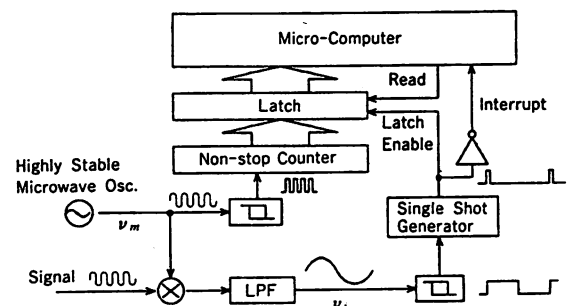


図3 アラン分散実時間測定装置の原理図<sup>6)</sup>

めの光学素子を組み込んだ測定装置も市販されている。光学的F/V変換器として、3.節で述べたスーパー・キャビティも市販されており、これを光スペクトラム・アナライザとして使った時の分解能が約150kHzに達するものもある。この場合、キャビティには高反射率の鏡が使われているので、被測定レーザへ戻り光が入射しないよう注意する必要がある。

### 5. 測定例

図4は波長0.8 $\mu$ m AlGaAsレーザのFM雑音のパワースペクトル測定例である<sup>7)</sup>。スーパー・キャビティを光学的F/V変換器として用いた。曲線Aはフリーランニング状態の値である。曲線BはFM雑音を抑圧するように半導体レーザ注入電流に電氣的負帰還制御を施した場合である。曲線Cは(9)式の値を推定して記してある。すなわちフリーランニング半導体レーザの量子雑音限界である。曲線A, Bを比較すると、電氣的負帰還制御の利得・帯域積は40THzに達しており、一方、曲線B, Cを比較するとフーリエ周波数  $f < 4.4$  MHzにおいては制御時のFM雑音はフリーランニング時の量子雑音以下になっている。これをハイパー・コヒーレント状態と呼んでいる<sup>8)</sup>。図5(a)は図4の曲線A, Bを用い(6)式によって

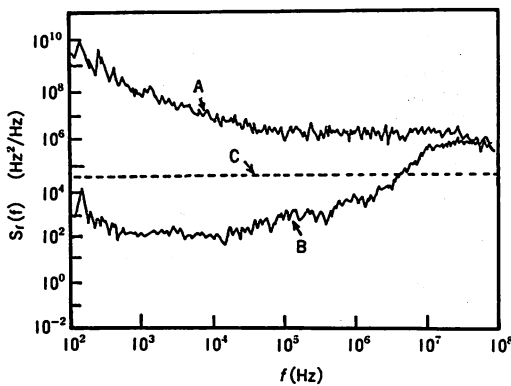


図4 波長0.8 $\mu$ m AlGaAsレーザのFM雑音のパワースペクトル密度<sup>7)</sup> A: フリーランニング時, B: 電氣的負帰還制御時, C: フリーランニング・レーザの量子雑音限界

発振スペクトル形状を求めた結果を示している。この図の曲線Aより、フリーランニング時のスペクトル線幅は4.5MHzであることがわかる。さらに、この値はファイバを用いた遅延自己ホモダイン法により測定した値と一致した。しかし、制御時の線幅は非常にせまいので、ファイバによる測定は困難で、(7)式を用いて求めざるを得ない。その結果が曲線Bであるが、この中心部分の横軸を拡大したものが図5(b)である。これより、線幅560Hzであり、これは半導体レーザでは世界最小の値である。

図6は波長0.67 $\mu$ m InGaAlPレーザの線幅を長さ2 kmのファイバを用いた遅延自己ホモダイン法により測

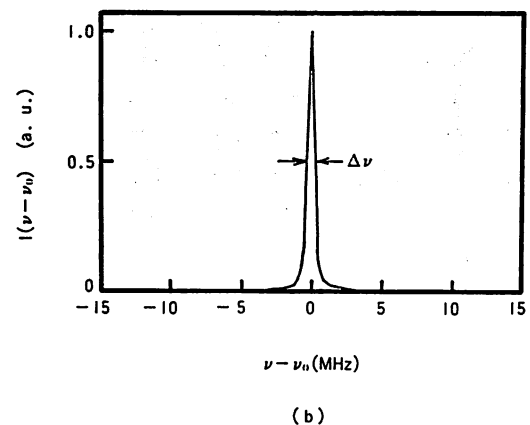
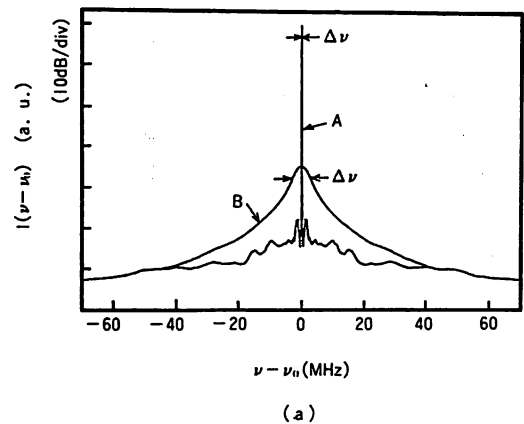


図5 (a) (6)式を用いて得られた発振スペクトル形状<sup>7)</sup>, A: フリーランニング時, B: 電氣的負帰還制御時, (b) 図(a)の曲線Bの横軸を拡大したもの<sup>7)</sup>

定したものである<sup>10)</sup>。フリーランニング状態では線幅は200MHzであったので、これをファブリ・ペロー共振器に入射し、その反射光をレーザに再注入する方法、すなわち光帰還法<sup>10)</sup>、により初めて線幅狭窄化に成功した結果である。図6のスペクトル形状の半値全幅は100kHz、従って3.節の議論により、レーザのスペクトル線幅は50kHzとなる。しかし、長さ2kmのファイバによって決まる測定分解能は3.節の議論によると50kHzである。このことは、図6のスペクトル線幅は光帰還により制御されたレーザの真のスペクトル線幅を測定しているのではなく、測定値は測定装置の分解能を表していることを意味する。すなわち、このレーザのスペクトル線幅は50kHz以下の小さい値になっている。

光帰還法は不安定であるが、広帯域FM雑音抑圧ができる利点をもつ。そこで、予め光帰還法によりAlGaAsレーザのFM雑音を抑圧し、さらに、その不安定性を除去するために電気的負帰還制御を同時に施した結果得られたFM雑音のパワースペクトル密度を図7(a)に示す<sup>11)</sup>。ここではフーリエ周波数1Hz以下でも安定にFM雑音が抑圧されていることを確認するためにFFTアナライザを低周波スペクトルアナライザとして用いた。図5(a)の曲線BよりもさらにFM雑音が低減していることがわかる。図7(a)の曲線より(7)式を用いて発振スペクトル形状を求めた結果を図7(b)に示す。このスペクトル線幅は7Hzである。これにより、周波数制御された超高安定気体レーザ、固体レーザ、などと同等の値が初めて実現したことが確認される。

レーザを2台用いてヘテロダイン形の光位相同期ループを構成し、ヘテロダイン信号の周波数揺らぎのラン分散の平方根を3.節のARPSで測定した結果を図8に示す<sup>12)</sup>。黒丸、白丸はそれぞれ非同期時、同期時の結果である。同期時は積分時間 $\tau=70$ (s)において $\sigma=1.1 \times 10^{-18}$ 、すなわち、ヘテロダイン信号周波数揺らぎ0.4mHzの値が測定されている。この結果よりこの光位相同期ループの残留位相雑音の分散値は0.02 (rad<sup>2</sup>)であることが確認される。この他、ホモダイン形位相同期ループの残留位相揺らぎのパワースペクトル密度もマイクロ波スペクトル・アナライザにより精密測定されている<sup>13,14)</sup>。この場合には光バランス検出器を光位相比較器

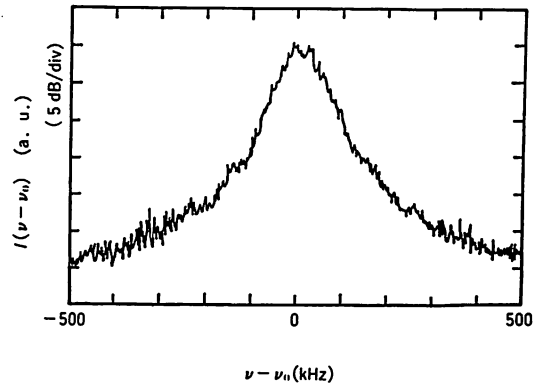


図6 波長0.67 $\mu$ m InGaAlPレーザのスペクトル形状を遅延自己ホモダイン法により測定した結果<sup>9)</sup>

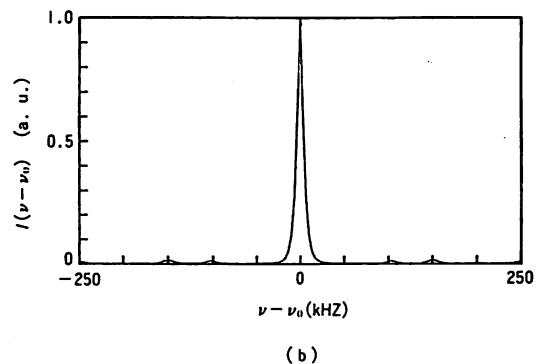
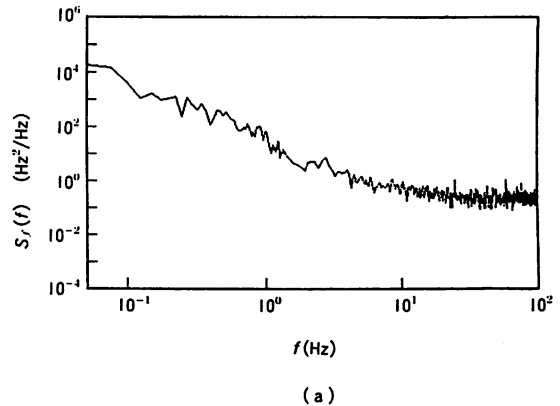


図7 波長0.8 $\mu$ m AlGaAsレーザに光帰還と電気的負帰還制御を同時に施した結果得られたFM雑音の測定結果<sup>11)</sup>

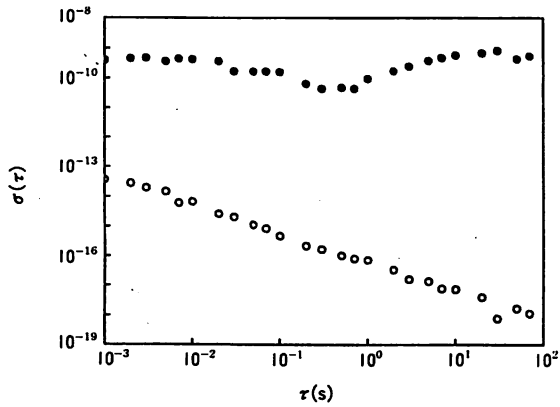


図8 ヘテロダイン形光位同期ループにおけるヘテロダイン信号周波数のFM雑音の大きさを表すアラン分散の平方根の測定結果<sup>12)</sup>。黒丸：非同期時，白丸：同期時

として使い，その出力，すなわち位相誤差信号，をマイクロ波スペクトル・アナライザに印加することにより測定する。

## 6. まとめ

レーザのFM雑音の量を表す尺度として，パワースペクトル密度，アラン分散，スペクトル線幅，の定義，測定法，測定装置について示した。これらの測定に関しては一般の物理量の測定と同様の測定論が適用できるのはいままでの間。すなわち，測定装置の雑音低減，感度向上，帯域拡大が必須である。ただし，感度と帯域とは互いにトレードオフの関係にあるので測定対象によってどちらを優先するのかを判断する必要がある。

本稿のうち尺度の定義のより詳細な記述に関しては文献<sup>15)</sup>を，さらに実験に関するより詳細な解説は文献<sup>16,17,18)</sup>などを参考にされたい。

### 参考文献

- 1) I. Mito and K. Kitamura : CLEO'89, Baltimore (1989) TUD5
- 2) H. Imai, CLEO'89, Baltimore (1989) FB 4
- 3) T. Okoshi, K. Kikuchi, and A. Nakayama : Electron.

- Let., vol.16 (1980) 630
- 4) 興梠元伸，他：応物学会講演会，1990年春，3laG5
- 5) K. Kuboki and M. Ohtsu, IEEE Trans. I. M. August issue. (1990)，印刷中
- 6) 申哲浩，他：応物学会講演会，1989年秋，29pZL4
- 7) M. Ohtsu, et.al. : IEEE J. Quantum Electron., vol.26 (1990) 231
- 8) 大津元一：サイエンス，1989年3月号，64
- 9) 鈴木宏昌，他：応物学会講演会，1990年春，3laG10  
および，M. Ohtsu, et.al. : Jpn. J. Appl. Phys., Part 2, vol.29, (1990) 印刷中
- 10) B. Dahmani, et. al. : Opt. Lett., vol.12 (1987) 876
- 11) C.-H. Shin and M. Ohtsu : IEEE/LEOS Topical Meeting on New Semiconductor Laser Devices and Applications. Monterey, 1990, SCW3
- 12) C.-H. Shin and M. Ohtsu : IEEE Photonics Tech. Lett., vol.2 (1990) 297
- 13) C.-H. Shin and M. Ohtsu : OEC'90. Makuhari, 1990, 12C3-3
- 14) 興梠元伸，他：応物学会講演会，1990年春，3laG4
- 15) 大津元一：レーザーと原子時計，オーム社，1986
- 16) M. Ohtsu and T. Tako : Prog. Opt., XXV, Ed. by E. Wolf, Elsevier, Amsterdam. 1988
- 17) 大津元一，中川賢一：応物学会誌，vol.58 (1989) 1428
- 18) 大津元一，他：通信学会誌，C-I, vol. J73-C-I (1990) 277

### Measurements of frequency fluctuations and field spectral linewidths of lasers

by Motoichi Ohtsu and Chul-Ho Shin, Graduate School at Nagatsuta, Tokyo Institute of Technology

Three kinds of measures representing the frequency stability of the lasers are defined, and their measurement methods and instruments are reviewed. The three measures are the power spectral density, the Allan variance, and the field spectral linewidth. Several measured results for ultra-high coherent semiconductor lasers, achieved by the authors, are demonstrated.

〈著者〉 オオツ モトイチ，シン チョルホ（東京工業大学総合理工学研究科）

〈連絡先〉 045-922-1111 ex.2526（大津）





# 超 高 コ ヒ ー レ ン ト レ ー ザ ー

中 川 賢 一

東京工業大学総合理工学研究科 〒227 横浜市緑区長津田町 4259

(1990年6月11日受理)

## Ultra-high Coherent Laser

Ken'ichi NAKAGAWA

Tokyo Institute of Technology Graduate School at Nagatsuta,  
4259, Nagatsuta-cho, Midori-ku, Yokohama 227

### 1. は じ め に

レーザーが発明されてから30年になり、現在レーザーは基礎研究から産業にわたる幅広い分野に応用されている。そのレーザーの性能も初期のものに比べて飛躍的に進歩しており、それに伴いその応用も多様かつ高度なものになってきている。とくにレーザーのコヒーレンス性・高輝度・高出力などの性質を利用した超精密測定、高感度微量検出などへの応用は物理・化学などの基礎研究の分野において必要不可欠なものになっている。

一方、このような応用分野においては従来のレーザーの性能では満足できなくなってきた。きわめて高い性能が要求されるようになってきた。たとえば、基礎物理の分野において最近計画されている重力波検出のためのレーザー干渉計においては、 $10^{-21}$ 程度の極微小な空間の歪を検出するためきわめて高い感度が要求される<sup>1)</sup>。検出感度はレーザーの周波数雑音や量子雑音で決まるため、超高安定かつ高出力なレーザーが必要とされている。また、将来の周波数標準として考えられているイオントラップ中の単一イオンを用いた原子時計においては $10^{-18}$ 以下の周波数精度が期待されるが<sup>2)</sup>、これにはきわめて周波数高安定なレーザーが必要になる<sup>3)</sup>。現在実用化されている半導体レーザーを用いた光通信においても、伝送距離および通信容量はレーザーの量子雑音によって最終的に制限される。このためこの従来の量子雑音限界を越えるものとしてスクィーズド光の利用などが提案されている<sup>4)</sup>。このスクィーズド光を利用した検出感度向上は先の重力波検出においても検討されてい

る。

このようにレーザーに対しての極限的な性能の追求はその応用分野に大きく貢献するだけでなく、スクィーズド光発生などのように光の量子状態を制御するなどそれ自身物理的にも非常に興味深い。そのなかでもレーザー光の特長であるコヒーレンス性の追求は多くの応用分野において必要とされる非常に重要なものである。今回は、このレーザーのコヒーレンス性向上について、その原理および最近の研究成果を含めて解説する。また、こうして得られる超高コヒーレンスレーザーの応用についてもいくつか取り上げ、要求される周波数安定度や現状の問題点などについても解説する。

### 2. レーザーの周波数雑音とその制御

レーザーの発振周波数は媒質の原子の遷移周波数と共振器の共振周波数によって決まり、その周波数はある有限の幅をもって揺らいでいる。機械的、熱的変動などによる共振器の共振周波数の変動が実際のレーザーの発振周波数の変動のおもな要因であるが、これらの外乱の影響をすべて取り除いたとしてもレーザー発振モードに混入する自然放出光によってランダムな位相揺らぎが生じこれが発振周波数の変動を引き起こす。ここでは後者の自然放出によって生ずる周波数雑音を簡単に説明し、これらの周波数雑音を負帰還制御することによって減少させる方法についても説明する。

#### 2.1 自然放出による周波数雑音の発生

レーザー周波数の揺らぎのうち、外乱による共振器長変動やレーザー媒質への揺らぎを完全になくしたとして

最後に残るのは自然放出に起因する量子雑音によるものである。これは簡単には次のように理解できる。励起された原子からレーザー共振器内に放出された自然放出光は誘導放出によってコヒーレントに増幅されるが共振器の線幅の逆数で決まる寿命で共振器の外に取り出される。このため共振器にはランダムな位相をもつ自然放出光がある一定の割合で混入して増幅および出力として取り出されるため、共振器内の光は平均的にはランダムな位相揺らぎを受けることになる。レーザー発振が自然放出光が種になっていることからこの自然放出光による揺らぎは本質的に避けることのできないものである。この自然放出によって生ずるレーザーの周波数揺らぎの影響はシャウロウ・タウンズらによって導出されており<sup>5)</sup>、これをレーザー周波数雑音のスペクトル密度  $\bar{\nu}$  で表すと、

$$\bar{\nu} = \Delta\nu_c \sqrt{\frac{2h\nu_0}{P}} \quad [\text{Hz}/\sqrt{\text{Hz}}] \quad (1)$$

と表される<sup>6)</sup>。ここで  $\Delta\nu_c$  はレーザー共振器の半値全幅 (FWHM) を、 $\nu_0$  はレーザーの発振周波数、 $P$  はレーザー出力を含んだ共振器の全パワー損失を表す。自然放出による周波数雑音がレーザー共振器の帯域内では白色雑音であることからこの周波数雑音スペクトル密度よりレーザーの線幅 (FWHM) を求めると、

$$\begin{aligned} \Delta\nu_0 &= \pi \bar{\nu}^2 \\ &= \frac{2\pi(\Delta\nu_c)^2 h\nu_0}{P} \end{aligned} \quad (2)$$

となる。この式を用いて実際のレーザーの線幅の限界を求めてみると、He-Ne レーザーの場合 ( $\Delta\nu_c = 2 \text{ MHz}$ ,  $\nu_0 = 4.7 \times 10^{14} \text{ Hz}$ ,  $P = 5 \text{ mW}$ ) には線幅  $\Delta\nu_0$  は約  $1 \text{ mHz}$  にまで達する。

一方、半導体レーザーの場合には自然放出によるキャリア数変動が屈折変動を介して周波数揺らぎを引き起こすため、先の(2)式にその補正を加えた式、

$$\Delta\nu_0 = \frac{h\nu}{8\pi P} \left( \frac{c}{nL} \right)^2 \left( \alpha_1 L + \ln \frac{1}{R} \right) \left( \ln \frac{1}{R} \right) n_{sp} (1 + \alpha^2) \quad (3)$$

が適用される<sup>7)</sup>。 $P$  はレーザー片端面からの出力パワー、 $n$  は屈折率、 $L$  は共振器長、 $\alpha_1 L$  は共振器内部損失、 $R$  は端面反射率、 $n_{sp}$  は自然放出光係数を表す。キャリア数変動による周波数雑音増加は  $\alpha$  によって表される。この式を用いて半導体レーザーの場合の線幅の限界を求めると、数百 kHz~数 MHz 程度の範囲になる。

このような自然放出光によるレーザーの位相揺らぎの影響は先の(2)式よりポンピングを大きくして出力を大きくする、またはレーザー共振器のQ値を高くすることによって小さくなり、レーザー光は理想的な単一モードのコヒーレント光に近づけることが可能である。

### 2.2 レーザーの周波数制御

レーザー光の自然放出による位相揺らぎや外乱による共振器長変動による周波数揺らぎは、外部のより安定な原子・分子の吸収線やファブリ・ペロー共振器などを周波数弁別器として用いて検出し、その誤差信号よりレーザー共振器長に負帰還制御を行うことによって減らすことができる。このような負帰還制御でレーザーのスペクトル線幅を狭窄化する方法としては、FM 側帯波法を用いてファブリ・ペロー共振器に周波数安定化する Pound-Drever 法と呼ばれる方法が広く用いられている<sup>8)</sup>。この FM 側帯波法は高感度かつ広帯域に周波数雑音を検出できるもので、この方法の原理については他の解説および論文を参考にしてもらいたい<sup>8,9)</sup>、ここでは簡単にその構成およびこれによって得られる周波数雑音の制御限界を示す。この Pound-Drever 法の基本構成を図 1 に示す。レーザーから出た光は E/O 変調器によって周波数  $\nu_m$  で FM 変調され偏光ビームスプリッターおよび  $\lambda/4$  波長板を通して基準共振器に入れられる。共振器からの反射光は再び  $\lambda/4$  波長板を通る際に偏光面が  $90^\circ$  回転するため偏光ビームスプリッターを通して分離して検出す

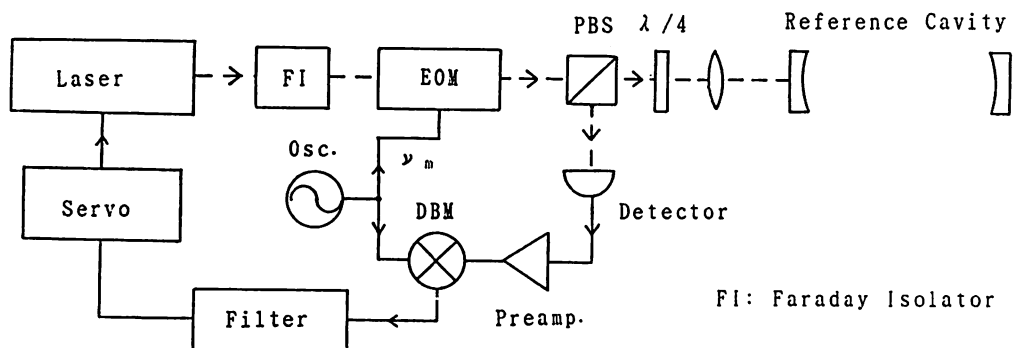


図 1 Pound-Drever 法によるレーザーの線幅狭窄化<sup>8)</sup>

る。こうして得られた光電流のうち変調周波数  $\nu_m$  の項をミキサによって変調周波数で復調することによって次の式、

$$I_s = 2I_0 \cdot \kappa^{1/2} \cdot J_0(M) J_1(M) \frac{2\Delta\nu/\Delta\nu_r}{1 + (2\Delta\nu/\Delta\nu_r)^2} \quad (4)$$

で表される誤差信号を得る。  $I_0$  はレーザー周波数が共振器の非共振状態のときの光電流で  $I_0 = e\eta P_0/h\nu$  で表され、  $\eta$  は検出器の量子効率、  $P_0$  は光出力、  $\nu$  はレーザーの周波数をそれぞれ表す。  $\Delta\nu = \nu_0 - \nu_r$  はレーザーの発振周波数  $\nu_0$  と基準共振器の共振周波数  $\nu_r$  の差、  $\Delta\nu_r$  は基準共振器の線幅 (FWHM) をそれぞれ表す。  $\kappa$  は入射光の共振器への結合効率で  $\kappa = (F \cdot T/\pi)^2$  と表され、  $F$  は共振器のフィネス、  $T$  は共振器入射鏡の強度透過率を表す。また  $M$  は周波数変調の変調指数を表す。こうして得られた誤差信号をもとにレーザーの共振器長に負帰還制御をかけることによって、レーザー周波数を基準共振器の共振周波数に安定化することができる。この方法の特長は、高い周波数 (>10 MHz) で FM 変調を行って誤差信号を得るためショット雑音 (量子雑音) 限界で決まる S/N 比が達成できる。また共振器からの反射光を検出することによって、その誤差信号は共振器の線幅より低い周波数領域では周波数弁別器として用いられ、帯域外の高い周波数領域では位相弁別器として用いることができるため共振器の線幅を越える広帯域制御ができる。

この方法で制御した場合の周波数雑音の抑圧限界を求めてみる。変調周波数  $\nu_m$  での検出器のショット雑音 (量子雑音) は、

$$I_n^2 = 2eI_{\min} \times 2 \quad (5)$$

で表される。  $I_{\min}$  はレーザー周波数が共振器の共振状態にあるときの検出器での DC 光電流で、  $I_{\min} = I_0 \{J_0(M)^2 \times (1 - \sqrt{\kappa})^2 + J_1(M)^2 + J_{-1}(M)^2\}$  で表される。周波数制御のゲインを十分大きくした場合、最終的に得られる周波数雑音限界は (5) 式のショット雑音によって決まり、その周波数雑音スペクトル密度は、

$$\tilde{\nu} = \Delta\nu_r \sqrt{\frac{h\nu}{\eta P_0}} \cdot \frac{1}{M} \cdot \frac{(1 - \sqrt{\kappa})}{\sqrt{\kappa}} \quad [\text{Hz}/\sqrt{\text{Hz}}] \quad (6)$$

になる。ただし  $M < 1$  として  $J_0(M) = 1$ ,  $J_1(M) = M/2$  とおき、  $I_{\min} = e\eta P_0(1 - \sqrt{\kappa})^2/h\nu$  とした。この式を用いて制御時の周波数雑音および線幅の限界を求めてみると、  $\Delta\nu_r = 150 \text{ kHz}$ ,  $P_0 = 1 \text{ mW}$ ,  $h\nu = 3.5 \times 10^{-19} \text{ J}$ ,  $\eta = 0.8$ ,  $M = 0.3$ ,  $\kappa = 0.1$  より  $\tilde{\nu} = 0.02 \text{ Hz}/\sqrt{\text{Hz}}$  となる。これは線幅にして約  $1 \text{ mHz}$  に相当する。

この式を先のシャウロウ・タウンズの関係式 (1) と比

較すると、レーザー共振器の線幅が外部基準共振器の線幅に、レーザー光出力が周波数弁別の際の検出器での実効的な光パワーにそれぞれ対応する。この (6) 式よりレーザー共振器よりも共振線幅の狭い基準共振器を用いることによって、周波数制御時の周波数雑音は非制御時の自然放出雑音限界以下に小さくすることが可能である。このことは負帰還によってレーザー共振器の  $Q$  値が実効的に向上することに相当しており、自然放出自身を制御しているわけではない。またこうして負帰還制御によって取り除ける周波数雑音は共振器の線幅および制御帯域によって制限されており、この帯域以上の高いフーリエ周波数の周波数雑音は取り除くことはできない。しかしこのように外部共振器を用いて周波数制御する方法がレーザー共振器自身の  $Q$  値を上げる方法よりも優っている点は、レーザーの外部のほうがより高い  $Q$  値と外乱の影響を受けにくい安定な基準共振器を得やすいからである。

一方、レーザー共振器の  $Q$  値を上げる方法として、外部共振器からの光帰還を用いた方法があり、半導体レーザーによく用いられる<sup>10)</sup>。半導体レーザーの場合、レーザー共振器長が短いことと端面反射率が小さいことによって共振器の  $Q$  値が小さいため、外部共振器を使って  $Q$  値を上げることは非常に有効である。ただし振動などによる外部共振器とレーザー共振器間の距離の変動によって帰還光の位相が変わり制御が不安定になる問題点がある。

### 3. 超高コヒーレントレーザー

高フィネスファブリペロー基準共振器を用いたレーザーの周波数制御による高コヒーレントレーザーの実現例をいくつか紹介し、その手法および得られた安定度を紹介する (表 1)。

J. Hall らのグループは  $1 \text{ Hz}$  を大幅に下回る線幅を He-Ne レーザーを用いて実現している (図 2)<sup>11)</sup>。これは 2 台の He-Ne レーザーの周波数をそれぞれ独立に安定な基準共振器にロックすることにより両者のビート信号から  $50 \text{ mHz}$  に相当する線幅が得られている。また中心周波数は基準共振器の共振周波数に対して  $\pm 1.5 \text{ Hz}$  の誤差の範囲にロックすることができた。この実験に用いている基準共振器はフィネス 3500 で線幅  $70 \text{ kHz}$  のものを用いている。この実験結果は現在報告されているなかで最も狭い線幅を示すものである。しかし、得られた線幅 ( $\Delta\nu = 50 \text{ mHz}$ ) は、先のシャウロウ・タウンズの式で与えられる自然放出による線幅の限界値 ( $\Delta\nu_0 \sim 1$

mHz) よりも 1 桁以上大きな値である。このグループの続報によると、同一の基準共振器に安定化した 2 台のレーザー間の相対的な周波数揺らぎはアラン分散にして  $8 \times 10^{-17}$  ( $\tau=300$  s) になる<sup>12)</sup>。また長期間の周波数安定度は共振器長のドリフトによって決まり、これは  $\sim 20 \times 10^{-10}/\text{day}$  であることが確認された。

色素レーザーは可視域を中心に広い波長範囲で発振可能でまた波長可変なためこのレーザーの周波数安定化は応用上非常に重要である。色素レーザーは色素ジェット面の揺らぎによる周波数雑音が比較的高い周波数領域まで存在するためその線幅はフリーラン状態では数十 MHz 程度である。このため高いフィネスのファブリペロー共振器と Pound-Drever 法を用いて数 MHz 以上の広帯域にわたって周波数制御する必要がある<sup>8)</sup>。周波数制御の結果、レーザー周波数は基準共振器の共振周波数に対して  $\pm 1$  Hz 以下の精度で安定化できることが確認されている<sup>13)</sup>。またこのように周波数安定化した色素レーザーを用いた単一イオンの高分解能分光によって線

幅約 80 Hz のスペクトルが得られていることから、レーザーの絶対周波数の揺らぎも 80 Hz 以下であることが確認されている<sup>3,14)</sup>。

最近、半導体レーザー励起固体レーザーがその高変換効率および高安定な性質から非常に注目されており、とくにこれをレーザー干渉計型重力波検出計のための周波数超高安定化レーザーとして用いることが検討されている<sup>1)</sup>。Shoemaker らは最近、半導体レーザー励起 Nd:YAG レーザーを周波数制御することにより mHz 程度に相当する線幅を得たことを報告している<sup>15)</sup>。周波数雑音のスペクトル密度は非制御時には 1 kHz で約  $100 \text{ Hz}/\sqrt{\text{Hz}}$  あったが、これに制御を施すと検出器のショット雑音で決まる値の  $\bar{\nu}=12.5 \text{ mHz}/\sqrt{\text{Hz}}$  にまで減少している (図 3)。この値から見積もられる線幅は mHz のオーダーになる。またこの値は (1) 式より得られる自然放出による周波数雑音の限界値、 $\bar{\nu}=200 \text{ mHz}/\sqrt{\text{Hz}}$  を大きく下回るものである。

同様の実験が Day らによっても報告され、半導体レ

表 1 超高コヒーレントレーザーの実現例

レ ー ザ ー	波 長	周 波 数 安 定 度	文 献
He-Ne	633 nm	$\Delta\nu$ (FWHM) $\sim 50 \text{ mHz}^{\text{a)}$	11)
Dye laser	486 nm	$\Delta\nu \sim 1 \text{ Hz}^{\text{b)}$	13)
Dye laser	563 nm	$\Delta\nu \sim 80 \text{ Hz}^{\text{c)}$	3), 14)
LD pumped Nd: YAG	1064 nm	$\nu=12.5 \text{ mHz/Hz}$ (@1 kHz), $\Delta\nu \sim 1 \text{ mHz}^{\text{b)}$	15)
LD pumped Nd: GGG	1062 nm	$\nu=0.834 \text{ Hz/Hz}$ , $\Delta\nu=3 \text{ Hz}^{\text{a)}$	16)
Diode laser	830 nm	$\Delta\nu=560 \text{ Hz}^{\text{b)}$	17)
Diode laser with O-F <sup>d)</sup>	830 nm	$\Delta\nu \sim 1 \text{ Hz}^{\text{b)}$	18)

- a) 2 本のレーザーのヘテロダイニート信号より評価した値。
- b) 周波数制御に用いた F-P 反射光の誤差信号から評価した値。
- c) 高分解能分光によってそのスペクトル線幅より評価した値。
- d) 外部 F-P 共振器からの光帰還を用いた半導体レーザー<sup>10)</sup>。

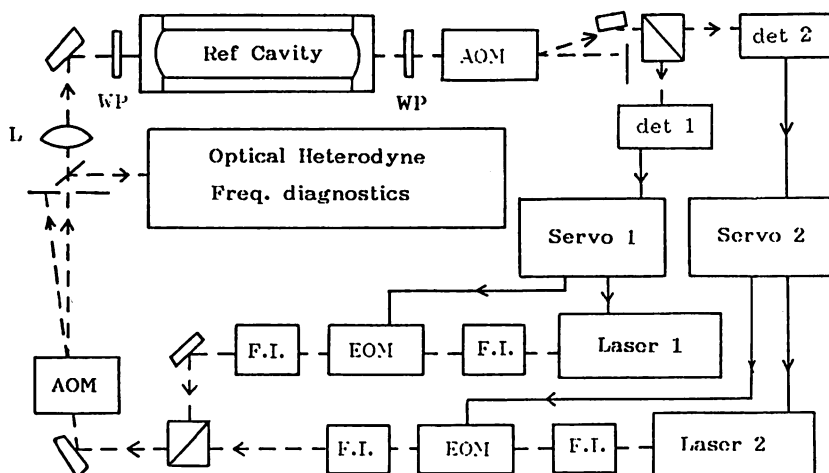


図 2 2 台の He-Ne レーザーを用いた周波数安定度の評価<sup>11)</sup>

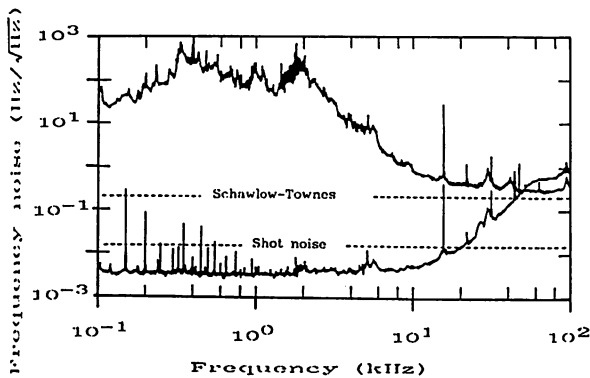


図3 半導体レーザー励起 Nd:YAG レーザーの周波数安定化<sup>15)</sup>  
 上の曲線: 非制御時の周波数雑音のスペクトル密度, 下の曲線: 制御時の周波数雑音スペクトル密度.

レーザー励起 Nd:GGG レーザーを周波数制御することによって 3 Hz 以下の線幅を実現している (図 4)<sup>16)</sup>. この報告では, それぞれ独立に制御を施した 2 台のレーザーのビート信号から線幅 3 Hz という値を直接求めており, これは検出器のショット雑音限界で決まる線幅よりも約 1 桁ほど大きい. これらの報告より半導体レーザー励起固体レーザーは周波数超安定化レーザーを実現するのにきわめて有望であることが確認された.

一方, 半導体レーザーの周波数雑音は非制御時には非常に大きく線幅にして数 MHz~100 MHz 程度である. しかし注入電流によって広帯域にわたって周波数変調が可能のため, 周波数制御を施すことによって周波数安定度をきわめて高くすることが可能である. Ohtsu らは高

フィネス外部共振器と注入電流による負帰還制御を使って約 560 Hz の線幅が実現できたことを報告している<sup>17)</sup>. この値は先の (3) 式で表される半導体レーザーの場合の自然放出雑音限界で決まる線幅を大きく下回るものである. また外部のファブリペロー共振器からの光帰還によって半導体レーザーの線幅は 10 kHz 程度にまで下げられることが Dahmani らによって示されている<sup>10)</sup>. さらに最近, Shin らによってこの光帰還を用いてあらかじめ線幅を約 10 kHz に狭窄化した半導体レーザーを高フィネス基準共振器を使って周波数制御することによって約 1 Hz の線幅に相当する周波数雑音の抑圧が実現されている<sup>18)</sup>.

このように基準共振器を用いた周波数制御によってレーザーの周波数安定度は先の (5) 式で表される検出器のショット雑音 (量子雑音) で決まる限界にほぼ達することが確認されている. しかしこうしたレーザーの周波数安定度向上は基準共振器に対する相対的な安定度の向上で, 外乱による基準共振器自身の揺らぎによってレーザーの絶対周波数の安定度は大きく制限されてしまう. このためレーザーの真の周波数超安定化を得るには基準共振器の安定度向上が必須である. 現在, ファブリペロー共振器に用いられている誘電体多層膜ミラーの性能は非常に良くなってきており, 反射率 99.99% 以上, 損失 100 ppm 以下, フィネスにして 70,000 以上が実現されている. これは共振器の線幅  $\Delta\nu_r < 10 \text{ kHz}$ ,  $Q$  値にして  $Q = \nu_r / \Delta\nu_r \sim 10^{11}$  に相当する. それに対して共振器の共振周波数をその分解能  $1/Q \sim 10^{-11}$  以下の安定度に保つ

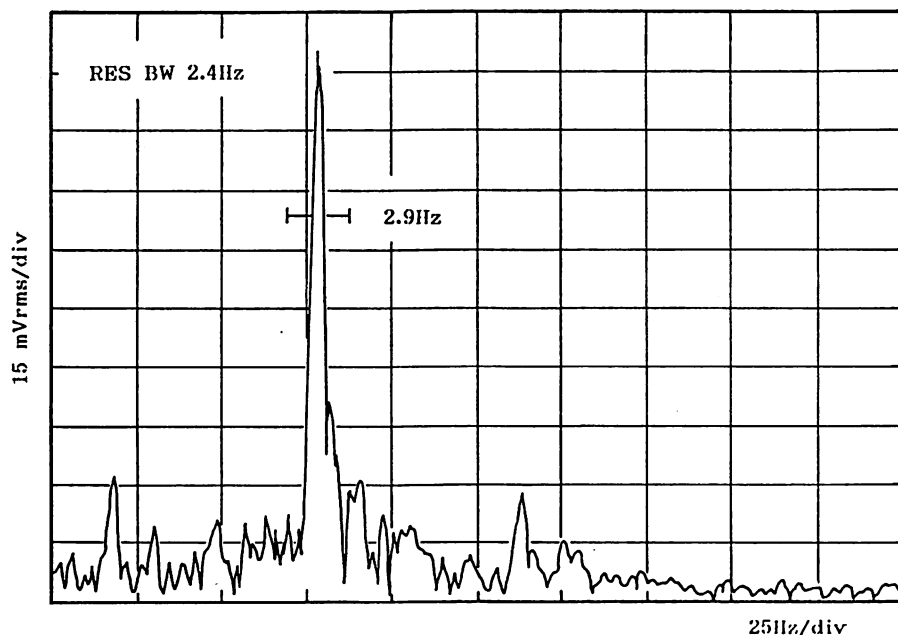


図4 周波数安定化した 2 台の Nd:YAG レーザーのヘテロダインビート信号<sup>16)</sup>

ためには、その共振器のスペーサーの長さをきわめて安定にしなければならない。たとえば可視域で数 Hz 以下のレーザーの周波数揺らぎは周波数安定度にして約  $10^{-14}$  に相当する。これは共振器長 0.25 m とすると共振器のスペーサー長の変化は実に  $2.5 \times 10^{-5}$  Å 以下にしなければならない。これはスペーサーの材料に温度膨張係数約  $10^{-8}$  のゼロデュアと呼ばれるセラミックガラスを用いたとしても温度揺らぎを  $10^{-6}$  K 以下に制御する必要がある。また周囲の温度揺らぎや振動および音響による影響を避けるため、 $P < 10^{-6}$  Torr 以下の高真空中にワイヤーで釣り下げられる。このように外部の揺らぎの影響を極力排除しても低い周波数領域 (<100 Hz) の振動を完全に取り除くことはむずかしく、これが実際の安定度を決めている。また長期の安定度は残留ガスの影響やスペーサーの材料自身の変形などによる大きなドリフトがある<sup>13)</sup>。このような基準共振器の安定度の限界によって、周波数高安定化レーザーの実質的な周波数変動は数 10 Hz、周波数安定度にして  $\Delta\nu/\nu_0 \sim 5 \times 10^{-14}$  程度であろう。

このため線幅 1 mHz 以下、周波数安定度が  $10^{-18}$  以下の周波数超高分解能レーザーを実現するには、いままで用いられてきたファブリ・ペロー基準共振器に代わる新しい周波数基準が必要になるだろう。その一つに原子および分子の高分解能分光を用いて絶対周波数を安定化する方法があり、これは現在長さの標準として用いられている周波数安定化 He-Ne レーザーに用いられている。レーザー周波数の短期安定度を高フィネスのファブリ・ペロー共振器を用いた周波数制御で向上し、振動および温度揺らぎによるドリフトが大きく影響する長期安定度は原子・分子の高分解能分光を用いて得ようとするものである<sup>14)</sup>。しかし先の超高分解能を得るには、原子・分子の吸収線の線幅は少なくとも 1 Hz 以下が要求される。このような超高分解能な分光を利用する具体的な応用については次の章でふれることとする。

#### 4. 超高分解能レーザーの応用

現在、最もレーザーの周波数安定性が要求される応用分野としてあげられるのはレーザー干渉計型重力波検出器のための光源である。この重力波検出に要求されるレーザーの性能に関しては詳しくは先の大橋らによる解説<sup>1)</sup>を参照してもらい、ここではこのためのレーザーの周波数安定化および高出力化についての最近の研究を紹介する。

周波数超高分解能および高出力なレーザーを実現する方

法としては、低出力の半導体励起 Nd:YAG レーザーを周波数安定化し、これをマスターレーザーとして高出力 (>10 W) のフラッシュランプ励起 Nd:YAG レーザー注入同期することが現在考えられている。マスターレーザーとしての半導体励起 Nd:YAG レーザーに関しては先の章でも示したようにきわめて高い周波数安定度が実現されており、周波数雑音密度にして  $\bar{\nu} = 12.5$  mHz/ $\sqrt{\text{Hz}}$  (@ 1 kHz) 程度である<sup>15)</sup>。しかし重力波検出に要求されるレーザーの周波数雑音は少なくともさらにこれよりも  $10^{-4}$  小さい値であるが<sup>1)</sup>、これはさらにフィネスが高いファブリ・ペロー共振器および高出力なレーザーを用いて周波数弁別感度の向上を図れば安定度はさらに向上すると思われる。一方、高出力化に関してはこの半導体励起 Nd:YAG レーザーをフラッシュランプ励起の Nd:YAG レーザーに注入同期を行うことによって 10 W 以上の高出力が得られている<sup>19,20)</sup>。得られた高出力スレーブレーザーの周波数雑音はマスターレーザーのそれより若干悪くなる程度である。この高出力スレーブレーザーもフラッシュランプ励起から高出力半導体レーザー励起に置き換えることが考えられており<sup>19)</sup>、これによって超高分解能・高出力・高効率なレーザーが実現できることになる。

現在、周波数および時間の標準として使われている Cs 原子時計の周波数安定度および周波数確度は、装置のサイズ、磁場の不均一性や二次のドップラー効果による周波数シフトなどの要因によって制限されており、これ以上の飛躍的な性能向上はむずかしい。これに対して最近、イオントラップ中の 1 個のイオンを原子時計に用いることが提案されており、これによって周波数安定度および確度を大幅に向上できる可能性が示唆されている<sup>21)</sup>。現在提案されているものはレーザー冷却によって 1 個の水銀イオン ( $\text{Hg}^+$ ) を極低温にして捕捉し、これからのマイクロ波 (40 GHz) または紫外光 (282 nm) の遷移を周波数標準として用いようとするものである。とくに紫外域 (282 nm) の電気四重極遷移の自然幅は 1 Hz 程度と見積もられているため、自然幅で決まる分解能を得るにはレーザーの線幅は 1 Hz 以下が要求される。現在、この 282 nm の紫外光は 563 nm の色素レーザーの SHG を利用している。高分解能分光の結果、約 80 Hz の分解能が得られており<sup>3,14)</sup>、これは用いた周波数安定化色素レーザーの線幅によっておもに制限されている (図 5)<sup>3)</sup>。この周波数安定化レーザーに使われている基準共振器のフィネスは約 70,000 で、線幅にして約 8 kHz である。先の章で述べたようにレーザー周波数は

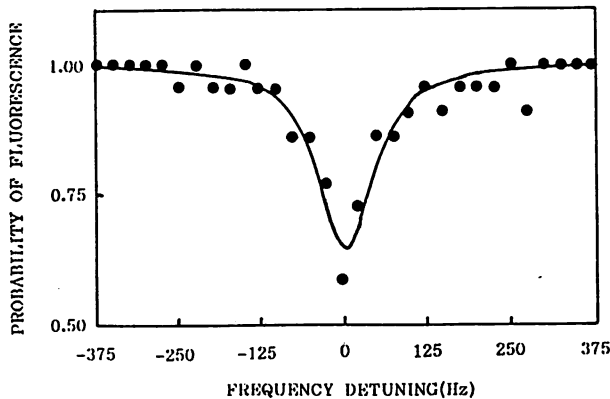


図5 イオントラップ中の単一  $\text{Hg}^+$  イオンの高分解能分光<sup>3)</sup>. 563 nm 色素レーザーの周波数に対する単一  $\text{Hg}^+$  イオンからの蛍光強度をプロットしたもの.

基準共振器の共振周波数に対して  $\pm 1$  Hz 程度の誤差範囲で安定化できるようになっているため、レーザーの真の周波数安定度は基準共振器の安定度によって決まる。この単一イオンの高分解能分光を用いることによってレーザー周波数の真の線幅および周波数安定度が評価できることになる。きわめて正確な温度制御および徹底的な除振によって基準共振器の短期安定度向上を行い、 $\text{Hg}^+$  イオンの自然幅 (1.3 Hz) で決まる高分解能分光を用いて長期安定度向上を行うことができれば、周波数精度  $10^{-15}$ 、周波数安定度  $10^{-15}$  以下の周波数超高安定化レーザーが実現しうる。現在この実験には  $\text{Ar}^+$  レーザー励起色素レーザーが用いられているが、これをさらに安定度が良い半導体レーザー励起固体レーザーなどに置き換えることが検討されている。

このような超高コヒーレントレーザーを用いた原子の高分解能分光はこの他にも基本的な物理定数の精密測定や物理の基本法則の検証などに応用することもいくつか考えられている。その一つに水素原子の 1S-2S 遷位の高分解能分光による遷移周波数の精密測定がある<sup>22)</sup>。この水素の 1S-2S 間の遷移周波数は約  $2.5 \times 10^{15}$  Hz (波長 121 nm) で、その自然幅は 1.3 Hz であるためこの自然幅で決まる分解能で測定すれば  $5 \times 10^{-16}$  の精度でその周波数を決定することができる。この 1S-2S 間の遷移周波数から、1S 準位のラムシフトを精密に導き出すことができ、量子電気力学 (QED) による計算値と比較してその検証を行うことができる。また現在約  $10^{-9}$  の精度で求められているリュドベルグ定数をさらに高精度で決定することも可能になる。現在までのところ測定はセル内の水素原子を用いているためその分解能は 10 MHz 程度であるが<sup>22)</sup>、低温に冷却した原子線源や原子噴水の方法を用いることによって自然幅 1.3 Hz 程度の

分解能を達成することも不可能ではない。このような高分解能分光を行うにはレーザーの線幅は少なくとも自然幅の 1.3 Hz 以下である必要がある。また測定した紫外光の遷移周波数を周波数領域で測定するには、周波数チェーンと呼ばれる手法を用いて紫外域のレーザーの周波数を赤外およびマイクロ波領域まで周波数変換して原子時計による周波数標準と比較する<sup>23)</sup>。このため紫外域から可視および赤外にわたって多くの周波数高安定化レーザーを用意する必要がある。

また物理の基本法則である特殊相対性理論の検証にも周波数超高安定化レーザーが必要とされており、その一つに空間の異方性の測定がある。ファブリ・ペロー共振器に周波数安定化したレーザーを用いて共振器の方向に依存するレーザー周波数の変化を測定した例があり、空間の異方性は長さの変化にして  $\Delta l/l = 1.5 \times 10^{-15}$  以内であることが確かめられている<sup>24)</sup>。しかしこれは共振器内では光が往復するため一方の光速は計れない。これに対して最近、Ne 原子ビームのドップラーフリー二光子吸収を用いた実験がある<sup>25)</sup>。これは2次のドップラー効果により生ずる周波数シフトを精密測定することによって一方の光速の方向依存性を調べるものである。この実験によると、光速の異方性の上限は  $\Delta c/c \leq 3 \times 10^{-9}$  であることが確認された。この結果は主に実験の系統的な誤差によって制限されているため、さらに高精度な実験が計画されている。

## 5. おわりに

以上、レーザーの極限的な性能の追求という観点から超高コヒーレントレーザーの実現およびその応用に関して紹介してきた。レーザーのコヒーレンスの追求はレーザーが発明されて以来の永遠のテーマであり、これから先も引き続き研究が続けられるであろう。周波数超高安定化レーザーは基礎物理だけでなく産業分野においても今後必要不可欠なものになっており、この実現はこれらの応用分野に大きなインパクトをもたらすだろう。また一方、レーザーの周波数安定度のさらなる向上にはきわめて安定な周波数基準が必要となっており、これには原子・分子の超高分解能分光などの手法が必要不可欠になると考えられる。このため、超高コヒーレントレーザーの実現はこの応用分野である原子物理、量子光学などの研究とともにその成果を互いに取り入れながら進めていく必要があるだろう。

## 文 献

- 1) 大橋正健, 藤本眞克: “レーザー干渉計による重力波検出”, 光学, **19** (1990) 505-510.
- 2) D. J. Wineland, W. M. Itano, J. C. Bergquist, J. J. Bollinger, F. Diedrich and S. L. Gilbert: “High accuracy spectroscopy of stored ions,” *Frequency Standards and Metrology*, ed. A. DeMarchi (Springer-Verlag, Berlin, 1989) pp. 71-77.
- 3) B. G. Levi: “Ion sits still for sharp ‘picture’ of its optical transition,” *Phys. Today*, **42**, 9 (1989) 17-18.
- 4) Y. Yamamoto and H. A. Haus: “Preparation, measurement and information capacity of optical quantum states,” *Rev. Mod. Phys.*, **58** (1986) 1001-1020.
- 5) A. Schawlow and C. Townes: “Theory of infrared and optical masers,” *Phys. Rev.*, **112** (1958) 1940-1949.
- 6) A. Yariv and W. Caton: “Frequency, intensity, and field fluctuations in laser oscillators,” *IEEE J. Quantum Electron.*, **QE-10** (1974) 509-515.
- 7) D. Welford and A. Mooradian: “Output power and temperature dependence of the linewidth of single-frequency cw (GaAl) As diode lasers,” *Appl. Phys. Lett.*, **40** (1982) 865-867.
- 8) R. Drever, J. Hall, F. Kowalski, J. Hough, G. Ford, A. Munley and H. Ward: “Laser phase and frequency stabilization using and optical resonator,” *Appl. Phys. B*, **31** (1983) 97-105.
- 9) 盛永篤郎: “位相安定レーザーの実現”, 光学, **16** (1987) 380-386.
- 10) B. Dahmani, L. Hollberg and R. Drullinger: “Frequency stabilization of semiconductor lasers by resonant optical feedback,” *Opt. Lett.*, **12** (1987) 876-878.
- 11) C. Salomon, D. Hils and J. L. Hall: “Laser stabilization at the milihertz level,” *J. Opt. Soc. Am. B*, **5** (1988) 1576-1587.
- 12) D. Halls and J. L. Halls: “Ultra-stable cavity-stabilized lasers with subhertz linewidth,” *Frequency Standards and Metrology*, ed. A. DeMarchi (Springer-Verlag, Berlin, 1989) pp. 162-173.
- 13) R. Kallenbach, C. Zimmermann, D. H. McIntyre and T. W. Hänsch: “A blue dye laser with sub-kilohertz stability,” *Opt. Commun.*, **70** (1989) 56-60; R. Kallenbach, T. W. Hänsch and R. G. DeVoe: “Locking of a 486 NM dye laser at the subhertz level,” proceeding of the CLEO '89 Postdeadline Papers PD 30 (1989).
- 14) M. G. Raisen, F. Elsner, J. C. Bergquist, W. M. Itano and D. J. Wineland: “Spectroscopy of a single  $^{199}\text{Hg}^+$  ion,” *Technical Digest of 17th IQEC* (Optical Society of America, Anaheim, 1990) p. 218.
- 15) D. Shoemaker, A. Brillet, C. N. Man, O. Cregut and G. Kerr: “Frequency-stabilized laser-diode-pumped Nd: YAG laser,” *Opt. Lett.*, **14** (1989) 609-611.
- 16) T. Day, E. K. Gustafson and R. L. Byer: “Active frequency stabilization of a 1.062- $\mu\text{m}$ , Nd: GGG, diode-laser-pumped nonplanar ring oscillator to less than 3 Hz of relative linewidth,” *Opt. Lett.*, **15** (1990) 221-223.
- 17) M. Ohtsu, M. Murata and M. Kouroggi: “FM noise reduction and subkilohertz linewidth of an AlGaAs laser by negative electrical feedback,” *IEEE J. Quantum Electron.*, **QE-26** (1990) 231-241.
- 18) C-H. Shin and M. Ohtsu: *Opt. Lett.* (投稿中).
- 19) C. D. Nabors, A. D. Farinas, T. Day, S. Y. Yang, E. K. Gustafson and R. L. Byer: “Injection locking of a 13-W cw Nd: YAG ring laser,” *Opt. Lett.*, **14** (1989) 1189-1191.
- 20) O. Cregut, C. N. Man, D. Shoemaker, A. Brillet, A. Menhert, P. Peuser, N. P. Schmitt, P. Zeller and K. Wallmeroth: “18 W single-frequency operation of an injection-locked, cw, Nd: YAG laser,” *Phys. Lett. A*, **140** (1989) 294-298.
- 21) D. J. Wineland, W. M. Itano, J. C. Bergquist and F. L. Walls: “Proposed stored  $^{199}\text{Hg}^+$  ion frequency standards,” *Proceedings of the 35th Annual Frequency Control Symposium* (USAERADCOM, Fort Monmouth, 1981) pp. 602-611.
- 22) R. G. Beausolei, D. H. McIntyre, C. J. Foot, E. A. Hildum, B. Couillaud and T. W. Hänsch: “Continuous-wave measurement of the 1S lamb shift in atomic hydrogen,” *Phys. Rev. A*, **35** (1987) 4878-4881.
- 23) D. A. Jennings, C. R. Pollack, F. R. Petersen, R. E. Drullinger, K. M. Evenson, J. S. Wells, J. L. Hall and H. D. Layer: “Direct frequency measurement of the I<sub>1</sub>-stabilized He-Ne 473-THz (633-nm) laser,” *Opt. Lett.*, **8** (1983) 136-138.
- 24) A. Brillet and J. L. Hall: “Improved laser test of the isotropy of space,” *Phys. Rev. Lett.*, **42** (1979) 549-552.
- 25) E. Riis, L-U. A. Andersen, N. Bjerre, O. Poulse, S. A. Lee and J. L. Hall: “Test of the isotropy of the speed of light using fast-beam laser spectroscopy,” *Phys. Rev. Lett.*, **60** (1988) 81-84.



## 超高安定レーザーの実現へ向けて

中 川 賢 一\*・大 津 元 一\*

重力波がもたらす空間の極微小な歪を検出する重力波検出器には極めて高い感度が要求され、現在のところレーザー干渉計による検出方法が最も有望とされている。しかしこの干渉計に用いるレーザー光源には周波数雑音にして  $\delta\nu/\nu \sim 10^{-21}/\sqrt{\text{Hz}}$  程度の極めて高い周波数安定度が要求され、さらにショット雑音による検出限界から光出力 1 kW 程度が必要とされる。しかしながらこの両方の性能を満足するレーザーは現在のところ実現されていない。そこでこのような超高安定・高出力レーザーの実現方法およびその問題点を考えてみる。

### レーザーの周波数安定度を決めるもの

単一周波数で発振しているレーザーからの光は共振器内に混入してくる自然放出によってその位相がランダムな揺らぎを受ける。このため次式、

$$\delta\nu = \Delta\nu_0 (2h\nu_0/P_0)^{1/2} \quad [\text{Hz}/\sqrt{\text{Hz}}] \quad (1)$$

で表される周波数雑音が本質的に存在する<sup>1)</sup>。  $\Delta\nu_0$  はレーザー共振器の共振線幅、  $\nu_0$  はレーザーの周波数、  $P_0$  は出力パワーを表す。この式よりレーザー共振器の  $Q$  値 ( $=\nu_0/\Delta\nu_0$ ) を高くし、さらに出力パワー  $P_0$  を増大すればより低い周波数雑音が得られる。しかしレーザー共振器内には利得媒質やモード選択素子等があるため  $Q$  値をあまり高くできないため、外部のより高い  $Q$  値の基準共振器を用いて制御する方法がとられる。この時のレーザーの周波数雑音の理論的限界は基準共振器の線幅  $\Delta\nu_r$  と制御に用いる光パワー  $P_r$  で決まる光検出器の量子雑音によって決まり、先の (1) 式と同様に、

$$\delta\nu = \Delta\nu_r (2h\nu_0/\eta P_r)^{1/2} \quad [\text{Hz}/\sqrt{\text{Hz}}] \quad (2)$$

によって与えられる。ここで  $\eta$  は光検出器の量子効率を

表す。この (2) 式より先に述べた重力波検出器に必要な条件を求めると、波長  $\lambda = 1.06 \mu\text{m}$  のレーザーを用いた場合には周波数雑音  $\delta\nu \sim 3 \times 10^{-7} \text{ Hz}/\sqrt{\text{Hz}}$  程度が必要で、このためには線幅  $\Delta\nu_r = 1.5 \text{ kHz}$  の基準共振器で光パワー  $P_r = 10 \text{ W}$  が最低限必要になる。

### 現在の周波数安定化および高出力化の実現状況とその問題点

先に述べたような高い周波数安定度および高出力パワーを実現できるレーザーとしては、高い励起効率、低雑音、高出力化が可能な半導体レーザー励起 Nd:YAG レーザーが現在、最も有望とされている。このレーザーと線幅  $\Delta\nu_r \sim 1 \text{ MHz}$  の基準共振器を用いて周波数安定化を行い、周波数雑音にして  $\delta\nu = 10^{-2} \text{ Hz}/\sqrt{\text{Hz}}$  程度が得られている<sup>2)</sup>。また高出力化は、ランプ励起の高出力 Nd:YAG レーザーに注入同期を行うことによって 10 W 以上の単一モード出力が得られている<sup>3)~4)</sup>。このためさらに線幅の狭い基準共振器を用いれば周波数雑音  $\delta\nu = 10^{-4} \text{ Hz}/\sqrt{\text{Hz}}$  ( $\delta\nu/\nu = 3 \times 10^{-19}/\sqrt{\text{Hz}}$ ) 程度が、またすべて半導体レーザー励起による Nd:YAG レーザーによって出力数 10 W 程度までは現在の技術の延長上で充分可能と思われる。

しかしこれ以上の安定度および出力向上を実現するためには多くの解決しなくてはならない技術的な問題に直面する。先に求めた基準共振器の線幅  $\Delta\nu_r = 1.5 \text{ kHz}$  を実現するには、共振器長  $L = 10 \text{ m}$  でフィネス  $F = 10000$  が必要で、注入する光パワー  $P_r = 10 \text{ W}$  の時には内部光パワーは実に 30 kW にも達する。このことから周波数安定化においては、

・高反射率、低損失、高いパワーに耐えられるミラーコーティング

\* 東京工大総合理工 Ken'ichi Nakagawa, Motoichi Ohtsu: Ultra Stable Laser

- 基準共振器の徹底的な除振
  - 入射光の共振器モードへのモードマッチング性能の向上
  - レーザー光の空間的なモードの安定化およびビーム方向制御
  - 高い量子効率で高い光パワーで使用できる光検出器の開発
  - 散乱光, 不必要な反射光の検出器への混入, およびレーザーへの戻り光を極力小さくする
- などの点をこれから解決していく必要がある。

出力パワー向上に関しては, 数 10 W 以上を越えると半導体レーザー励起 Nd:YAG レーザーを用いてもレーザー媒質の熱的な揺らぎや放熱による振動等の影響が無視できなくなり, 周波数およびモードの安定度向上は非常に難しくなると思われる。このため複数のレーザー光出力をコヒーレントに足し合わせる方法が有望である<sup>9)</sup>。これを実現するにはレーザー間の正確な周波数・位相トラッキングや正確なモードマッチングおよびビーム方向制御を行う必要がある, 先の周波数安定化と同様の問題を解決する必要がある。

#### 今後の展望

超高安定レーザー実現に向けて解決しなくてはならない問題点の多くは重力波検出器である干渉計においてもあてはまる共通の問題である。このためレーザーと干渉計を独立に考えることはあまり意味がなく, これからは

両者を一体のものとして基本設計をする必要があるだろう。これは例えば基準共振器およびレーザーまでも干渉計の一部に取り込んだ構造なども考えられる。こう考えるとこの重力波検出用干渉計の実現は巨大な超高安定レーザーの実現と言っても良いだろう。またこの干渉計は  $10^{23}$  個もの光子を 1 ms 近くの時間にわたって共振器に閉じ込める事に相当し, 光ストレージリングと言えるかも知れない。この様な観点から考えるとこれから必要なのは光の状態をもれなく測定してかつ任意に制御するための理論および技術であろう。このような問題点が解決されて重力波検出器が実現されればこれは単に物理の基本法則の検証と言う本来の目的だけでなく, 量子光学, 超精密計測, 光デバイス等の幅広い分野の発展に多く貢献するだろう。

#### 参考文献

- 1) A. Schawlow, C. Townes, *Phys. Rev.*, 112 (1958), 1940-1949.
- 2) D. Shoemaker, A. Brillat, C. N. Man, O. Cregut and G. Kerr, *Opt. Lett.*, 14 (1989), 609-611.
- 3) C. D. Nabors, A. D. Farinas, T. Day, S. Y. Yang, E. K. Gustafson and R. L. Byer, *Opt. Lett.*, 14 (1989), 1189-1191.
- 4) O. Cregut, C. N. Man, D. Shoemaker, A. Brillat, A. Menhert, P. Peuser, N. P. Shmitt, P. Zeller and K. Wallmeroth, *Phys. Lett. A*, 140 (1989), 294-298.
- 5) G. A. Kerr and J. Hough, *Appl. Phys. B*, 49 (1989), 491-495.

# 5

## Spectroscopy by Semiconductor Lasers

M. OHTSU AND K. NAKAGAWA

*Graduate School at Nagatsuta, Tokyo Institute of Technology, Midori-ku,  
Yokohama, Kanagawa, Japan*

### 5.1. INTRODUCTION

Stable gas, dye, and solid-state lasers have been employed as coherent light sources for high resolution, nonlinear laser spectroscopy. Recent progresses in semiconductor devices have made it possible to achieve high output power, low frequency fluctuations, and wideband tunability in room-temperature and continuous-wave (CW) operated semiconductor lasers. It can be claimed that the performance of some of these lasers has already surpassed that of other types of lasers. This progress has made it possible to use semiconductor lasers for high-resolution laser spectroscopy. Furthermore, it is interesting to note that these semiconductor lasers oscillate at the wavelength range of between 0.7 and 1.6  $\mu\text{m}$ , which has not been obtained by other types of lasers. Because of this wavelength range, a new field of spectroscopy, for example, spectroscopy of overtones or combination tones in organic molecular vapors, can be exploited. Furthermore, low price, small volume, and low power consumption in semiconductor lasers are quite attractive for spectroscopists who have been troubled with expensive maintenance charges and huge laser systems.

Considering these facts pointed out above, semiconductor lasers could play an essential role in several fields of high-resolution spectroscopy. This chapter will demonstrate such techniques. Prior to this demonstration, FM noise characteristics of semiconductor lasers and their control techniques will be reviewed in Sections 5.2 and 5.3. Very high quality and low noise semiconductor lasers are required for high-resolution laser spectrometer systems, which is quite different from other application systems. A part of these sections may overlap with those of other chapters in this book.

---

*Coherence, Amplification, and Quantum Effects in Semiconductor Lasers*, Edited by Yoshihisa Yamamoto.

ISBN 0-471-512494 © 1991 John Wiley & Sons, Inc.

However, most of the parts are discussed from a viewpoint of its applications to spectroscopy. Several topics in the laser spectroscopy and their applications will be described in Sections 5.4 and 5.5. A summary is given in 5.6.

## 5.2. CHARACTERISTICS OF SEMICONDUCTOR LASERS TO BE CONSIDERED TO REALIZE SINGLE-MODE OSCILLATION

A semiconductor laser exhibits essentially multilongitudinal-mode oscillation because the linewidth of its gain spectrum is about 100 times broader than separation between the adjacent longitudinal modes. Such the laser has the following specific oscillation characteristics:

1. *Mode-Hopping.* Semiconductor lasers usually shows multilongitudinal-mode oscillation if they employ a conventional Fabry-Perot-type cavity that is fabricated by cleaving or chemical etching of the crystal facets. In this case, power switching between the longitudinal modes occurs.
2. *Mode Partition.* Even though the power of the specific longitudinal mode is larger than those of others, that is, in the case of nearly single-longitudinal-mode oscillation, transient decrease of the main mode power and increase of the other submode power occurs. This decrease in the main mode power is called *power dropout*.

Both phenomena have been interpreted as quantum-mechanical phenomena, which are triggered by mutually uncorrelated spontaneous emission fluctuations introduced into each mode. Power fluctuation characteristics due to these phenomena are governed by cross-saturation characteristics of the gains in these modes, for which intraband relaxation of the carrier in the conduction band plays an essential role. Mode power fluctuations stemmed from these phenomena follow the statistics of a Poisson process, and unified theoretical models have been presented by introducing an analogy with phase transition of the first order in classical thermodynamics [1]. From this theoretical work, it was pointed out that the frequency of occurrences of these power fluctuations decrease exponentially with the increase of the bias level. It can also be decreased by enhancing the cross-gain saturation. For this enhancement, the tellurium (Te) was doped into the clad layer so that the DX center formed by this dopant worked as a saturable absorber [2, 3].

The 1.3- and 1.5- $\mu\text{m}$ -wavelength InGaAsP lasers have more advanced cavity structures: DFB (distributed feedback) or DBR (distributed Bragg reflector)-type laser cavities, to realize a more reliable nearly single-longitudinal-mode oscillation for applications in optical communication sys-

tems. This DFB structure has recently been employed successfully for 0.8- $\mu\text{m}$ -wavelength AlGaAs lasers [4]. Even for these longitudinal-mode controlled lasers, the mode partition phenomenon cannot be neglected if the power ratio between the main and sublongitudinal modes are less than 40 dB, which could induce errors in spectral assignments in high resolution and highly sensitive laser spectrometers [5]. To overcome this difficulty, electrodes for current injection into the laser were divided into two or three parts to suppress the spatial hole burning of the carrier so that the power of the sublongitudinal modes could be reduced [6].

Even when the nearly single-longitudinal-mode oscillation can be realized by solving these problems, deterministic instability can be induced if the emitted light from the laser is injected back into the laser itself from the external reflecting surface [7, 8]. To avoid this instability, a high-quality optical isolator with the isolation of higher than 60 dB is required.

For the discussions given in Section 5.3, it is assumed that each problem presented above has been solved to realize a reliable nearly single-longitudinal-mode oscillation.

### 5.3. REALIZATION OF A WIDEBAND HYPERCOHERENT OPTICAL SWEEP GENERATOR FOR SPECTROSCOPY

A highly coherent and widely tunable light source is required for spectrometer systems. It is demonstrated in this section that such a light source can be realized by utilizing efficiently frequency-controllable semiconductor lasers.

#### 5.3.1. Frequency Fluctuations of a Single-Longitudinal-Mode Semiconductor Laser

The primary measures that have been used for representing the magnitude of optical frequency fluctuations (FM noise) are power spectral density and the Allan variances [9, 10]. They are measures in the Fourier frequency and the time domain, respectively. In the case of white FM noise, the field spectral profile of laser oscillation takes a Lorentzian shape and its half-linewidth could be used as a convenient measure for representing the FM noise magnitude because the linewidth is proportional to the magnitude of the white noise power spectral density.

Figure 5.1 shows a power spectral density of the intrinsic FM noise. Most fundamental noise source is the spontaneous emission fluctuations (curve *A*). It gives a quantum noise limit of the free-running laser, which corresponds to the FM noise of the coherent state or is called the *Schawlow-Townes limit* of the field spectral linewidth [11]. Probability of

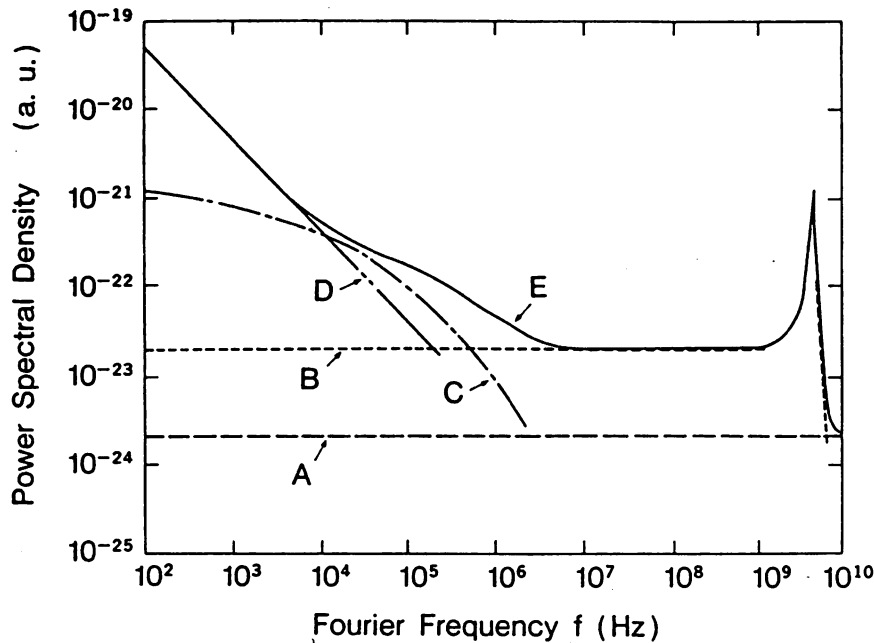


**Figure 5.1.** Power spectral density of the FM noise of a semiconductor laser induced by intrinsic noise sources. Curve *A*, spontaneous emission fluctuations; *B*, carrier-density fluctuations; *C*, temperature fluctuations; *D*,  $1/f$  fluctuations. Curve *E* represents the total intrinsic FM noise by superposing the values of curves *A*–*D*.

occurrences of spontaneous emission events is proportional to the number of cavity modes, and the magnitude of FM noise due to spontaneous emission are proportional to cavity loss.

Carrier density could also be varied by the spontaneous emission, which could induce the fluctuations of refractive index of the cavity and give additional FM noise (curve *B* in Figure 5.1). Since the carrier density fluctuations are very fast, the adiabatic approximation of this fluctuation cannot be made. Frequency modulation noise due to the carrier density fluctuations have the second-order lag characteristics due to the interband relaxation time and photon lifetime, which exhibits the low-pass characteristics with the cutoff determined by the relaxation oscillation frequency of several gigahertz. The power spectral density of this FM noise exhibits a resonant peak at this frequency. Since center frequencies of the real and imaginary parts of the complex gain spectrum of the laser medium differ, the FM noise could be induced by the carrier density fluctuations, which simultaneously induce the power fluctuations (IM noise) also. The ratio between the FM noise magnitudes due to spontaneous emission and carrier density fluctuations can be expressed by  $\alpha^2$ . The quantity  $\alpha$  has been called a *linewidth enhancement factor* or “ $\alpha$ -parameter,” which takes the values of 2–9 [12].

The third source of the FM noise is the temperature fluctuation (curve *C* in Figure 5.1) induced by the carrier density fluctuation. There is also a low-pass characteristic with a cutoff frequency determined by the thermal

response time constant of the laser device. These three kinds of FM noise give the intrinsic quantum noise originated from the laser.

In addition to these factors,  $1/f$  noise could be observed at a low Fourier frequency range (curve *D* in Figure 5.1). It could give the power-independent width of the field spectrum [13]. Although the origin of this fluctuation has not yet been identified, possible origins are fluctuations of carrier mobility [14], fluctuations of state occupation probability of active carriers [15], and so on. Furthermore, current fluctuations from the current source and ambient-temperature fluctuations could contribute as external noise sources to generate additional FM noise. All of these noise sources contribute to the FM noise of a free-running laser [16].

### 5.3.2. Frequency Modulation Characteristics

Direct frequency modulation (FM) capability by modulating the injection current plays an essential role in reducing FM noise. Therefore, it could be important to investigate the direct FM response characteristics because they could limit the performance of negative electrical feedback and optical feedback systems designed for FM noise reduction. Figure 5.2 shows those of a 1.5- $\mu\text{m}$  InGaAsP laser and a 0.8- $\mu\text{m}$ -wavelength AlGaAs laser (CSP, or channeled substrate planar, type) [17]. Mechanisms of the direct FM are attributed to thermal effect and carrier density effect at lower and higher modulation frequency ranges, respectively. They have a low-pass characteristic with the cutoff determined by a thermal response time constant of the device and relaxation oscillation frequency, respectively. Since the direct FM response characteristics are a superposition of these two effects, modulation efficiency shown by Figure 5.2*a* is, in general, inhomogeneous for a wide modulation frequency range. These characteristics depend on the transverse spatial distributions of the carrier density and  $\alpha$  parameter [18]. In particular, the phase lag characteristics shown by Figure 5.2*b* limit the frequency control bandwidth. Homogeneous modulation characteristics have been obtained recently by controlling the spatial carrier density distribution by segmenting electrodes for current injection [19]. Curve *C* in Figure 5.2 represents the result.

### 5.3.3. Principle and Method of Frequency Control

The magnitude of laser FM noise  $\delta\nu(t)$  can be expressed as [20, 21]

$$\delta\nu(t) = \kappa_{cl} \cdot (1 + \alpha^2) \cdot \Gamma_s(t) + \Gamma_{ex}(t) - \int_0^\infty h(\tau) \cdot \{\delta\nu(t - \tau) + \Gamma_n(t - \tau)\} \cdot d\tau \quad (5.1)$$

where  $\kappa_{cl}$  is the cavity loss,  $\alpha$  is the  $\alpha$  parameter,  $\Gamma_s(t)$  is the spontaneous

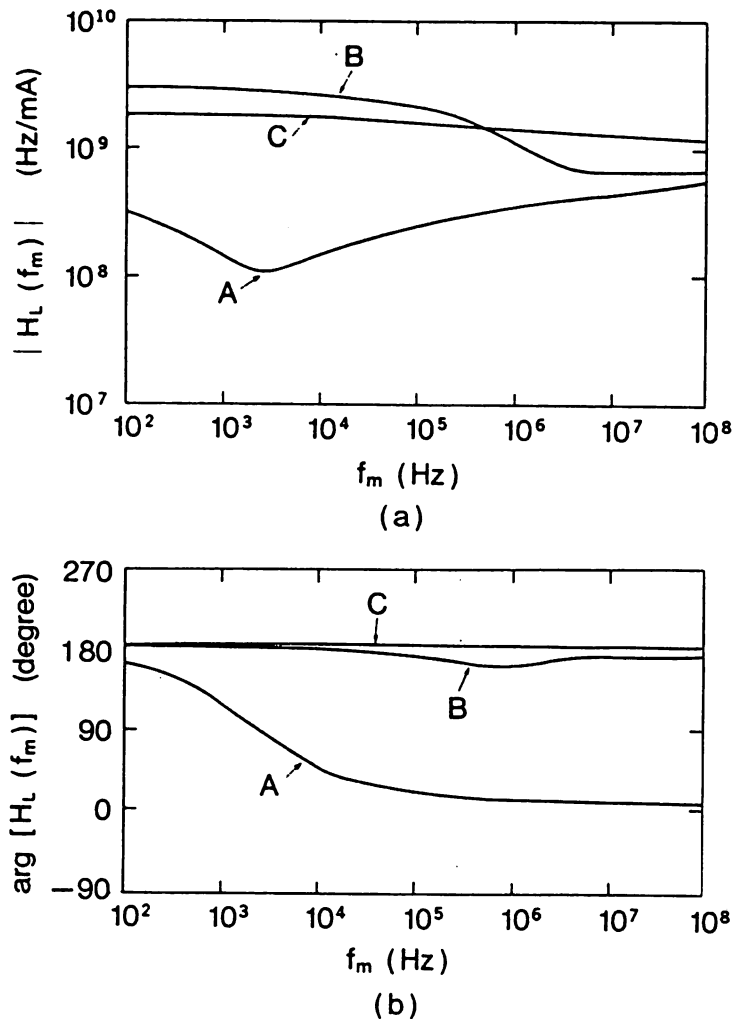


**Figure 5.2.** Complex transfer function  $H_L(f_m)$  representing the direct FM responses of a 1.5- $\mu\text{m}$  InGaAsP laser (curve *A*) and a 0.8- $\mu\text{m}$  CSP-type AlGaAs laser (curve *B*) [17, © 1988 IEEE]. Curve *C* represents a 1.5- $\mu\text{m}$  segmented electrode InGaAsP laser [19, © 1987 IEEE]. Panels (a) and (b) illustrate for the absolute value and argument of  $H_L(f_m)$ , respectively.

emission fluctuation, and  $\Gamma_{\text{ex}}(t)$  is the fluctuation due to external noise sources. These terms represent the magnitude of the FM noise of the free-running laser. An convolution integral in the right-hand side of this equation represents the effect of negative electrical feedback described below. In this integral,  $h(\tau)$  is the impulse response function of the feedback loop,  $\delta\nu(t - \tau)$  is the magnitude of the FM noise detected by the feedback loop, and  $\Gamma_n(t - \tau)$  is the noise magnitude originating from the frequency discriminator element of the feedback loop. On the basis of this equation, at least four methods can be found to reduce the FM noise: (1) negative electrical feedback [21], (2) optical feedback [22], (3) improvements in performance of laser devices, and (4) suppressing the spontaneous emission by the method of cavity quantum electrodynamics (cavity QED). These methods are described and compared with each other in the following.



**5.3.3.1. Negative Electrical Feedback.** As is represented by the convolution integral in Eq. (5.1), an operating parameter (e.g., the injection current) is controlled to vary the laser frequency to compensate for the detected FM noise. Features of this method are:

1. A laser cavity structure does not have to be modified.
2. The feedback loop has a high gain and narrow-to-medium bandwidth.
3. Selective feedback is possible within a specific range of Fourier frequency. In this case, quite a high gain of the feedback loop can be realized, which will provide a promising system for FM laser spectroscopy, a very long baseline laser interferometer for a resonant-type antenna of gravitational wave detection, and so on.
4. The magnitude of the FM noise can be reduced below the spontaneous emission level (coherent state) of the free-running laser by using a high-gain and low-noise feedback loop. That is, Fourier transform of Eq. (5.2) gives

$$F(f) = \frac{\kappa_{cl} \cdot (1 + \alpha^2)}{1 + H(f)} \cdot \Pi_s(f) + \frac{1}{1 + H(f)} \cdot \Pi_{ex}(f) - \frac{H(f)}{1 + H(f)} \cdot \Pi_n(f) \quad (5.2)$$

where  $f$  is a Fourier frequency and  $F$ ,  $\Pi_s$ ,  $\Pi_{ex}$ ,  $\Pi_n$ , and  $H$  represent the Fourier transforms of  $\delta\nu$ ,  $\Gamma_s$ ,  $\Gamma_{ex}$ ,  $\Gamma_n$ ; and  $h$  of Eq. (5.1), respectively. This equation means that the first and second terms of Eq. (5.2), that is, the contributions from the quantum and external noise sources, can be suppressed by the infinite gain of the feedback loop ( $|H| \rightarrow \infty$ ). The magnitude of the last term converges to  $|\Pi_n|$  by the infinite gain; thus, the FM noise reduction limit is given by the magnitude of the shot noise from the photodetector used for FM noise detection. In other words, the shot noise corresponds to the quantum noise limit of the laser under negative electrical feedback condition. The magnitude of FM noise at the shot noise limit can be lower than that of the spontaneous emission limit (coherent state) of the free-running laser. Therefore, such a state of low FM noise by negative electrical feedback can be called the *hypercoherent state* [23].

5. Stability of the system is high because the feedback is negative.
6. The feedback loop can be designed optimally by computer simulation of the feedback loop through analogy with the design criteria of the conventional analog electrical feedback circuit. By this optimum design technique, highly reproducible experimental results can be obtained.

**5.3.3.2. Optical Feedback.** The convolution integral in Eq. (5.1) does not appear in this method. Instead, the cavity loss  $\kappa_{cl}$  is reduced by modifying cavity structures. Characteristics of this method are:

1. Feedback loop has a medium to high gain and medium to wide bandwidth that depends on the inverse of the photon lifetime in the modified cavity.
2. Modified cavity structure is simple. For this reason, this method has been used for more than 15 years [22].
3. Deterministic instability, such as coherent collapse [24], can be induced. Effective optical coupling and moderate optical feedback should be required to avoid this instability by fixing thin films on a laser cavity facet for an antireflection coating. Furthermore, feedback control of the external cavity length is also required by using, for example, a piezoelectric transducer. Therefore, this method can be called an *optomechanical feedback*. The hypercoherent state is not generated because of the absence of a FM noise detection system and an external feedback loop.
4. Mode-hopping between adjacent longitudinal modes of the external cavity can be induced. A method of monitoring and suppressing this mode-hopping has been proposed [25, 26].
5. Efficiency of direct frequency modulation is drastically reduced.

By injecting a reflected light from an external reflector, the field spectral linewidth of 2 kHz has been realized [27]. Laser frequency can be swept by using a diffraction grating as the external reflector. However, continuous sweep is difficult because of the hopping between the external longitudinal modes, as well as that between the internal longitudinal modes of the laser itself. In spite of these mode-hoppings, a total sweep range as wide as 100 nm has been demonstrated by fabricating the laser device by introducing a quantum well structure [28].

To keep the optical feedback system stable enough by controlling the phase of the reflected light, the optical path length between the external reflector and the laser facet should be controlled by using, a device such as a piezoelectric transducer (PZT). In order to avoid this control system, a self-pumping-type phase conjugation mirror has been used as an external reflector [29]. However, the stability characteristics of this optical feedback system have been limited because of the slow response of the phase conjugation medium.

As a more stable version of optical feedback, the method of using a confocal Fabry–Perot interferometer as an external reflector has been proposed [30], and a field spectral linewidth of about 10 kHz has been realized. The experimental setup of this system is shown in Figure 5.3. In

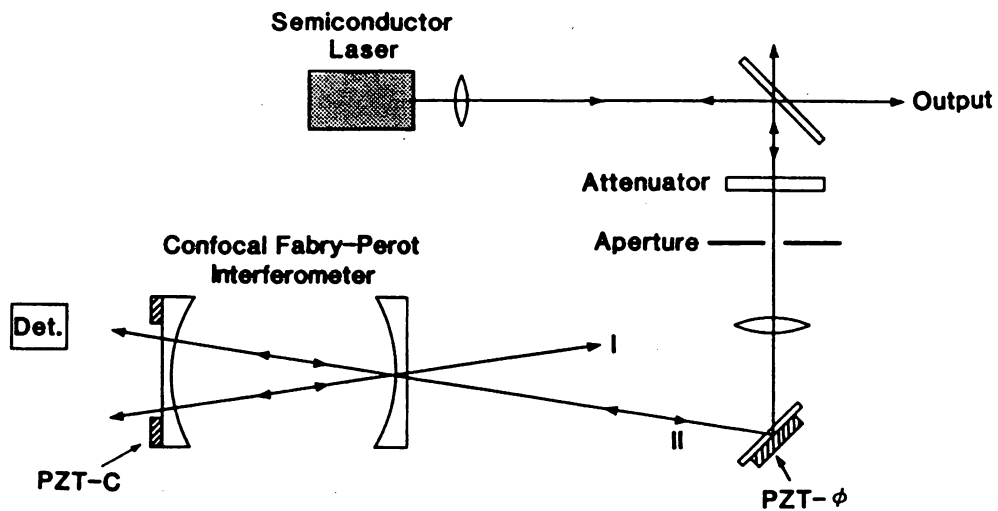
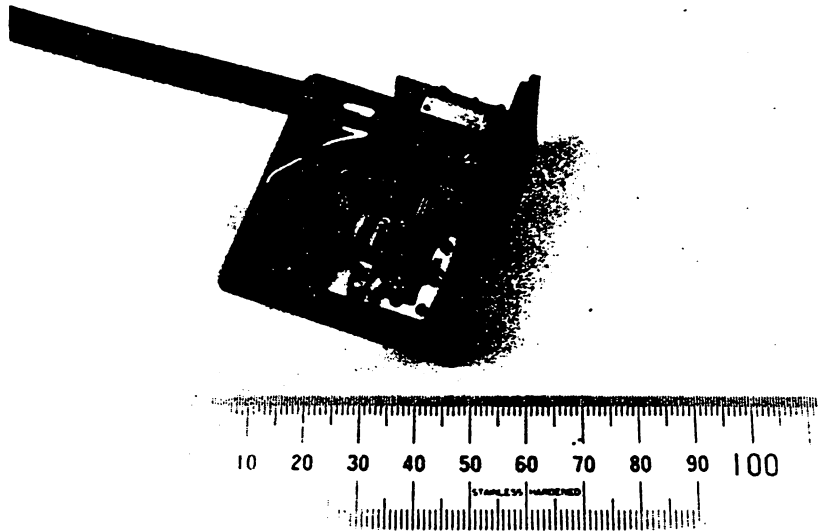


Figure 5.3. Experimental setup of FM noise reduction by optical feedback from a confocal Fabry-Perot interferometer [30].

this system, transmitted light, after resonating in the Fabry-Perot interferometer, is injected into the laser. Since the Fabry-Perot interferometer works as a frequency-dependent reflector, the laser frequency is pulled into the resonance frequency of this interferometer, and the laser FM noise is reduced. Control bandwidth is given by the half-width at the half-maximum of the resonance curve of the Fabry-Perot interferometer, which corresponds to the inverse of the photon lifetime of the interferometer. As is the case of using a single reflecting plate described above, the optical pass length between the laser and the Fabry-Perot interferometer should be controlled to maintain the stable optical feedback system. However, the precision of its control may be lower than that of the previous system [31]. In addition to this fact, this system has two more advantages. First, strong optical feedback from the Fabry-Perot interferometer is not required, by which intrinsic laser cavity structure is maintained. This laser system shows that the external mode suppression ratio is much higher than that of the conventional external-cavity lasers. Second, direct frequency modulation is still possible at the modulation frequency which is related by rational fractions to the free-spectral range of the Fabry-Perot interferometer [31, 32].

A compact and frequency-modulatable laser module has been fabricated by employing the techniques of microoptics and fiber optics to make a compact Fabry-Perot interferometer [33–35]. This module is demonstrated by Figure 5.4. This technique has also been applied for a  $0.67\text{-}\mu\text{m}$  visible AlGaInP laser to reduce its FM noise. As is shown in Figure 5.5, the half-linewidth of its field spectrum has been reduced to 50 kHz [36, 37]. This measured value was limited by a resolution of the delayed self-homodyne system of the linewidth measurements. It was confirmed that this value was  $2 \times 10^{-4}$  times that of the free-running laser. By



**Figure 5.4.** A compact and frequency-modulatable AlGaAs laser module [33–35, © 1990 IEEE]. The Fabry–Perot interferometer for optical feedback was made by employing the technique of microoptics.

employing simultaneously the optical feedback from a diffraction grating, the wavelength of this visible laser could be swept for over 5 nm.

**5.3.3.3. Improvements in Performances of the Laser Devices.** External optical and electrical elements should be connected to the laser devices for application of two methods described in Sections 5.3.3.1 and 5.3.3.2. However, it could sometimes be inconvenient for some practical industrial applications to use additional elements because of the increasing cost and

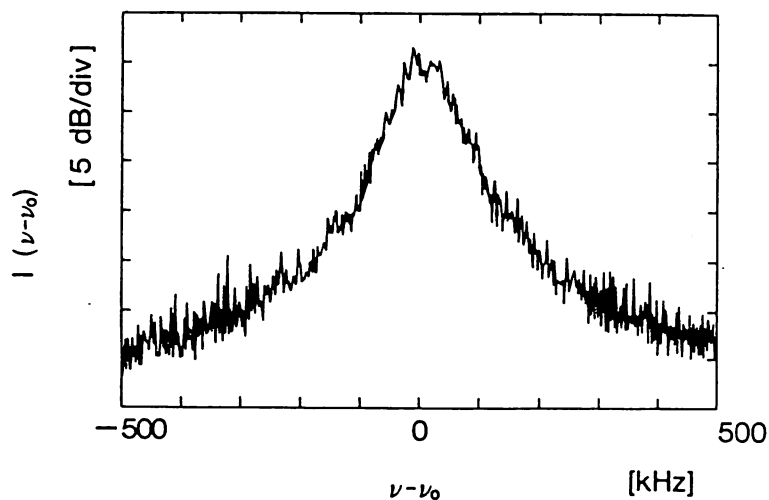


**Figure 5.5.** Field spectral profile  $I(\nu - \nu_0)$  of a 0.67- $\mu\text{m}$  AlGaInP laser whose FM noise was reduced by the optical feedback of Figure 5.3 [36, 37] ( $\nu_0$  is the center frequency of the spectrum). Its half-linewidth was 50 kHz, which was estimated by using a delayed self-homodyne technique with an optical fiber about 2 km long.

system volume. To overcome these difficulties, performance of laser device itself has been improved to realize a stable laser, which can be an interesting approach for laser device designers. This method provides a low to medium feedback gain, and the bandwidth is medium to wide because the photon lifetime in the laser cavity is shorter than that of the method described in Section 5.3.3.2. Even for this method, the negative electrical feedback loop should usually be added to improve the stability and reliability of these improved laser devices, and to increase the feedback gain. This method can be divided into two categories:

1. *Reductions of the Cavity Loss and  $\alpha$  Parameter.* Cavity loss of the laser device can be reduced by increasing the cavity length. Furthermore, segmented electrodes are fixed to the laser in order to reduce the spatial hole burning by controlling the currents injected into the segmented electrodes. As a more advanced method, a quantum well structure is introduced to adjust the center frequency of the real and imaginary parts of the complex gain spectrum to reduce the value of the  $\alpha$  parameter [38].

2. *Integration of the System Described in Section 5.3.3.1 or 5.3.3.2.* An external reflector and an optical waveguide for the optical feedback have been integrated with laser devices [39]. To avoid occurrences of deterministic instability, a phase controller was also integrated between the gain part for the laser oscillation and an external distributed Bragg reflector. As a result of this integration, a field spectral linewidth of about 100 kHz has been realized [40,41]. Furthermore, corresponding to the optical feedback system illustrated in Figure 5.3 two distributed Bragg reflectors and an optical waveguide were integrated to reduce the field spectral linewidth of a 1.5- $\mu\text{m}$  InGaAsP laser to 150 kHz [42]. The future problem of this system is the integration of these external components with the laser. For an negative electrical feedback system, the principal factor for limiting the feedback bandwidth is the length of the feedback loop. If frequency demodulators, photodetectors, and amplifiers can be integrated with the laser devices, its bandwidth can be expanded. From this point of view, electrical negative feedback is compatible with the technique of optoelectronics integration.

**5.3.3.4. Using the Method of Cavity Quantum Electrodynamics.** The magnitude of the spontaneous emission fluctuations, specifically, the value of  $\Gamma_s$  of Eq. (5.1), can be reduced by the method of cavity QED [43]. In this method, spontaneous emission rate is reduced by reducing the number of cavity modes by using a microcavity. Since this method is still at the early stage of development, several problems remain to be solved; for instance, the spontaneous emission rate is enhanced at the resonance frequency of the cavity. It should be inhibited to realize a low-noise laser.

Several experiments have already been carried out at the microwave frequency region. Similar experiments have recently been carried out at

the optical frequency region to control the spontaneous emission rate [44], and fabrication techniques of optical microcavity have been developed [45]. As another approach to control the spontaneous emission rate, realization of band structure of photon energy has been proposed by localizing the photon in the medium with the three-dimensionally periodical distribution of the refractive index [46,47]. By utilizing these new quantum optical approaches, realization of novel laser devices with low quantum noise is expected in the future.

#### 5.3.4. Example of a Hypercoherent Optical Sweep Generator by Negative Electrical Feedback

To realize a stable optical sweep generator for high-resolution laser spectroscopy, a reliable method is the negative electrical feedback. Although the feedback bandwidth is about 100 MHz, it is wide enough for the spectroscopy because most of the spectrometer system have a bandwidth narrower than 100 MHz. The bandwidth of the negative electrical feedback can be expanded by employing the optoelectrical integration technique in the future.

At least five subjects should be considered to realize a reliable optical sweep generator: (1) stabilization of the center frequency of the field spectrum, (2) improvement of the accuracy of the stabilized center frequency, (3) linewidth reduction of the field spectrum, (4) frequency tracking to the other coherent laser, and (5) accurate and wideband frequency sweep. Experimental results obtained by the authors' group and future outlook of the improvement of the system performances are introduced in the following.

Figure 5.6 represents the synthesized system of negative electrical feedback to solve simultaneously the five problems presented above [21]. It appears rather complicated; however, the total volume of the system can be maintained far smaller than those by using other kinds of lasers. Further reductions of the total volume can be expected if several optical or electrical components will be integrated with the lasers in the future.

**5.3.4.1. Center Frequency Stabilization of the Field Spectrum.** The center frequency of the field spectrum can be stabilized if a slow FM noise components (e.g.,  $f < 1$  Hz) are reduced by using a DC servocontrol loop. Since these slow FM noise components are usually caused by temperature fluctuations and  $1/f$  fluctuations, a low drift and stable frequency demodulator, composed of frequency reference and discriminator, is indispensable for this feedback system. Resonance spectral lines in atomic or molecular vapors can be used for such the frequency demodulators.

Absorption spectral lines due to higher harmonics or combination tones of vibration-rotation transitions in organic molecular vapors (e.g.,  $\text{NH}_3$  [48],  $\text{H}_2\text{O}$  [48, 49],  $\text{C}_2\text{H}_2$  [50],  $\text{HCN}$  [51]) can be used conveniently because

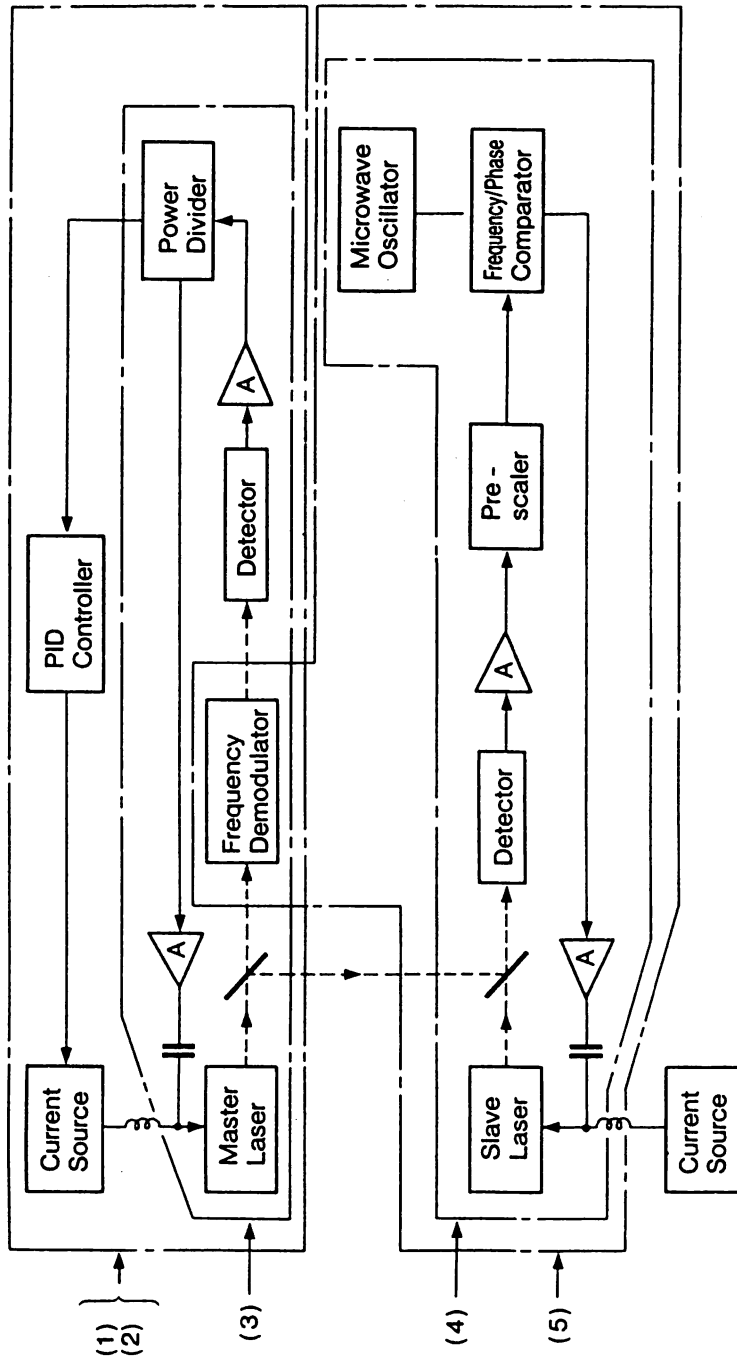


Figure 5.6. The synthesized system of negative electrical feedback to solve the five problems simultaneously [21, © 1988 IEEE]. The five blocks in this figure represent (1) stabilization of the center frequency of the field spectrum, (2) improvement of the accuracy of the stabilized laser frequency, (3) linewidth reduction of the field spectrum, (4) frequency tracking to the other coherent laser, and (5) accurate and wideband frequency sweep.

a great number of these spectral lines are distributed around the wavelength region of 0.7–1.6  $\mu\text{m}$ . The problems are their broad spectral linewidths, weak absorption coefficients, and difficulties in spectral assignments. To overcome these difficulties, strong spectral lines at the 0.8- $\mu\text{m}$ -wavelength region due to electronic transitions in atomic vapor (e.g., Rb [52], Cs [53]) have been used because their spectral assignments have been completed. They have further advantages in realizing a Doppler-free, narrow-linewidth saturation absorption spectral lines, reducing the volume of the gas cells, and so on. Since optogalvanic spectral lines in rare gases exhibit a large signal-to-noise ratio, it can be considered as another candidate [54]. Although it is rather difficult to realize a high-frequency stability because the reference frequency would be shifted as a result of plasma instability and the Stark effect in the discharged gases, a compact discharge lamp has been employed to realize a low-price frequency demodulator for 1.5- $\mu\text{m}$  InGaAsP lasers in order to realize a practical light source for optical communication systems [55]. As a novel method, the second harmonic frequency, which is generated from the active layer of the InGaAsP laser, has been stabilized to the Rb linear absorption spectral line in order to stabilize the 1.56- $\mu\text{m}$  InGaAsP laser frequency [56]. Although this second harmonic power is low, detection sensitivity of absorption spectral line can be increased by using a heterodyning technique with a 0.78- $\mu\text{m}$  AlGaAs laser, and furthermore, a technique of optical-optical double resonance could make it possible to detect Doppler-free absorption spectral lines in Rb by using a 0.78- $\mu\text{m}$  AlGaAs laser as a pumping light source [57]. From these facts, it can be claimed that low power in the internally generated second harmonics does not present any essential problems. Using a nonlinear organic waveguide, investigators have recently attempted to increase the efficiency of second harmonic generation [57]. For a stable frequency demodulator for a 0.67- $\mu\text{m}$  AlGaInP laser, several atomic vapors (e.g., Li) can be used.

Although a Fabry–Perot interferometer does not provide any absolute reference frequencies, it has been conveniently used as a frequency demodulator because of its simple structure. Since the value of its finesse has recently been increased up to several ten thousands, it has been demonstrated that high short-term stability (at the Fourier frequency range of  $f > 0.1$  mHz or the integration time range of  $\tau < 1 \times 10^4$  s) can be realized by using this supercavity, which has been higher than by using atomic or molecular spectral lines [58].

By using the frequency demodulators described above, a frequency stability as high as  $2 \times 10^{-12}$  has been obtained at the integration time of 100 s [59]. Although this value has not yet reached the shot noise limit generated from the photodetector in the feedback loop, theoretical analysis has estimated that the stability as high as  $1 \times 10^{-15}$  can be obtained if this shot noise limit is realized [21]. The most accurate frequency stability measurement is made by measuring the residual FM noise of the beat



frequency between the independently stabilized two lasers. For this purpose, an Allan variance real-time processing system has been developed for the accurate evaluation of frequency stability [60, 61].

#### 5.3.4.2. Improvement in the Accuracy of the Stabilized Center Frequency.

In high-resolution, high-precision laser spectroscopy system, the stabilized laser frequency should be accurately calibrated for precise spectral assignments and determining structural constants of atoms and molecules. From these critical requirements, accuracy of the stabilized laser frequency has to be improved. One of the principal phenomenon of limiting the accuracy of semiconductor laser frequency is a blue-shift (about  $20 \text{ MHz h}^{-1}$ ) due to the drift of the thermal resistance of the free-running laser device [62]. Furthermore, a drift of the reference frequency also limits the accuracy of the stabilized frequency. For example, a saturated absorption spectral line in Rb exhibits a frequency shift induced by the changes in incident laser power and ambient temperature [63]. Typical values of this frequency shift have been evaluated as  $-5 \text{ MHz}/(\text{mW cm}^{-2})$  and  $-0.8 \text{ MHz K}^{-1}$ , respectively. Those of  $\text{H}_2\text{O}$  vapor are about 10 times larger [64]. Furthermore, those of optogalvanic spectral lines in rare gases could be much larger because of the plasma instability and the Stark effect in the discharged gas, which can be concluded from a popular historical story that a Lamb-dip stabilized He-Ne laser has been replaced by a  $\text{CH}_4$ -stabilized He-Ne laser to avoid the frequency shift of the Lamb-dip of the He-Ne discharged gas [65]. From the comparison between the results reported so far, it can be concluded that spectral lines due to electronic transitions in atomic vapors are used as more accurate frequency demodulators than those of the higher harmonics or combination tones of vibration-rotation transitions in organic molecular vapors.

To calibrate accurately the stabilized laser frequency, absolute measurements of laser frequency are required. Harmonic mixers using metal-insulator-metal (MIM) point-contact diodes or Josephson devices have been conventionally used for this purpose [66]. However, since the MIM diodes have low sensitivities and the response of Josephson devices is slow [67], it is not practical to use them for the semiconductor lasers with wavelengths shorter than  $1.5 \mu\text{m}$ . Instead of measuring frequency, wavelength measurements have been employed by a scanning Michelson interferometer-type wavemeter for convenient and rough evaluations of the accuracy with the error of  $1 \times 10^{-7}$ – $10^{-8}$  [48, 49].

Several trials have recently been reported to realize a sensitive and fast photodetector by using a tunnel junction between thin films of a high- $T_c$  superconductor and a metal film [68], and by using a virtual charge-induced optical nonlinearity in a quantum well structure semiconductor device [69]. If these devices could be used as reliable harmonic mixers, practical systems of absolute frequency measurement may be realized to improve the accuracy as high as  $1 \times 10^{-10}$ .

**5.3.4.3. Linewidth Reduction of the Field Spectrum.** The half-linewidth of the field spectrum can be reduced by negative electrical feedback if its bandwidth  $B$  is wider than the half-linewidth of the free-running laser  $\Delta\nu_{FR}$  (i.e.,  $B > \Delta\nu_{FR}$ ). A sensitive and wideband frequency demodulator is required to realize a high gain and wideband feedback loop. For this purpose, a high-finesse Fabry–Perot interferometer described in Section 5.3.4.1, especially its reflection mode, has been used [70, 71]. Since the reflection mode works as an optical frequency differentiator, it exhibits a wider bandwidth of frequency demodulation than does the transmission mode [70–72]. Furthermore, to obtain a dispersive frequency demodulation output signal without modulating the laser frequency, several types of frequency demodulators have been proposed, such as (1) installing a Fabry–Perot interferometer in a Mach–Zehnder interferometer [73], (2) installing a polarizer in a Fabry–Perot interferometer [74], and so on. Figure 5.7 shows such a dispersive profile of the output signal from the frequency demodulator (installation method 1). It has also been confirmed that the gain of this demodulator is 10 dB larger and the bandwidth is equal to those of the reflection mode of the Fabry–Perot interferometer [73].

Optimum design of a phase compensation circuit in the feedback loop can be carried out in order to realize the largest gain and widest bandwidth of the feedback loop. For this design, computer-aided analog network design criteria can be employed based on the frequency response characteristics of each feedback element, such as a laser (see Figure 5.2), a frequency demodulator, and so on. Curve  $B$  of Figure 5.8 shows an experimental result for an  $0.8\text{-}\mu\text{m}$  AlGaAs laser (CSP type) by using such the optimized slow and fast feedback loops simultaneously [70, 71]. It represents the power spectral density of the residual FM noise. Curve  $A$  is the value of the free-running laser. It can be seen by comparing these curves that the feedback bandwidth is 40 MHz and the FM noise was reduced to 60–70 dB within the Fourier frequency range of 100 Hz–1 kHz. It means that the gain–bandwidth product of this feedback loop was as

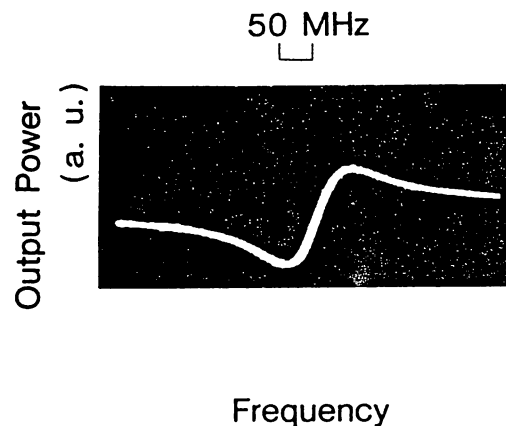


**Figure 5.7.** Relation between the laser frequency and the output power from the Mach–Zehnder interferometer, in which a Fabry–Perot interferometer is installed [73]. The sharp slope is used as a frequency demodulator.

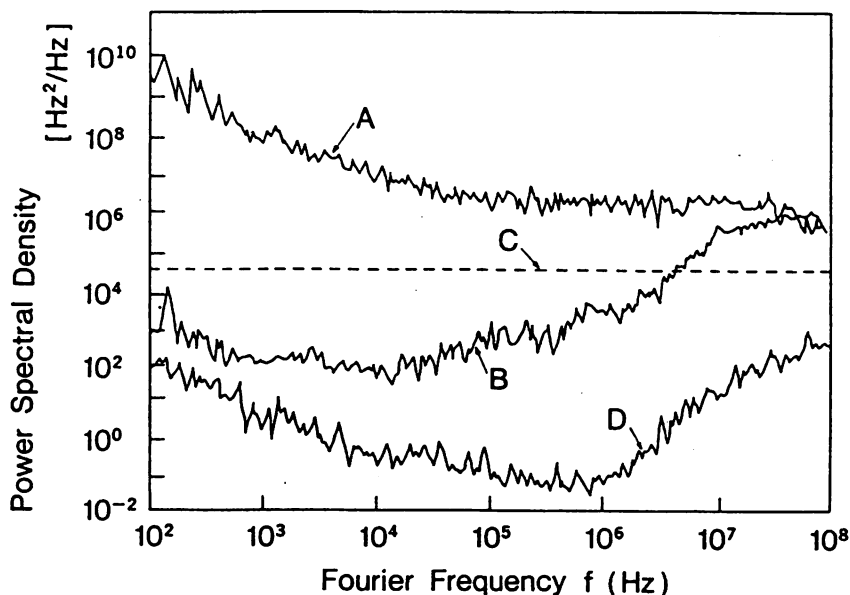


**Figure 5.8.** Power spectral density of the FM noise of a CSP-type AlGaAs laser [70, 71, © 1990 IEEE]. Curve *A*, free-running laser; *B*, under condition of negative electrical feedback; *C*, magnitude of the spontaneous emission noise, that is, FM noise in the coherent state of the free-running laser or the so-called Schawlow–Townes limit; *D*, limit of FM noise detection of the present experimental setup.

large as 50 THz (terahertz). For most laser spectrometers, the bandwidth obtained here could be sufficiently wide. Curve *C* represents the magnitude of the spontaneous emission noise, that is, the FM noise in the coherent state of the free-running laser, which was estimated by assuming the value of the  $\alpha$  parameter as 9 [12]. It can be confirmed that the value of curve *B* is lower than that of curve *C* at the Fourier frequency range below 4.4 MHz; thus, the hypercoherent state was realized in this range.

Curve *D* in Figure 5.8 represents the sensitivity of the frequency demodulator employed here, that is, the limit of FM noise reduction, which was determined by intrinsic IM noise of the laser. An optical balanced detector [75–77] could be effective to eliminate the contributions from this IM noise in order to realize the shot-noise limit of the feedback loop. It has been confirmed that the contribution from the IM noise can be reduced to 20–30 dB within the Fourier frequency range below 20 MHz [78]. Curves *A* and *B* of Figure 5.9 represent the field spectral profiles derived by applying the computer program of the fast Fourier transform to curves *A* and *B* of Figure 5.8, respectively [70, 71]. Curve *A* represents that the half-linewidth of the free-running laser is 4.5 MHz, while it can be seen from by comparing curves *A* and *B* that the FM noise within the  $\pm 40$ -MHz region around the center has been drastically reduced by the feedback. From the magnified profile given by Figure 5.9*b*, it is confirmed that the half-linewidth was reduced to 560 Hz, which is, to the authors' knowledge, the narrowest linewidth among the formally reported values.

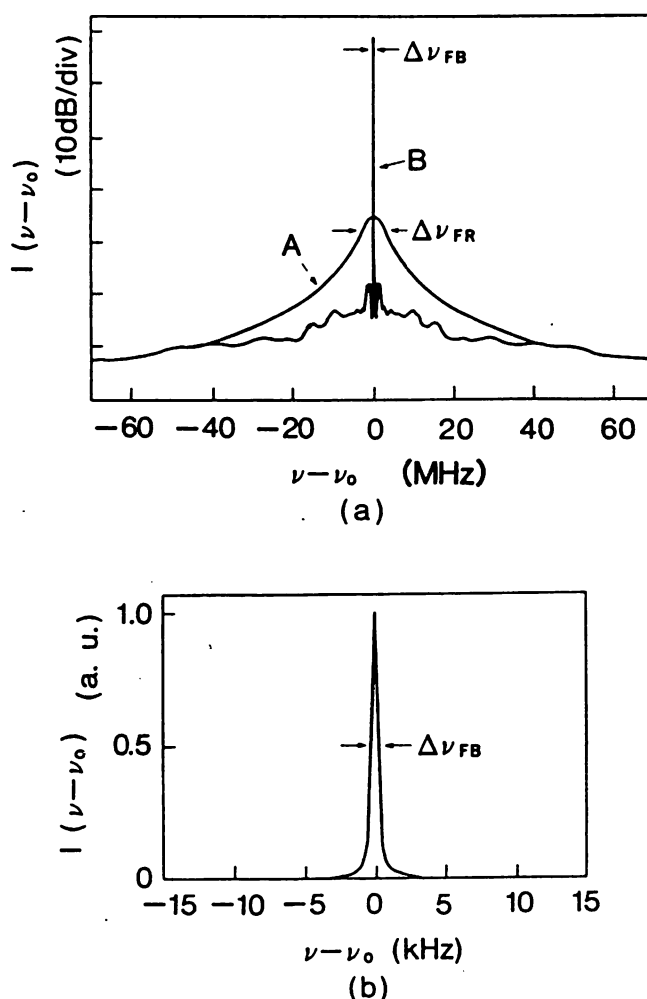


**Figure 5.9.** Field spectral profile  $I(\nu - \nu_0)$  of a CSP-type AlGaAs laser [70, 71, © 1990 IEEE], where  $\nu_0$  is the center frequency of the spectrum. (a) Curves *A* and *B* correspond to curves *A* and *B* in Figure 5.8, respectively. (b) Magnified profile of curve *B* in Figure 5.9a. The values of the half-linewidths for curves *A* and *B* are  $\Delta\nu_{FR} = 4.5$  MHz and  $\Delta\nu_{FB} = 560$  Hz, respectively.

This linewidth has been narrow enough even for ultra-high-resolution laser spectroscopy such as the subnatural linewidth spectroscopy, laser cooling, and so on. The half-linewidth estimated from curve *D* of Figure 5.8 is about 1 Hz, which corresponds to the linewidth reduction limit of the present experimental setup. It was estimated that the shot-noise limit of the present experimental setup could realize the half-linewidth of about 50 mHz [21].

**5.3.4.4. Frequency Tracking to the Other Coherent Laser.** If a stable laser can be realized by solving the problems mentioned in Sections 5.3.4.1–5.3.4.3, frequency tracking of the second laser (a “slave” laser) to this coherent laser (a “master” laser) is also an essential technique for a heterodyne-type or homodyne-type detection system for laser spectroscopy. Block 4 in Figure 5.6 represents such a frequency tracking loop,

that is, a frequency locked loop. To realize a heterodyne-type frequency locked loop, injection current of the slave laser is controlled so that the beat frequency between the two lasers is locked to the microwave local oscillator frequency, which has been called the *frequency offset locking* [79]. By this technique, the residual FM noise of the beat signal has been reduced to 0.2 Hz at the integration time of 100 s, which corresponds to the square root of the Allan variance of  $5 \times 10^{-16}$ , where the magnitude of this FM noise was normalized to the optical frequency [80]. This value is much smaller than that of the residual FM noise of the master laser, which means that the slave laser frequency tracks very accurately to the stable master laser. The capture and locking ranges of this loop were as wide as 2 GHz, which were limited by the bandwidth of the photodetector used as a heterodyne receiver [80].

It has been estimated that this FM noise can be reduced to about  $1 \times 10^{-18}$  by improving the performance of the feedback elements such as a frequency–phase comparator [33, 80]. By these improvements, phase fluctuations (PM noise) of the beat signal can also be reduced to lower than 1 radian; in other words, a heterodyne-type phase locked loop can be realized [81]. Figure 5.10 shows experimental results to demonstrate the low residual PM noise of the beat signal between two semiconductor lasers obtained by the heterodyne optical phase-locked loop [33]. Curves *A* and *B* of Figure 5.10*a* represent the signal waveforms of the local microwave oscillator and of the beat signal, respectively. By the magnitude of the timing jitter on curve *B*, the root mean-square value of the residual PM noise has been estimated as 0.6 radian [33, 82]. Figure 5.10*b* shows the field spectrum of the beat signal under optical phase locking, of which the control bandwidth was about 1 MHz. The beat signal was also observed at 2-kHz span, where its half-linewidth was 60 Hz, which was limited by the resolution bandwidth of the RF spectrum analyzer. A homodyne-type phase locked loop can be also realized by fixing the frequency of the local microwave oscillator to zero, where the photodetector becomes an optical phase comparator. Figure 5.11 shows the experimental result of the power spectral density of the PM noise of the homodyne phase-locked loop [83]. Within the Fourier frequency range below 12 MHz, drastic reduction of the PM noise can be seen. The bandwidth of this phase-locked loop, 12 MHz, could be large enough for the most of the homodyne phase-locked system for high-resolution laser spectroscopy. To evaluate quantitatively the magnitude of these residual FM or PM noise, the measurement system with about 100 times more accurate [82] than those of conventional ones [60, 61] has been developed.

For FM laser spectroscopy [84], the beat signal between the two lasers has to be measured. In such a case, measurement accuracy could be limited by the magnitude of the FM noise of the beat signal, which depends on the uncorrelated spontaneous emissions introduced into each laser mode. To improve this accuracy, a method of making a correlation

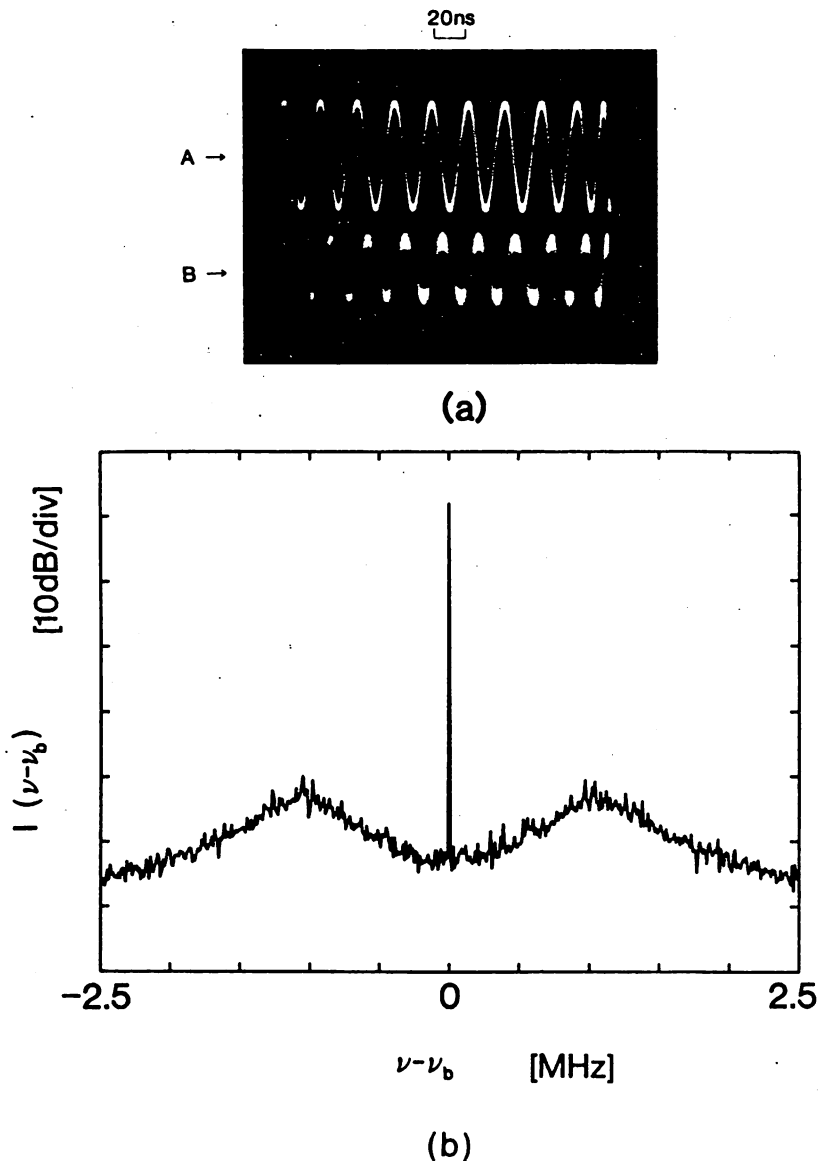


**Figure 5.10.** (a) A waveform of the beat signal obtained by the heterodyne-type phase-locked loop [33]. Curves *A* and *B* are the waveforms from the microwave local oscillator and the beat signal, respectively. Their frequencies are 50 MHz. (b) A field spectrum  $I(\nu - \nu_b)$  of the beat signal under optical phase locking ( $\nu_b$  is the center frequency of the spectrum). The resolution bandwidth and sweep time were 1 kHz and 30 s, respectively.

between these spontaneous emission fluctuations has been proposed [85]. Since the spontaneous emission corresponds to the stimulated emission driven by the zero-point fluctuations in vacuum, any correlations would not exist between those for different modes. However, if a number of upper energy levels are engaged in laser transitions, correlation can be generated between these spontaneous emissions by making a quantum correlation between these upper levels by applying a resonant external modulation. The correlated spontaneous emission has already been observed for the external-cavity semiconductor laser [86]. However, one

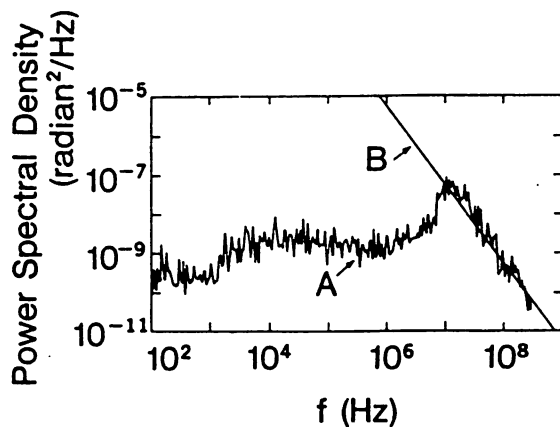


**Figure 5.11.** Power spectral density of the PM noise of the homodyne phase-locked loop [83]. Curve *A* shows experimental results for locked condition. The locking bandwidth was 12 MHz. The solid line *B* represents the unlocked condition estimated by extrapolating an unlocked part of curve *A*.

should not confuse this with the active mode locking phenomenon because some of the characteristics in correlated spontaneous emission are similar to those of the active mode locking. A method of highly precise evaluation has recently been proposed by measuring the Allan variance of short-term PM noise in the beat signal [87].

**5.3.4.5. Accurate and Wideband Frequency Sweep.** In the heterodyne-type frequency locked loop described in Section 5.3.4.4, the slave laser frequency can be swept by sweeping the frequency of the microwave local oscillator while maintaining the stability of the slave laser frequency very high. For a conventional AlGaAs laser with a Fabry–Perot cavity, a continuous tunable range of 64 GHz has been already realized [80], which is large enough for high-resolution laser spectroscopy. By using a longitudinal-mode controlled laser, such as a DFB or DBR laser, tunable range as wide as 1 THz can be realized [88].

Furthermore, as is shown by Figure 5.12, a novel system of realizing a petahertz (PHz;  $10^{15}$  Hz) class coherent optical sweep generator has been proposed [89, 90]. In this system, four commercially available semiconductor lasers, with wavelengths of 1.56, 1.34, 0.78, and  $0.67\ \mu\text{m}$ , are employed as primary light sources. Negative electrical feedback loops as described above are applied to these lasers to reduce their FM noises. As additional passive elements, nonlinear optical waveguides using organic materials such as MNA and DAN, are used for second harmonic generation, parametric frequency conversion, sum, and difference frequency generations. In this system, frequency tracking between the  $1.56\text{-}\mu\text{m}$  laser and the  $0.78\text{-}\mu\text{m}$  laser has been realized by locking simultaneously the frequencies of the  $0.78\text{-}\mu\text{m}$  laser and the second harmonics of the  $1.56\text{-}\mu\text{m}$  laser to the center frequency of the pump–probe spectral shape in Rb atomic vapor (see Figure 5.16 later in this chapter). Similar frequency tracking between the  $1.34\text{-}\mu\text{m}$  laser and the  $0.67\text{-}\mu\text{m}$  laser can be realized by using the Li atomic vapor. By incidenting these stabilized lasers into organic nonlinear waveguides used for parametric frequency converters, fre-

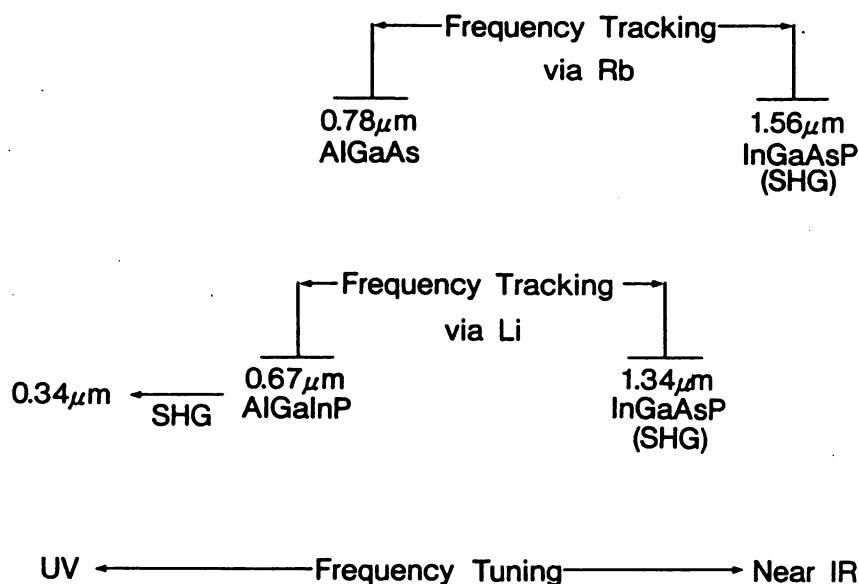


**Figure 5.12.** Schematic explanation of the principle for a petahertz-class hypercoherent optical sweep generator [89, 90]. Four coherent semiconductor lasers are used as primary light sources. Frequency links between these lasers are realized by using absorption lines of Rb and Li vapors as frequency references for negative electrical feedback. Nonlinear organic waveguides are used for generations of the second harmonic wave for this link. For wideband frequency sweep, other organic nonlinear waveguides are used to realize parametric frequency conversion and sum or difference frequency generation. Another inorganic oxide nonlinear optical crystal is used to generate the second harmonic wave from the 0.67- $\mu\text{m}$  laser. Maximum of the wavelength tuning range expected by this system is 1.22  $\mu\text{m}$  (i.e., from 1.56  $\mu\text{m}$  to 0.34  $\mu\text{m}$ ), which corresponds to 700-THz frequency range.

quency-converted coherent lights can be generated, which can be frequency-tunable within the wavelength range of 1.56–0.67  $\mu\text{m}$ . Inorganic oxide nonlinear optical crystals should be used for efficient second harmonic generation from the 0.67- $\mu\text{m}$  laser. By summarizing these techniques, rough frequency tuning between the wavelength range of 1.56–0.34  $\mu\text{m}$  can be expected, which corresponds to the frequency-tunable range of 700 THz, or approximately 1 PHz. Such a wideband frequency tuning, to the authors' knowledge, has never been realized by other kind of laser systems. For practical applications to high-resolution laser spectroscopy, expensive dye laser systems may be replaced by this inexpensive and compact system. Fine and accurate tuning can be carried out by employing simultaneously the technique of frequency offset locking. Essential problems to be solved to realize the petahertz frequency sweep range could be crystal growing and fabrication of efficient organic nonlinear optical waveguides. Theoretical analysis, crystal growing, and fabrication of the DFB-type channel waveguides are now in progress [91].

Table 5.1 summarizes the present status and future outlook of performance of the optical sweep generator that could be realized by considering five subjects described above [90]. It can be claimed that a highly precise



**Table 5.1 Present Status and Future Outlook of Optical Sweep Generator Performance [90]**

	Present Performance	Future (Predicted) Performance
Center frequency stabilization	$2 \times 10^{-12}{}^a$	$1 \times 10^{-15}{}^a$
Reproducibility and accuracy	$1 \times 10^{-8}$	$1 \times 10^{-10}$
Linewidth reduction	560 Hz	50 mHz
Frequency/phase tracking	$5.5 \times 10^{-16}{}^a$ 0.6 radian <sup>b</sup>	$< 1 \times 10^{-18}{}^a$ $< 0.1$ radian <sup>b</sup>
Accurate and continuous frequency sweep	1 THz	700 THz

<sup>a</sup>The value at the integration time of 100 s.

<sup>b</sup>Root mean square.

optical sweep generator has been realized, and further improvements can be expected in the near future.

## 5.4. TOPICS OF SPECTROSCOPY

Spectroscopic data of atoms and molecules at the near-infrared region of about 0.7–1.6- $\mu\text{m}$  wavelength have not been documented sufficiently because of the lack of the reliable coherent light sources. However, the improvements of semiconductor lasers have made it possible to carry out highly sensitive and high-resolution spectroscopy at this wavelength region. Several examples in experimental results of spectroscopy, obtained by frequency controlled semiconductor lasers, are demonstrated in the following subsections.

### 5.4.1. Linear and Nonlinear Laser Spectroscopy

A great number of Doppler-broadened spectral lines due to higher harmonics and combination tones of vibration–rotation transitions in organic molecular vapors can be observed within the wavelength range of 0.7–1.6  $\mu\text{m}$ . Although their absorptions are weak, spectral lines due to  $2\nu_1$ ,  $2\nu_3$ , or  $\nu_1 + \nu_3$  vibration transitions in  $\text{NH}_3$  and  $2\nu_2 + \nu_3$  vibration transition in  $\text{H}_2\text{O}$  have been observed at the 1.5- $\mu\text{m}$  wavelength with the detection sensitivity of  $2.3 \times 10^{-3}$  torr per a meter optical pass length [48]. Furthermore, those due to the  $2\nu_1 + \nu_2 + \nu_3$  vibration transition in  $\text{H}_2\text{O}$  have been measured at the wavelength range of 0.8  $\mu\text{m}$  [49]. In this case, fairly strong absorptions were observed because the  $2\nu_1 + \nu_2 + \nu_3$  band is coupled with the  $\nu_2 + \nu_3$  band by Darling–Dennison resonance [92]. The wavelengths of these absorption lines have been calibrated within the

error of  $1 \times 10^{-7}$  to  $1 \times 10^{-8}$ . After these pioneering works, spectroscopic data have been accumulated for several organic molecular vapors. For example, spectral lines in  $C_2H_2$  [50] and HCN [51] have been measured by sweeping a DFB laser frequency for over 1.5 THz. A highly sensitive spectrometer for studying the wavelength regions of 0.75–0.88  $\mu\text{m}$ , 1.3  $\mu\text{m}$ , and 1.5  $\mu\text{m}$  has recently been constructed [93], which was sensitive to the absorption of  $2 \times 10^{-6}$ . By using this spectrometer, the systematic study on the characteristics of spectral measurements of the vibration transitions in  $NH_3$  has been carried out. As a result of this study, the transfer from the normal mode vibration to local mode vibration was found with increase of the vibration quantum number. These experimental data were confirmed with theoretical analysis. Further improvements in sensitivity of these spectrometers can be expected by employing the technique of frequency modulation (FM) spectroscopy [84], which is compatible to semiconductor lasers because of their high efficiency of direct frequency modulation. Several experimental results of FM spectroscopy have already been demonstrated [94]. A problem to be solved in FM spectroscopy by semiconductor lasers is that IM is induced simultaneously by FM, which limits the measurement sensitivity. However, the contribution from IM could be reduced by employing a two-tone FM technique. As a result of it, the sensitivity was improved by 10 times that of the conventional one [95].

Spectral lines due to electronic transitions in atomic vapors have been measured at the 0.8- $\mu\text{m}$  wavelength region. Systematic studies on Rb [52] and Cs [53] have been reported. For rare gases, the technique of optogalvanic spectroscopy has been employed because a great number of optogalvanic spectral lines are distributed between the near-infrared and the visible spectra [96]. Although sufficiently reproducible frequency measurements could be rather difficult because of the frequency shift due to plasma instability and the Stark effect, fairly high sensitivity in measurements have been obtained [54].

Since most spectral lines due to electronic transitions in atomic vapors are distributed within the visible region, short wavelength lasers could be required for these measurements. For this purpose, a second harmonic wave generated from the active layer of an AlGaAs laser has been used to measure the strong spectral lines in K (transitions  $5p^2P_{1/2}-4s^2S_{1/2}$ , and  $5p^2P_{3/2}-4s^2S_{1/2}$ ) and Al (transition  $3p^2P_{3/2}-4s^2S_{1/2}$ ) vapors at the 0.4- $\mu\text{m}$  wavelength range [97]. Similar measurements of Rb lines by using the second harmonic wave generated internally from a 1.56- $\mu\text{m}$  InGaAsP laser have also been carried out [56].

Doppler-free spectroscopy of atomic vapors has been carried out by using a technique of atomic beam or nonlinear spectroscopy. Atomic beam spectroscopy has been carried out, for Cs, Rb, and so on. Examples of Doppler-free fluorescence spectroscopy experimental and calculated re-

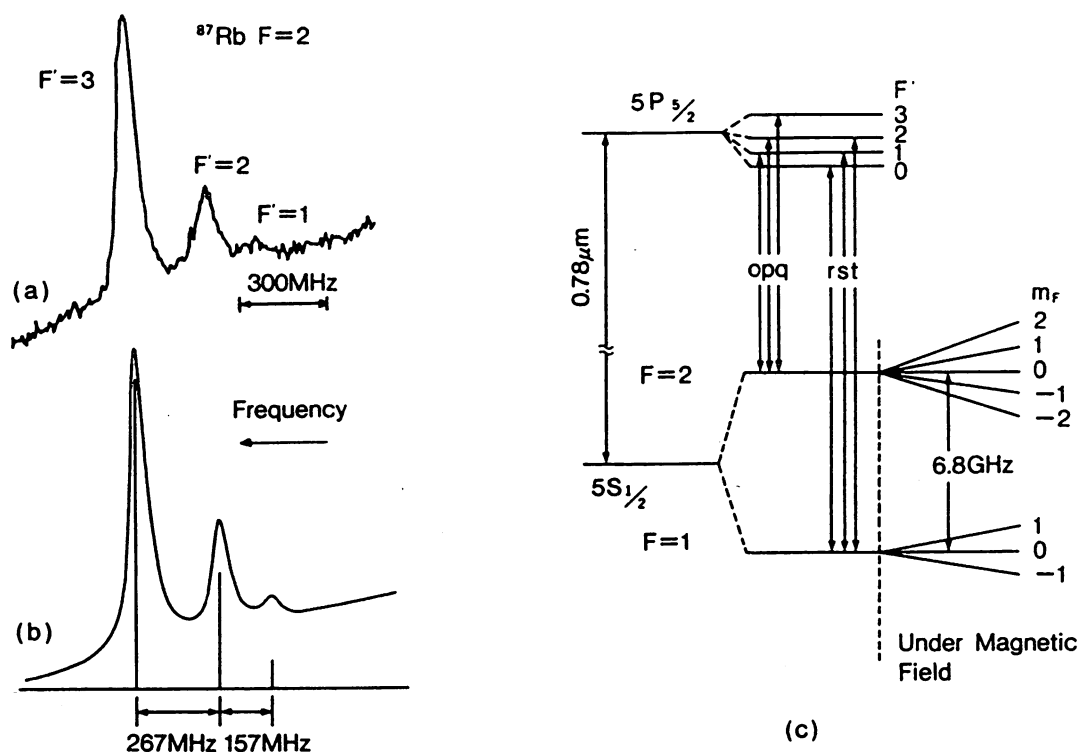


**Figure 5.13.** Doppler-free fluorescence spectral shape of  $^{87}\text{Rb}$  atomic beam [98]. (a) Experimental results; (b) calculated results; (c) relevant energy-level diagram of the Rb atom.

sults are shown by Figures 5.13a and 5.13b, respectively [98]. It was obtained by using a  $0.78\text{-}\mu\text{m}$  AlGaAs laser, and the half-linewidths of the fluorescence spectral profiles due to the transitions from  $F' = 1, 2,$  and  $3$  levels of the excited state to the  $F = 2$  level of the ground state was as narrow as  $70\text{ MHz}$ . This linewidth was determined by the residual Doppler broadening due to the  $5^\circ$  divergence of the atomic beam [98]. However, it is narrow enough that each spectral component represented by Figure 5.13c is clearly resolved.

As the first example of nonlinear spectroscopy, a saturated absorption technique has been employed for Cs [53], Rb [52, 99], and other elements. Figure 5.14a shows the derivatives of saturated absorption lineshapes in the  $^{87}\text{Rb}$   $D_2$  line obtained by using a  $0.78\text{-}\mu\text{m}$  AlGaAs laser, in which 11 narrow spectral lines, including cross-resonance lines, are resolved [99]. They have linewidths as narrow as  $40\text{ MHz}$ , which is limited by the lifetimes of relevant energy levels. Their spectral strengths and positions on the abscissa agree well with those estimated by theoretical analyses (see Figure 5.14b).

As the second example, optical-optical double resonance has been carried out for the  $D_1$  [100] and  $D_2$  lines in Rb by using a  $0.79\text{-}\mu\text{m}$  and  $0.78\text{-}\mu\text{m}$  AlGaAs lasers, respectively. Figure 5.15 shows the double reso-

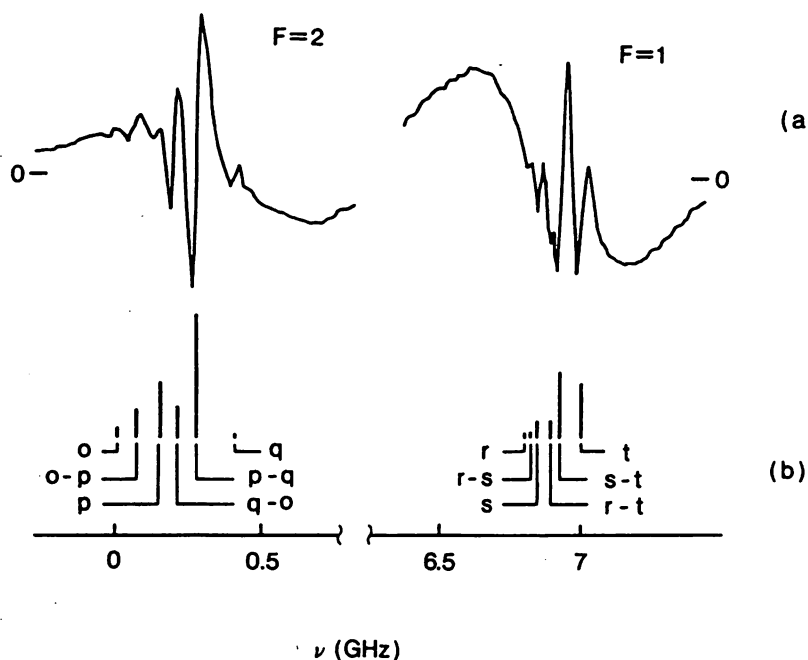


**Figure 5.14.** Derivative of saturated absorption spectral lineshapes in  $^{87}\text{Rb}$  [99, © 1985 IEEE]. (a) Experimental results. (b) Assigned spectral lines. For the notations of this spectral lines, see the relevant energy-level diagram presented in Figure 5.13c. For the transition from the  $F = 1$  level of the ground state, two saturated absorption lines ( $s$  and  $t$ ) and three cross-resonance lines ( $r-s$ ,  $r-t$ , and  $s-t$ ) were observed. For the transition from the  $F = 2$  level, three saturated absorption lines ( $o$ ,  $p$ , and  $q$ ) and three cross-resonance lines ( $o-p$ ,  $q-o$ , and  $p-q$ ) were observed.

nance spectral shapes for the  $D_2$  component of an  $^{87}\text{Rb}$  atomic beam [98], which exhibit clear Doppler-free spectral shapes. Because the pump laser frequency was fixed to the transition frequency between the  $F = 2$  and  $F' = 3$  levels, the strength of the spectral component  $F' = 3$  is weaker than that of the other two components as the result of saturation. Figure 5.16a shows a novel experimental setup for a nonlinear pump-probe

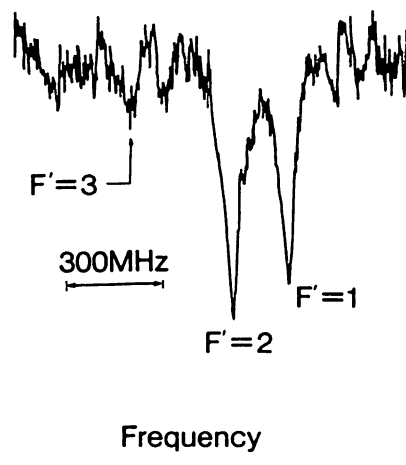


**Figure 5.15.** Optical-optical double-resonance spectral shapes of  $^{87}\text{Rb}$  atomic beam [98]. The pump laser frequency was fixed to the transition frequency from  $F = 2$  to  $F' = 3$ .

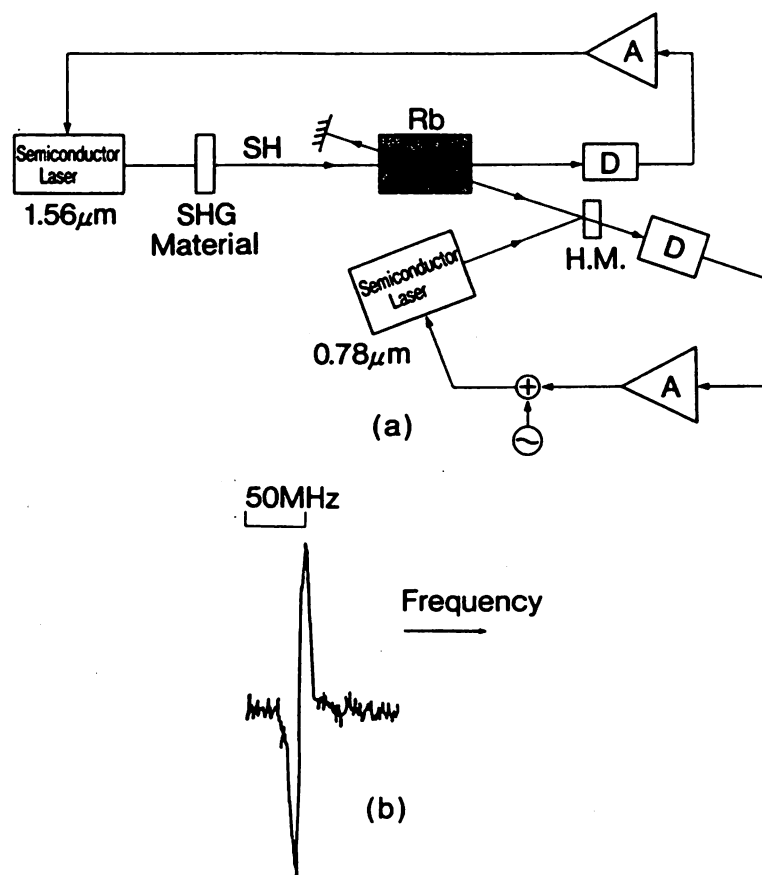


**Figure 5.16.** Novel Doppler-free pump-probe spectroscopy of Rb by using an AlGaAs laser and the second harmonics of the InGaAsP laser as the pumping and probe light sources, respectively [90]. (a) Experimental setup; (b) an example of the first derivative of the spectral profile.

spectroscopy [90]. Doppler-free spectral profiles, which are due to the saturation by the pumping from a  $0.78\text{-}\mu\text{m}$  AlGaAs laser, can be probed by using a second harmonic wave generated from a  $1.56\text{-}\mu\text{m}$  InGaAsP laser. Figure 5.16b shows an experimental result of the first derivative of the Doppler-free spectral shape. This spectral shape can be used as a frequency reference to stabilize the frequency of the pump and probe lasers simultaneously, which can realize a stabilized frequency link between the  $0.78\text{-}\mu\text{m}$  AlGaAs and  $1.56\text{-}\mu\text{m}$  InGaAsP lasers, and will be used as stable master lasers for wideband optical sweep generator represented by Figure 5.12. Similar results can be expected for Li atoms by using  $0.67\text{-}\mu\text{m}$  AlGaInP and  $1.34\text{-}\mu\text{m}$  InGaAsP lasers.

The third example is the Doppler-free two-photon spectroscopy for Li atomic vapor, which has been carried out by using a dye laser and an AlGaAs laser [101]. By using a thermoionic heat pipe diode as a sensitive detector for spectral measurements, clear spectral profiles, shown by Figure 5.17, have been obtained. It can be seen from this figure that the hyperfine components in  ${}^6\text{Li}$  and  ${}^7\text{Li}$  have been clearly resolved.

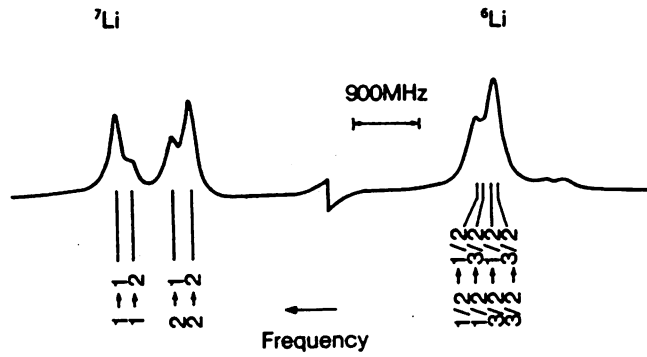


**Figure 5.17.** Spectral profile due to the Doppler-free two photon transitions  $2S-2P-3S$  in the  ${}^6\text{Li}$  and  ${}^7\text{Li}$  atoms [101]. The numbers below the spectra denote the quantum numbers  $F$  and  $F'$  of the initial and final states, respectively.

As one of the other applications of semiconductor lasers to alkali vapor spectroscopy, Rydberg states of alkali atoms can be produced by stepwise excitation, which is shown in Figure 5.18 for Cs and Rb [102]. By using this spectroscopic method, information about highly excited states can be obtained [103]. The Rydberg atoms prepared by this method have also been used for one atom maser in the microwave region, which is one branch of the cavity QED described in Section 5.4.4.

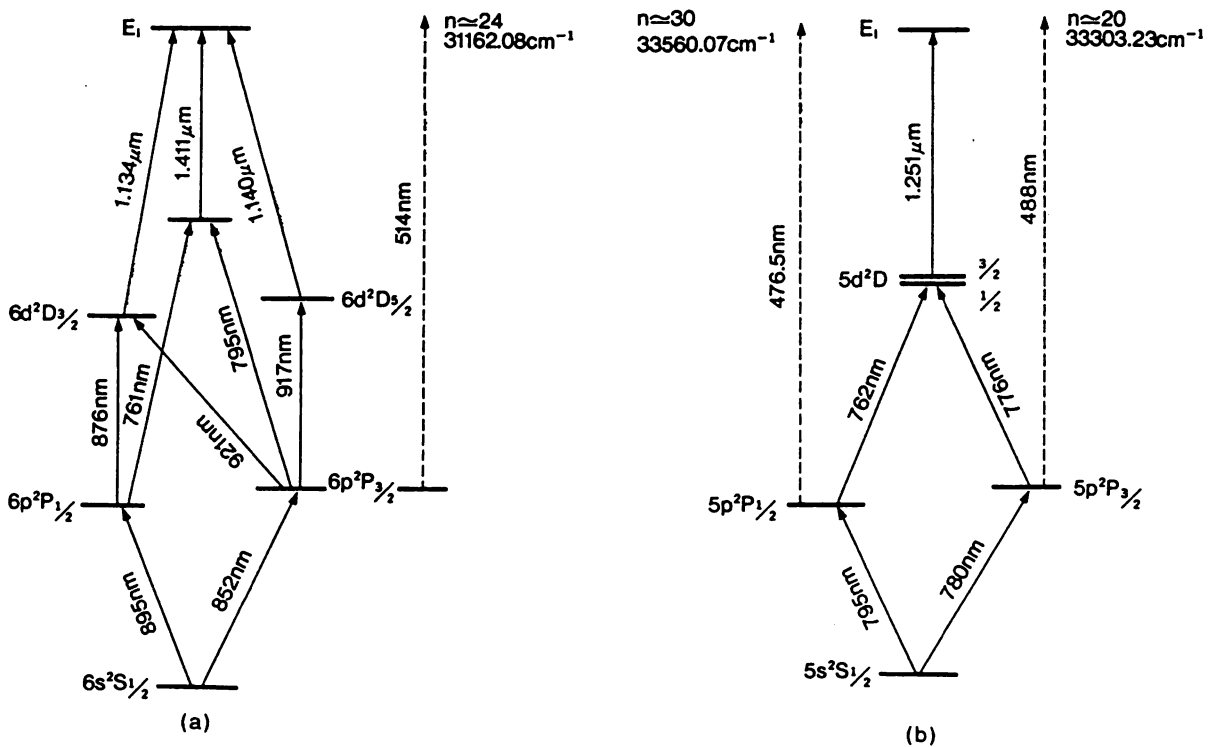


**Figure 5.18.** Stepwise excitation schemes to obtain the Rydberg states of Cs (a) and Rb (b);  $E_1$  is the ionization level [102]. Most of the transitions indicated by solid arrows in this figure can be driven by the semiconductor lasers. The broken arrows indicate transitions driven by argon ion lasers.

### 5.4.2. Test of Parity Nonconservation

The existence of weak interaction between elemental particles in atoms has been predicted by the standard electroweak theory developed by Glashow, Weinberg, and Salam. Experimental tests for this theory have been carried out in the field of high-energy physics using a huge accelerator. However, it has been found that a method of precision laser spectroscopy could be used as a more convenient and less expensive tool for this test [104, 105]. Since the parity conservation of the wave function of the atom could be violated by the weak interaction, a weak optical transition due to this violation can be detected by a carefully designed sensitive laser spectrometer. Figure 5.19 shows such an experimental setup for detecting the change of polarization of the transmitted light through the Pb atomic vapor, in which a 1.3- $\mu\text{m}$  InGaAsP laser is used as a coherent light source [106]. The optical transition due to magnetic dipole interaction in Pb atoms was monitored to detect the change of polarization induced by the parity nonconservation. This sensitive spectrometer, employing the techniques of polarization modulation and phase-sensitive detection, was sensitive to the polarization rotation of 0.1  $\mu\text{radian}$ . Stark coefficients in Cs atoms have also been accurately measured by using a carefully frequency controlled AlGaAs laser, by which several structural constants of Cs have been estimated to test the parity nonconservation [107].

Semiconductor lasers can be also used for accurate measurement of the Lamb shift of muonic atoms [108]. A frequency controlled 0.73  $\mu\text{m}$  AlGaAs laser is used as the master laser for the injection locking of a high-power solid-state Alexandrite laser to reduce its FM noise. The third harmonic radiation from the locked Alexandrite laser is generated by using nonlinear optical media. This ultraviolet light can be used as a pumping source of the muonic atoms.

### 5.4.3. Manipulations of Atoms and Ions

Experimental studies of deceleration of atomic motion in vacuum (i.e., laser cooling [109]) and confinement of atoms in a limited volume by laser beams have been recently progressed rapidly with the aid of improvements in the laser frequency control technique. Deceleration of atomic motion is possible by the light pressure imposed by the laser beam. The lowest equivalent temperature of the cooled atom is lower than the value determined by the Doppler effect [ $< 40 \mu\text{K}$  (microkelvins)] [110, 111]. Furthermore, a recent experiment has revealed a temperature lower than 2  $\mu\text{K}$ , which corresponded to the thermal velocity of several centimeters per second [112]. This is lower than the value determined by the recoiling between the atom and photon.

It has become possible to confine a number of atoms (e.g.,  $1 \times 10^7$  atoms) in a limited volume in vacuum for more than several minutes with

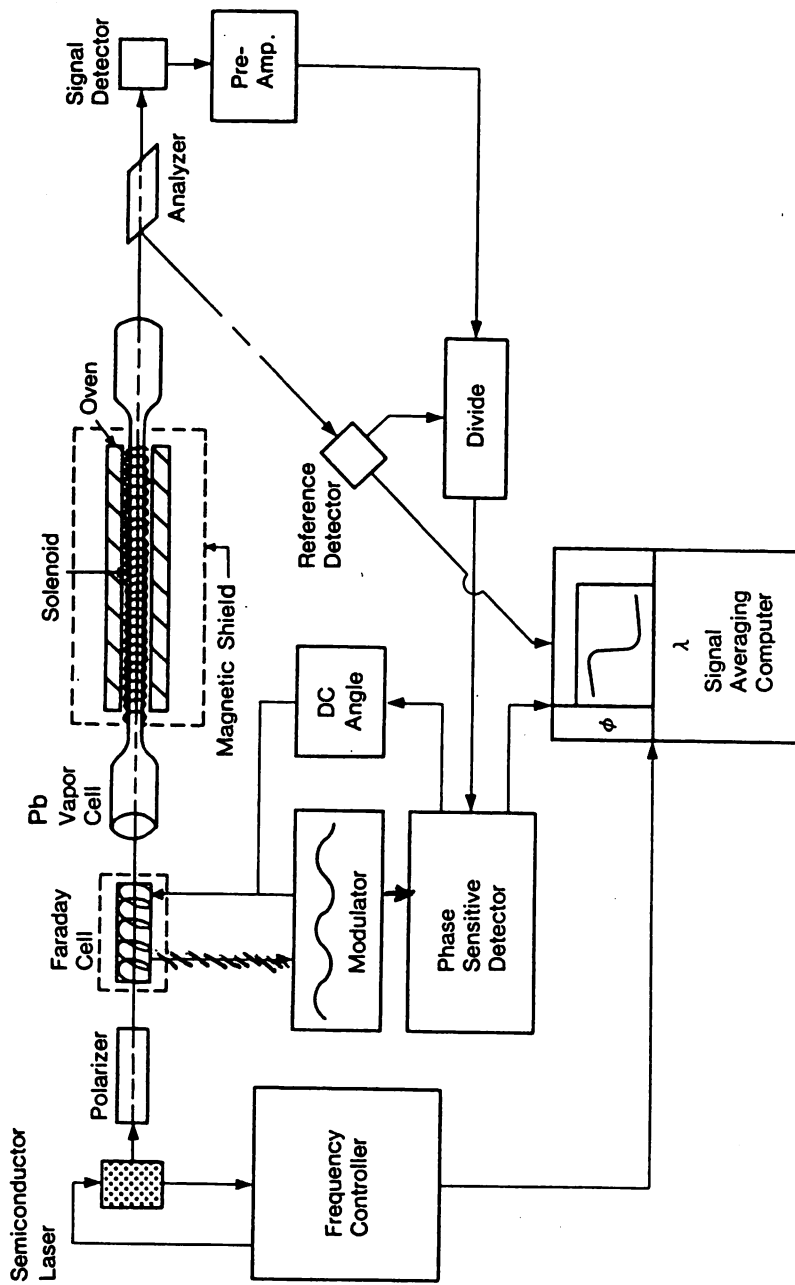


**Figure 5.19.** Experimental setup for testing the parity nonconservation in Pb atoms [106]. A  $1.3\text{-}\mu\text{m}$  InGaAsP laser beam was incident into the Pb atomic vapor. Its frequency was tuned to the transition frequency due to the magnetic dipole moment interaction in Pb. Change in the polarization of the transmitted light was precisely measured by employing the techniques of the polarization modulation and the phase-sensitive detection.



atomic density as high as  $1 \times 10^{11} \text{ cm}^{-3}$  [113]. In such high-density situation, the confined atomic mass exhibits a specific characteristics similar to those of viscous fluids. For this reason, this confined atomic mass has been called “optical molasses.”

For these experiments, it is advantageous to utilize a high efficiency of frequency modulation and controllability in semiconductor lasers. Figure 5.20 shows such an experimental setup using  $0.85\text{-}\mu\text{m}$  AlGaAs lasers for optical pumping, laser cooling, and producing optical molasses of Cs atoms [114]. Laser coolings of Rb atoms [115] and rare gases [116] have also been carried out by using AlGaAs lasers. These experiments have been carried out by using expensive and complicated atomic beam apparatus. However, a simple experimental configuration using an inexpensive Cs vapor cell has recently been employed to produce the optical molasses [117].

The experimental study of an ion trap, that is, confining a single ion in a limited volume of an electromagnetic potential such as a Penning trap or Paul trap, has been remarkable progress by simultaneously utilizing the technique of laser cooling. Several specific characteristics, such as quantum jump [118], have been observed for a cooled and confined single ion [119]. By further improvements of performances in confinement technique, squeezing between uncertainties of the momentum and the position of the ion have recently been observed [120]. Furthermore, by confining and cooling high-density atoms, it was observed that their characteristics were similar to those of ionic crystal and solid-state plasma [121].

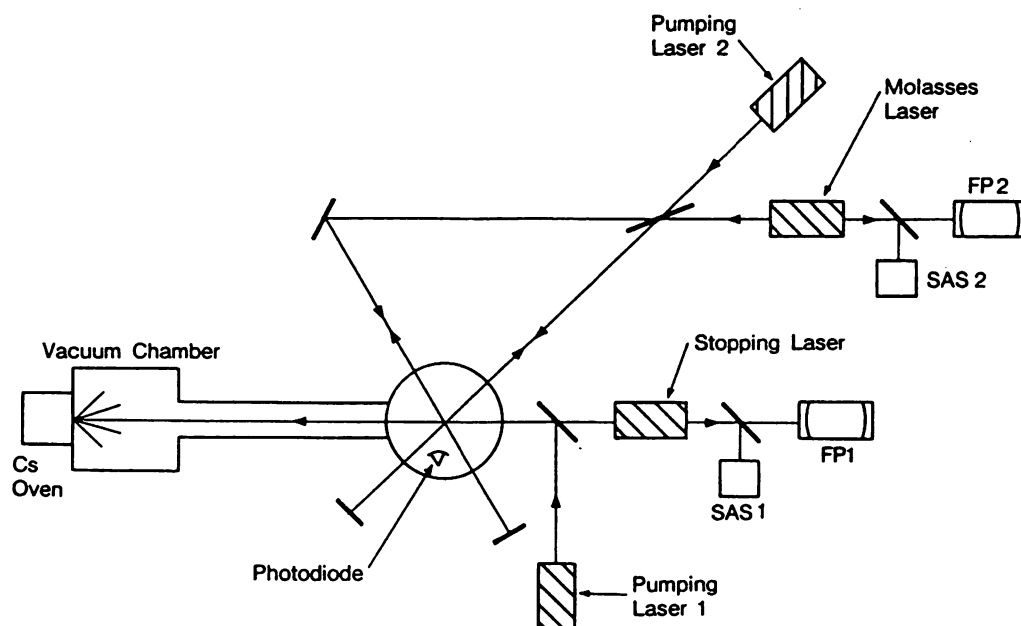


**Figure 5.20.** Experimental setup for laser cooling and for producing the optical molasses of Cs atoms [114]. AlGaAs lasers were used for optical pumping, laser cooling, and producing optical molasses.

Since most of the ions have their resonant frequencies in the visible–ultraviolet region, several expensive dye lasers and their second harmonic or sum-frequency radiations have been used. However, the efficiency of these wavelength conversion is rather low in these short-wavelength regions. To overcome these difficulties, the possibility of using easily controllable semiconductor lasers have been examined [120]. For this purpose, it is expected that a hypercoherent optical sweep generator such as that described in Section 5.3.4 can be used as a reliable coherent light source.

#### 5.4.4. Cavity Quantum Electrodynamics

As was described in Section 5.3.3 [4], enhancement or inhibition of spontaneous emission from atoms can be realized by using a microcavity with the dimension of a wavelength order. At the initial stage of the cavity QED study, experiments were carried out in the microwave frequency region. Controlled rate of the spontaneous emission and specific Rabi oscillation driven by vacuum fluctuations were observed by using a microcavity and single-atom maser [122]. To prepare the atoms of a large transition dipole moment, Cs atoms were excited to the Rydberg state by using AlGaAs lasers as pumping sources.

Because of the technical difficulty of fabricating a microcavity in the optical frequency region, experiments of optical cavity QED have been carried out by installing atoms in a high-finesse and mode-degenerated confocal Fabry–Perot cavity. Enhancement and inhibition of the spontaneous emission from Yb atoms have been observed at the resonant and nonresonant frequencies of the confocal Fabry–Perot cavity, respectively [123]. Experimental study of the single-atom laser is also in progress. As is shown by Figure 5-21, FM sidebands on the spontaneous emission spectral line from Na atoms in the high-finesse Fabry–Perot cavity have recently been observed, which were attributed to vacuum Rabi oscillation [124]. The techniques of cavity QED could be useful to realize a novel light-emitting semiconductor device, such as a low-threshold semiconductor laser. For this purpose, the Fabry–Perot microcavity with the dimensions of optical wavelength has been fabricated, as is shown by Figure 5.22 [45]. Enhancement and inhibition of spontaneous emission from a semiconductor quantum well have also been demonstrated by using a multilayer distributed Bragg reflector used as a microcavity [125]. Since the study of optical cavity QED is still at the early stage, several problems remain to be solved. For example, conventional studies on cavity QED have demonstrated that spontaneous emission has been enhanced at the cavity resonance frequency. However, for low-noise laser devices, it should be inhibited to reduce the quantum noise. It is expected that these problems will be solved in the near future, and that novel and stable semiconductor

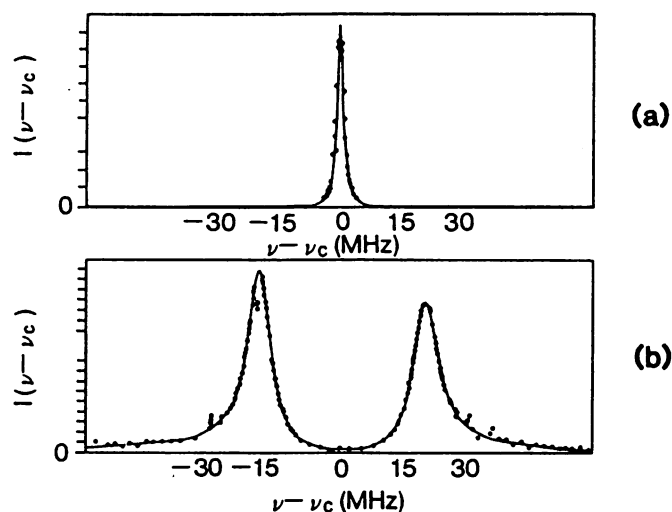


**Figure 5.21.** Experimental results for measuring the vacuum Rabi oscillation in Na atoms [124]. (a) Spectral profile  $I(\nu - \nu_c)$  of the empty Fabry-Perot cavity. (b) Spectral profile  $I(\nu - \nu_c)$  of the cavity with Na atoms. This profile has two peaks representing the FM sidebands due to the vacuum Rabi oscillation ( $\nu_c$  is the cavity resonance frequency).

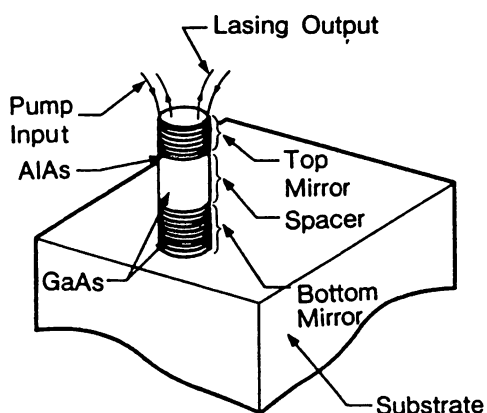


**Figure 5.22.** Schematic diagram of the Fabry-Perot microcavity created by employing a semiconductor device fabrication technique [45]. Its diameter and lengths are about 1.5 and 4.0  $\mu\text{m}$ , respectively. Laser operation has been observed by this cavity.

lasers will be realized by utilizing the cavity QED technique. Furthermore, such advanced lasers could be used as powerful light sources for further improvements in the study of laser spectroscopy.

## 5.5. APPLICATIONS OF SPECTROSCOPY

Results of atomic and molecular spectroscopy have been used for a great number of applications. In the case of spectroscopy by semiconductor lasers, wider fields of practical applications can be opened because of low price, small size, and low power consumption of semiconductor lasers. These include several specific applications that cannot be essentially

realized without using semiconductor lasers. These examples are described in the following subsections.

### 5.5.1. Analytical Spectroscopy

**5.5.1.1. Isotope Separation.** Several kinds of lasers have been used for laser isotope separation of U for nuclear fusion and Li, Ba, and Ga for tracers in medical diagnoses, and so on. Frequency-stable, frequency-tunable, and high-power lasers should be used for efficient selective excitation of a specific isotope by utilizing isotope shifts of the center frequencies of resonant spectral lines between each species of isotopes. For this purpose, several high-power lasers, such as dye lasers pumped by copper-vapor lasers, have been conventionally employed. However, some of the dye lasers have recently been replaced by frequency controlled semiconductor lasers to reduce the cost of the laser systems.

One successful example is the isotope separation of Rb and Cs by the light-induced drift method [126]. Although conventional systems have used dye lasers, the efficiency of isotope separation has not been sufficiently high because of the deexcitation occurred at the process of selective optical pumping. To improve this efficiency, dye lasers have been replaced by AlGaAs lasers. Since the direct FM response characteristics of these semiconductor lasers exhibit the resonant peak at the relaxation oscillation, a series of FM sidebands appear in the field spectrum of these lasers. By careful adjustment of the bias level, the frequency separation between the optical carrier and the FM sideband of the second order can be coincided with the frequency separation between the two hyperfine energy levels of the ground state (e.g.,  $F = 1$  and  $F = 2$  levels in Rb). By pumping Rb atoms by an optical carrier and this FM sideband simultaneously, cyclic excitation can be realized. By this cyclic excitation, most of  $^{87}\text{Rb}$  atoms are maintained at the excitation states so as to realize a large cross section of the collision with buffer gases. As a result, drift velocity of  $^{87}\text{Rb}$  in buffer gases could become different from that of  $^{85}\text{Rb}$ , by which separation efficiency has been improved. Frequency stability of the laser can be maintained high enough by locking the optical carrier frequency to the Rb resonant frequency by following the technique of negative electrical feedback. As is represented by Figure 5.23 [126], separation efficiency as high as the one obtained by using a conventionally used dye laser (150-mW power) has been realized by the AlGaAs laser with the power of only 3.3 mW. This result has also been confirmed by the theoretical analysis based on the density matrix formulation for Rb atoms [127].

For isotope separations of Li, Ba, Ga, and so on, by using the Doppler-free two-photon transition process, one of the dye lasers has been replaced by a semiconductor laser, and as is shown by Figure 5.17, clearly resolved Doppler-free spectral shapes of  $^7\text{Li}$  and  $^6\text{Li}$  have been obtained and the magnitude of the isotope shift has been evaluated with the

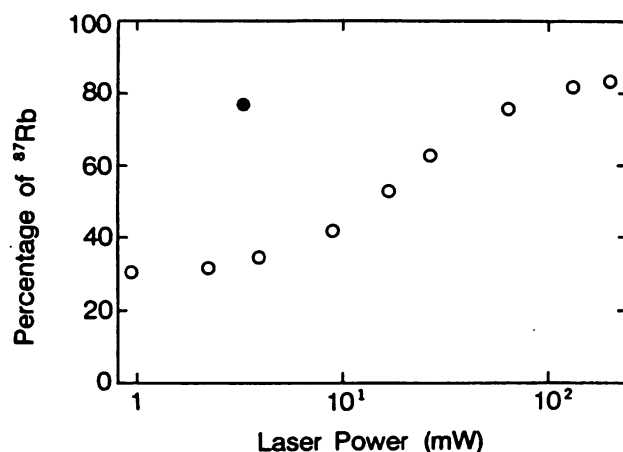


**Figure 5.23.** Percentage of  $^{87}\text{Rb}$  in a natural Rb atomic vapors obtained as the result of laser-induced drift [126]. Closed circle represents the result using the AlGaAs laser with relaxation oscillation sidebands at the power of 3.3 mW. Open circles represent results using a dye laser.

accuracy of about  $1 \times 10^{-7}$  [101]. For the isotope separation of  $^{235}\text{U}$ , there are two possibilities [127]:

1. High power AlGaAs lasers can be used as one of the pumping sources for two-step excitation because the  $^{235}\text{U}$  atoms have fairly large excitation cross sections at the wavelength region of about  $0.8\text{--}0.7 \mu\text{m}$ .
2. A stable and coherent visible AlGaInP laser can be used as the master laser for injection locking of a pulsed high-power dye laser.

With all of these possibilities, low-cost light sources for practical isotope separation systems can possibly be realized in the near future.

As has been widely known, several atomic isotopes, such as Li, Ga, and Ba, as described above, can be used as tracers for medical diagnoses. Molecular isotopes can also be used for this medical application. Since stable isotopes contained in a human respiration by doping several molecules, such as  $^{13}\text{CO}$ , can be sensitively detected by using a semiconductor laser spectrometer, the result of this detection can also be used as an useful information for medical diagnoses [128].

**5.5.1.2. Analysis of  $\text{SiH}_x$  Radicals.** Fabrication of amorphous silicon film by chemical vapor deposition has been a key technology for the semiconductor device industry. For accurate control of deposited film thickness, quantitative analysis and assignment of species of  $\text{SiH}_x$  are required. For example, it has been confirmed by UV photolysis that the  $\text{SiH}_2$  radical could emit fluorescence due to transitions between the vibration levels. It can be expected that visible AlGaInP lasers will be used as a coherent

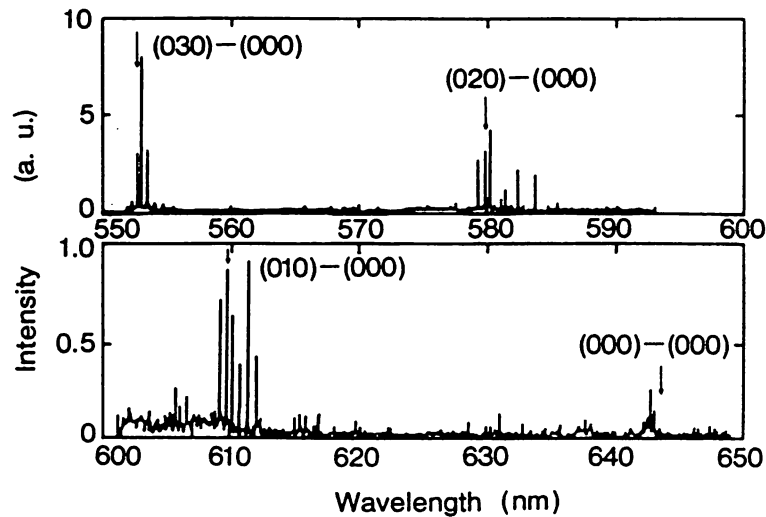


**Figure 5.24.** Laser excitation fluorescence spectra of  $\text{SiH}_2$  radical [129]. The assignment of the vibrational progression and the band origin are indicated by vibration quantum numbers and arrows, respectively.

light source for efficient and practical spectral analysis in UV photolysis systems because the fluorescence spectra emitted due to the excitation by a pulsed ArF excimer laser are distributed at the wavelength region of  $0.6 \mu\text{m}$  [127, 129] (see Figure 5.24).

**5.5.1.3. Laser Radar.** Although the power of a semiconductor laser usually is lower than that of  $\text{CO}_2$ , Ar, and YAG lasers, the small size and low power consumption of the semiconductor laser are advantageous features for use as a practical airborne or automobile-borne laser radar (lidar) system. Furthermore, by utilizing a high efficiency of direct modulation of a semiconductor laser, the pseudorandom modulation technique can be employed to realize high sensitivity and high spatial resolution in lidar operation. Figure 5.25 shows an example of the measurement of aerosols and clouds in the sky [130]. It was confirmed from the results of these field tests that this pseudorandom modulation CW lidar had the maximum measurable distance of 1 km for aerosol, and 3–5 km for cloud or dust with the spatial resolution of 9 m.

A FM–CW lidar has been proposed, which requires a  $< 100\text{-kHz}$ -linewidth AlGaAs laser for a range finding with the target range of 10–100 m, spatial resolution of  $10 \mu\text{m}$ , and data rate of 10–100 pixels per second [131]. To prepare the coherent semiconductor laser for this system, techniques of negative electrical feedback and optical feedback described in Section 5.3.3 have been utilized.

### 5.5.2. Optical Pumping of Atomic Clocks

Frequency-stable microwave oscillators have been used as key devices for microwave communication, broadcasting, navigation, earthquake predic-

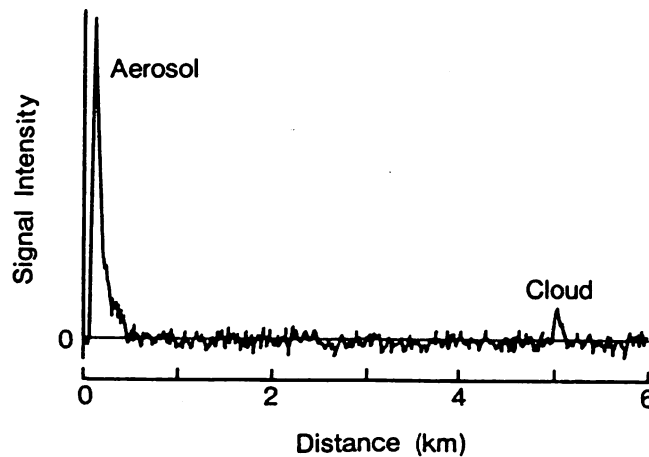


**Figure 5.25.** An example of the measurement of aerosols and clouds in the sky by using a semiconductor laser radar (lidar) by employing the technique of pseudorandom modulation [130].

tion (seismology), astronomy, and so on. For these systems, the most reliable oscillators are atomic clocks. Drastic improvements in the performances in these atomic clocks have been attained by using semiconductor lasers as coherent optical pumping source. Two examples of these improvements are described in the following.

**5.5.2.1. Cesium (Cs) Atomic Clock at 9.2 GHz.** A Cs atomic clock is a microwave oscillator, for which the transition frequency (9.2 GHz) between two hyperfine levels ( $F = 4, m_F = 0$  and  $F = 3, m_F = 0$ ; see Figure 5.26a) in the ground state of Cs has been used as the frequency reference to control the frequency of a voltage-controlled crystal oscillator [102]. Since the frequency accuracy of this clock is very high, it has been used as a primary standard of time. This clock has been studied and developed in a number of national research institutes in the world and used as a time-keeping clock. A compact and portable Cs atomic clock has been developed for a satellite-borne system.

In the conventional Cs atomic clock, deflection of the Cs atomic beam by DC magnetic fields has been used to select the atoms at the energy levels of  $F = 4, m_F = 0$  and  $F = 3, m_F = 0$ . In this state selection scheme, atoms at  $m_F \neq 0$  levels among the  $2F + 1$  magnetic sublevels cannot be used, which limited the efficiency of the state selection. Furthermore, this clock has had several error sources limiting frequency accuracy, such as the frequency shift induced by the magnetic fields, which were used to deflect the atomic beam. To overcome these difficulties, an optical pumping scheme has been proposed [132]. Figure 5.26b shows a typical experimental setup for an optically pumped Cs atomic clock. Two  $0.85\text{-}\mu\text{m}$  AlGaAs laser frequencies,  $\nu_1$  and  $\nu_2$ , are tuned to the transition frequencies from  $F = 4$  to  $F' = 4$ , and from  $F = 3$  to  $F' = 4$ , respectively, where

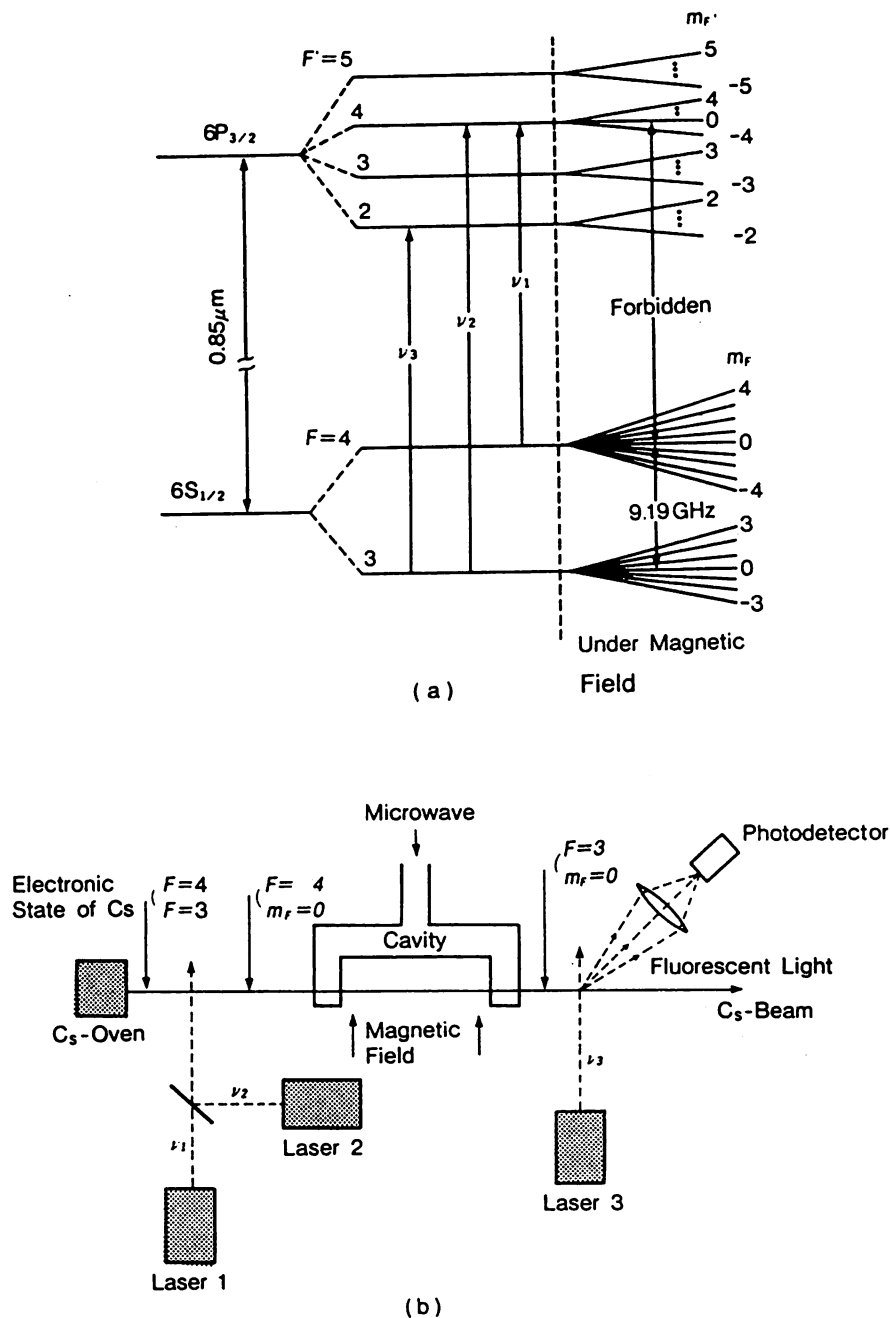


**Figure 5.26.** (a) Energy levels of Cs atoms. (b) Experimental setup for optical pumping of a Cs atomic clock [102].

$F'$  represents the quantum number of the excited state. After the cyclic transitions between the ground and the excited states due to the simultaneous optical pumping by the two lasers, all the atoms are transferred to the  $F = 4$ ,  $m_F = 0$  level of the ground state. Therefore, efficiency of state selection is increased eight times that of the conventional magnetic deflection scheme. After this state selection, atoms pass through the spatially isolated two microwave cavities, by which a fringe-shaped microwave Ramsey spectral profile can be observed. Figure 5.27 represents a typical



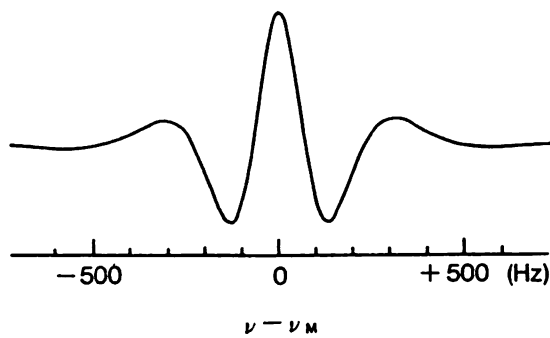


**Figure 5.27.** An example of fringe-shaped microwave Ramsey spectral profile obtained by an optically pumped Cs atomic clock [133, © 1988 IEEE]. The half-linewidth of the center part of this fringe was 200 Hz.

fringe-shaped Ramsey spectral profile. The half-linewidth of the center part of this fringe was as narrow as 200 Hz [133], which is determined by the inverse of the separation between the two microwave cavities. This narrow spectral line is used as a sensitive and stable frequency demodulator to control the microwave frequency. The third AlGaAs laser are used to measure this Ramsey spectral shape. Its frequency  $\nu_3$  is tuned to the transition frequency between  $F = 3$  and  $F' = 2$  to excite the atoms of the  $F = 3$  level that have been deexcited from the  $F = 4$  level due to the microwave transition. Ramsey spectral shape can be measured by detecting the fluorescence from the  $F' = 2$  level, which can be emitted by the optical pumping from  $F = 3$  to  $F' = 2$  by this laser.

Although the optical pumping scheme has been proposed for more than 10 years ago [132], experiments with this scheme have progressed at a slow speed because of the lack of frequency controlled AlGaAs lasers. Rapid progress in developing frequency controlled AlGaAs lasers, as was described in Section 5.3.3, made remarkable progress in this scheme. By this optical pumping, frequency accuracy higher than  $5 \times 10^{-14}$  can perhaps be realized in the near future. For further improvements of this optically pumped Cs atomic clock, employments of the laser cooling technique have been proposed [134].

**5.5.2.2. Rubidium (Rb) Atomic Clock at 6.8 GHz.** Although the frequency accuracy of a Rb atomic clock is lower than that of the Cs atomic clock, it has been popularly used as a compact and low-price microwave oscillator because the short-term frequency stability was rather higher than that of Cs atomic clocks. A block diagram of the Rb atomic clock is shown by Figure 5.28. As is shown by Figure 5.13c, transition frequency (6.8 GHz) between the two hyperfine levels in the ground state ( $F = 2$ ,  $m_F = 0$  and  $F = 1$ ,  $m_F = 0$ ) is used as the frequency demodulator to control the voltage controlled crystal oscillator.

To detect the spectral profile of this frequency demodulator, a technique of microwave-optical double resonance has been employed, for which optical pumping from the ground state to the excited state is required by using a light source of  $0.78\text{-}\mu\text{m}$  wavelength. The double-resonance spectral profile can be measured by detecting the light power

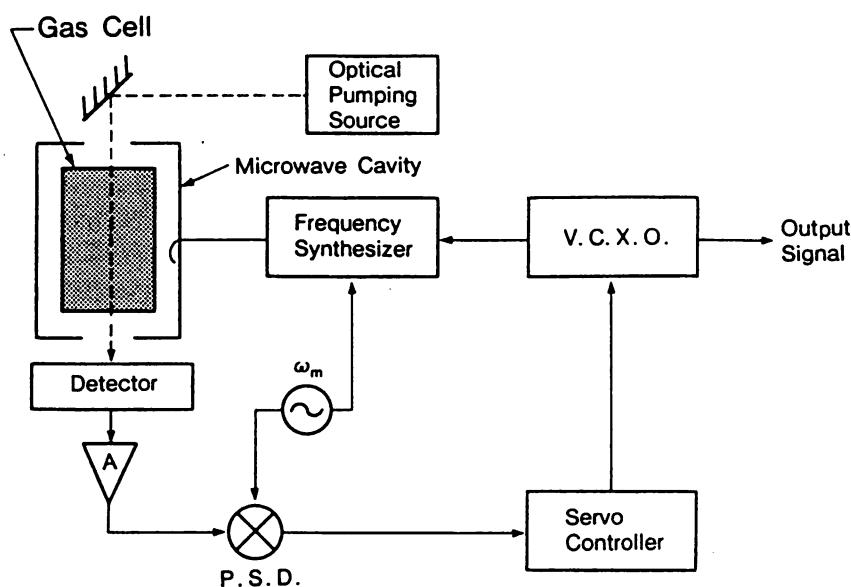


**Figure 5.28.** Experimental setup of a Rb atomic clock. VCXO and PSD represent a voltage-controlled crystal oscillator and a phase-sensitive detector, respectively.

transmitted through the Rb vapor cell. Buffer gases such as Ne, and Ar have been filled in the Rb vapor cell to reduce the double-resonance spectral width by atomic collisions so as to increase the sensitivity of frequency demodulation. By this collisional narrowing, termed *Dicke narrowing*, a spectral width as narrow as 100–500 Hz has been obtained. Microwave frequency is modulated and a phase-sensitive detector is used to measure the derivative of double-resonance spectral shape in order to use it as a frequency demodulator. Conventional Rb atomic clocks have used an incoherent discharge lamp for optical pumping. However, center frequency of the double-resonance spectral profile could be shifted as a result of variations of lamp power. This shift, called “light shift,” is induced by the AC Stark effect by the optical field, which could not be avoided as long as the incoherent lamp has been used. This light shift has limited the long-term frequency stability. Furthermore, the frequency accuracy has been limited by the frequency shift induced by the collision between the Rb and buffer gas atoms. For these reasons, the Rb atomic clock has been considered as the secondary standard of time.

Improvements in short- and long-term frequency stabilities, and frequency accuracy also, can be expected by using an AlGaAs laser as a coherent optical pumping source. In this pumping scheme, the effect of microwave frequency modulation could be transferred to the coherent optical field of the laser in the Rb vapor cell. This modulation transfer occurs as a result of the nonlinear susceptibility of the Rb atoms that interact with the optical and microwave fields simultaneously. Since the double-resonance spectral signal is detected by using this modulated laser light, the effect of this modulation transfer induces a kind of interference

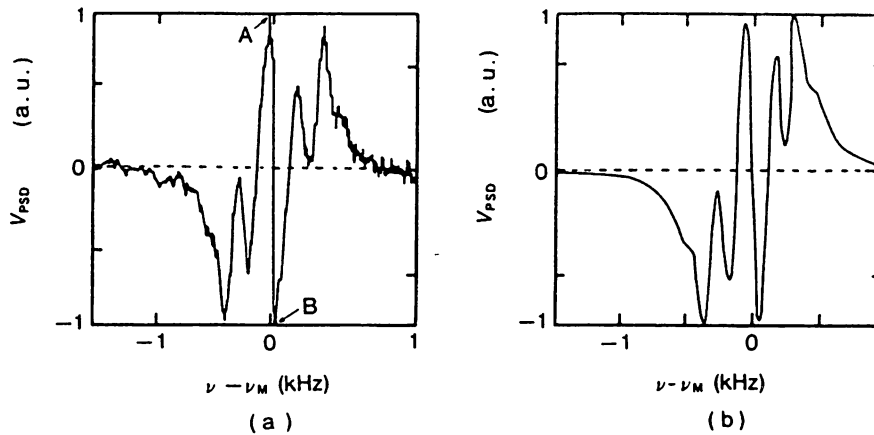


**Figure 5.29.** Derivative of double-resonance spectral shape measured by the AlGaAs laser pumped Rb atomic clock [135, © 1987 IEEE]. (a) Experimental result. The linewidth of the center of this fringe-shaped spectral profile (i.e., the separation between points *A* and *B*) is about  $\frac{1}{20}$  times narrower than that for the conventional lamp-pumped Rb atomic clock. (b) Calculated result [136].

fringe on the double-resonance spectral profile, as is shown by Figure 5.29a [135]. The width of the center part of this fringe-shaped spectral profile was about  $\frac{1}{20}$  times narrower than that for the conventional lamp-pumped Rb atomic clock. The principle of obtaining such a fringe-shaped spectral profile is equivalent to that of FM laser spectroscopy [136]. As is shown by Figure 5.29b, such a specific spectral profile could be accurately reproduced by using the theoretical model based on the density matrix for the three-level atoms. It has also been confirmed that the fringe-shaped spectral profile of Figure 5.29 was equivalent to the fringe-shaped Ramsey spectral profile in the Cs atomic clock (see Figure 5.27). In the case of the Cs atomic clock, the perturbations from the microwave fields were applied to the Cs atoms at the two separate positions along the spatial axis of Cs atomic beam trajectory. On the other hand, in the Rb atomic clock, the perturbations from the optical fields were applied to the Rb atoms at separate positions along the optical frequency axis, which is a result of modulation transfer. The effect of this separated perturbation induced the fringe on the double-resonance spectral shape. By using this narrow-linewidth spectral shape as a frequency demodulator, it was confirmed that the short-term frequency stability was improved 40 times that of the conventional Rb atomic clocks [136].

Further improvements of short-term frequency stability was confirmed by reducing the FM noise of the laser at the Fourier frequency of the microwave modulation frequency because the noise contained in the double-resonance signal was mainly originated from the laser FM noise [137]. It has been demonstrated by Figure 5.8 that the negative electrical feedback can reduce the laser FM noise as large as 60 dB at around 1-kHz Fourier frequency range, in which region the microwave is frequency-mod-

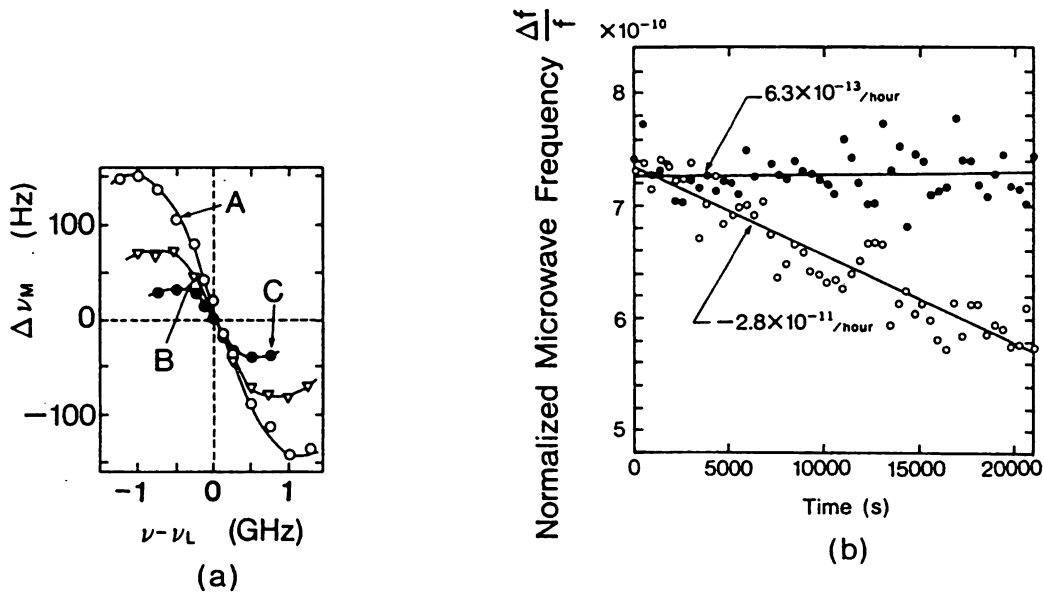


**Figure 5.30.** (a) Measured relation between the light shift and laser frequency detuning [138, © 1990 IEEE]. The laser power densities were 1008, 360, and 144  $\mu\text{W}/\text{cm}^2$  for curves A, B, and C, respectively. (b) Drift of microwave frequency [138, © 1990 IEEE]. The closed and open circles represent the results obtained with and without using the self-tuning technique, respectively.

ulated. This reduction is large enough to reach the shot-noise level, which is determined by the photodetector for the detection of the double-resonance signal. At the shot-noise limit, it has been estimated that the short-term frequency stability of the Rb atomic clock can be improved to as high as  $5 \times 10^{-15} \tau^{-1/2}$ , where  $\tau$  is the integration time [136]. This stability is 1000 times higher than that of the presently developed laser-pumped Rb atomic clock.

The magnitude of the light shift induced by the AC Stark effect due to the optical field can be quantitatively evaluated by varying the laser power and frequency. The result is shown by Figure 5.30a [138]. Negative electrical feedback system has been developed to control the laser frequency in order to suppress the light shift of the microwave frequency. By this self-tuned system, drift of the microwave frequency, which originated from the drifts of the optical pumping power and frequency, has been reduced. The result is shown by Figure 5.30b [138], from which it can be confirmed that the long-term frequency stability was improved 40 times that of the conventional ones.

It has been also confirmed that the performances of the long-term frequency stability is higher than those of the portable Cs atomic clocks [137]. The replacement of the Rb vapor cell by the Rb atomic beam has been proposed to improve the frequency accuracy by eliminating the atomic collision with the buffer atoms [139].

By the intensive studies described above, it is expected that a novel, high-performance, compact, and low-price Rb atomic clock will be realized in the near future, and will be, thus, employed to the key applications

such as the global positioning system (GPS), a novel primary standard of time, and so on.

### 5.5.3. Optical Pumping of Solid-State Lasers

Since a wavelength of an AlGaAs laser coincides with that of the absorption spectral band of a Nd:YAG crystal and the AlGaAs laser power has been increased up to, for example, 76 W, by employing an array structure [140], arc lamps used for optical pumping sources for CW Nd:YAG lasers have been replaced by these efficient AlGaAs lasers. The IM noise of the high-power, multi-longitudinal-mode oscillation of AlGaAs lasers, due to its mode-hopping or mode-partition phenomenon, limits the power and frequency stabilities of the Nd:YAG laser. To solve this problem, a careful design of the AlGaAs laser as a stable optical pumping source has been carried out by using a rate equation formalism [141]. Figure 5.31 shows

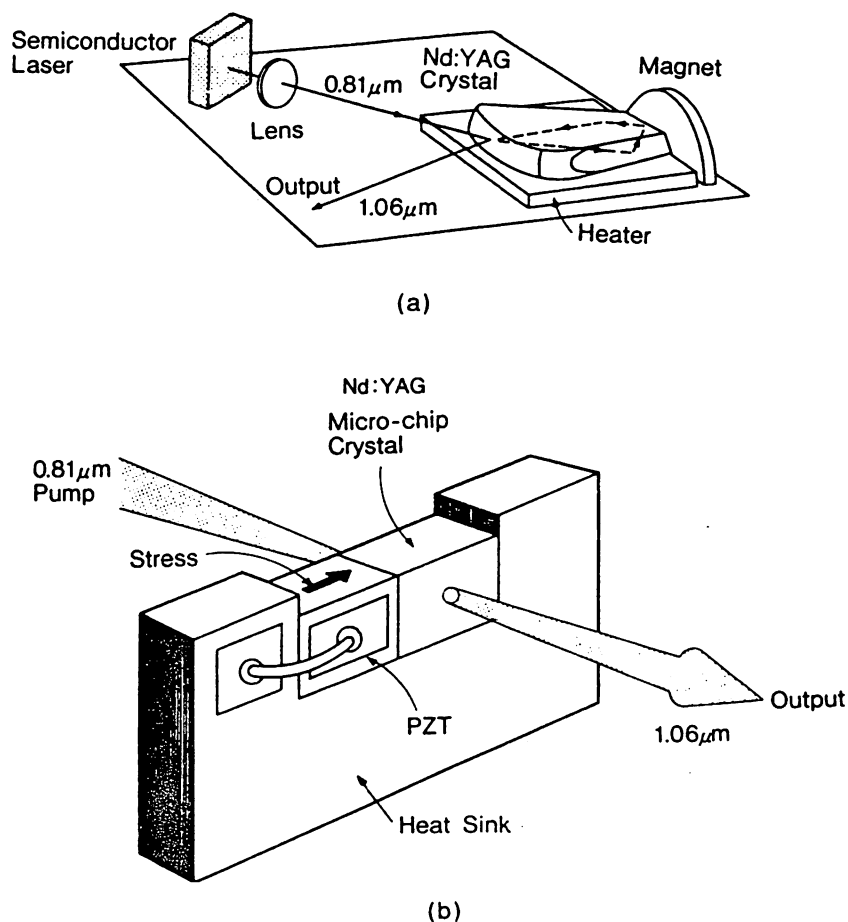


**Figure 5.31.** Configurations of semiconductor laser-pumped Nd:YAG lasers. (a) NPRO (nonplanar ring oscillator) or MISER (monolithic isolated single-mode end-pumping ring)-type laser [142, © 1989 IEEE]. (b) A Nd:YAG laser by using a microchip YAG crystal [145, reprinted with permission of Lincoln Laboratory, Massachusetts Institute of Technology, Lexington, Massachusetts].

typical structures of such the all-solid-state Nd:YAG lasers. Figure 5.31a shows the laser structure called *nonplanar ring oscillator* (NPRO) or (*monolithic isolated single-mode end-pumping ring* (MISER) type, where the laser crystal itself forms a ring cavity and the end-pumping scheme from the AlGaAs laser is employed [142]. A DC magnetic field is applied to the crystal to control the polarization of the laser beam by utilizing the Faraday effect of the crystal. By this control, a unidirectional ring cavity configuration with only a clockwise running wave could be realized. Wavelength tuning is also possible by varying the crystal temperature. Stability of the laser oscillation frequency is high because the cavity was monolithically integrated with the laser crystal. The field spectral linewidth under the free-running condition was less than 10 kHz. A stress applied to the crystal by a piezoelectric transducer (PZT) can modulate the laser frequency with the FM efficiency of about 500 kHz/V. By utilizing this FM response characteristics, the laser frequency was stabilized to a high-finesse ( $> 20,000$ ) Fabry–Perot cavity by negative electrical feedback, which realized a linewidth below 30 Hz [143]. Recent studies of this system revealed the linewidth to be as narrow as 3 Hz [144]. Since the Schawlow–Townes limit of the free-running laser was estimated as 1 Hz at 1 MW of output power, this value of 3 Hz has almost reached this limit. It can be expected that the hypercoherent state is realized by improving the performance of the feedback loop in the near future.

Figure 5.31b shows the laser using a microchip of the YAG crystal ( $0.7 \times 1.0 \times 2.0$  mm in size) to realize a single-longitudinal-mode oscillation by end-pumping scheme [145]. The laser frequency can be modulated by applying a stress to the crystal by a PZT. The FM efficiency was about 0.3 MHz/V up to the modulation frequency of 80 kHz. The maximum modulatable frequency was about 25 MHz, which was limited by the acoustic resonances of the Nd:YAG crystal.

In addition to the Nd:YAG lasers, a great number of solid-state lasers can be optically pumped by semiconductor lasers. For example, a Ho:YAG laser oscillates at  $2.1\text{-}\mu\text{m}$  wavelength [146], which can be applied to the laser radar system because it guarantees safety for the eye and low propagation loss in the atmosphere. Furthermore, if a Ti:sapphire laser can be pumped by an AlGaAs laser-pumped Nd:YAG laser, a low noise and all-solid-state laser with an oscillation wavelength of  $0.67\text{--}1.1\ \mu\text{m}$  could be realized, which could, thus, replace the dye lasers and semiconductor lasers for various applications, such as high-resolution spectrometer for atoms and molecules [147].

These low-noise solid-state lasers can be used as powerful coherent light sources for basic studies of science. For example, a low-noise Nd:YAG laser has been designed for a very long-baseline interferometer for gravitational wave detection [148]. Typical performance required for this laser is frequency stability higher than  $1 \times 10^{-15}$ , output power higher than 100 W, and so on. To realize these performances, negative electrical

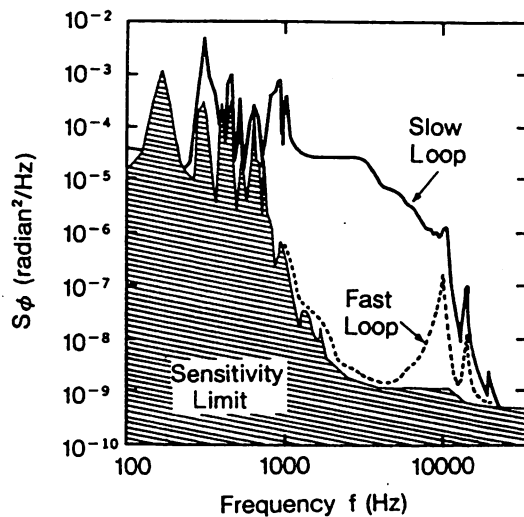


**Figure 5.32.** Power spectral density of the PM noise representing the phase fidelity of the injection-locked high-power Nd:YAG laser to the master laser [150].

feedback loop, composed of an electrooptical modulator and high-finesse Fabry–Perot interferometer, has been designed to obtain a very high gain with a bandwidth of about 50 kHz [149]. Furthermore, to obtain high power, the injection locking of a 13-W continuous-wave Nd:YAG laser has been carried out by using a semiconductor laser-pumped Nd:YAG laser with 40 mW of output power as the master laser [150]. Figure 5.32 shows the phase fidelity of the injection-locked laser obtained by using a slow and fast feedback loop, which is similar to the case for the frequency control of a semiconductor laser (see Figure 5.8 [70, 71]). It can be seen from this figure that phase noise reduction is about 40 dB for the Fourier frequency range of 1–20 kHz, from which the total root-mean-square phase noise can be estimated as about 0.3 radian. Further increases in injection-locked laser power up to 100 W can be expected while maintaining the frequency stability as low as that of the master laser.

Performance of these lasers can be improved to as high as that required for the gravitational wave detection system in the near future. The problems remained to be solved include (1) using a phase-squeezed light to save the laser power in order to avoid optical damages to the high-quality interferometer mirrors and (2) realizing the quantum nondemolition measurement system to measure the tiny displacement of the interferometer mirror by the gravitational wave [151].

## 5.6. SUMMARY

In this chapter, the topics of laser spectroscopy were reviewed by following the performance of frequency controlled semiconductor lasers and a petahertz-class hypercoherent optical sweep generator. These findings are based on at least two factors: (1) high-resolution spectroscopy cannot be realized without using these stable light sources, and (2) novel results of

spectroscopy can be used to improve the performance of these lasers; for example, very narrow spectral lines in atoms or molecules can be used as a sensitive frequency demodulator for the laser frequency control. These facts indicate that progress in spectroscopy and progress in laser technology are mutually positively fed back and thus are interrelated. It can be concluded from this discussion that further development of semiconductor laser spectroscopy is essential for progress in quantum electronics, quantum optics, atomic physics, and a wide variety of practical industrial application systems. Further details of the characteristics of semiconductor laser operations and possible applications can be found in ref. 102.

### ACKNOWLEDGMENTS

The authors would like to thank Mr. C.-H. Shin of their research group for his critical reading and comments on the manuscript, and to graduate students for their active cooperation in the authors' work. Figure 5.31(b) was reprinted with permission by the Lincoln Laboratory, Massachusetts Institute of Technology, Lexington, Massachusetts.

### REFERENCES

1. M. Ohtsu and Y. Teramachi, *IEEE J. Quantum Electron.* **25**, 31–38 (1989).
2. N. Chinone, T. Kuroda, T. Otsoshi, T. Takahashi and T. Kajimura, *IEEE J. Quantum Electron.* **QE-21**, 1264–1269 (1985).
3. M. Ohtsu, Y. Teramachi, and T. Miyazaki, *Opt. Commun.* **61**, 203–207 (1987).
4. K. Kojima, S. Noda, K. Mitsunaga, K. Fujiwara, and K. Kyuma, "Low threshold current AlGaAs/GaAs DFB lasers grown by MBE," in *IEICE Technical Report on Optical and Quantum Electronics*, June 1985 (IEICE, Tokyo, 1985), pp. 93–98 (in Japanese).
5. K.-Y. Liou, M. Ohtsu, C. A. Burrus, Jr., U. Koren, and T. L. Koch, *IEEE J. Lightwave Technol.* **7**, 632–639 (1989).
6. M. Usami, S. Akiba, and Y. Matsushima, "Mode characteristics of  $\lambda/4$ -shifted DFB lasers with the distributed current injection along the cavity," *Extended Abstracts of the 49th Autumn Meeting of Jpn. Soc. Appl. Phys., Tokyo 1988* (Jpn. Soc. Appl. Phys., Tokyo, 1988), 6p-ZC-16 (in Japanese).
7. R. Lang and K. Kobayashi, *IEEE J. Quantum Electron.* **QE-16**, 347–355 (1980).
8. M. Ohtsu, "Noises in lasers," *Physics Monthly* **6**, 297–303 (1985) (in Japanese).
9. P. Kartaschoff, *Frequency and Time*, Academic Press, London, 1978.
10. M. Ohtsu, *Lasers and Atomic Clocks*, Ohm-sha, Tokyo, 1986 (in Japanese).
11. A. Blaquiére, *Compt. Rend.* **26**, 2929–2931 (1962).
12. M. Oshinski and J. Buus, *IEEE J. Quantum Electron.* **QE-23**, 9–29 (1987).



13. D. Welford and A. Mooradian, *Appl. Phys. Lett.* **40**, 560–562 (1982).
14. M. Ohtsu and S. Kotajima, *Jpn. J. Appl. Phys.* **23**, 760–764 (1984).
15. K. Vahala and A. Yariv, *Appl. Phys. Lett.* **43** 140–142 (1983).
16. M. Ohtsu, H. Fukada, T. Tako, and H. Tsuchida, *Jpn. J. Appl. Phys.* **22**, 1157–1166 (1983).
17. M. Ohtsu and M. Tabuchi, *IEEE J. Lightwave Technol.* **6**, 357–369 (1988).
18. O. Nilsson and Y. Yamamoto, *Appl. Phys. Lett.* **46**, 223–225 (1985).
19. Y. Yoshikuni and G. Motosugi, *IEEE J. Lightwave Technol.* **LT-5**, 516–522 (1987).
20. Y. Yamamoto, O. Nilsson, and S. Saito, *IEEE J. Quantum Electron.* **QE-21**, 1919–1928 (1985).
21. M. Ohtsu, *IEEE J. Lightwave Technol.* **6**, 245–256 (1988).
22. A. Mooradian, “High resolution tunable infrared lasers,” in *Laser Spectroscopy*, R. G. Brewer and A. Mooradian, eds., Plenum Press, New York, 1973, pp. 223–236.
23. M. Ohtsu, “Realization of hyper-coherent light,” *Science* (Japanese version of *Scientific American*), March 1989, pp. 64–73 (in Japanese).
24. D. Lenstra, B. H. Verbeek, and A. J. den Boef, *IEEE J. Quantum Electron.* **QE-21**, 674–679 (1985).
25. M. Ohtsu, K.-Y. Liou, E. C. Burrows, C. A. Burrus, and G. Eisenstein, *Electron. Lett.* **23**, 1111–1113 (1987).
26. M. Ohtsu, K.-Y. Liou, E. C. Burrows, C. A. Burrus, and G. Eisenstein, *IEEE J. Lightwave Technol.* **7**, 68–76 (1989).
27. N. A. Olsson and J. P. Van der Ziel, *IEEE J. Lightwave Technol.* **LT-5**, 510–515 (1987).
28. D. Mehuys, M. Mittelstein, and A. Yariv, “(GaAl)As quantum well semiconductor lasers tunable over 105 nm with an external grating,” *Proc. Conf. Lasers and Electro-Optics (CLEO '89)*, Baltimore, 1989 (LEOS/IEEE and OSA, Washington, D.C., 1989), FL4.
29. K. Vahala, K. Kyuma, A. Yariv, S. K. Kwong, M. Cronin-Golomb, and K. Y. Kau, *Appl. Phys. Lett.* **49**, 1563–1565 (1986).
30. B. Dahmani, L. Hollberg, and R. Drullinger, *Opt. Lett.* **12**, 876–878 (1987).
31. M. Ohtsu, “A frequency modulatable narrow-linewidth semiconductor laser,” *IEICE Technical Report on Optical and Quantum Electronics* (1987), pp. 35–40 (IEICE, Tokyo, 1987) (in Japanese).
32. L. Hollberg and M. Ohtsu, *Appl. Phys. Lett.* **53**, 944–946 (1988).
33. C.-H. Shin, M. Teshima, M. Ohtsu, T. Imai, J. Yoshida, and K. Nishide, “Modulatable, high coherent and compact semiconductor laser modules,” *Proc. 7th International Conf. Integrated Optics and Optical Fiber Communications (IOOC '89)*, July 1989, Kobe, Japan (IEICE, Tokyo, 1989) 21D4-5, pp. 116–117.
34. J. Yoshida, T. Imai, K. Nishide, C.-H. Shin, M. Teshima, and M. Ohtsu, “Modulatable high coherent laser for fiber optic gyroscope,” *Reports on Topical Meeting of the Laser Society of Japan, Tokyo, 1989* (Laser Society of Japan, Osaka, 1989), pp. 33–38 (in Japanese).

35. C.-H. Shin, M. Teshima, M. Ohtsu, T. Imai, J. Yoshida, and K. Nishide, *IEEE Photonics Technol. Lett.* **2**, 167–169 (1990).
36. H. Suzuki, I. Koshiishi, K. Nakagawa, and M. Ohtsu, "Frequency control of visible semiconductor laser," *Extended Abstracts of the 59th Autumn Meeting of Jpn. Soc. Appl. Phys., 1989* (Jpn. Soc. Appl. Phys., Tokyo, 1989), 29p-ZL-7 (in Japanese).
37. M. Ohtsu, H. Suzuki, K. Nemoto, and Y. Teramachi, *Jpn. J. Appl. Phys. Part 2*, **29**, L1463–L1465 (1990).
38. Y. Arakawa and A. Yariv, *IEEE J. Quantum Electron.* **QE-22**, 1887–1899 (1986).
39. T. Fujita, J. Ohya, K. Matsuda, M. Ishino, H. Sato, and H. Serizawa, *Electron. Lett.* **21**, 374–376 (1985).
40. I. Mito and K. Kitamura, "GaInAs/GaInAsP multiquantum well DFB lasers," *Proc. Conf. on Lasers and Electro-Optics* (CLEO '89), Baltimore, 1989 (LEOS/IEEE, OSA, Washington, DC, 1989), TUD5.
41. H. Imai, "Optical devices for high speed transmission including widely tunable DFB/DBR lasers," *Proc. Conf. on Lasers and Electro-Optics* (CLEO '89), Baltimore, 1989 (LEOS/IEEE, OSA, Washington, DC, 1989), FB4.
42. N. A. Olsson, C. H. Henry, R. F. Kazarinov, H. J. Lee, B. H. Johnson, and K. J. Orlowsky, *Appl. Phys. Lett.* **51**, 1141–1142 (1987).
43. S. Haroche and D. Kleppner, "Cavity quantum electrodynamics," *Physics Today*, January 1989, pp. 24–30.
44. A. Anderson, S. Haroche, E. A. Hinds, W. Jhe, D. Mechede and L. Moi, "Atomic physics experiments in micronized cavities: suppressing spontaneous decay at optical frequency," *Proc. 15th International Quantum Electronics Conference* (IQEC '87), Baltimore, 1987 (OSA, Washington, DC, 1987), THAA1.
45. J. L. Jewell, S. L. McCall, Y. H. Lee, A. Scherer, A. C. Gossard, and J. H. English, *Appl. Phys. Lett.* **54**, 1400–1402 (1989).
46. E. Yablonovitch, "Inhibited spontaneous emission in solid-state electronics," *Proc. 15th International Quantum Electronics Conference* (IQEC '87), Baltimore, 1987 (OSA, Washington, DC 1987), THAA4.
47. E. Yablonovitch, "Photonic band structure: Observation of an energy gap for light in 3-D periodic dielectric structures," *Proc. Conf. Quantum Electronics and Laser Science* (QELS '89), Baltimore, 1989 (OSA, Washington, DC, 1989), TUKK6.
48. M. Ohtsu, H. Kotani and H. Tagawa, *Jpn. J. Appl. Phys.* **22**, 1553–1557 (1983).
49. K. Fukuoka, M. Ohtsu and T. Tako, *Jpn. J. Appl. Phys.* **23**, L117–L120 (1984).
50. S. Kinugawa, H. Sasada, and K. Uehara, "Detection of C<sub>2</sub>H<sub>2</sub> absorption lines with 1.5 μm DFB lasers," *Extended Abstracts of the 49th Autumn Meeting of Jpn. Soc. Appl. Phys., 1988* (Jpn. Soc. Appl. Phys., Tokyo, 1988), 6p-Q-13 (in Japanese).
51. H. Sasada, *J. Chem. Phys.* **88**, 767–777 (1988).

52. H. Tsuchida, M. Ohtsu, T. Tako, N. Kuramochi, and N. Oura, *Jpn. J. Appl. Phys.* **21**, L561–L563 (1982).
53. T. Yabuzaki, A. Ibaraki, H. Hori, M. Kitano, and T. Ogawa, *Jpn. J. Appl. Phys.* **20**, L451–L454 (1981).
54. S. Yamaguchi and M. Suzuki, *Appl. Phys. Lett.* **41**, 597–598 (1982).
55. Y. C. Chung, *Photon. Technol. Lett.* **1**, 135–136 (1989).
56. M. Ohtsu and E. Ikegami, *Electron. Lett.* **25**, 22–23 (1989).
57. E. Ikegami, H. Kusuzawa, K. Nakagawa, and M. Ohtsu, “Nonlinear organic waveguides for a LD-based optical sweep generator I,” *Extended Abstracts of the 50th Autumn Meeting of the Jpn. Soc. Appl. Phys.*, 1989 (Jpn. Soc. Appl. Phys., Tokyo, 1989), 28p-ZP-16 (in Japanese).
58. Ch. Salomon, D. Hills, and J. L. Hall, *J. Opt. Soc. Am. B* **5**, 1576–1587 (1988).
59. M. Ohtsu, *Opt. Quantum Electron.* **20**, 283–300 (1988).
60. T. Kato, K. Kuboki, and M. Ohtsu, “Evaluation of performance of frequency offset locking system,” *Extended Abstracts of the 48th Autumn Meeting of Jpn. Soc. Appl. Phys.*, 1987 (Jpn. Soc. Appl. Phys., Tokyo, 1987), 20p-ZQ-4 (in Japanese).
61. K. Kuboki and M. Ohtsu, *IEEE Trans. Instrum. Meas.* **39**, (in press). August issue, 1990.
62. M. Ohtsu, M. Hashimoto, and H. Ozawa, “A highly stabilized semiconductor laser and its application to optically pumped Rb atomic clock,” *Proc. 39th Annual Frequency Control Symp. Philadelphia, 1985* (IEEE, Piscaway, NJ, 1985), pp. 43–53.
63. H. Furuta and M. Ohtsu, *Appl. Opt.* **28**, 3737–3743 (1989).
64. V. Pevtshin and S. Ezekiel, *Opt. Lett.* **12**, 172–174 (1987).
65. M. Ohi, *Jpn. J. Appl. Phys.* **12**, 1377–1381 (1973).
66. D. A. Jennings, K. M. Evenson, and D. J. E. Knight, *Proc. IEEE* **74**, 168–179 (1986).
67. Y. Miki, “Josephson devices for optical frequency measurements,” *Proc. Symp. on Quantum Measurements, Tokyo, 1987* (Society of Promotion for Industry and Technology in Japan, Tokyo, 1987), pp. 19–28 (in Japanese).
68. Y. Enomoto and T. Murakami, “Optical detector using oxide superconductor,” *Extended Abstracts of the 36th Spring Meeting of Jpn. Soc. of Appl. Phys. and Related Soc.*, Tokyo, 1989 (Jpn. Soc. Appl. Phys., Tokyo, 1989), 2p-ZD-4, p. 1112 (in Japanese).
69. M. Yamanishi, “Ultrafast optical processes through virtual charge polarization in quantum well structures,” *Oyo Buturi* **58**, 1696–1707 (1989) (in Japanese).
70. M. Ohtsu, M. Murata, and M. Kouroggi, “Subkilohertz linewidth of a semiconductor laser by electrical feedback and its network analysis,” *Proc. Conf. on Lasers and Electro-Optics (CLEO '89)*, Baltimore, 1989 (LEOS/IEEE and OSA, Washington, DC, 1989), THK30.
71. M. Ohtsu, M. Murata, and M. Kouroggi, *IEEE J. Quantum Electron.* **25**, 231–241 (1990).

72. M. Murata and M. Ohtsu, "FM noise reduction of a semiconductor laser by reflection mode of high finesse Fabry-Perot resonator," *Extended Abstracts of the 35th Spring Meeting of the Jpn. Soc. Appl. Phys. and Related Soc.*, 1988 (Jpn. Soc. Appl. Phys., Tokyo, 1988), 29p-ZP-9 (in Japanese).
73. M. Kouroggi, A. Kiyohara, and M. Ohtsu, "Improvement of the electrical negative feedback system for FM noise reduction of a semiconductor laser," *IEICE Technical Report on Optical and Quantum Electronics* (1989), pp. 19-24 (IEICE, Japan, Tokyo, 1989) (in Japanese).
74. T. W. Hänsch and B. Coullaud, *Opt. Commun.* **35**, 441-444 (1980).
75. H. P. Yuen and V. W. S. Chan, *Opt. Lett.* **8**, 177-179 (1989).
76. G. Abbas, V. W. S. Chan, and T. K. Lee, *IEEE J. Lightwave Technol.* **LT-3**, 1110-1122 (1985).
77. S. B. Alexander, *IEEE J. Lightwave Technol.* **LT-5**, 523-537 (1987).
78. M. Teshima, S.-H. Shin, and M. Ohtsu, "FM characteristics of optical feedback LD for homodyne OPLL," *Extended Abstracts of the 50th Autumn Meeting of the Jpn. Soc. Appl. Phys.*, 1989 (Jpn. Soc. Appl. Phys., Tokyo, 1989), 29p-ZL-3 (in Japanese).
79. M. Ohtsu, S. Katsuragi, and T. Tako, *IEEE J. Quantum Electron.* **QE-17**, 1100-1106 (1981).
80. K. Kuboki and M. Ohtsu, *IEEE J. Quantum Electron.* **25**, 2084-2090 (1989).
81. C.-H. Shin, K. Kuboki, and M. Ohtsu, "Simulation for the heterodyne type optical phase-locked loop by semiconductor lasers," *Trans. IEE Japan*, **108-C**, 678-684 (1988) (in Japanese).
82. S.-H. Shin, M. Teshima, and M. Ohtsu, "Heterodyne optical phase-locked loop by semiconductor lasers," *Extended Abstracts of the 50th Autumn Meeting of the Jpn. Soc. Appl. Phys.*, 1989 (Jpn. Soc. Appl. Phys., Tokyo, 1989), 29p-ZL-4 (in Japanese).
83. M. Kouroggi, A. Kiyohara, and M. Ohtsu, "Homodyne OPLL of semiconductor lasers by all electrical negative feedback," *Extended Abstracts of the 37th Spring Meeting of the Jpn. Soc. Appl. Phys.*, 1990 (Jpn. Soc. Appl. Phys., Tokyo, 1990), 31a-G-4 (in Japanese).
84. G. C. Bjorklund, *Opt. Lett.* **5**, 15-17 (1980).
85. M. O. Scully, *Phys. Rev. Lett.* **55**, 2802-2805 (1985).
86. M. Ohtsu and K.-Y. Liou, *Appl. Phys. Lett.* **52**, 10-12 (1988).
87. M. Winters, Joint Institute for Laboratory Astrophysics, University of Colorado, (1989), private communication.
88. Y. Tohmori, K. Komori, S. Arai, and Y. Suematsu, *Electron. Lett.* **21**, 743-745 (1985).
89. H. Kusuzawa, E. Ikegami, K. Nakagawa, and M. Ohtsu, "Nonlinear organic waveguides for a LD-based optical sweep generator II (Frequency sweep)," *Extended Abstracts of the 50th Autumn Meeting of the Jpn. Soc. Appl. Phys.*, 1989 (Jpn. Soc. Appl. Phys., Tokyo, 1989), 28p-ZP-17 (in Japanese).
90. M. Ohtsu, "Progress toward highly coherent semiconductor lasers," *Proc. 7th International Conf. on Integrated Opt. and Optical Fiber Communications*, (IOOC '89), July 1989, Kobe, Japan, (IEICE of Japan, Tokyo, 1989) 19A3-1.

91. H. Kusuzawa, E. Ikegami, K. Nakagawa, and M. Ohtsu, "Basic study on a LD-based Peta-Hertz class ultrahigh coherent optical sweep generator," *Proc. 4th Meeting on Lightwave Sensing Technology, 1989, Osaka* (Lightwave Sensing Technol. Group, Jpn. Soc. Appl. Phys., Tokyo, 1989), LST4-8 (in Japanese).
92. B. T. Darling and D. M. Dennison, *Phys. Rev.* **57**, 128–139 (1940).
93. K. Nakagawa, "Local mode vibrations in overtone vibration of  $\text{NH}_3$ ," Ph.D. thesis, University of Tokyo, 1989.
94. W. Lenth, *Opt. Lett.* **8**, 575–577 (1983).
95. L.-G. Wang, H. Riris, C. B. Carlisle, and T. F. Gallagher, *Appl. Opt.* **27**, 2071–2077 (1988).
96. F. M. Phelps III, *M.I.T. Wavelength Tables*, Vol. 2, *Wavelengths by Element*, The MIT Press, Cambridge, MA, 1982.
97. K. Sakurai and N. Yamada, *Opt. Lett.* **14**, 233–235 (1989).
98. H. Furuta, M. Hashimoto, H. Suzuki, K. Nakagawa, and M. Ohtsu, "Optical-microwave spectroscopy for rubidium beam atomic clocks," *Proc. Electronic Circuit Technical Meeting, IEE Jpn., 1989* (IEE Jpn., Tokyo, 1989), ECT-89-12 (in Japanese).
99. M. Ohtsu, M. Hashimoto, and H. Ozawa, "A highly stabilized semiconductor laser and its application to optically pumped Rb atomic clock," *Proc. 39th Annual Symp. Frequency Control, Philadelphia, 1985* (IEEE, Piscaway, NJ, 1985), pp. 43–53.
100. M. Suzuki and S. Yamaguchi, *IEEE J. Quantum Electron.* **24**, 2392–2399 (1988).
101. C. Vadla, A. Obrebski, and K. Niemax, *Opt. Commun.* **63**, 288–292 (1987).
102. M. Ohtsu and T. Tako, "Coherence in semiconductor lasers," in *Progress in Optics XXV*, E. Wolf, ed., Elsevier, Amsterdam, 1988, pp. 191–278.
103. H. Rinnenberg, "Ultrahigh  $n$  Rydberg atoms," *Technical Digest of 14th International Conf. on Quantum Electronics, San Francisco, 1986* (LEOS of IEEE, OSA, Washington, DC 1986), THKK1.
104. S. L. Gilbert and C. E. Wieman, *Phys. Rev. A* **34**, 792–803 (1986).
105. M. C. Noecker, B. P. Masterson, and C. E. Wieman, *Phys. Rev. Lett.* **61**, 310–313 (1988).
106. T. P. Emmons, J. M. Reeves, and E. N. Forston, *Phys. Rev. Lett.* **51**, 2089–2092 (1983).
107. C. E. Tanner and C. E. Wieman, *Phys. Rev. A* **38**, 162–165 (1988).
108. S. Chu (AT & T Bell Laboratories), private communication, 1986.
109. T. W. Hänsch and A. L. Schawlow, *Opt. Commun.* **13**, 68–69 (1975).
110. P. D. Lett, R. N. Watts, C. I. Westbrook, W. D. Phillips, P. L. Gould, and H. J. Metcalf, *Phys. Rev. Lett.* **61**, 169–172 (1988).
111. R. N. Watts, P. D. Lett, C. I. Westbrook, S. L. Rolston, C. E. Tanner, W. D. Phillips, P. L. Gould, and H. J. Metcalf, "Laser cooling below the Doppler limit," *Proc. Conf. on Quantum Electronics and Laser Science (QELS '89), Baltimore, 1989* (OSA, Washington, DC, 1989), THLL1.

112. A. Aspect, E. Arimond, R. Kaiser, N. Vansteenkiste, and C. Cohen-Tannoudji, *Phys. Rev. Lett.* **61**, 826–829 (1988).
113. E. L. Raab, M. G. Prentiss, A. E. Cable, S. Chu, and D. E. Pritchard, *Phys. Rev. Lett.* **59**, 2631–2634 (1987).
114. D. Sesko, C. G. Fan, and C. E. Wieman, *J. Opt. Soc. Am. B* **5**, 1225–1227, (1988).
115. R. N. Watts, D. H. Yang, B. Sheehy, and H. Metcalf, “Deceleration and cooling of a thermal beam of rubidium,” *Proc. 15th International Quantum Electronics Conference (IQEC '87)*, Baltimore, 1987 (OSA, Washington, DC, 1987), TUGG37.
116. H. Katori, K. Yamashita, and F. Shimizu, “Laser cooling of rare gas atoms by semiconductor lasers,” *Extended Abstracts of the Autumn Meeting of the Jpn. Soc. of Phys.*, 1989 (Jpn. Soc. Phys., Tokyo, 1989), 5a-ZF-11 (in Japanese).
117. C. E. Wieman, Joint Institute for Laboratory Astrophysics, University of Colorado, 1989, private communication.
118. E. Schrödinger, *Br. J. Phil. Sci.* **3**, 109–123 (1952).
119. J. C. Bergquist, R. G. Hulet, W. M. Itano, and D. J. Wineland, *Phys. Rev. Lett.* **57**, 1699–1702 (1986).
120. J. Bergquist, National Institute for Standards and Technology, 1989, private communication.
121. S. L. Gilbert, J. J. Bollinger, and D. Wineland, *Phys. Rev. Lett.* **60**, 2022–2025 (1988).
122. D. Meschede, H. Walther, and G. Muller, *Phys. Rev. Lett.* **54**, 551–554 (1985).
123. D. J. Heinzen, J. J. Childs, J. F. Thomas, and M. S. Feld, *Phys. Rev. Lett.* **58**, 1320–1323 (1987).
124. M. G. Raizen, R. J. Thompson, R. J. Brecha, H. J. Kimble, and H. J. Carmichael, *Phys. Rev. Lett.* **63**, 240–243 (1989).
125. K. Igeta, Y. Yamamoto, and S. Machida, “Control of spontaneous emission from a GaAs quantum well,” *Extended Abstracts of the Autumn Meeting of the Jpn. Soc. Phys.*, 1989 (Jpn. Soc. Phys., Tokyo, 1989) 4a-ZF-6 (in Japanese).
126. A. D. Streatere, J. Mooibroek, and J. P. Woerdman, *Appl. Phys. Lett.* **52**, 602–604 (1988).
127. M. Ohtsu, “Investigation on applicability of visible semiconductor lasers to elementary analysis,” *Proc. 1st Meeting on Lightwave Sensing Technology, Tokyo, 1988* (Lightwave Sensing Technol. Research Group, Jpn. Soc. Appl. Phys., Tokyo, 1988), LSTI-4 (in Japanese).
128. U. Lachish, S. Rotter, E. Adler, and U. El-Hanany, *Rev. Sci. Instrum.* **58**, 923–927 (1987).
129. G. Inoue and M. Suzuki, *Chem. Phys. Lett.* **105**, 641–644 (1984).
130. N. Takeuchi, *Development of Pseudo-Random Modulation CW Lidar and Its Application to Field Measurement* (Research Report from the National Institute for Environmental Studies, Japan, No. 122, 1989) (in Japanese).

131. R. G. Beausoleil, J. A. McGarvey, R. L. Hagman, and C. S. Hong, "Narrow-linewidth semiconductor laser for frequency modulated continuous-wave ladar," *Proc. Conf. on Lasers and Electro-Optics (CLEO '89)* Baltimore, 1989 (LEOS/IEEE, OSA, Washington, DC, 1989), WN3.
132. J. L. Picque, *Metrologia* **13**, 115–119 (1977).
133. S. Ohshima, Y. Nakadan, and Y. Koga, *IEEE Trans. Instrum. Meas.* **37**, 409–413 (1988).
134. D. W. Sesko and C. E. Wieman, *Opt. Lett.* **14**, 269–271 (1989).
135. M. Hashimoto and M. Ohtsu, *IEEE J. Quantum Electron.* **QE-23**, 446–451 (1987).
136. M. Hashimoto and M. Ohtsu, *J. Opt. Soc. Am. B* **6**, 1777–1789 (1989).
137. M. Ohtsu, H. Hashimoto, and H. Suzuki, "Performance evaluation of a semiconductor laser pumped Rb atomic clock," *Extended Abstracts of the 50th Autumn Meeting of the Jpn. Soc. Appl. Phys., 1989* (Jpn. Soc. Appl. Phys., Tokyo, 1989), 29a-X-5 (in Japanese).
138. M. Hashimoto and M. Ohtsu, *IEEE Trans. Instrum. Meas.* **39**, 458–462 (1990).
139. H. Furuta, K. Nakagawa, and M. Ohtsu, "Rubidium-atomic-beam clock pumped by a semiconductor laser I," *Extended Abstracts of the 50th Autumn Meeting of the Jpn. Soc. Appl. Phys., 1989* (Jpn. Soc. Appl. Phys., Tokyo, 1989), 29a-X-6 (in Japanese).
140. M. Sakamoto, D. F. Welch, J. G. Endriz, D. R. Scifres, and W. Streifer, *Appl. Phys. Lett.* **54**, 2299–2300 (1989).
141. T. M. Baer, "Diode-pumped solid state lasers," *Proc. Conf. on Lasers and Electro-Optics (CLEO '89)*, Baltimore, 1989 (LEOS/IEEE and OSA, Washington, DC, 1989), FJ1.
142. A. C. Nilsson, E. K. Gustafson, and R. L. Byer, *IEEE J. Quantum Electron.* **25**, 767–790 (1989).
143. T. Day, A. C. Nilsson, M. M. Fejer, A. D. Farinas, E. K. Gustafson, C. D. Nabors, and R. L. Byer, *Electron. Lett.* **25**, 810–812 (1989).
144. T. Day, E. K. Gustafson, and R. L. Byer, *Opt. Lett.* **15**, 2221–223 (1990).
145. J. J. Zayhowski and A. Mooradian, *Opt. Lett.* **14**, 618–620 (1989).
146. T. Y. Fan, G. Huber, R. L. Byer, and P. Mitzscherlich, *Opt. Lett.* **12**, 678–680 (1987).
147. K. Ishikawa and S. Imai, "Tunable solid state lasers," *Optronics*, No. 78 (1988) (Optronics Corp., Tokyo, 1988), pp. 81–86 (in Japanese).
148. R. W. P. Drever, J. Hough, A. J. Munley, S.-A. Lee, R. Spero, S. E. Whitcomb, H. Ward, G. M. Ford, M. Hereld, N. A. Robertson, I. Kerr, J. R. Pugh, G. P. Newton, B. Meers, E. D. Brooks III, and Y. Gursel, "Gravitational wave detectors using laser interferometer and optical cavities: Ideas, principles and prospects," in *Quantum Optics, Experimental Gravitation, and Measurement Theory*, P. Meystre and M. O. Scully, eds., Plenum Press, New York, 1981, pp. 503–514.

149. D. Shoemaker, A. Brillet, C. Nary Man, O. Crequit, and G. Kerr, *Opt. Lett.* **14**, 609–611 (1989).
150. C. D. Nabors, A. D. Farinas, T. Day, S. T. Yang, E. K. Gustafson, and R. L. Byer, *Opt. Lett.* **14**, 1189–1191 (1989).
151. M. Hillery and M. O. Scully, “Quantum noise and QND measurements,” in *Quantum Optics, Experimental Gravitation, and Measurement Theory*, P. Meystre and M. O. Scully, eds., Plenum Press, New York, 1981, pp. 661–674.





# 超高コヒーレントレーザーの周波数ゆらぎの測定

東工大総理工 申 哲 浩

## 1. まえがき

高性能光計測システム、コヒーレント光通信、高分解能分光、新しい光周波数標準、超精密光周波数掃引発振器などの光源として超高コヒーレントレーザーの研究開発が行われ、スペクトル線幅が1Hz以下になるNd:YAGレーザー、He-Neレーザー、色素レーザーが報告されている<sup>1)</sup>。最近、光・電気2重帰還法により発振線幅7Hzの半導体レーザーが実現している<sup>2)</sup>。これらの高安定レーザーの周波数安定度評価のためにはFM雑音のパワースペクトル密度、アラン (Allan) 分散、発振線幅パワー集中度が主に使われる。本稿ではそれらの定義、測定方法、測定例について記す。

## 2. 周波数揺らぎの尺度

パワースペクトル密度がフーリエ周波数 ( $f$ ) 領域での尺度であるのに対し、アラン分散は時間領域での尺度である。アラン分散は測定時間 (積分時間)  $\tau$  にわたり測定した公称周波数値  $\nu_0$  で規格化した周波数揺らぎの瞬時値  $y(t)$  を  $\bar{y}_k$  とし、

$$\sigma_y^2(\tau) = \left( \frac{\bar{y}_{k+1} - \bar{y}_k}{2} \right)^2 \quad (1)$$

で定義する。これとFM雑音の片側パワースペクトル密度  $S(f)$  との間には

$$\sigma_y^2(\tau) = \frac{2}{\nu_0^2} \int_0^\infty S(f) \frac{\sin^4(\pi f \tau)}{(\pi f \tau)^2} df \quad (2)$$

の関係がある<sup>3)</sup>。さらに、発振スペクトル形状は  $S(f)$  を用いて

$$I(\nu - \nu_0) = 4 \cdot \text{Re} \left[ \int_0^\infty \exp \left\{ j2\pi (\nu - \nu_0)\tau - 2(\pi\tau)^2 \int_0^\infty S(f) \frac{\sin^2(\pi f \tau)}{(\pi f \tau)^2} df \right\} d\tau \right] \quad (3)$$

により与えられる<sup>4)</sup>。 $S(f)$  が全  $f$  にわたって一定値  $S_0$  をとる場合、すなわち、スペクトル形状がローレンツ形であれば、

発振線幅  $\Delta\nu$  は  $\pi S_0$  に等しい。

$|\nu - \nu_0| < B$  ( $B$  は考慮する帯域) に集中されるレーザーのパワー率  $R_{PC}$  は

$$R_{PC} = \left| \int_0^\infty \left[ 2 \int_B^\infty \frac{S(f)}{f^2} df \right]^{1/2} \right|^2 \quad (4)$$

で与えられる<sup>5)</sup>。スペクトル形状がローレンツ形の場合  $B = \Delta\nu/2$  の  $R_{PC}$  は50%である。

以上からわかるようにFM雑音のパワースペクトル密度  $S(f)$  を測定することによって他の尺度は決定できる。発振線幅は必ずしもFM雑音の大きさを正確に表す尺度ではないが、パワー集中度とあわせて表示すれば、この2つの尺度の対によりFM雑音の大きさを概観できる。

## 3. 測定法

紙面の制限より発振線幅とFM雑音のパワースペクトル密度の測定方法を主に記述する。アラン分散の測定方法は文

献<sup>5,6)</sup>を参照されたい。被測定レーザーより周波数安定度がよい基準レーザーがある場合には、2つのレーザーのビート信号を測定することによって発振線幅とFM雑音のパワースペクトル密度が決定できるが、ここでは被測定レーザーを超高コヒーレントレーザーとするので、基準レーザーがない時の測定法を中心に説明する。図1にFM雑音と線幅の測定法を示す。

スペクトル形状はA-①のように光ファイバーを使う方法とA-②のように掃引形ファブリ・ペロー干渉計 (FPI) を使う方法がある。まず、A-①を説明する。レーザーの光を2つに分け、一方を長い光ファイバーを通して遅延させた後、2つの光を再合成する。このとき、両者の光の揺らぎはもはや無相関とみなされるので、再合成に使った光検出器の出力をマイクロ波スペクトラム・アナライザーに加えれば、被測定レーザーのスペクトルの2倍の線幅をもつスペクトル形状が観測される。これは遅延自己ホモダイナ法と呼ばれる<sup>7)</sup>。この測定の分解能は遅延後の無相関性が破れることに起因するので、ファイバーの長さ  $L_f$  に反比例し、 $c/2n_f L_f$  である。ここで  $n_f$  はファイバーの屈折率である。分けられた2つのレ

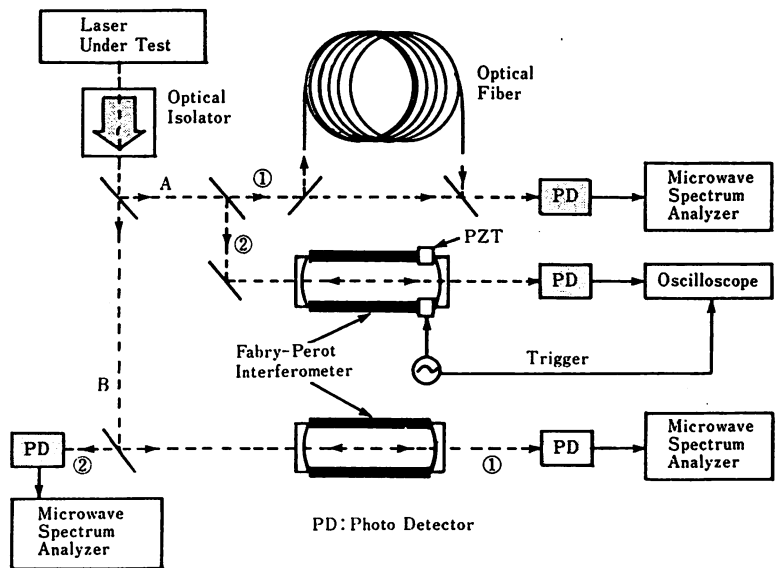


図1 FM雑音の測定法。  
A: 発振線幅測定法 (A-①遅延自己ホモダイナ法、A-②スキャニング光スペクトラム分析法。)  
B: FM雑音のパワースペクトル密度測定法。(B-①ファブリ・ペロー干渉計の透過モード利用法、B-②ファブリ・ペロー干渉計の反射モード利用法。)

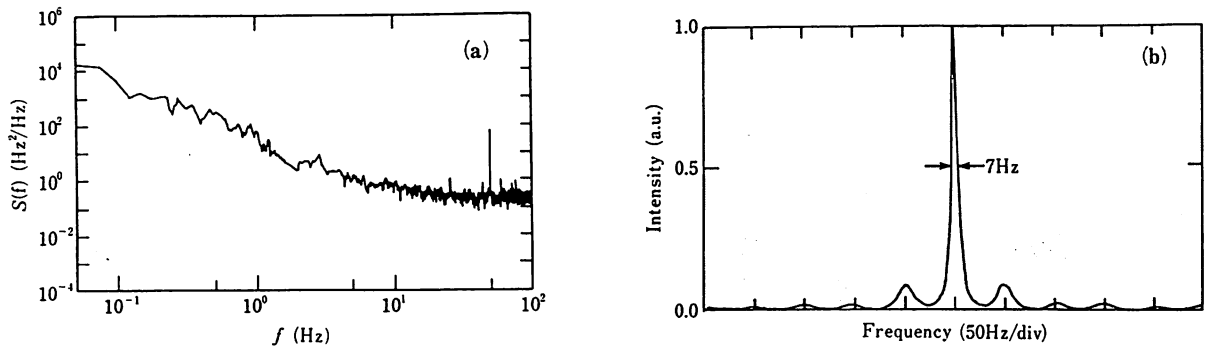


図2 FM雑音の測定例。波長0.8 $\mu$ m AlGaAsレーザに光帰還と電気的負帰還制御とを同時に施した結果得られたFM雑音の測定結果(a)とそれを用いて計算したスペクトル形状(b)。

ーザ光の一方を音響光学変調器で周波数シフトさせ測定するヘテロダイン法もある。この遅延法は分解能以下の低いフーリエ周波数雑音成分はカットされるので、測定された線幅には1/f雑音と周波数ドリフトの影響が現れてこない。A-②の場合にはレーザ光をファブリ・ペロー干渉計に入射させ、干渉計の長さを掃引すると光検出器で検出された干渉計透過光の強度変化によりスペクトル形状が測定できる。測定分解能は干渉計の共振曲線の幅によって決まる。

FM雑音のパワースペクトル密度の測定のためには、図1に示したように、光検出器の前に、光学的F/V変換器を設置する。これにはファブリ・ペロー干渉計の透過モード(図1のB-①)と反射モード(図1のB-②)、マイケルソン干渉計、原子、分子の吸収線、などを使う。この中、ファブリ・ペロー干渉計は装置の簡便さ、高S/N、高い短期周波数安定度、の利点があるので最もよく利用される。この場合、検出帯域幅は干渉計の共振曲線の線幅の1/2であり、その帯域より高いフーリエ周波数では透過モードでは-40dB/dec、反射モードでは-20dB/dec、の割合で検出感度が落ちる。検出帯域内での検出感度Kは次式で与えられる<sup>2,4)</sup>。

$$K = K_s \frac{\eta_c PR}{\Delta\nu_c} \quad (5)$$

ここで、 $K_s$ は検出に使う干渉計の共振線の傾き(共振ピークの1/2の所を使うと $\approx 1$ )、 $\eta_c$ は干渉計の効率(共振ピークと入射光の強度との比)、 $P$ は検出に使う光パワー、 $R$ は検出に使う光検出器の感度、 $\Delta\nu_c$ は干渉計の共振半値全幅である。(5)式から分かるように、検出感度は干渉計の共振曲線の線幅が狭いほど高い。しかし上述の理由により検出帯域は減少する。最近ではフィネス10,000以上のファブリ・ペロー干渉計、すなわちスー

パーキャビティが市販されている。スーパーキャビティでは効率が重要な量であるが、最近では60%以上のものも実現されている。さらに、実験室レベルではフィネス100,000以上のスーパーキャビティも超高コヒーレントレーザ用の周波数基準として使われている。この場合、レーザ光の強度雑音が測定感度を制限する場合があるので、高精度測定には強度雑音だけが除去できる光バランス検出器を使う必要がある。ただし、これらの光学的F/V変換器を使う場合、F/V変換器の固有周波数へのレーザ周波数追従度を測っていることになるので、固有周波数の揺らぎが十分小さく安定なF/V変換器を使うことが重要である。以上により測定されたFM雑音のパワースペクトル密度と(2)、(3)式とを利用するとアラソ分散、スペクトル形状が求められる。

#### 4. 測定例

図1に示した測定法B-②によるFM雑音のパワースペクトル密度の測定例とそれを用いた発振線幅の計算例を紹介する。光帰還法は不安定であるが、広帯域FM雑音抑圧ができる利点をもつ。そこであらかじめ光帰還法によりAlGaAsレーザのFM雑音を抑圧し、さらに、その不安定性を除去するために電気的負帰還制御を同時に施した結果得られたFM雑音のパワースペクトル密度を図2(a)に示す<sup>2)</sup>。電気的負帰還制御はフィネス35,000のスーパーキャビティの反射モードを用いた。図2の結果は制御時のFM雑音の弁別信号を測定したものである。ここでは、フーリエ周波数1Hz以下でも安定にFM雑音が抑圧されていることを確認するためにFFTアナライザを低周波スペクトラムアナライザとして用いた。図2(a)の測定結果と(3)式を用いて求めた発振スペクトル形状を図2(b)に示す。この発振線幅は7Hzである。ま

た、制御帯域1.5MHz以内のパワー集中度率は98%であった。これにより、周波数制御された超高安定気体レーザ、固体レーザ、などと同等の値が半導体レーザとしては初めて実現したことが確認された。

#### 5. むすび

レーザのFM雑音の量を表す尺度として、パワースペクトル密度、アラソ分散、発振線幅、パワー集中度の定義と相互関係、測定法、測定例、について示した。これらの測定に関しては一般の物理量の測定と同様の測定論が適用できるのはいうまでもない。すなわち、測定装置の雑音低減、感度向上、帯域拡大、が必須である。

- 1) 中川賢一: 光学 19, 642 (1990).
- 2) C. H. Shin and M. Ohtsu: Opt. Lett. 15, 1455 (1990).
- 3) L. S. Cutler and C. L. Searle: Proc. IEEE 54, 136 (1966).
- 4) M. Ohtsu and N. Tabuchi: J. Lightwave Technol. 6, 357 (1988).
- 5) K. Kuboki and M. Ohtsu: IEEE Trans. Instrum. Meas. 39, 637 (1990).
- 6) C. H. Shin and M. Ohtsu: Electron. Lett. 26, 1571 (1990).
- 7) T. Okoshi, K. Kikuchi and A. Nakayama: Electron. Lett. 16, 630 (1980).

分類番号 7.8, 7.10

Measurement of frequency fluctuations in ultra-high coherent lasers. Chul-Ho SHIN. Graduate School at Nagatsuta, Tokyo Institute of Technology.

SCW1

## Frequency Stabilization of Diode Lasers

M. OHTSU

Graduate School at Nagatsuta, Tokyo Institute of Technology,  
4259 Nagatsuta, Midori-ku, Yokohama 227, Japan  
Tel. +81-45-922-1111 (ext. 2526), Fax. +81-45-921-1156

Ultra-stable diode lasers have been required for various application systems. In this presentation, we review performances of our frequency-stabilized diode lasers and their application systems.

For reliable and accurate linewidth reduction, an electrical feedback was employed, and the half linewidth of a 0.83  $\mu\text{m}$  AlGaAs laser was reduced to 560 Hz[1], which was about -25 dB from that of the Schawlow-Townes' limit of the solitary laser device. Optical feedback from an external confocal Fabry-Perot cavity was also employed to realize a moderately narrow linewidth of 20 kHz[2]. A compact module of this system was developed by using techniques of micro-optics. Figure 1 shows a photograph of this module[3]. This optical feedback was also employed to reduce the linewidth of a visible 0.67  $\mu\text{m}$  AlGaInP laser to less than 50 kHz[4]. Optical feedback was combined with the electrical feedback for further linewidth reduction, and thereby the linewidth of an AlGaAs laser as narrow as 1 Hz was realized[5].

To avoid the instability of the optically feedback laser induced by the phase change of the reflected light from the external reflector, a phase conjugate wave generated from the other diode laser was injected into the laser. This novel optical feedback realized a stable linewidth reduction independent on the separation between the two lasers, as is shown by Fig.2[6].

A frequency synchronization link between two different wavelength lasers, i.e., 0.78  $\mu\text{m}$  AlGaAs and 1.56  $\mu\text{m}$  InGaAsP lasers, was realized by locking the frequencies of the AlGaAs laser and the second harmonics of InGaAsP laser simultaneously to the Doppler-free optical-optical double resonance line in Rb. The second harmonics internally generated from the active waveguide of the InGaAsP laser was used for this experiment.

Homodyne optical phase locked loop (OPLL) by purely electrical feedback realized a bandwidth as wide as 100 MHz and reduced the residual phase variance to 0.15 ( $\text{rad}^2$ ). Homodyne OPLL using the optically feedback lasers realized the residual phase variance of 0.002 ( $\text{rad}^2$ ). Heterodyne OPLL using the optically feedback laser has realized the residual phase variance of 0.02 ( $\text{rad}^2$ ) and residual heterodyne frequency fluctuations of 0.4 mHz (i.e.,  $1 \times 10^{-18}$  heterodyne frequency stability) at the integration time of 70(s)[7]. This heterodyne OPLL was advantageously used for fine tuning of the laser frequency for the range of 1 THz[8]. To realize a Peta-Hz class optical sweep generator, organic nonlinear optical waveguides were fabricated for coarse and wideband frequency tuning[9].

These frequency-stabilized diode lasers were employed in the following application systems:

- (1) For analytical spectroscopy, opto-galvanic spectral lines in Li were observed by a 0.67  $\mu\text{m}$  AlGaInP laser. To improve the efficiency of these experiments, the power of this diode laser was amplified by a YAG laser-pumped dye (LDS698) solution, and then an amplification gain was 25 dB, as is shown by Fig.3[4].
- (2) A Rb atomic clock was optically pumped by a frequency-stabilized AlGaAs laser, which improved the short-term microwave frequency stability more than  $10^3$  times that of the conventional Rb atomic clocks[10]. The long-term microwave frequency stability was also improved 40 times by compensating for the light shift[11]. An atomic beam-type Rb clock is being developed to improve the microwave frequency accuracy, and a novel microwave Ramsey fringe was observed by using a microwave cavity[12].
- (3) A super-resolution and a reflection-type photon scanning tunneling microscope was proposed in which the tunnel-chip was made of a fiber Fabry-Perot cavity or a diode laser[13]. For drastic improvements of the sensitivity, the frequency-shift of the resonance frequency of this cavity is measured instead of measuring the power of the evanescent light. As is shown by Fig.4, the lateral and normal resolutions of 1 nm were estimated by using the accurate heterodyne OPLL technique described above.
- (4) Using the cavity quantum electrodynamics technique was proposed to improve the laser cooling limit of the atoms[14], in which frequency-stabilized diode lasers play essential roles as pumping and cooling sources.

## References

- [1] M. Ohtsu, et.al.: IEEE J. Quantum Electron., 26, 231 (1990)
- [2] B. Dahmani, et.al.: Opt. Lett., 12, 876 (1987)
- [3] C.-H. Shin, et.al.: Photonics Technol. Lett., 2 (1990), March Issue, in press
- [4] H. Suzuki, et.al.: Extended Abstracts (The 37th Spring Meeting, 1990) Jpn. Soc. Appl. Phys., March 1990, paper No. 31a-G-10 (In Japanese)
- [5] C.-H. Shin and M. Ohtsu, to be presented at this meeting
- [6] I. Koshilishi, et.al.: Extended Abstracts (The 37th Spring Meeting, 1990) Jpn. Soc. Appl. Phys., March 1990, paper No. 31a-G-9 (In Japanese)
- [7] C.-H. Shin and M. Ohtsu: Photonics Technol. Lett., 2 (1990), April Issue, in press
- [8] K. Kuboki and M. Ohtsu: IEEE J. Quantum Electron., 25, 2084 (1990)

- [9] M. Ohtsu, et.al.: to be presented at CLEO'90, May 1990, Anaheim, CA, paper No.CME5
- [10] M. Hashimoto and M. Ohtsu : J. Opt. Soc. Am. B. 6, 1777 (1989)
- [11] M. Hashimoto and M. Ohtsu : IEEE Trans. Instrum. and Meas., June Issue, 1990, in press
- [12] H. Furuta and M. Ohtsu : to be presented at CPEM'90, June 1990, Ottawa
- [13] M. Ohtsu, et.al.: to be presented at OEC'90, July 1990, Makuhari
- [14] K. Nakagawa and M. Ohtsu : Extended Abstracts ( The 37th Spring Meeting, 1990 ) Jpn. Soc. Appl. Phys., March 1990, paper No. 28a-A-8 ( in Japanese )

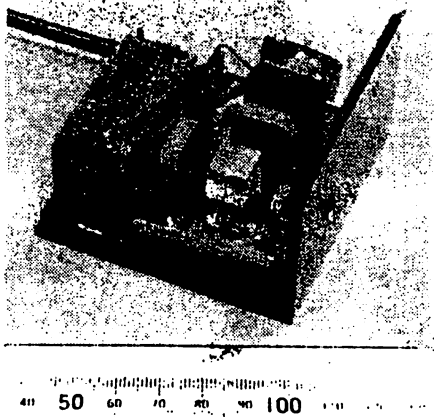


Fig. 1. A photograph of a compact module of a AlGaAs laser stabilized by optical feedback from a micro-lens Fabry-Perot cavity[3].

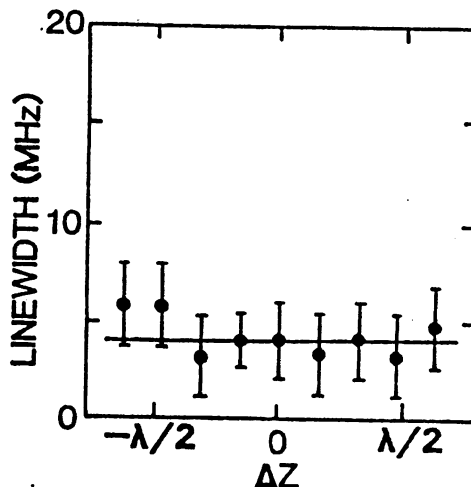


Fig. 2. A relation between the separation  $\Delta z$  between the two lasers and the half linewidth of a laser which was reduced by optical feedback of a phase conjugate wave from the other laser[6]. The linewidth without any feedbacks was 20 MHz.  $\lambda$ : Optical wavelength.

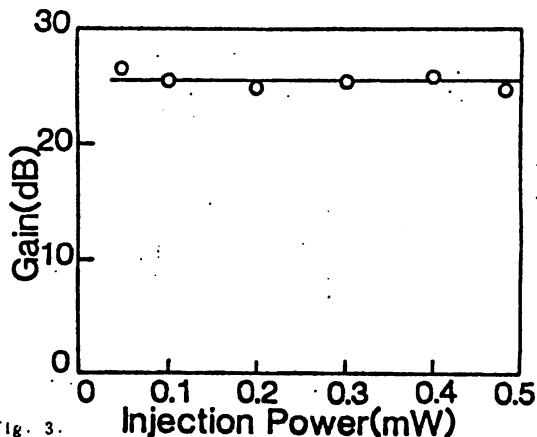


Fig. 3. A relation between the injection power from a 0.67  $\mu\text{m}$  AlGaInP laser and the amplification gain of a YAG laser-pumped dye ( LDS698 ) solution.

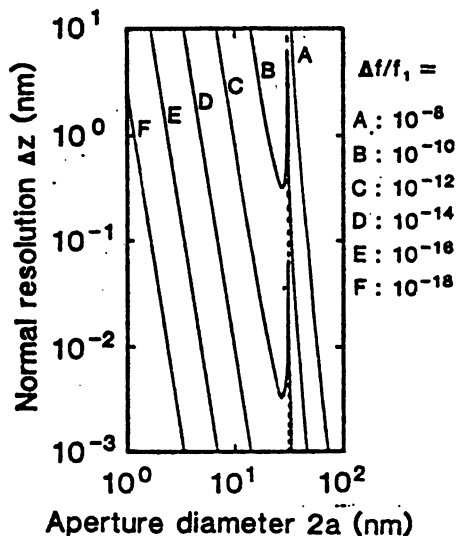


Fig. 4. Estimated relation between the aperture diameter ( which determines the lateral resolution ) and the normal resolution of a reflection-type photon scanning tunneling microscope with super-resolution.  $\Delta f/f_1$  is a frequency-shift of the resonance frequency of a fiber Fabry-Perot cavity used as a tunnel-chip, which was normalized to the optical frequency  $f_1$  [13].

## SCW3 Very Precise Phase/Frequency Control of Confocal Fabry-Perot Cavity Coupled Semiconductor Laser

Chul-Ho Shin and Motoichi Ohtsu

Graduate School at Nagatsuta, Tokyo Institute of Technology  
4259 Nagatsuta, Midori-ku, Yokohama, Japan  
Tel 045-922-1111(ext.2526) Fax 045-921-1156

Ultra narrow linewidth semiconductor lasers are attractive for the applications to precise measurements and high resolution spectroscopy, and coherent communication systems.

The confocal Fabry-Perot cavity coupled semiconductor laser (CFP-LD) shows a wide band frequency noise suppression characteristics with narrow linewidth[1][2]. The FM characteristics of the CFP-LD had been reported in [3]. We had carried out the experiment on the heterodyne optical phase-locked loop (OPLL) using two AlGaAs CFP-LD's of 10 kHz linewidths, with the phase error of 8.1 degrees and the frequency tracking error between two lasers of 0.4MHz at the integration time of 70sec [4]. The linewidth of the heterodyne signal under phase locking with PLL noise bandwidth of about 1 MHz was less than 30 Hz, which was limited by the resolution bandwidth of the spectrum analyzer used in the measurement.

We have also carried out the experiment on the homodyne OPLL using these lasers, where a balanced detector consisted of two pin-PD's was used as the phase comparator. The phase/frequency of the slave laser was controlled by using two routes via CFP cavity length control for lower frequency components upto about 10 kHz and injection current control for higher frequency components to secure a wide control bandwidth. Figure 1 shows the phase error spectral density under phase-locked condition, where phase noise spectra are fully suppressed within the PLL noise bandwidth of about 1.3 MHz. The RMS phase error was 2.6 degrees, which was measured by comparing with the output signals from the phase detector under phase-locked and unlocked conditions.

From the results of [4] and Fig.1, it is expected that the linewidth of the CFP-LD can be narrowed to less than the order of 10Hz if its frequency is locked to a stable reference with a control bandwidth of the order of 1 MHz. In this connection, we selected a hermetically-sealed and temperature-controlled super-cavity with the finesse of more than 30,000 and the free spectral range of 6 GHz as the frequency reference. According to the maker's specification, the frequency drift of the cavity resonance frequency is 150 kHz/3minutes, so it can be considered as a stable reference. Figure 2 shows the schematic of the experimental set-up for linewidth narrowing of the CFP-LD. The FM noise of the CFP-LD was demodulated by the reflection mode of the super-cavity[5]. And then the demodulated signal is negatively feedback to the laser via the CFP cavity length and the injection current controls. A part of the reflected light from the super-cavity of about nW was optically feedback to the CFP-LD, simultaneously. This optical feedback is, of course, not indispensable, but useful for the FM noise suppression. If optical feedback power is large, the mode competition between the CFP cavity and the super cavity modes may be occur. The severe optical isolation and the optical axis alignment is required for using only electrical negative feedback scheme. However, the electrical feedback is essential for stable locking. As can be seen by Fig.3, FM noise power spectral density(FSD) of the CFP-LD was suppressed about 45dB by this scheme. This means that the linewidth of the CFP-LD was narrowed to the order of 1 Hz. We are preparing to measure the FM noise PSD for Fourier frequency lower than 100 Hz, which was not measured in Fig.3. The result shows

that a ultra narrow linewidth semiconductor laser can be made by using double optical feedback scheme in cooperating with electrical negative feedback technique.

References

- [1] B. Dahmani, L. Holberg and R. Drullinger, *Opt. Lett.*, V.12, 876-878, 1987
- [2] C.H. Shin et. al., 7th IOOC in Kobe, Japan, 21D4-5, 1989
- [3] C.H. Shin et.al., *IEEE Photon. Technol. Lett.*, 2, March issue, 1990
- [4] C.H. Shin and M. Ohtsu, *IEEE Photon. Technol. Lett.*, 2, April issue, 1990
- [5] M. Ohtsu et.al, *IEEE Quantum Electron.*, 26, 231-341, 1990

Fig.1 Power spectral density of phase error in homodyne phase-locked loop.

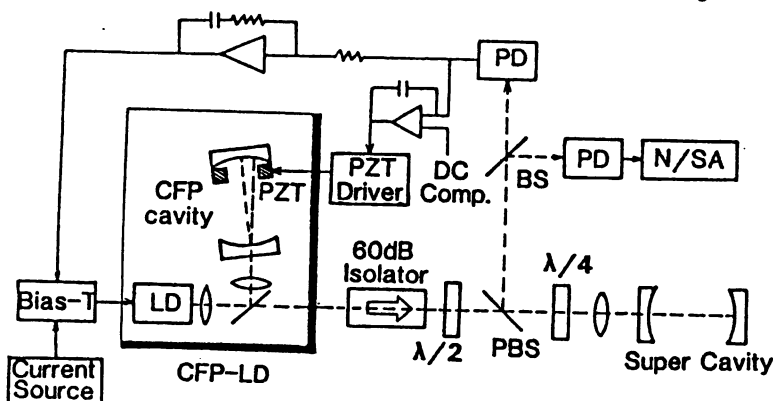
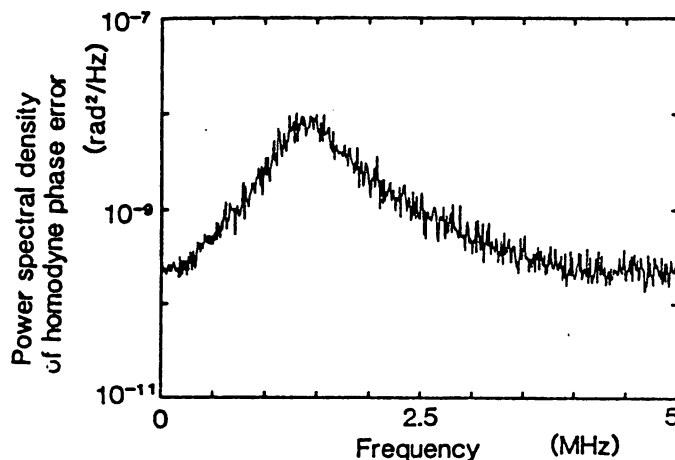
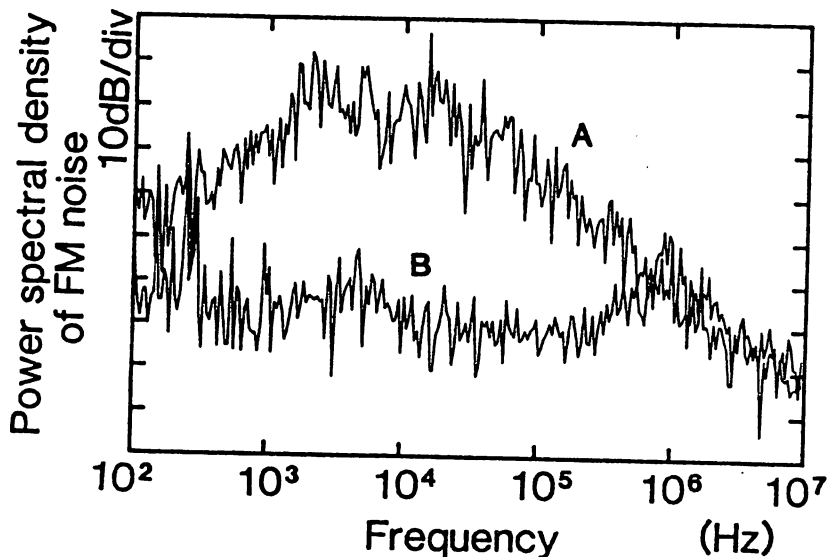


Fig.2 Experimental set-up for linewidth narrowing of the CFP-LD. PBS:polarization beam splitter. PD:photo-diode. DC comp.:DC compensation.  $\lambda/2$ ,  $\lambda/4$  :wavelength plates. N/SA :network/spectrum analyzer.

Fig.3 Controlled power spectral densities of FM Noise with narrow bandwidth (A) and wide bandwidth (B). Linewidth of the non-controlled CFP-LD was less than 10 kHz.



IR TO UV COHERENT OPTICAL SWEEP GENERATOR BY SEMICONDUCTOR LASERS

Motoichi Ohtsu

Graduate School at Nagatsuta, Tokyo Institute of Technology,  
4259 Nagatsuta, Midori-ku, Yokohama, Kanagawa 227, Japan

Our experimental results on frequency stabilization, linewidth reduction, homodyne- and heterodyne-type phase lockings, and accurate frequency sweep of semiconductor lasers, including recently developed 671nm semiconductor lasers, are reported. Based on these results, a method of stable frequency sweep from near-IR to near-UV is proposed to realize a Peta-Hertz class coherent optical sweep generator. Experimental results on fabrications of organic nonlinear optical waveguides and frequency link between different wavelength lasers are presented to realize this sweep generator. As applications of these high quality semiconductor laser systems, an optical fiber gyroscope, a rubidium atomic clock, a photon scanning tunneling microscope, and cavity QED experiments are demonstrated.

JAPAN-UNITED STATES SEMINAR  
(pp.451-472)

FREQUENCY CONTROL OF SEMICONDUCTOR LASERS AND ITS APPLICATIONS

M. OHTSU

The Graduate School at Nagatsuta, Tokyo Institute of Technology  
4259 Nagatsuta, Midori-ku, Yokohama, Kanagawa 227, JAPAN

Phone : +45-922-1111 (ext.) 2526. FAX : +45-921-1156

[ ABSTRACT ]

Our recent experimental results on frequency stabilization, linewidth reduction, phase locking, and Peta-Hz class frequency sweep are reviewed. For these experiments, we employed mainly the stable and reproducible technique of negative electrical feedback. Optical feedback was also employed auxilarily in order to increase the gain of the negative electrical feedback loop. Possibility of using an oxide superconductor film for optical frequency counting system is proposed. As an application system of these high quality semiconductor laser system, we proposed a reflection-type photon scanning tunneling microscope ( photon STM ), and demonstrated some preliminary experimental results. Results are summarized as :

(1) Frequency stability of  $2 \times 10^{-12}$  was obtained, and a modified Fabry-Perot interferometer with a polarization rotator was proposed as a sensitive and wideband optical frequency discriminator.

(2) The half linewidth of the field spectral profile was reduced

to 7 Hz.

(3) Phase error variance and loop bandwidth of  $0.15 \text{ radian}^2$  and 100 MHz, respectively, were obtained in the homodyne optical phase locked loop. In the heterodyne optical phase locked loop, the phase error variance and heterodyne frequency fluctuations of  $0.02 \text{ radian}^2$  and 0.4 MHz, respectively, were obtained.

(4) For the frequency sweep, we have realized a frequency link between the different wavelengths lasers by utilizing an optical double resonance spectral lines in Rb vapor. Organic nonlinear optical waveguides were fabricated for the second harmonic generation and optical parametric oscillation, resulting the total frequency sweep range of 700 THz.

(5) For optical frequency counting system, we have observed a non-bolometric signal in an oxide superconductor film by irradiating a chopped laser beam. Such a phenomenon can be used as a novel, sensitive, and fast photo-detector.

(6) For application, we proposed a reflection-type Photon STM to achieve a resolution of 0.1 nm, which can be used as a quantum optical microscope for real-time and non-destructive diagnostics of biomembranes and ultra-thin organic films.



The 2nd INTERNATIONAL FORUM ON THE FRONTIER OF  
TELECOMMUNICATIONS TECHNOLOGY

COHERENT QUANTUM OPTICS AND TECHNOLOGY

Motoichi OHTSU

The Graduate School at Nagatsuta,

Tokyo Institute of Technology

4259 Nagatsuta, Midori-ku, Yokohama, Kanagawa 227, Japan

Phone : 045-922-1111 ( extension 2526 )

[ ABSTRACT ]

Our recent works on coherent quantum optics and technology, i.e., improvement of coherence of lasers, development of novel light emitting devices, and its applications to atomic physics and advanced systems for industry, will be reviewed. There are three parts in this talk : (1) experimental results on frequency stabilization, linewidth reduction, phase locking, and Peta-Hz frequency sweep are reviewed. (2) Novel optical frequency counting system and the possibility of using an oxide superconductor film for optical frequency counter are proposed. (3) As an application system, a photon scanning tunneling microscope, a laser-pumped rubidium atomic clock, and a passive ring cavity-type fiber gyroscope are demonstrated.

## QELS '91/THURSDAY AFTERNOON

Thursday Afternoon  
 May 16, 1991 QThL  
 Hyatt Regency Ballroom C

3:00 pm Symposium on Stabilized Lasers II

J. L. Hall, *JILA-NIST, Presider*

3:00 pm Invited  
 QThL1 7-Hz-linewidth diode lasers,  
 wideband optical phase locking,  
 and applications

M. Ohtsu, C.-H. Shin, H. Furuta,  
 M. Kouguri, H. Kusuzawa, S. Jiang, and  
 K. Nakagawa  
*Graduate School at Nagatsuta, Tokyo Institute of  
 Technology, 4259 Nagatsuta, Midori-ku,  
 Yokohama, Kanagawa 227, Japan*

Highly coherent laser diodes (LD's) are indispensable for studying basic physics (e.g., manipulation of atoms, experiments on P and T violation in atoms, and cavity QED) and for a variety of photonics technology systems. We review here the performances of highly coherent LD's and their application systems. Two kind of experiments were carried out to reduce linewidth of LD's. In the first experiment, the linewidth of a 1.5- $\mu\text{m}$ -wavelength three-electrode distributed-feedback LD was reduced by using a negative electrical feedback (NEF) loop. Because its free-running linewidth was 350 kHz and a flat FM response could be obtained by adjusting the dc bias level to each electrode, a NEF loop with a very high gain could be optimally designed. The linewidth could be reduced to 300 Hz with a 10-MHz-bandwidth NEF loop. In the second experiment, the linewidth of a Fabry-Perot AlGaAs LD with a 0.8- $\mu\text{m}$  wavelength was reduced to 560 Hz by NEF.<sup>1</sup> As an auxiliary, optical feedback (OF) was used to increase the NEF loop gain. By applying the NEF to this OF laser, a linewidth as narrow as 7 Hz was achieved with the power concentration as high as 81% of the controlled spectral profile. Figure 1 shows the progress of the half-linewidth reduction by NEF and by carefully designed solitary distributed-feedback and distributed-Bragg-reflector, InGaAsP lasers. It is expected that the NEF technique will provide a sub-hertz-linewidth LD if a more advanced optical frequency discriminator is used.<sup>2</sup>

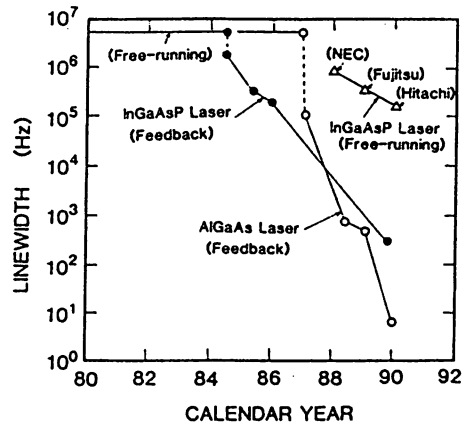
A bandwidth as wide as 134 MHz was achieved in the homodyne optical phase-locked loop (OPLL). By using an auxiliary OF technique, the heterodyne OPLL achieved a phase error variance as low as  $2 \times 10^{-3} \text{ rad}^2$  and a 0.4-mHz frequency tracking error at an integration time of 70 s.<sup>3</sup>

We have proposed a highly coherent petahertz optical sweep generator ranging from UV to IR by using these highly coherent LDs as master oscillators.<sup>4</sup> Nonlinear optical frequency converters, e.g., OPO, are being developed by fabricating organic nonlinear optical waveguides. An optical frequency measurement system was proposed for these coherent light sources, especially for the 1.5- $\mu\text{m}$  wavelength region, by nonlinear optical frequency conversion. Two frequency-stabilized He-Ne lasers (0.63- $\mu\text{m}$  and 3.39- $\mu\text{m}$  wavelengths) are used as primary frequency references to achieve mea-

surement accuracy as high as  $1 \times 10^{-9}$ . For this system, an optical-frequency comb generator was proposed as the local oscillator, and an oxide superconductor film was proposed as the wavelength-independent fast photodetector for efficient heterodyne detection.

As application systems, LD-pumped Rb atomic clocks (gas-cell type<sup>5</sup> and atomic-beam type) and photon scanning tunneling microscopes<sup>6,7</sup> were developed. Their performances will be presented in the session. The possibility of using the photon scanning tunneling microscope for single-atom manipulation will be also discussed.

1. M. Ohtsu, M. Murata, and M. Kouguri, *IEEE J. Quantum Electron.* 26, 231-241 (1990).
2. M. Kouguri and M. Ohtsu, *Opt. Commun.*, in press.
3. C.-H. Shin and M. Ohtsu, *Opt. Lett.*, in press.
4. M. Ohtsu, *et al.*, in *Technical Digest, Conference on Lasers and Electro-Optics* (Optical Society of America, Washington, D.C., 1990), paper CME5.
5. M. Hashimoto and M. Ohtsu, *IEEE Trans. Instrum. Meas.* 39, 458-462 (1990).
6. M. Ohtsu, *et al.*, in *Proceedings of the Third Optoelectronics Conference*, Makuhari, Japan, July 1990, paper 12D1-1.
7. S. Jiang, *et al.*, in *Proceedings of the Third Optoelectronics Conference*, Makuhari, Japan, July 1990, paper 12D1-3.



QThL1 Fig. 1. Progress in linewidth reduction of diode lasers.

by applying the ac electric field parallel to the  $c$  axis of  $\text{KNbO}_3$  crystal.

The experimental arrangement is shown in Fig. 1. The fundamental light is provided by a GaAlAs laser diode (SDL-5411-G1). The output is mode matched to the three-mirror, ring built-up cavity. A 5-mm-long  $\text{KNbO}_3$  crystal is placed in the beam waist of the cavity. Noncritical phase matching using nonlinear coefficient  $d_{32}$  can be achieved at room temperature.

The stabilization of the laser-diode frequency to the cavity-resonance frequency is achieved by optical feedback from the counter-propagating fundamental mode, reflected from the  $\text{KNbO}_3$  crystal facet.<sup>2</sup> To provide stable locking, we controlled the optical path length between the laser diode and the ring cavity by applying P-I feedback to a piezoelectric-transducer-mounted mirror, by which the laser frequency was locked to the peak of the resonance. Even though the  $\text{KNbO}_3$ -loaded ring cavity had finesse as low as 16 for the fundamental wavelength, a frequency-locking range of as wide as 20 GHz was achieved,  $\sim 3$  times wider than the free spectral range (6 GHz) of the cavity.

The maximum second-harmonic power is 3.3 mW at 87 mW of fundamental power incident to the resonant cavity. With the P-I control loop closed, the blue output fluctuation is less than  $\pm 0.1\%$  over several hours, as shown in Fig. 2. The linewidth of the resonant fundamental output is  $< 1$  MHz (measured by the delayed, self-homodyne technique), 1 order smaller than that of free running. The relative intensity noise (RIN) is about  $-130$  dB/Hz for a Fourier frequency range up to 20 MHz.

The modulation characteristics of the blue radiation are shown in Fig. 3. The electric field is applied parallel to the  $c$  axis of a 3-mm-thick  $\text{KNbO}_3$  crystal. Blue-radiation intensity is selectively modulated because the fundamental and blue-radiation beams are orthogonally polarized. Further, EO coefficient  $r_{33}$  (effective for blue radiation) is 50 times larger than  $r_{23}$  for fundamental radiation. Therefore, modulation for blue radiation is realized by the SHG phase mismatch because of the EO effect; stable frequency locking is maintained because of the negligibly small change in the refractive index for fundamental radiation. A representative result of this modulation experiment is 78% in modulation depth and several hundred kilohertz in bandwidth. Improving the driving circuit should expand the bandwidth up to several megahertz.

*\*Tokyo Institute of Technology, Graduate School at Nagatsuta, 4259 Nagatsuta, Midori-ku, Yokohama 227, Japan*

9:15 am

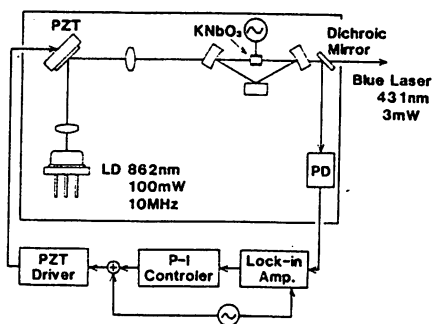
**CWA6 Direct modulation of stable blue radiation from frequency-doubled GaAlAs laser diode by using EO effect in  $\text{KNbO}_3$  nonlinear crystal**

Tadanori Senoh, Yousuke Fujino, Yuzuru Tanabe, Motoichi Ohthu,\* and Ken'ichi Nakagawa

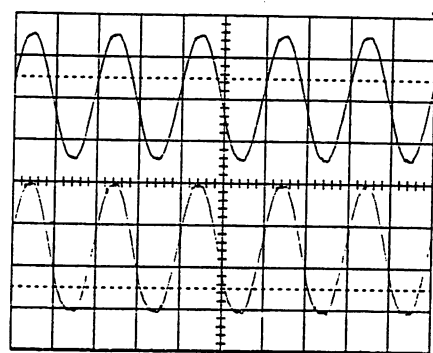
*Asahi Glass Company, Ltd., Research Center, 1150 Hazawa, Kanagawa-ku, Yokohama 221, Japan*

Efficient frequency doubling of a laser diode using  $\text{KNbO}_3$  crystal has recently been reported.<sup>1,2</sup> Modulatable blue-laser sources could offer applications for laser printers and optical data storage; however, direct modulation for doubling radiation has not yet been reported. We propose here a novel method for modulating frequency-doubled blue radiation. We used the optical feedback-locking technique from a ring built-up cavity to generate the 3.3-mW stable, blue radiation of 431 nm wavelength. We succeeded in intensity modulation, for the first time, with a modulation depth as high as 78%,

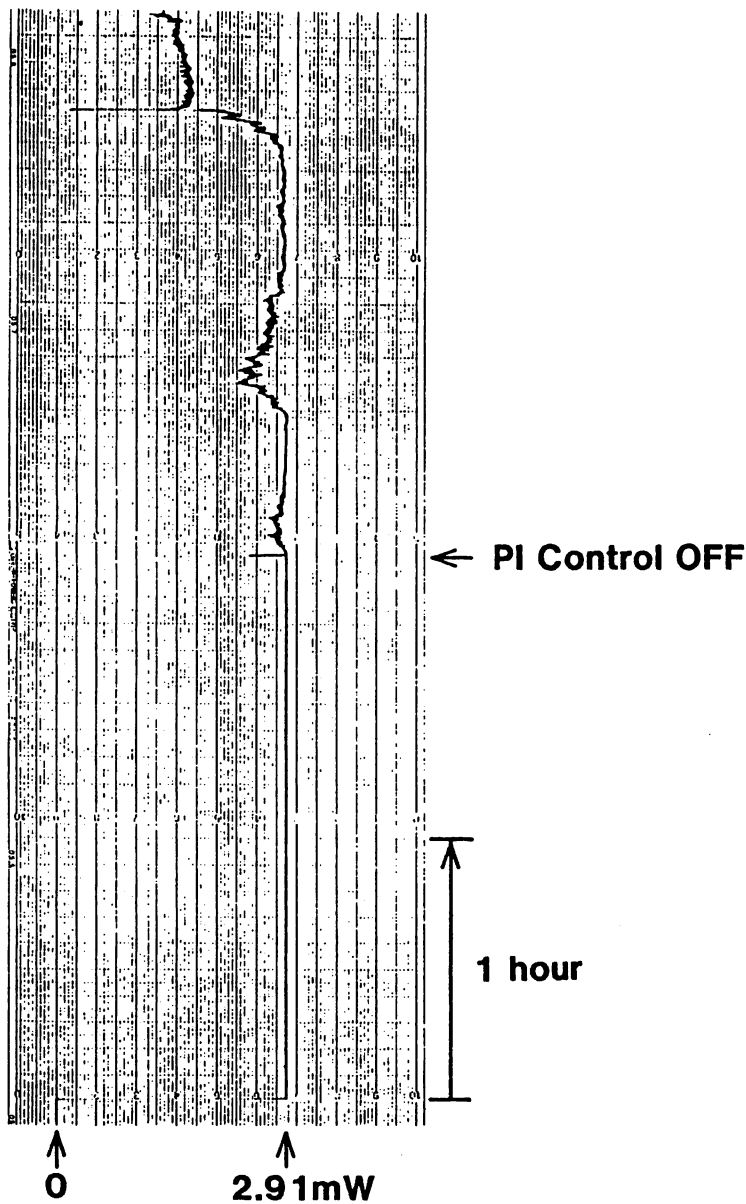
1. W. J. Kozlovsky, W. Lenth, E. E. Latta, A. Moser, and G. L. Bona, *Appl. Phys. Lett.* 56, 2291 (1990).
2. A. Hemmerich, D. H. McIntyre, C. Zimmermann, and T. W. Hänsch, *Opt. Lett.* 15, 372 (1990).



CWA6 Fig. 1. Experimental arrangement for frequency doubling of GaAlAs laser diode using a KNbO<sub>3</sub> crystal in the built-up ring cavity. The KNbO<sub>3</sub> crystal is used both as a frequency doubler and as a modulator.



CWA6 Fig. 3. Modulation waveform of the second-harmonic power (lower trace), with application of 130-V ac voltage (upper trace) to KNbO<sub>3</sub> crystal.



CWA6 Fig. 2. Time variation of cw, second-harmonic output power, with and without the phase of feedback light control. Output power is stabilized remarkably when P-I control is applied.

11:15 am

**CThF4 Genuine optical frequency discriminator with wide recovery range and high gain for FM noise reduction of semiconductor lasers**

M. Kouroggi and M. Ohtsu

*Graduate School at Nagatsuta, Tokyo Institute of Technology, 4259 Nagatsuta, Midori-ku, Yokohama 227, Japan*

Highly coherent semiconductor lasers are indispensable for accurate coherent optical systems, and a field spectral linewidth as narrow as 7 Hz has been achieved by employing negative electrical feedback (NEF) technique.<sup>1</sup> Because using genuine optical frequency discriminators (OFD) have not existed, the slope of the resonance spectral shape of a super Fabry-Perot interferometer (FPI) has been tentatively used in the NEF experiment. However, demand is growing for a high quality OFD for use in a computer-aided channel selection scheme of frequency division multiplexing coherent optical communications,<sup>2</sup> and for a very long-baseline interferometer for gravitational wave detection.

A genuine OFD, proposed here, is schematically explained by Fig. 1, together with three types of modified stable and compact devices. Figure 2 shows the output signal from the OFD as having specific dispersive spectral shapes, which provides an ideal error signal for servo-locking the laser frequency to one of the FPI resonant frequencies  $f_0$  without any frequency modulation (FM). This shape originates from interference between two degenerated, orthogonal, linearly polarized modes of the FPI whose degeneracy was removed by a wave plate installed in the FPI. The proposed OFD has several outstanding advantages. The first is that even though some electrical surges cause out of lock, OFDs can be recovered to  $f_0$  because the dispersive shape has far-reaching non-zero wings. It should be pointed out that a similar idea has also been presented by Hansch and Couillaud.<sup>3</sup> It was found experimentally that, by dithering the locked laser frequency, the recovery range was  $2F$  times wider than that of a conventional FPI ( $F$ ; finesse of an FPI).

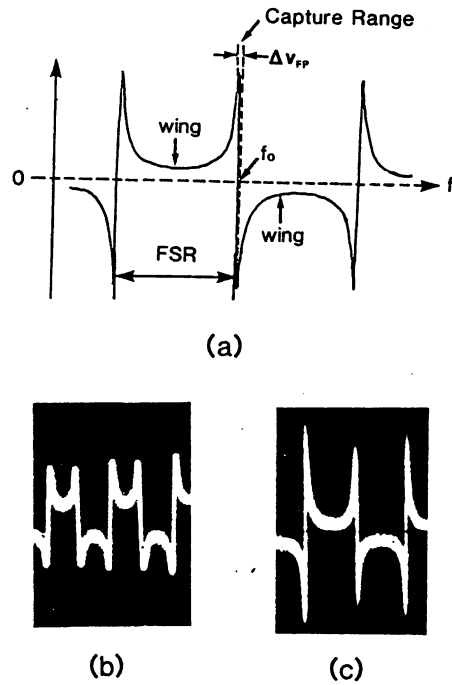
Figure 3 shows calculated results of the transfer function of the OFD. The gain transfer functions were measured by using a cw free-running laser diode as a white FM noise generator. The functions are also in this figure, and they agree with the calculated results.

Second, by comparing curve A with curves B and C (calculated results for conventional FPIs), the OFD gain is 10 dB larger than those of others because two counterpropagating lightwaves in the FPI contribute to the output signal, and the FM discrimination sensitivity is higher at the center of the dispersive profile than on the slope of the resonance curve of the conventional FPI.

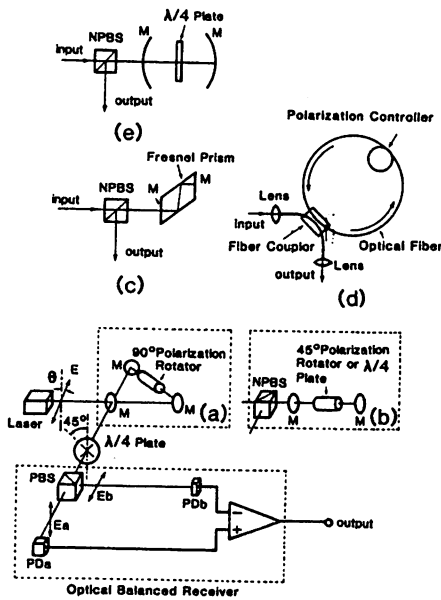
It is also advantageous that an optical balanced receiver can be used to suppress the additional discrimination noise originated from the laser IM noise, by which the OFD sensitivity can reach to the short-noise limit. Furthermore, it is seen that the maximum phase delay of the OFD is only  $90^\circ$ . These properties are advantageous in designing a high-gain and wideband NEF loop. A NEF experiment, using the simple device in Fig. 1(e) ( $F=25$  and  $FSR=1.5$  GHz), easily achieved the 35-dB maximum FM noise reduction and the 10-MHz bandwidth.

In summary, a genuine OFD with a wide recovery range and high gain was presented for the first time.

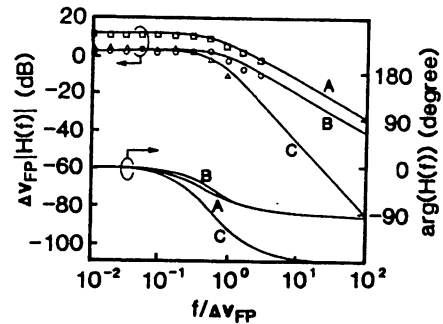
1. C. H. Shin and M. Ohtsu, *Opt. Lett.* **15** (1990), in press.
2. B. Grance, T. L. Koch, *Electron. Lett.* **25**, 883 (1989).
3. T. W. Hänsch and B. Couillaud, *Optics Comm.* **35**, 441 (1980).



CThF4 Fig. 2. Spectral profile of the proposed OFD. (a) Calculated result. FSR: Free-spectral range.  $f_0$ : One of the FPI resonant frequency.  $\Delta\nu_{FP}$ : Half linewidth of the FPI resonance curve. (b), (c) Experimental results obtained by the device in Figs. 1(c) and 1(e), respectively.



CThF4 Fig. 1. Concept of the proposed OFD using (a) a ring FPI and (b) a standing wave FPI with a polarization rotator. Modified and compact devices using (c) a Fresnel prism, (d) a ring-fiber FPI incorporated with a polarization controller, and (e) a FPI incorporated with a quarter-wave plate. M: Mirror. NPBS: Nonpolarized beam splitter. PBS: Polarized beam splitter.



CThF4 Fig. 3. Transfer functions of the OFD. A: Proposed OFD. B and C: The reflection and transmission modes of a FPI, respectively. Squares, open circles, and triangles are measured results.

Thursday, May 16

**CThR57 Accurate frequency measurement system for 1.5- $\mu\text{m}$  wavelength laser diodes**

M. Kourogi, K. Nakagawa, C. H. Shin, M. Teshima, and M. Ohtsu

*Graduate School at Nagatsuta, Tokyo Institute of Technology, 4259 Nagatsuta, Midori-ku, Yokohama, Kanagawa 227, Japan*

Future optical systems (e.g., coherent optical communication systems with more than 1,000 channels frequency division multiplexing) require highly accurate optical-frequency measurement systems in the 1.5- $\mu\text{m}$  wavelength region. However, the conventionally used wavelength-measurement methods are not accurate enough to meet this requirement. To solve this problem, we have proposed a novel optical-frequency measurement system with an accuracy as high as  $1 \times 10^{-9}$  as shown in Fig. 1(a).

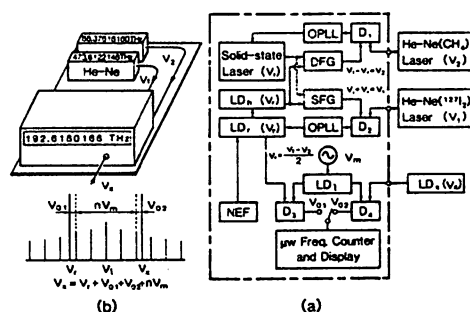
This high accuracy is secured by using an  $\text{I}_2$ -stabilized and  $\text{CH}_4$ -stabilized He-Ne laser, whose frequencies  $\nu_1$  and  $\nu_2$  have already been calibrated within the accuracy of  $1 \times 10^{-9}$ .<sup>1</sup> A 1.5- $\mu\text{m}$  wavelength, highly coherent laser diode ( $\text{LD}_i$ ) can be realized by negative electrical feedback (NEF),<sup>2,3</sup> and its frequency  $\nu_i$  is maintained to be  $(\nu_1 - \nu_2)$  as long as the two optical phase-locked loops (OPLL) in this figure are closed by using two nonlinear, optical-frequency converters (difference frequency generator (DFG) and sum frequency generator (SFG)). A solid-state laser (e.g., an LD-pumped YAG or a  $\text{Ti}:\text{Al}_2\text{O}_3$  laser) and an injection-locked, high-power LD ( $\text{LD}_h$ ) are used as local oscillators for highly efficient, nonlinear frequency conversions. It should be pointed out that a similar and preliminary proposal has also been presented recently for a different wavelength region.<sup>4</sup> Finally, the frequency  $\nu_x$  of the laser under test  $\text{LD}_x$  is measured by heterodyning with the frequency-calibrated  $\text{LD}_r$ . A local oscillator LD ( $\text{LD}_l$ ) is used if the heterodyne frequency is too high to detect with the photo detectors  $\text{D}_1 \sim \text{D}_3$ . In this case the heterodyne frequencies  $\nu_{01}$  and  $\nu_{02}$  between  $\text{LD}_l$  and  $\text{LD}_i$ , and between  $\text{LD}_l$  and  $\text{LD}_x$ , are measured by an rf frequency counter, and thereby,  $\nu_x$  is given by  $\nu_i + \nu_{01} + \nu_{02} + m\nu_m$  (see Fig. 1(b)). For these heterodynings, the  $\text{LD}_l$  is used as a wideband-frequency comb generator, as is explained schematically in Fig. 1(b). A wideband frequency comb can be realized by sidebands of Fabry-Perot electro-optic modulator<sup>5</sup> and/or ultrashort pulse techniques.

To prepare a prototype of the system, we carried out the experiments on reducing the field-spectral linewidth of the  $\text{LD}_i$ , injection locking, and OPLL. Figure 2 shows the measured results of the power-spectral density of FM noise in the  $\text{LD}_i$  to confirm its field-spectral linewidth reduction by NEF. In the Fourier frequency range of  $100 \text{ Hz} \leq f \leq 100 \text{ kHz}$ , the FM noise magnitude is lower than  $300/\pi \text{ (Hz}^2/\text{Hz)}$ , which corresponds to a 300-Hz spectral linewidth. This is, to our knowledge, the narrowest linewidth documented so far for 1.5- $\mu\text{m}$  LDs. A high-power multimode LD was injection locked by the narrow linewidth LD, by which the 32-mW, power-coherent light was obtained, which is sufficiently high for the efficient nonlinear frequency conversion. The bandwidth as wide as 134 MHz was also achieved for the homodyne OPLL, as is shown in Fig. 3. This is the widest among the formally documented OPLL systems.

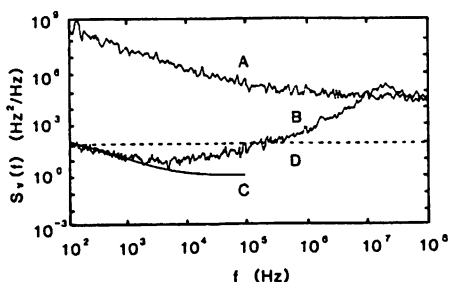
In summary, we proposed a highly accurate frequency measurement system for 1.5- $\mu\text{m}$  wavelength LDs.

1. D. A. Jennings, K. M. Evenson, and J. J. E. Knigt, *Proc. IEEE*, **74**, 168 (1986).
2. M. Ohtsu, M. Murata, and M. Kourogi, *J. Quantum Electron.* **26**, 231 (1990).
3. C. H. Shin and M. Ohtsu, *Opt. Lett.* **15**, (in press, 1990).
4. D. H. McIntyre and T. W. Hänsch, in *Technical Digest, Optical Society of America Annual Meeting* (Optical Society of America, Washington, D.C., 1988), p. 131.
5. T. Kobayashi, T. Sueta, Y. Cho, and Y. Matsuo, *Appl. Phys. Lett.* **21**, 341 (1972).

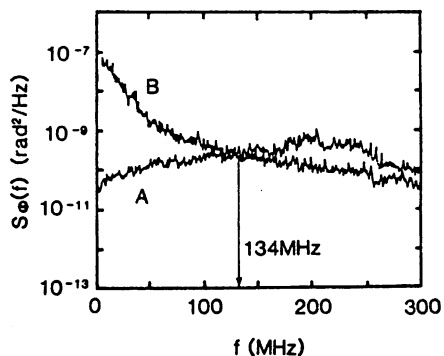




CThR57 Fig. 1. (a) Proposed frequency-measurement system for a 1.5- $\mu\text{m}$  wavelength LD.  $D_1 \sim D_3$ : Photo detectors. (SFG using, for example, a  $\text{LiNbO}_3$  crystal; DFG using, for example, an  $\text{AgGaSe}_2$  or  $\text{AgGaS}_2$  crystal). (b) Schematic explanation of the relative frequency locations of LD<sub>1</sub> ( $\nu_1$ ), LD<sub>2</sub> ( $\nu_2$ ), and LD<sub>3</sub> ( $\nu_3$ ).  $\nu_m$  is the modulation frequency of the LD<sub>1</sub>;  $n$  is the number of FM sidebands of LD<sub>1</sub> located between  $\nu_1$  and  $\nu_2$ .



CThR57 Fig. 2. Measured power-spectral density of the FM noise in the LD, under free-running condition (A) and NEF condition (B). The curve C represents the magnitude of the IM noise of the LD<sub>1</sub>, which limited the FM noise detection. Broken line D represents a FM noise level corresponding to 300-Hz Lorentzian spectral linewidth.



CThR57 Fig. 3. Power-spectral density of homodyne optical phase-locked loop (A). The curve B represents the result for the unlocked condition.

Poster Thursday

## SEMICONDUCTOR LASERS FOR HIGHLY COHERENT OPTICAL SWEEP GENERATOR

K. Nakagawa, M. Ohtsu, C.-H. Shin, and M. Kourogi

Graduate School at Nagatsuta, Tokyo Institute of Technology,

4259 Nagatsuta, Midori-ku, Yokohama 227, JAPAN

We review our recent activities on frequency control of semiconductor lasers, which can be used as novel light sources for laser spectroscopy and basic physics. Applications to rubidium atomic clocks and photon STM will be also demonstrated at the session. By negative electrical feedback (NEF), i.e., a reliable and reproducible method, the linewidth of a 1.5  $\mu\text{m}$  InGaAsP laser was reduced to 250 Hz with the power concentration ratio (PCR) within the controlled bandwidth of 99%. By adding a high gain NEF loop to an optical feedback loop from a confocal cavity, the linewidth of the AlGaAs laser was reduced to 7 Hz with the PCR of 98%. For heterodyne optical phase locked loop (OPLL), the frequency tracking error of 0.4 MHz and the residual phase error variance of  $2 \times 10^{-3}$  radian<sup>2</sup> were obtained. For homodyne OPLL, the bandwidth as wide as 134 MHz was achieved. To realize a peta-Hz class coherent optical sweep generator, organic nonlinear optical waveguides were fabricated for SHG and OPO. Furthermore, a multi-longitudinal mode high power laser was injection-locked to a narrow-linewidth master laser, by which the FM noise of the high power laser was reduced to that of the master laser with the PCR of 99%. Coherent addition between these high power lasers were also realized. To calibrate the optical frequency of this sweep generator, a highly accurate optical frequency counting system was proposed.

## Semiconductor Lasers for Highly Coherent Optical Sweep Generator

K. Nakagawa, M. Ohtsu, C. H. Shin\*, M. Kouroggi, and Y. Kikunaga  
Graduate School at Nagatsuta, Tokyo Institute of Technology,  
4259 Nagatsuta, Midori-ku, Yokohama 227, Japan

### ABSTRACT

We review our recent studies on frequency control of semiconductor lasers. We discuss a highly coherent sweep generator realized by the present semiconductor lasers. We also present several applications of present semiconductor lasers under way.

#### 1. Introduction

Recent progresses in semiconductor lasers have realized highly coherent and high power light sources in wide wavelength region. These lasers made it possible to realize novel advanced and sophisticated experiments on laser spectroscopy and basic physics.

Here we present our recent studies of frequency control of semiconductor lasers. We will show several techniques to realize highly coherent, high power and wide range frequency tunable lasers. It is shown how a highly coherent optical sweep generator covering from near-infrared to ultra-violet can be realized based on the use of the present semiconductor laser and nonlinear frequency conversions. Finally, we briefly show the applications of the present highly coherent semiconductor lasers.

#### 2. Frequency control of semiconductor lasers

##### 2.1. Linewidth reduction and optical phase locking

The spectral linewidth of the semiconductor laser is typically several MHz to several hundreds of MHz in free running. By using a

-----  
\* National Mokpo Merchant Marine College, Monko, Chun-Nam, Republic of Korea

optical feedback from a confocal cavity<sup>1</sup>, the linewidth can be reduced to typically 10 kHz. This method is useful for the high resolution spectroscopy of atoms and molecules.

Further linewidth reduction can be obtained by using an electrical feedback method<sup>2</sup>. The laser frequency is stabilized to the mid-point of a reflection fringe in a high finesse Fabry-Perot cavity by using a wide bandwidth current feedback. The linewidth of a  $0.83\mu\text{m}$  laser was reduced to about 560 Hz. In the case of a  $1.5\mu\text{m}$  multi-electrode DFB laser, its linewidth was reduced to about 250 Hz<sup>3</sup>. We also applied both optical and electrical feedback method to a  $0.83\mu\text{m}$  laser and its linewidth was reduced to as narrow as 7 Hz (Fig. 1)<sup>4</sup>. In the above cases, the residual FM noise was mainly caused by the intensity modulation (IM) noise at low frequency (<1kHz). This IM noise can be suppressed by using a FM modulation technique (Pound-Drever method)<sup>5</sup>. We applied it to the  $1.5\mu\text{m}$  DFB laser by using current modulation at 20 MHz and its linewidth was reduced to less than 100 Hz. The linewidth of less than 1 Hz will be realized in the near future.

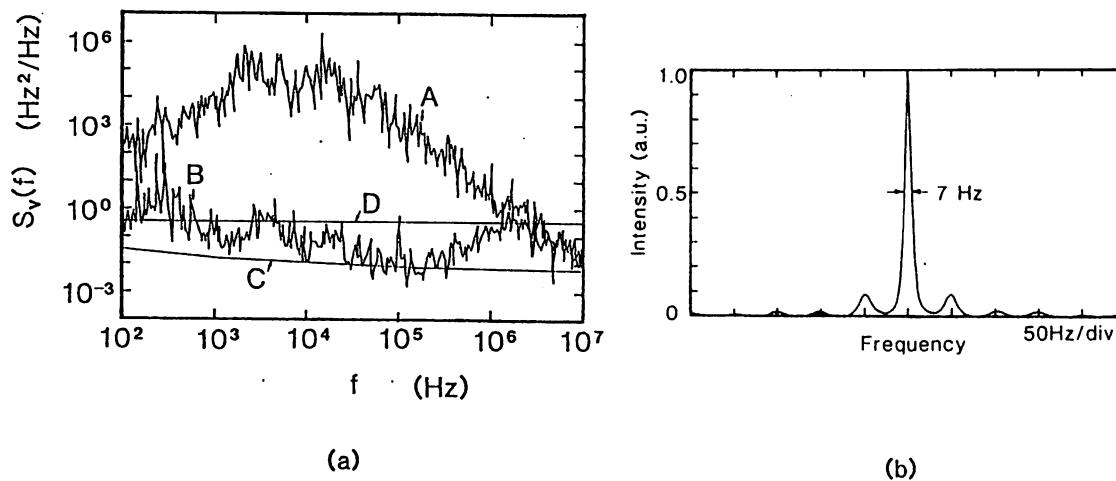


Fig.1 Power spectrum density of FM noise(a). A: free running, B: under feedback, C: IM noise level, D: FM noise level corresponds to the linewidth of 1 Hz. Calculated field spectral profile(b).

The optical phase locking between two lasers have been carried out by using the electrical feedback. The homodyne phase locking was realized with a bandwidth as wide as 134 MHz and a phase error variance of  $0.15 \text{ rad}^2$  by using two free running  $0.83\mu\text{m}$  lasers<sup>6</sup>. The heterodyne phase locking was also realized with a phase error variance

of  $0.02 \text{ rad}^2$  and frequency tracking error of  $0.4 \text{ mHz}$  at an integration time of  $70 \text{ sec}$  by using two optical feedback lasers<sup>7</sup>.

## 2.2 Injection locking and coherent addition

High power semiconductor lasers show a multi-mode oscillation in general. By using an injection locking method, high power single mode oscillation can be obtained by these lasers. We applied this method to  $1.5 \mu\text{m}$  high power ( $P_{\text{max}} = 60 \text{ mW}$ ) laser by using a narrow linewidth ( $700 \text{ kHz}$ ) multi-electrode DFB laser as a master laser. Single mode oscillation was realized with its output power of  $40 \text{ mW}$  and its linewidth of nearly  $700 \text{ kHz}$  (Fig. 2). We also realized a coherent addition between the master and the injection-locked slave lasers with a phase error of less than  $0.2 \text{ rad}$ .

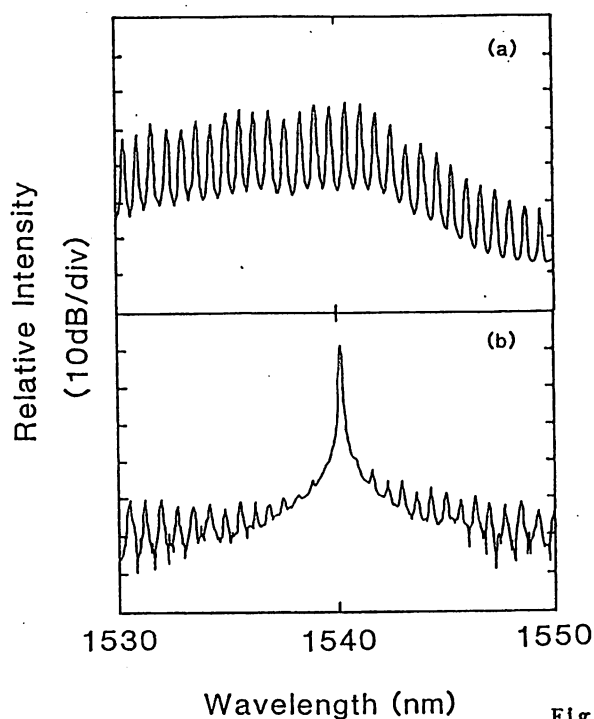


Fig.2 Spectra of the high power slave laser: (a) free running, (b) injection locked.

## 2.3 Frequency tunability and sweep

Frequency tunability and continuous frequency sweep are very important for atomic and molecular spectroscopy. By using an external grating feedback, frequency tunability was extended to wider than  $10 \text{ THz}$  or  $100 \text{ nm}$  at  $1.3 \mu\text{m}$ . This method was also helpful to obtain high power ( $> 60 \text{ mW}$ ) single mode emission from high power lasers at  $1.3 \mu\text{m}$ .

A continuous frequency sweep of wider than  $1 \text{ THz}$  was easily obtained by sweeping the temperature of DFB lasers at  $1.3$  and  $1.5 \mu\text{m}$ .

## 2.4 Highly coherent optical sweep generator

Available wavelengths of the present semiconductor lasers are roughly grouped into four regions, 0.75-0.9  $\mu\text{m}$ , 1.2-1.6  $\mu\text{m}$ , 0.63-0.68  $\mu\text{m}$ , and recently available 0.9-1.1  $\mu\text{m}$  (Fig. 3(a)). Further extensions of the wavelength are expected by using nonlinear frequency conversions such as SHG, SFG, and OPO. We expect efficient frequency conversions by using nonlinear optical materials as  $\text{LiNbO}_3$ ,  $\text{KTP}$ ,  $\text{KNbO}_3$  and recently developed organic materials. We are fabricating organic nonlinear waveguides for SHG, SFG and OPO.

By combining the present techniques of frequency control and nonlinear frequency conversion, highly coherent optical sweep generator will be realized and it will cover the wavelength range from 0.32  $\mu\text{m}$  to 1.6  $\mu\text{m}$  (Fig. 3(b)). Highly coherent and high power lasers will be realized by narrow linewidth ( $< 1\text{kHz}$ ) master lasers and injection locking of high power ( $> 100\text{ mW}$ ) lasers. Precise frequency tracking will be realized by using heterodyne optical phase locking.

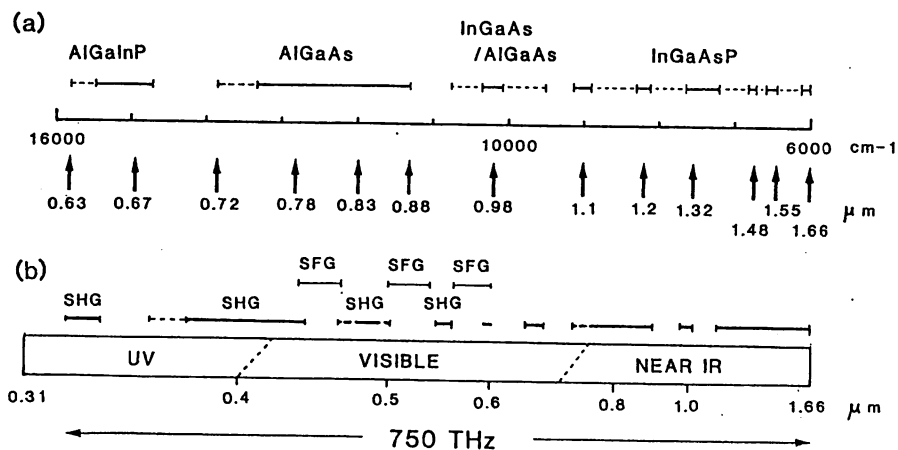


Fig.3 Wavelengths generated by the semiconductor lasers(a) and nonlinear frequency conversions(b).

## 3. Applications of highly coherent semiconductor lasers

### 3.1 Optical frequency synthesis

Optical frequency standards and absolute frequency measurement are needed in the near-infrared region of 1.3-1.5  $\mu\text{m}$ . We propose an optical frequency synthesis based on visible and infrared He-Ne lasers to measure the absolute frequency of 1.55  $\mu\text{m}$  lasers (Fig. 4)<sup>8</sup>. At first, the sum and difference frequencies between the 1.064  $\mu\text{m}$  Nd:YAG

laser and two  $1.5\mu\text{m}$  semiconductor lasers will be compared with two He-Ne lasers of  $0.633\mu\text{m}$  and  $3.392\mu\text{m}$  respectively. Next, we will measure frequency difference ( $\sim 1.5\text{ THz}$ ) between two  $1.5\mu\text{m}$  lasers by using a wideband optical comb generator, which can be realized by using an electro-optic modulator inside a Fabry-Perot cavity<sup>9</sup>. Finally, we will determine the absolute frequencies of both  $1.064\mu\text{m}$  and  $1.5\mu\text{m}$  lasers with an accuracy of two reference He-Ne lasers. The  $1.5\mu\text{m}$  lasers can be stabilized by using the absorption lines of molecules such as  $\text{NH}_3$ ,  $\text{HCN}$ , and  $\text{C}_2\text{H}_2$ . The present injection-locked high power lasers will help to obtain saturation spectroscopy of these lines and also efficient frequency mixings between  $1.5\mu\text{m}$  lasers and the Nd:YAG laser.

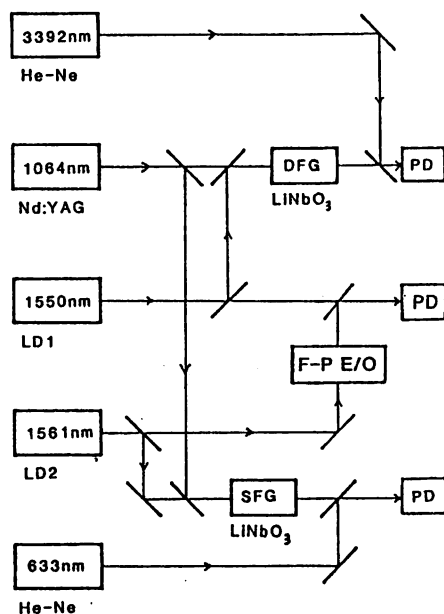


Fig.4 Schematic diagram for the proposed optical frequency synthesis.

### 3.2 Laser cooling and high resolution spectroscopy of atoms and ions.

The laser cooling and trapping of atoms is suitable for the application of semiconductor lasers because it is quite easy to prepare many tunable lasers for cooling, pumping and probing. Cooling and trapping of Rb atoms in a small glass cell<sup>10</sup> is now underway by using optical feedback  $0.78\mu\text{m}$  lasers. We will study the cavity QED by using the trapped atoms.

High resolution spectroscopy is also attractive application for the highly coherent semiconductor lasers. We are preparing a ultra high resolution spectroscopy of laser cooled  $\text{Sr}^+$  ions in RF trap<sup>11</sup>. Cooling and pumping laser can be provided by frequency doubled  $0.843\mu\text{m}$  AlGaAs laser and  $1.09\mu\text{m}$  InGaAsP laser respectively. The narrow(0.4 Hz) transition at  $0.674\mu\text{m}$  can be probed by a AlGaInP visible laser whose linewidth is reduced by the optical and electrical feedback method.

#### 4. Summary

We have obtained narrow linewidth(7 Hz), accurate phase locking between lasers(0.4 mHz), an injection-locked high power laser, wide frequency tuning range(10 THz) by using semiconductor lasers. These results encourage to realize a highly coherent frequency tunable light source covering from near-infrared to ultra-violet, which will be widely applied to atomic and molecular spectroscopies, optical frequency synthesis, and quantum optics.

#### References

1. B. Dahmani, L. Hollberg, and R. Drullinger, Opt.Lett.12, 876(1987).
2. M. Ohtsu, M. Murata, and M. Kourogi, IEEE J.Quantum Electron.26, 231(1990).
3. M. Kourogi, C. H. Shin, and M. Ohtsu, IEEE Photon.Technol.Lett., to be published in June issue.
4. C. H. Shin and M. Ohtsu, Opt.Lett.15, 1455(1990).
5. R. W. P. Drever, J. L. Hall, F. V. Kowalski, J. Hough, G. M. Ford, A. J. Munley, and H. Ward, Appl.Phys.B31, 97(1983).
6. M. Kourogi, C. H. Shin, and M. Ohtsu, IEEE Photon.Technol.Lett.3, 270(1991).
7. C. H. Shin and M. Ohtsu, IEEE Photon.Technol.Lett.2, 297(1990).
8. M. Kourogi, K. Nakagawa, C. H. Shin, M. Teshima, M. Ohtsu, in Technical Digest, Conference on Lasers and Electro-Optics(Optical Society of America, Baltimore, 1991), paper CThR57.
9. T. Kobayashi, T. Sueta, Y. Cho, and Y. Matsuo, Appl.Phys.Lett.21, 341(1972).
10. C. Monroe, W. Swann, H. Robinson, and C. Wieman, Phys.Rev.Lett.65, 1571(1990).
11. A. A. Majei and J. D. Sankey, Opt.Lett.15, 634(1990).



OVERVIEW OF COHERENT LIGHTWAVE COMMUNICATION

M. OHTSU, C.-H. SHIN\* and M. KOUROGI

Graduate School at Nagatsuta, Tokyo Institute of Technology,  
4259 Nagatsuta, Midori-ku, Yokohama, 227 Japan

\* Present address : National Mokpo Merchant Marine College,  
Mokpo, Chun-Nam, Korea

Principle of operation of the coherent lightwave transmission systems is essentially the same as that in the microwave system. However, in order to realize the practical system, one has to solve several problems which result from the very high optical carrier frequency, the large magnitude of frequency fluctuations of semiconductor lasers and the variation of the polarization axes of lightwaves transmitted through the optical fibers. Based on these situations, following subjects will be reviewed for present and future coherent lightwave communication systems.

1. Principle of coherent lightwave communications.

(1) Why are the coherent lightwave communication systems required ? ( High carrier frequency, parallel transmission, long transmission length )

(2) Relation between the transmission capacity and modulation ( ASK, FSK, and PSK ) and demodulation ( heterodyne and homodyne ) schemes.

## 2. Performances of the light sources.

(1) Narrow linewidth semiconductor lasers ( Fig. 1[1] )

Novel devices, electrical feedback method, and optical feedback method.

(2) Wideband tunable semiconductor lasers for FDM systems.

(3) Frequency stabilized semiconductor lasers.

(4) Other promising coherent light sources, e.g., LD-pumped solid state lasers.

## 3. Optical phase locking.

(1) Heterodyne optical phase locked loops ( Fig.2 [2] ).

(2) Homodyne optical phase locked loops ( Figs. 3 [3] and 4 [4] )

## 5. Optical amplification.

(1) Semiconductor laser amplifiers.

(2) Fiber amplifiers.

(3) Novel semiconductor lasers for pumping the fiber amplifiers.

## 6. Possible coherent optical lightwave systems.

(1) Local area networks.

(2) Space communication systems.

## 7. Related technologies

- (1) Highly accurate optical frequency counting systems.
- (2) Polarization diversity methods.

## 8. Toward the future

- (1) Ultra-low loss optical fiber communications.

Performances of ultra-low loss optical fibers and semiconductor lasers at several  $\mu\text{m}$  wavelength region.

### [ References ]

- [1] M. Ohtsu, C.-H. Shin, H. Furuta, M. Kourogi, H. Kusuzawa, S. Jiang, and K. Nakagawa, "7-Hz linewidth diode lasers, wideband optical phase locking and applications", Quantum Electronics and Laser Science, IEEE LEOS and Opt. Soc. Am., May 12 - 17, Baltimore, MA, paper number QTh1.1
- [2] C.-H. Shin and M. Ohtsu, "Heterodyne Optical Phase-Locked Loop by Confocal Fabry-Perot Cavity Coupled AlGaAs Lasers", IEEE Photonics Technol. Lett., Vol.2, No.4, April 1990, pp.297-300
- [3] C.-H. Shin, "Optical Phase-Locking of Semiconductor Lasers", Ph. D. Thesis, Tokyo Institute of Technology, January 1991
- [4] M. Kourogi, C.-H. Shin, and M. Ohtsu, "A 134 MHz Bandwidth Homodyne Optical Phase-Locked-Loop of Semiconductor Laser Diodes", IEEE Photonics Technol. Lett., to be appeared in Vol.3, No. 3, March 1991

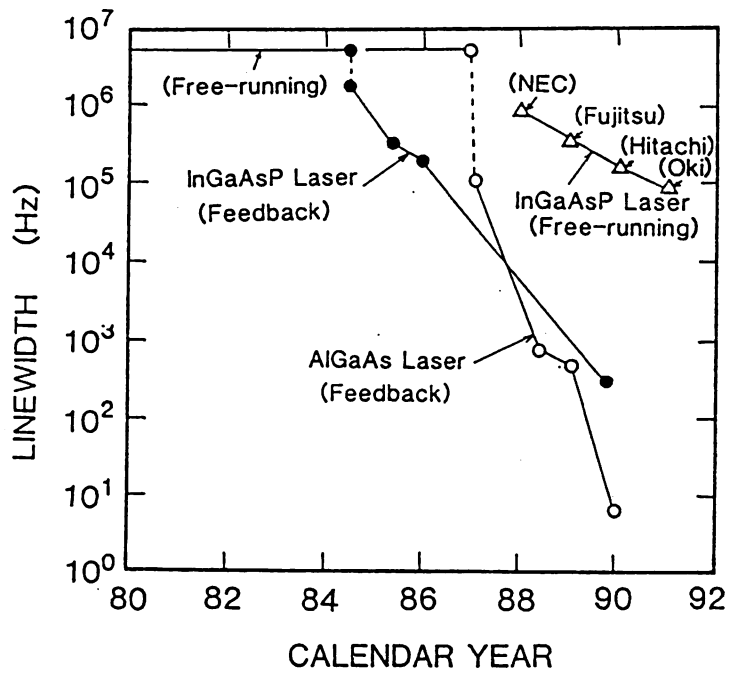


Fig. 1

Improvements of spectral field spectral linewidth reduction of semiconductor lasers[1].

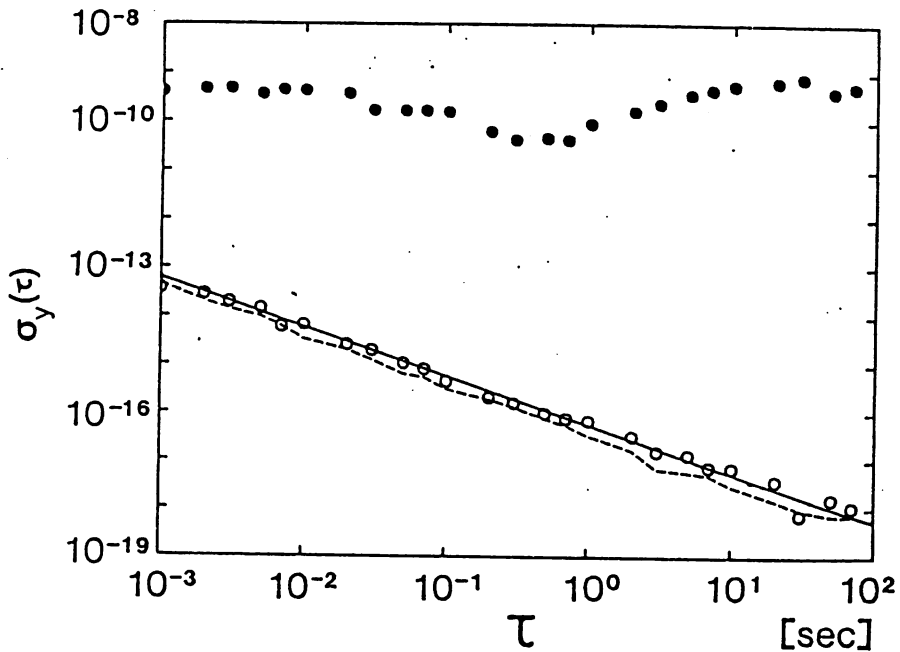


Fig. 2

Square root of variances of residual frequency fluctuations of the phase locked heterodyne signal( Open circles and a solid line ) [2]. Closed circles represent the fluctuations under the unlocked condition. Broken curve represents the fluctuations of the local microwave oscillators. All of these fluctuations are normalized to the nominal optical frequency.

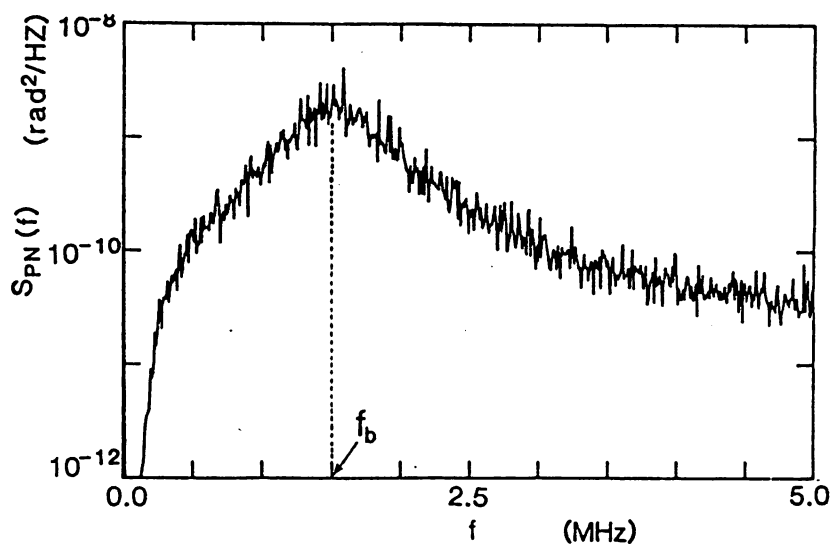


Fig. 3

Power spectral density of the residual phase fluctuations of the homodyne phase locked loop, which was achieved by optical-electrical double feedback method[3].

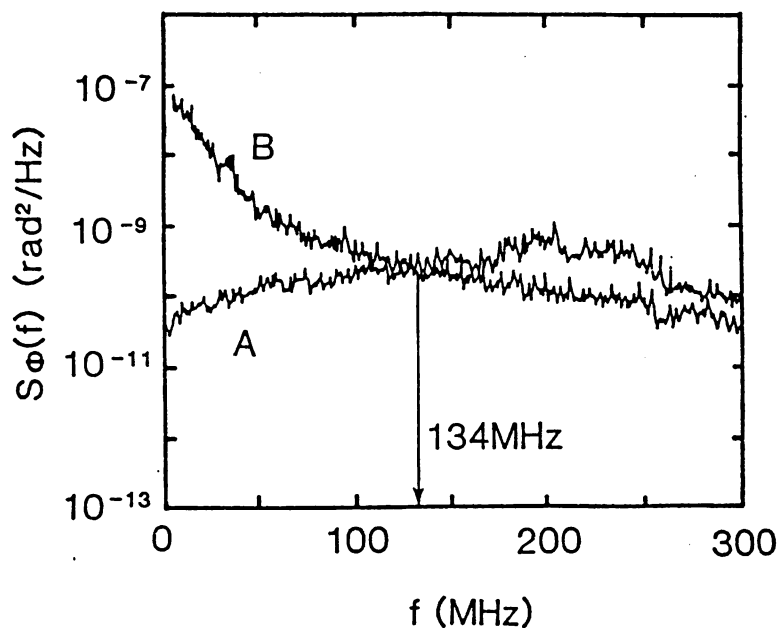


Fig. 4

Power spectral density of the residual phase fluctuations of the wideband homodyne phase locked loop, which was achieved by negative electrical feedback method[4]. The curves A and B represent the results measured under the locked and unlocked conditions, respectively.

## Observation of Ramsey-Type Resonant Fringe Using a Cylindrical Microwave Cavity for a Diode Laser-Pumped Rb Beam Atomic Clock

Hiroyuki FURUTA, Hiromasa SUZUKI and Motoichi OHTSU

Graduate School at Nagatsuta, Tokyo Institute of Technology  
4259 Nagatsuta, Midori-ku, Yokohama, Kanagawa 227

(Received November 8, 1990; accepted for publication January 19, 1991)

A novel Ramsey-type resonance signal is observed by using a simple microwave cylindrical cavity in a diode laser-pumped rubidium atomic clock. Its linewidth is 1.1 kHz. The signal lineshapes depend on the modal profile of the microwave magnetic field inside the cavity. The lineshapes are reproduced by numerical calculation. Conditions to achieve the maximum frequency discrimination sensitivity are derived by the theoretical analysis.

**KEYWORDS:** diode laser, rubidium atomic clock, Ramsey-type fringe, frequency accuracy

### §1. Introduction

Highly precise and compact rubidium (Rb) atomic clocks have been required for various applications, e.g., the signal sources for GPS satellites, and ISDN systems. For the improvement of their performances, Rb atomic clocks pumped by diode lasers have been investigated.<sup>1-3)</sup> By using a diode laser on a conventional gas cell-type clock, Hashimoto and Ohtsu have demonstrated that the stability of the microwave frequency has drastically been improved.<sup>4)</sup> To obtain high short-term stability, a sensitive discriminator with a 20-Hz resonant linewidth has been achieved by utilizing the effect of modulation transfer in the optical-microwave double resonance.<sup>4,5)</sup> For the improvement of medium- and/or long-term stability, the self-tuning system was invented to compensate for the light shift due to the AC Stark effect by the pumping laser.<sup>6)</sup>

The accuracy of the microwave frequency has been limited by the frequency shifts due to various origins. The principal origins were the AC Stark effect and the collisions between rubidium-87 (<sup>87</sup>Rb) atoms and buffer gases. As mentioned above, the light shift (AC Stark effect) has been compensated<sup>6)</sup> or can be avoided by spatially separating interaction regions of atoms with lightwaves and microwaves. However, as long as the Rb gas cells with some kinds of buffer gas are used for Rb atomic clocks, it is impossible to remove the frequency shift induced by the collisions of Rb atoms with the buffer gases. When a Rb gas cell without any buffer gas is used, the linewidth of the microwave resonance signal is broadened by the Doppler effect and the self-collisions of <sup>87</sup>Rb atoms. In the conventional Rb atomic clocks, <sup>87</sup>Rb gas cells with the buffer gases have been used because the collisional narrowing effect by the high-pressure buffer gases reduces the Doppler effect and the self-collisions and make the resonant linewidth narrower. It has also been difficult to remove the collision-induced frequency shift by the effect of collisions with walls of the gas cell. Since such frequency shifts have deteriorated the frequency accuracy of the atomic clock, conventional Rb

atomic clocks have not been employed as the primary frequency standards. In this connection, we proposed a diode laser-pumped Rb beam atomic clock for achieving high frequency accuracy by eliminating the effects of collisions.<sup>7)</sup>

The lineshape characteristics of microwave resonance signal are important since it is used as the frequency reference and discriminator for the microwave frequency stabilization of an atomic clock. In the present work, a novel method is proposed to obtain a Ramsey-type resonance\* signal by using a simple and compact cylindrical microwave cavity. This novel Ramsey-type resonance signal can be advantageously used as a stable frequency reference and discriminator. Ramsey-type resonance can occur in a TE<sub>012</sub> mode cavity with its cylindrical axis perpendicular to the atomic beam trajectory. The occurrences of the Ramsey-type resonance can be attributed to the spatial profile of the microwave magnetic field in the microwave cavity. Compared with a U-shaped cavity, which has been used for conventional cesium (Cs) beam atomic clocks,<sup>8)</sup> the present method is advantageous in its compact size and simplicity of design. It should be pointed out that DeMarchi *et al.* have recently observed Ramsey-type resonances using a TE<sub>013</sub> mode cylindrical cavity.<sup>9)</sup> This cavity was used in a preliminary test of the optical pumping in a Cs beam atomic clock.

In this paper, the experimentally obtained Ramsey-type resonance signals are fully explained theoretically. By using the theoretical model, the optimal design criteria of the resonance are obtained to achieve the maximum frequency discrimination. Also, even in the presence of modal perturbations in the cavity, it is confirmed that the magnitude of the cavity phase shift is negligibly small in this type of resonance.

### §2. Experimental

Figure 1 shows the experimental setup of a diode laser-

\*This resonance is a kind of Rabi resonance which has a signal characteristic similar to that in Ramsey resonance. To distinguish this resonance with the Ramsey resonance, "Ramsey-type" was used here.

pumped Rb beam atomic clock. The vacuum chamber was composed of a stainless steel oven, a PYREX glass tube in which the atomic beam propagated, and a stainless steel cold trap cooled by liquid nitrogen, where Rb atoms were collected. The chamber was evacuated by a diffusion pump to  $10^{-6}$  Torr. The Rb atomic beam from the oven was collimated by two small apertures, i.e., the aperture at the oven and that 10 cm away from the oven. Their diameters were 2 mm. The atomic beam

interacted with a microwave and laser lightwaves during the propagation in the glass tube. The length and the inner diameter of the glass tube were 22 cm and 1.2 cm, respectively. The inner diameter and the length of the cylindrical microwave cavity were 10 cm and 5 cm, respectively. The cavity mode used in the present experiment was the  $TE_{012}$  mode. The cylindrical axis of the cavity was set perpendicular to the atomic beam trajectory. Figure 2(a) schematically illustrates the modal patterns of the

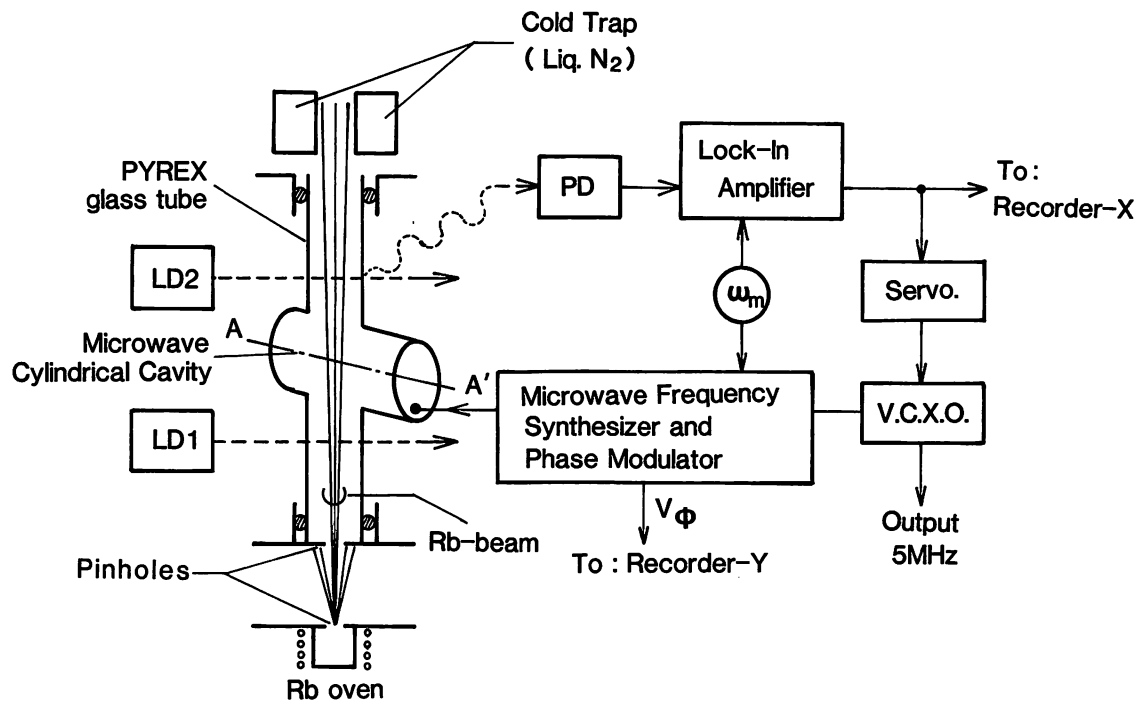


Fig. 1. Diode laser-pumped Rb beam atomic clock.

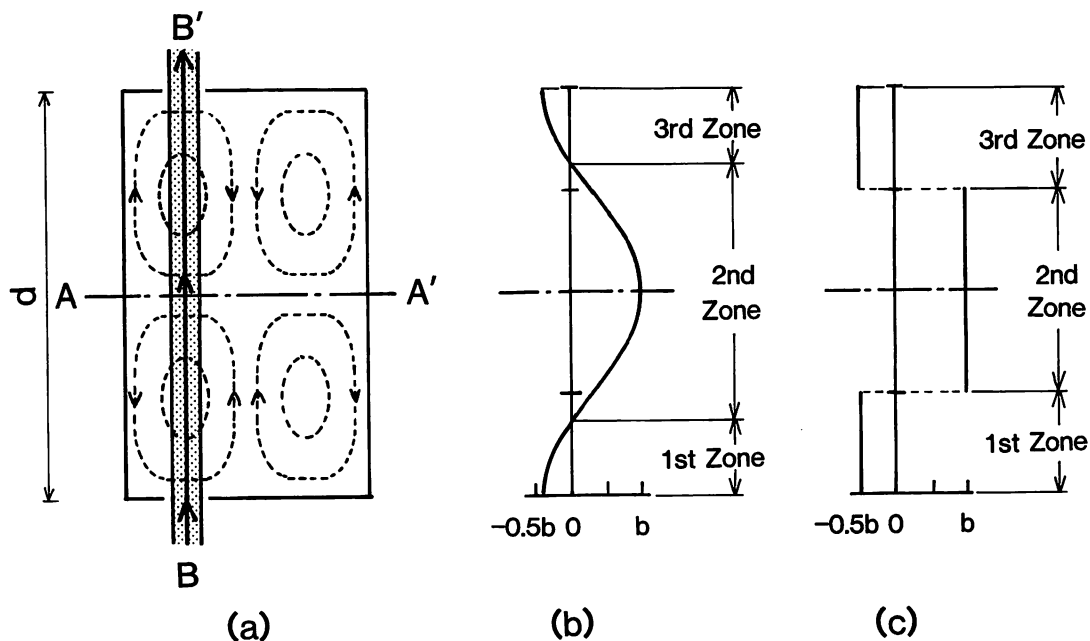


Fig. 2. Modal pattern of the cavity  $TE_{012}$  (a) and magnetic field amplitude (b) corresponding to the line B-B' of (a). The line A-A' represents the cylindrical axis of the cavity corresponding to that in Fig. 1, while (c) gives the approximated magnetic field amplitude used for the calculation corresponding to (b).

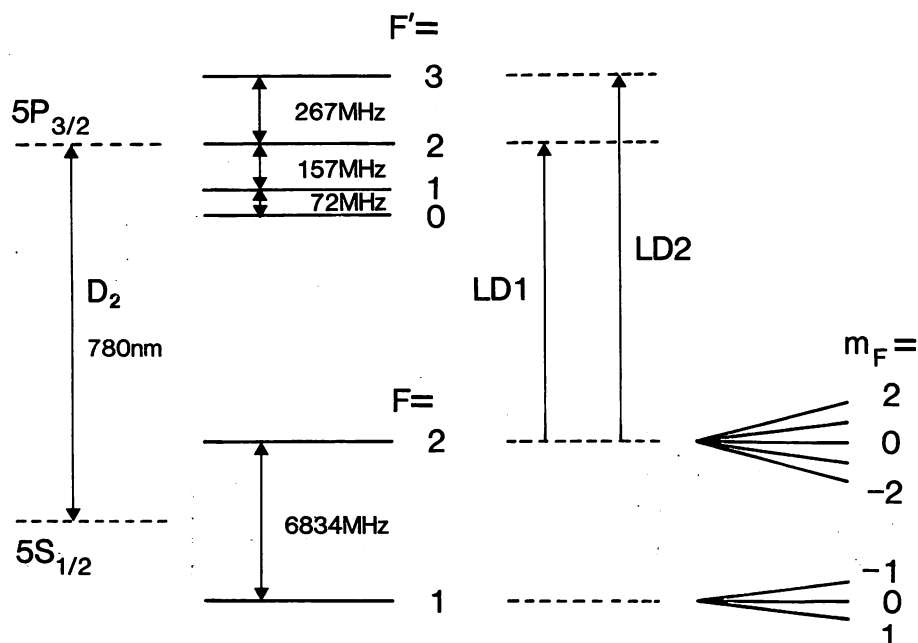


Fig. 3. The energy level of  $^{87}\text{Rb}$   $D_2$  line; LD1 and LD2 indicate the transitions on which the frequencies of diode lasers LD1 and LD2 (see Fig. 1) were stabilized.

magnetic field in the  $\text{TE}_{012}$  mode cylindrical microwave cavity. Here the cylindrical axis of this cavity is shown by the line A-A'. As illustrated in Fig. 2(a), the modal patterns of the magnetic field are symmetric with its cylindrical axis. When an atomic beam passes through the cavity perpendicular to its axis, i.e., along the line B-B' in Fig. 2(a), atoms interact with the microwave magnetic field, whose amplitude has the profile shown in Fig. 2(b). The amplitude is expressed by the Bessel function of the 0th order. Since the magnetic fields of the 1st and the 3rd zones of the cavity (see Fig. 2(b)) are in phase with each other and the magnetic field in the 2nd zone is out of phase to them, the interaction between the atoms and microwave, during propagation through these zones, can generate the Ramsey-type resonance. The loaded Q of the cavity used in the present experiment was  $1,600 \pm 100$ .

Figure 3 shows the energy level diagram of the  $^{87}\text{Rb}$   $D_2$  line. The optical pumping on the transition from  $F=2$  to  $F'=2$  of the  $^{87}\text{Rb}$   $D_2$  line induces a population difference between ground state hyperfine levels of  $^{87}\text{Rb}$   $|F=1, m_F=0\rangle$  and  $|F=2, m_F=0\rangle$ . The diode laser LD1 (Fig. 1) was used for this pumping as is shown in Fig. 3. The spectral lineshapes of the microwave transition at 6.834 GHz were measured by detecting the fluorescence from  $^{87}\text{Rb}$  atoms pumped by the diode laser LD2 (Fig. 1). As is shown in Fig. 3, the recycling transition between  $F=2$  and  $F'=3$  was used for the detection because the fluorescence is enhanced at this transition without changing the population difference between the ground state hyperfine levels. The frequencies of diode lasers LD1 and LD2 for optical pumping and detection were stabilized to each transition frequency by using absorption lines in  $^{87}\text{Rb}$  gas cells.<sup>10)</sup>

Two curves in Fig. 4(a) show the observed and calculated fluorescence signals of optically pumped

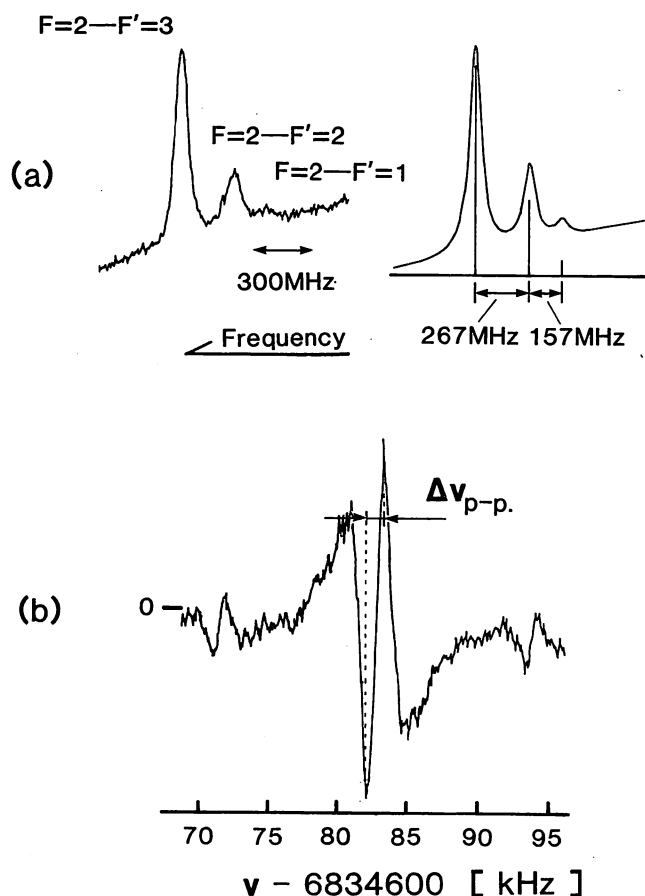


Fig. 4. (a) Fluorescence signal of optically pumped  $^{87}\text{Rb}$  atoms and calculated lineshape as a function of the laser frequency. (b) Phase-sensitively detected microwave resonance signal as a function of microwave frequency  $\nu$ . The modulation frequency of the microwave was 420 Hz and the temperature of the Rb source  $T_{\text{Rb}}$  was 433 K.



atomic beam as a function of the laser frequency. These figures show a good agreement with each other. The observed hyperfine spectral lines were clearly resolved. The full-linewidth at half-maximum (FWHM) of the spectral line is 70 MHz. The divergence angle of the atomic beam can be calculated from this value as 30 mrad, where a 40 MHz spectral linewidth of the diode laser was taken into account in the calculation.

Figure 4(b) shows an experimental result of the first derivative of the microwave resonance signal as a function of the applied microwave frequency  $\nu$ . This signal was obtained by phase-sensitive detection by modulating the microwave frequency. The linewidth  $\Delta\nu_{p-p}$  was  $(1.1 \pm 0.2)$  kHz when the temperature of Rb source  $T_{Rb}$  was 433 K. This value can be transferred to the value of FWHM of the central part of the resonance as 1.4 kHz for the Gaussian or as 1.6 kHz for the Lorentzian profile. In the conventional Ramsey resonance, the FWHM of the resonant lineshape is expressed as  $1/2T$  [Hz] ( $T$ : transit time in drift space).<sup>9)</sup> By using this relation, the FWHM for the cavity used in this work was calculated as 2.5 kHz. The experimental value is, therefore, about half as narrow as that in the Ramsey cavity with the same value of  $T$ .

### §3. Theoretical Analysis and Discussions

#### 3.1 Theoretical model

The amplitude of the microwave magnetic field across the line B-B' has the spatial modal profile given by the Bessel function of 0th-order  $J_0(r)$ , where  $r$  represents the position of the atoms inside the cavity and depends on time, i.e.,  $r(t)$ . The interaction between atoms and the microwave magnetic field can be described by using the following time-dependent Bloch equations.

$$(d/dt)a_1(t) + \Omega_0 a_2(t) = 0 \quad (1)$$

$$-\Omega_0 a_1(t) + (d/dt)a_2(t) - bJ_0(r(t))a_3(t) = 0 \quad (2)$$

$$bJ_0(r(t))a_2(t) + (d/dt)a_3(t) = 0, \quad (3)$$

where  $a_1(t)$ ,  $a_2(t)$ , and  $a_3(t)$  are quantities related to the density matrix elements  $\rho_{1,2}(t)$ ,  $\rho_{1,1}(t)$  and  $\rho_{2,2}(t)$  for the ground state hyperfine levels  $|F=1, m_F=0\rangle$  and the  $|F=2, m_F=0\rangle$  as

$$\rho_{1,2}(t) = (1/2)(a_1(t) + ia_2(t)) \exp(-i\omega t) \quad (4)$$

and

$$\rho_{1,1}(t) - \rho_{2,2}(t) = a_3(t) \quad (5)$$

with the initial conditions

$$a_1(0) = a_2(0) = 0 \text{ and } a_3(0) = 1, \quad (6)$$

and  $b$  is the real part of the Rabi frequency and is proportional to the amplitude of the microwave magnetic field. The value  $r(t)$  is expressed as

$$r(t) = |v_M t - d/2| \quad (7)$$

where  $v_M$  is the most probable velocity of atoms\* and  $d$  is the diameter of the microwave cylindrical cavity.  $\Omega_0$  is the

angular frequency detuning from the microwave resonance, defined as

$$\Omega_0 = \omega - \omega_0 \quad (8)$$

where  $\omega$  is the microwave angular frequency and  $\omega_0$  is the atomic resonance angular frequency. The transition probability giving the microwave resonance signal is expressed as

$$P(\tau_0) = (1/2)(1 - a_3(t_0)) \quad (9)$$

where  $\tau_0 (=d/v_M)$  is the transit time of the atoms with the velocity  $v_M$ . By using eq. (9), the spectral profiles of microwave resonance signal can be calculated.

In the recycling transition for the optical detection, it has been experimentally confirmed that the signal has the Maxwellian distribution weighed by  $1/v$ , where  $v$  is the velocity of atoms.<sup>11)</sup> Thus, the transition probability  $P(\tau_0)$  is averaged over the velocity of atoms by using  $1/v$  weighed Maxwellian distribution. To simplify the calculations, the spatial profile of the microwave magnetic field along the atomic beam trajectory was approximated as shown in Fig. 2(c). Under this approximation, the solutions of eqs. (1)–(3) are

$$\begin{pmatrix} a_1(\tau_0) \\ a_2(\tau_0) \\ a_3(\tau_0) \end{pmatrix} = R(0.5b, 0, \Omega_0, \tau) R(-b, 0, \Omega_0, \tau') \\ \times R(0.5b, 0, \Omega_0, \tau) \begin{pmatrix} 0 \\ 0 \\ 1 \end{pmatrix} \quad (10)$$

where  $\tau$  and  $\tau'$  are the transit times of atoms with the velocity  $v_M$  through the microwave magnetic field in the 1st (and 3rd) and 2nd zones of the cavity in Fig. 2(c), respectively, and  $\tau_0 = \tau + \tau' + \tau$ .  $R$  is the matrix which has been given by eq. (5.2.23) of ref. 8.

#### 3.2 Signal profiles

Figures 5 and 6 show the microwave resonance signal profiles  $P(\tau_0)$  and their first derivatives, respectively, which were numerically calculated by using eqs. (9) and (10). Horizontal axes are the frequency detuning of microwave  $(\nu - \nu_0) = \Omega_0/2\pi$ . The results shown in Figs. 5(a) and 6(a) were obtained at  $b\tau = 0.2\pi$ , where  $\tau = 0.08$  ms at  $T_{Rb} = 433$  K, corresponding to the present experimental conditions. The calculated profile of Fig. 6(a) shows a good agreement with that of Fig. 4(b), from which it can be confirmed that our theoretical model accurately describes the Ramsey-type resonance obtained by the microwave cavity. The linewidth  $\Delta\nu_{p-p}$  shown in Fig. 6(a) was  $(1.3 \pm 0.2)$  kHz.

The signal profile for  $b\tau = 1.1\pi$  is shown in Figs. 5(b) and 6(b). The linewidth  $\Delta\nu_{p-p}$  in Fig. 6(b) and the FWHM of central part  $\Delta\nu$  in the profile of Fig. 5(b) were  $(2.3 \pm 0.2)$  kHz and  $(2.7 \pm 0.2)$  kHz, respectively. The 2.7 kHz FWHM is approximately the same with the value calculated from  $1/2\tau'$  because the transit time  $\tau'$  is 0.17 ms in the approximation of Fig. 2(c). This corresponds to the FWHM of conventional Ramsey resonance with a U-

\*In general, the velocity  $v$  of atoms is used. In convenience remarking velocity-averaged results, the most probable velocity  $v_M$  of atoms is used here.

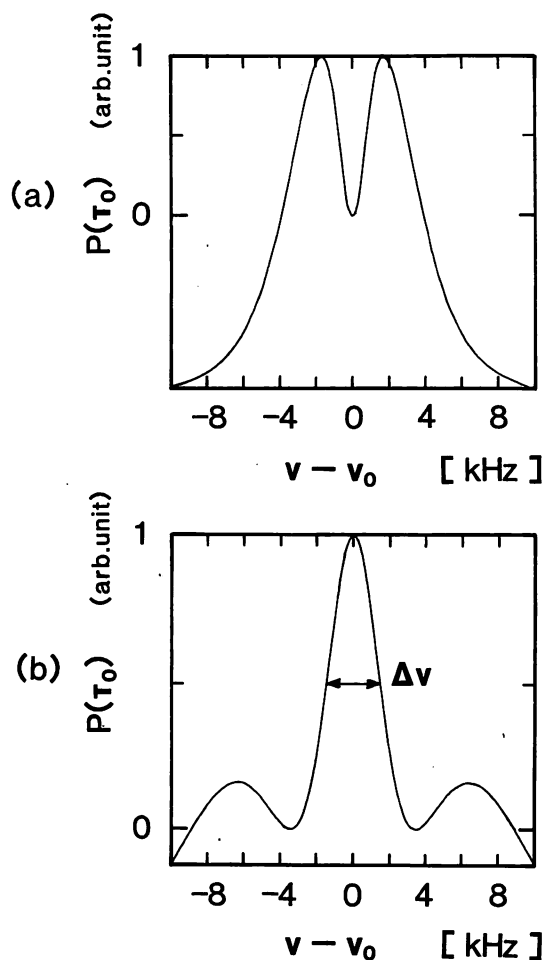


Fig. 5. The microwave resonance signals  $P(\tau_0)$  as a function of frequency detuning  $\nu - \nu_0 = \Omega_0/2\pi$ . The lineshapes were numerically calculated at  $b\tau = 0.2\pi$  (a), and at  $b\tau = 1.1\pi$  (b), when  $T_{Rb} = 433$  K.

shaped cavity.

### 3.3 Optimization and improvement of the frequency discrimination sensitivity

The optimum conditions of the frequency discrimination sensitivity were considered. The optimum condition is defined here as the maximum steepness of the slope of the derivative of the microwave resonance signal at the resonance frequency.

The temperature of the Rb source  $T_{Rb}$  was adjusted in the range between 350 K and 450 K, where the moderate intensities of the atomic beam were obtained. Figure 7 shows the peak-to-peak linewidth  $\Delta\nu_{p-p}$  and the slope  $(d^2/d\nu^2)P(\tau_0)$  at the resonance frequency ( $\nu = \nu_0$ ) of the derivative of the signal as a function of the Rabi frequency  $b$ . Here  $b\tau$  is used instead of  $b$  since the transition probability  $P(\tau_0)$  depends on  $b\tau$  in the conventional Rabi and Ramsey interactions. From this figure, the optimum value of  $b\tau$  can be obtained. In the range of  $0 < b\tau < 2\pi$ , the maximum of the slope  $(d^2/d\nu^2)P(\tau_0)$  was achieved at  $b\tau = 1.1\pi$ , i.e., point A in Fig. 7. The calculated lineshape in Fig. 5(b) (and Fig. 6(b)) was obtained at this condition. However, the peak value of  $(d^2/d\nu^2)P(\tau_0)$  at  $b\tau = 0.2\pi$ , i.e., point B, is almost the same with that of point A. The measured and calculated lineshapes in Figs.

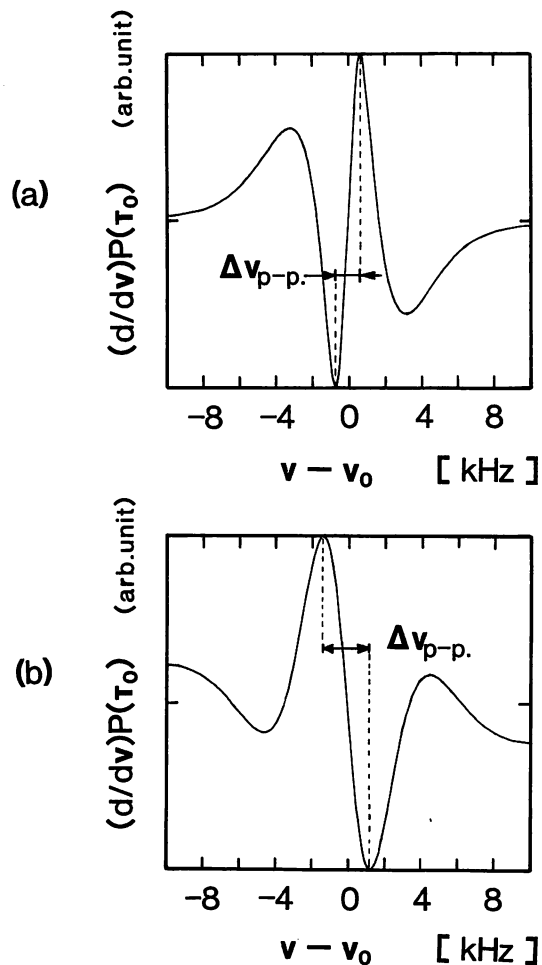


Fig. 6. The derivatives of the lineshapes. (a) and (b) correspond to those in Figs. 5(a) and 5(b), respectively.

4(b) and 5(a) (and 6(a)) were obtained under the condition corresponding to point B. Consequently, the optimum signal lineshapes are obtained both at points A and B of microwave magnetic field amplitudes, i.e., at  $b\tau = 1.1\pi$  and  $0.2\pi$ , at which the frequency discrimination takes the maximum sensitivity.

It is worth noting that, in a diode laser pumping system, a little wider linewidth of microwave resonance signal, compared with those in conventional Rb atomic clocks, can be compensated by the reduction of  $N$  value in  $S/N$  of the signal to achieve the maximum frequency discrimination. Since most of the noise is determined by the optical pumping and detection and not by the signal lineshapes of the microwave resonance, the  $N$  value can be reduced by suppressing the frequency (FM) noise of the diode lasers. In order to confirm this, we investigated the improvement of the  $S/N$  in the microwave resonance signal by selectively reducing the FM noise at the modulation frequency. Figure 8 shows the result obtained in the preliminary test for a gas cell-type Rb atomic clock pumped by a diode laser. Here  $10 \log(\Delta S_{LD}(f_m)/S_{LD}(f_m))$  means the magnitude of FM noise reduction at the modulation frequency  $f_m$  through the band-pass filter with  $Q=10$ . For the reduction of FM noise, the frequency of the diode laser was stabilized to the slope of a

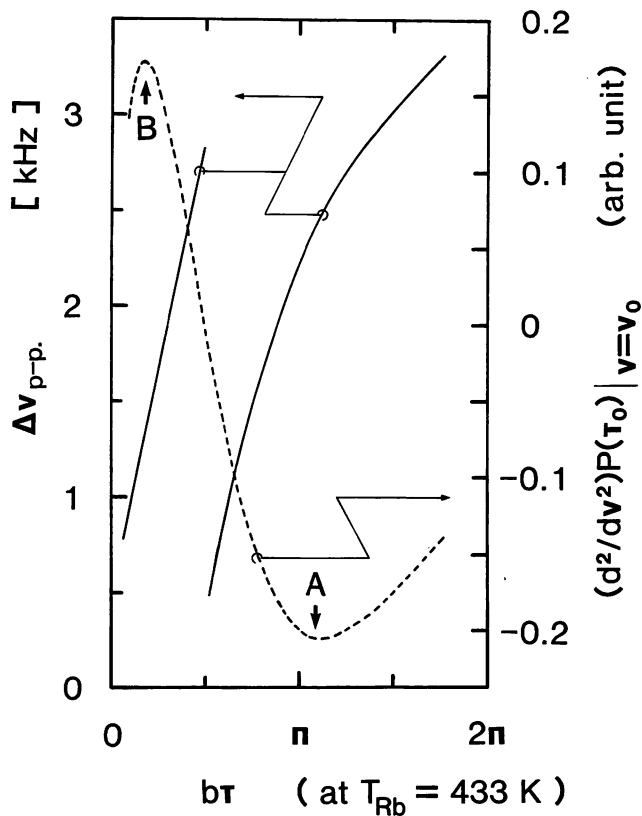


Fig. 7. The peak-to-peak linewidth  $\Delta v_{p-p}$ , and the slope  $(d^2/dv^2)P(\tau_0)$  at the resonance frequency ( $v=v_0$ ) of the derivative of the microwave resonance signal as a function of  $b\tau$ , where  $\tau$  is the transit-time in which an atom of velocity  $v_M$  goes through the 1st zone in Fig. 2(c). The results were obtained at  $T_{Rb}=433$  K. Solid lines represent the linewidth and the broken line represents the slope. Symbols A and B represent the conditions for the calculated lineshape in Fig. 6(b) and the experimentally obtained lineshape in Fig. 4(b), which corresponds to the calculated one in Fig. 6(a), respectively.

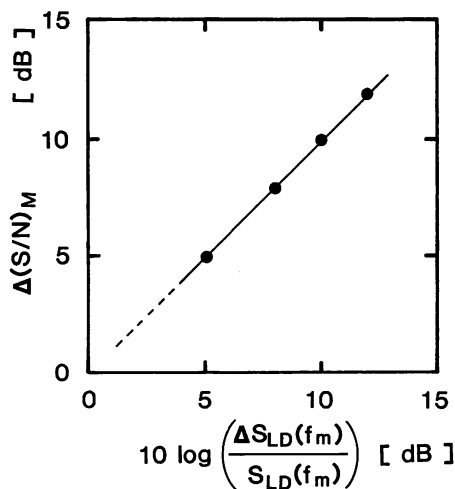


Fig. 8. Improvement of  $S/N$  in the microwave resonance signal  $\Delta(S/N)_M$  obtained by the selective reduction of FM noise of the diode laser  $\Delta S_{LD}(f_m)/S_{LD}(f_m)$  at the modulation frequency of the microwave signal  $f_m (=480$  Hz).

resonant line-shape of a Fabry-Perot interferometer. From this figure, it was confirmed that the magnitude of the improvement of  $S/N$  for the microwave resonance

signal is proportional to the magnitude of the FM noise reduction in the diode laser. In this result, 12 dB of the  $S/N$  improvement was achieved. Ohtsu *et al.* have demonstrated the FM noise reduction as low as  $-60$  to  $-70$  dB relative to that of free-running condition.<sup>12)</sup> If the same level of FM noise reduction is incorporated in the present system, 60 dB of the  $S/N$  improvement in the microwave resonance signal will be possible.

### 3.4 Frequency shifts

Frequency shifts in the present system can be produced by phase variations in the cavity or misalignment of atomic beam trajectory, in analogy with the end-to-end phase shifts in Ramsey cavities of Cs atomic clocks. Such frequency shifts in the frequency discriminator reduce the accuracy of the clock frequency. In highly accurate frequency standards, these shifts must be considered.

The microwave phase variations inside the cavity can cause the frequency shifts when they are associated with other modes. In our cavity, however, other TE modes have resonance frequencies far away from the  $TE_{012}$  and have a mode symmetry that will not produce frequency shifts. Even though other modes are fed in the cavity, the effects of these modes are quite small, i.e., the floor intensities caused by such other modes are less than a part in  $10^6$  relative to the resonant mode in our cavity. To achieve the  $10^{-12}$  level of frequency accuracy, the frequency shifts by the other TE modes do not cause any problems. Furthermore, the degenerate  $TM_{112}$  modes can be eliminated by using a  $\lambda/4$  mode filter.<sup>9)</sup> Thus, the phase variations inside the cavity cannot be a problem.

For the misalignment of atomic beam trajectory, the numerical calculation for the microwave resonant lineshapes was carried out including the effects of misalignments. As a result, it was found that even if the atoms flow 10 mm away from just the output point of the cavity (the misaligned angle is about 0.1 rad.), the frequency shift is less than a part in  $10^{13}$ . Since it is easy to adjust the atomic beam trajectory more precisely, the frequency shifts by the misaligned angle would be much smaller.

It is concluded that the present microwave resonance would not cause any specific frequency shifts. It can, therefore, be considered that the performance of the resonant method in the present work is sufficiently high to achieve a highly accurate laser-pumped Rb beam atomic clock.

## §4. Summary

A novel microwave resonance method for a laser-pumped rubidium (Rb) beam atomic clock was proposed. A microwave cylindrical cavity was used with its axis perpendicular to the atomic beam trajectory. A Ramsey-type fringe was observed in the microwave resonance signal. Its linewidth was 1.1 kHz. The characteristics of microwave resonance were theoretically explained by the spatial modal profile of microwave magnetic field inside the cylindrical cavity. The conditions for the maximum sensitivity of frequency discrimination on this type of resonance were discussed. The cavity frequency shifts for the present work in analogy with end-to-end cavity phase

shifts of conventional Cs atomic clocks were evaluated. The results showed that the shifts are not a problem in the present method. This novel method can be used to obtain a high-accuracy performance in atomic clocks because the atoms are free from collisions.

#### Acknowledgements

The authors would like to thank Dr. K. Yoshimura, Dr. K. Nakagiri and Mr. J. Umezumi of Communications Research Laboratory, and Dr. K. Nakagawa and Mr. C.-H. Shin of their institute for valuable discussions. They also wish to thank Mr. K. Chiba, Mr. H. Sumiyoshi and Mr. Y. Nakajima of Fujitsu, Ltd., for their support in the experiments.

#### References

- 1) L. L. Lewis and M. Feldman: *Proc. 35th Annual Symp. Frequency Control* (IEEE, Ft. Monmouth, 1981) p. 612.
- 2) M. Feldman, J. C. Bergquist, L. L. Lewis and F. L. Walls: *Proc. 35th Annual Symp. Frequency Control* (IEEE, Ft. Monmouth, 1981) p. 625.
- 3) J. C. Camparo, R. P. Frueholz and C. H. Volk: *Phys. Rev. Lett.* **27** (1983) 1914.
- 4) M. Hashimoto and M. Ohtsu: *IEEE J. Quantum Electron.* **QE-23** (1987) 446.
- 5) M. Hashimoto and M. Ohtsu: *J. Opt. Soc. Am. B, Series 2.* **6** (1989) 1777.
- 6) M. Hashimoto and M. Ohtsu: *IEEE Trans. Instrum. & Meas.* **39** (1990) 458.
- 7) H. Furuta, K. Nakagawa and M. Ohtsu: *Digest Conf. Precision Electromagnetic Measurements (CPEM '90)* (IEEE, Ottawa, 1990) p. 428.
- 8) J. Vanier and C. Audoin: *The Quantum Physics of Atomic Frequency Standards* (Adam Hilger, Bristol and Philadelphia, 1989) Vol. 2, Chap. 5, p. 603.
- 9) A. DeMarchi, R. E. Drullinger and J. H. Shirley: *Proc. 44th Annual Symp. Frequency Control* (IEEE, Baltimore, 1990) p. 34.
- 10) H. Furuta and M. Ohtsu: *Appl. Opt.* **28** (1989) 3737.
- 11) G. Avila, E. de Clercq, M. de Labachellerie and P. Cerez: *IEEE Trans. Instrum. & Meas.* **IM-34** (1985) 139.
- 12) M. Ohtsu, M. Murata and M. Kourogi: *IEEE J. Quantum Electron.* **26** (1990) 231.

## フォトン走査トンネル顕微鏡

大 津 元 \*

光を使ったSTM, すなわちフォトンSTM (PSTM) は数年前まではNFM (近視野顕微鏡) と呼ばれ, 初歩的な研究結果が報告されていたが<sup>1)</sup>, システム構造, 要素技術, などが未熟であったため, かならずしも高い分解能が得られていなかった. しかし, 以下に示すように半導体レーザと光通信用単一モード光ファイバを用いると, より高い分解能が可能となる. 透過形PSTM (T-PSTM, 同様のT-PSTMは文献2)でも提案されている) ではレーザのもつ高い光パワー密度, 波長可変性, を利用すると, 試料に強制的に光化学反応を誘起させ, 試料の特性変化の実時間観測, さらに局所的な分光分析が可能となる. 一方, レーザのもつ高コヒーレンスを利用した反射形PSTM (R-PSTM) では高分解能, 非破壊・非接触測定が可能である. 特に, 光源として半導体レーザを用いる場合, このレーザの応答時定数は1 ns以下であるので, 超高速での実時間測定ができる. さらに, 光検出においてはその量子雑音限界, すなわち光検出器のショット雑音レベルが容易に達成でき, これにより高感度の量子顕微鏡の実現が期待される.

図1 (a)にT-PSTMの原理を示す<sup>3)</sup>. 試料裏面から全反射角をもって光を入射させるとエバネッセント光が試料表面にしみ出す(光子のトンネル現象に対応). この光のパワーは縦方向(試料厚み方向)には指数関数的に減少するので, これを先鋭化されたファイバでピックアップすれば高い縦分解能が得られる. さらに, ファイバ先端に金属膜をコーティングした後, 先端に波長以下の直径の微小開口をあければ, 高い横分解能(試料面内方向)が得られる. 測定感度は光検出器のショット雑音およびピックアップされる光パワーにより制限されるので, 縦, 横分解能は互いに相関をもつ. STMと同様の制御装置でファイバを掃引すれば試料の3次元形状が測定できる.

図1 (b)は反射形PSTMの装置を示す<sup>3,4)</sup>. ピックアップとしてはファイバを用いて作ったファブリ・ペロー共振器(FPC)を使う. FPCの一端面に波長以下の微小開口を開けるとエバネッセント光はFPCからしみだした後, 試料に反射されてFPCに再入射する. 再入射光の位相は試料の形状に依存するのでFPCの位置を掃引しながらFPCの共振周波数の変化を測定すればよい. そ

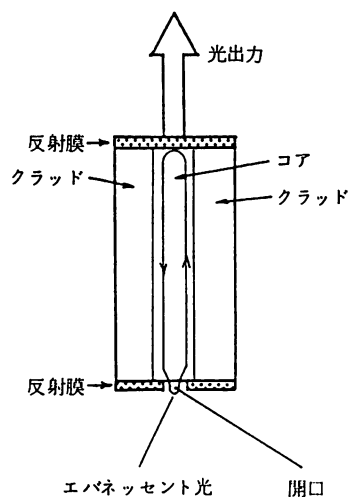
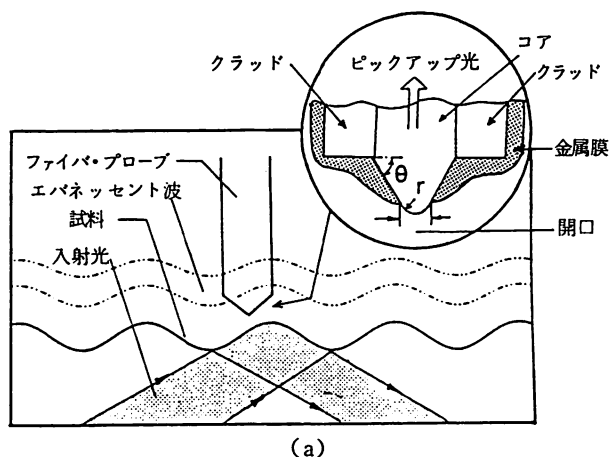


図1 (a) T-PSTM, (b) R-PSTMの原理図

### Photon Scanning Tunneling Microscope

\*MOTOICHI OHTSU 東京工業大学総合理工学研究科助教授  
筆者紹介 [最終学歴] 1978年東京工業大学大学院博士課程修了. [専門] 光量子エレクトロニクス. [趣味] 水泳, ダンス, ウッドクラフト. [連絡先] 227 横浜市緑区長津田 4259 (勤務先)

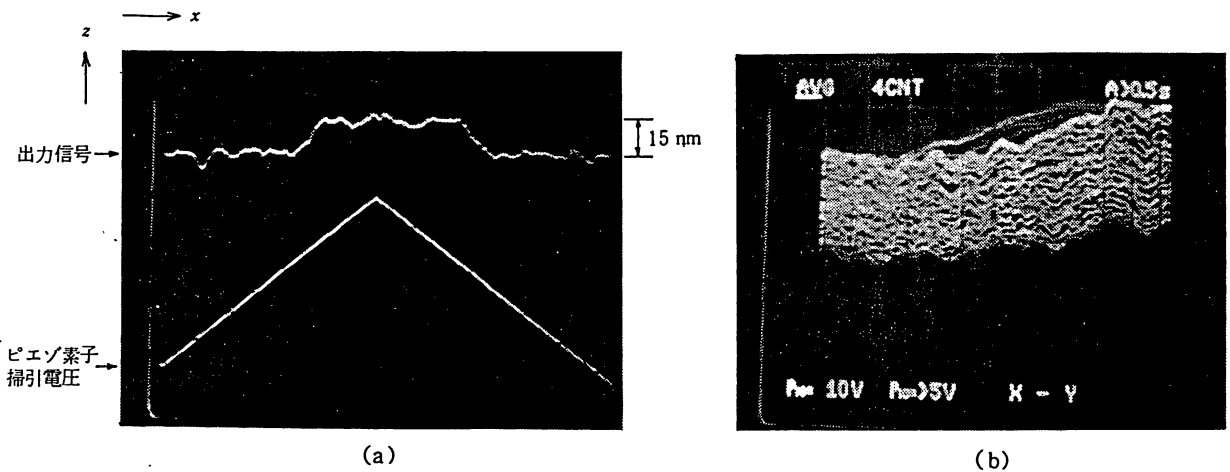


図2 (a)厚み 15 nmの SiO<sub>2</sub> 薄膜をプリズム表面の半分にコーティングし、T-PSTMで測定した結果  
 ファイバはx軸方向を往復させているので写真中央を境に左右対称となっている。  
 (b)ファイバをxy方向に掃引させて得られた試料の3次元形状

の測定には FPC の共振周波数に周波数固定されたレーザと、基準となるレーザとの間でのヘテロダイン法が利用できる。この FPC のかわりに端面に微小開口をあけた半導体レーザを使うことも可能である。

これらのシステムに必要な素子としてレーザとファイバとがある。前者についてはすでに小形・コヒーレント半導体レーザモジュールが開発され<sup>5)</sup>、そのスペクトル幅は 100 kHz 以下になっている。これは大形の市販気体レーザの性能よりもすぐれている。ファイバの先端はフッ酸による選択エッチングにより極率半径 100 nm 以下まで研磨することが可能である<sup>3,4)</sup>。さらに、R-PSTM ではヘテロダイン形光位同期ループの技術が必要であるが、すでに半導体レーザを用いてこれが実現し、0.4 mHz の光周波数変化も測定可能である<sup>6)</sup>。

図2にT-PSTMによる測定結果の例を示す。ここでは試料として厚み 15 nm の SiO<sub>2</sub> 薄膜をプリズム面の半分に蒸着したものをを用いた。ファイバを掃引することにより同図(a)には2次元形状が得られている。測定の時定数は 1 ms であり、短時間での測定である。それにもかかわらずこの図から推定される縦分解能は 1 nm である。これは従来の NFM の分解能より1桁以上よい。現在の装置のままでも、測定系のパラメータ最適化により、さらに高い分解能が期待できる。横分解能も縦分解能と大差ない値と推定している。同図(b)はこの試料の3次元形状を示す。

図3はR-PSTMのシミュレーション実験結果を示す。筆者らの手元には適当な標準試料がなかったので、ここでは動作原理の正当性を証明するために波長  $\lambda = 44 \mu\text{m}$  のマイクロ波共振器を使ってシステムを構成した。同図中に示したような断面形状をもつ試料を作り、測定を行

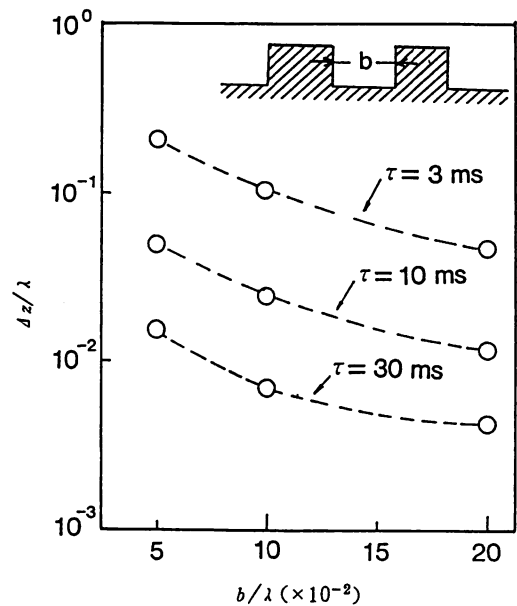


図3 R-PSTMのシミュレーション実験結果  
 図中の右上にあるのは試料の断面図 横軸は試料の二つの突起間隔  $b$ 。縦軸は縦分解能  $\Delta z$ 。パラメータは測定時定数  $\tau$ 。

った。縦軸、横軸は波長  $\lambda$  で規格化してある。測定時定数  $\tau = 30 \text{ ms}$  のとき、縦分解能は  $0.005 \lambda$  に達している。開口直径はまだ大きく、 $0.2 \lambda$  であるのにもかかわらず、このように非常に高い分解能が得られているのは、マイクロ波パワーが開口中心部に集中しているからである。この縦分解能は  $\lambda = 1 \mu\text{m}$  の光を使った場合、0.5 nm に相当する。動作パラメータ最適化により、より高い分解能が期待される。

将来の可能性の一つとして、PSTMを超高精度加工装置として使うことが考えられる。筆者らは特に単原

子結晶成長を提案している<sup>3,7)</sup>。レーザを用いた光糖蜜 (optical molasses)の方法<sup>8)</sup>によって真空中での原子集団を捕獲し、原子の熱運動の等価温度を予め数 $\mu\text{K}$ まで下げておく。ここにR-PSTM用のファイバ・ピックアップを近づけ、開口からのエバネッセント光のもつ勾配力により光糖蜜中の原子を捕獲する。これを結晶成長用の冷却結晶基板上に運び、レーザ周波数を変化させて基板上に原子を落下させ、付着させる。この際、問題となるのは必要なレーザパワーであるが、計算の結果、数mWでよいことが確認された<sup>3,7)</sup>。この方法はシリコン、ゲルマニウム、ガリウム、ひ素など、半導体産業に必須の元素に適用可能であり、将来の極限結晶成長のための重要な方法となりうる。

## 文 献

- 1) U. Durig et al., *J. Appl. Phys.*, **59**, 3318 (1986)
- 2) R. C. Redick et al., *Phys. Rev. B*, **39**, 767 (1989)
- 3) M. Ohtsu et al., Proc. OEC '90, Makuhari, July (1990), paper No. 12D1-1
- 4) S. Jiang et al., Proc. OEC '90, Makuhari, July (1990), paper No. 12D1-3
- 5) C.-H. Shin et al., *IEEE Photonics Technol. Lett.*, **2**, 167 (1990)
- 6) C.-H. Shin et al., *IEEE Photonics Technol. Lett.*, **2**, 297 (1990)
- 7) 大津 他, 第51回応用物理学会学術講演会発表, 講演番号 27aL9 (1990年9月)
- 8) D. Sesko et al., *J. Opt. Soc. Am. B*, **5**, 1225 (1988)

# 解説

## フォトン走査トンネル顕微鏡

蔣 曙 東・富田 直幸・大津 元一

東京工業大学総合理工学研究科 〒227 横浜市緑区長津田町 4259

(1990年11月12日受理)

### Photon Scanning Tunneling Microscope

Shudong JIANG, Naoyuki TOMITA and Motoichi OHTSU

Department of Information Processing, Tokyo Institute of Technology,  
4259, Nagatsuta, Midori-ku, Yokohama 227

#### 1. はじめに

有機超薄膜の診断・開発<sup>1)</sup>さらに、生体類似機能素子、バイオリアクターの設計、生体細胞膜のゲート機構解明、細胞プロセッシングなどの研究のために、横および縦分解能がおおの数十 nm, 数 nm 以内、広視野、非接触、非破壊、実時間観測可能な顕微鏡の需用が最近急速に高まっている。従来、光学顕微鏡、レーザー顕微鏡、電子顕微鏡(SEM)、走査型トンネル顕微鏡(STM)<sup>2)</sup>、原子間力顕微鏡(AFM)<sup>3)</sup>、などが開発されている。しかし、これらの顕微鏡では視野の広さ、分解能、測定条件、非接触・非破壊性などについては表1に示すようにいずれも一長一短がある。これらの問題点を解決するために、フォトン走査トンネル顕微鏡 (photon scanning tunneling microscope: PSTM) が最近注目されている。これは光学顕微鏡のもつ特長 (広視野・非接触・非破壊) と走査トンネル顕微鏡のもつ特長 (高分解能) とを組み合わせたものと考えられる。本稿ではこの PSTM の原理、研究の現状、今後の研究展望について筆者らの研究内容などをもとにご紹介し、さらに、今後の装置改良により、1 nm 以内の高分解能が可能であることを指摘する。

#### 2. PSTM の原理

光学顕微鏡の分解能は回折限界により制限され、波長と同程度の値になることは周知のとおりである。この分解能限界を超えるためには、マイクロ波の場合には超長基線電波干渉計(VLBI)、開口合成法<sup>4)</sup>などが使われている。しかし、光波の場合、波長  $\lambda$  は  $1 \mu\text{m}$  以下であるた

め、これらの方法を直接適用することは容易ではない。しかし、エバネッセント光 (すなわち、フォトンのトンネル効果)、と微小開口をもつプローブとを利用すれば、光波領域でも回折限界を超えることが可能である。この考え方に基づいて構成されたシステムが PSTM である。

図1に PSTM の基本原理を示す<sup>13)</sup>。試料表面内に沿って  $x$ - $y$  軸をとり、境界面に垂直方向は  $z$  軸をとる。全反射条件下では、試料表面上の法線方向  $z \ll \lambda$  なる近視野で考えると、振幅が  $z$  軸方向に指数関数的に減少し、エバネッセント光が発生する<sup>5)</sup>。光をフォトンと見なしてこの発生機構を解釈すると、二つの媒質の屈折率の値によって決まるフォトン閉じ込めのポテンシャル障壁の高さに依存して、フォトンがトンネル効果により試料外にしみだす現象と考えられる。トンネリング・フォトンの観測確率は  $z$  の増加とともに指数関数的に減衰するため、高い縦分解能が得られる。また、このフォトンの場合は光波長  $\lambda$  より小さい開口直径  $a$  ( $< \lambda$ ) をもつプローブにより破壊測定され、フォトンの運動量の測定誤差 (これは光の波長の測定誤差  $\Delta\lambda/\lambda = (\lambda/a)$  に比例) は

$$\Delta p = \hbar k \cdot \Delta\lambda/\lambda = h/a \quad (1)$$

となる。ここで、 $\hbar$  は  $h/2\pi$ 、 $h$  はプランク定数、 $k$  は光の波数である。ハイゼンベルグの不確定性原理によると、この誤差により開口で検出されるフォトンの位置測定 の最小不確定性  $\Delta x$  は

$$\Delta x = a/2\pi \quad (2)$$

となり、開口直径  $a$  で決まる高い横分解能が得られる。すなわち、従来の光学顕微鏡は回折効果に基づく不確定性原理に従う分解能をもつのに対し、ここでは微小開口



表 1 各種高分解能顕微鏡の特徴比較 (実用的なシステムの性能の代表値)

	試料の導電性	測 定 量	分 解 能		視 野	測 定 環 境
			縦	横		
光学顕微鏡	不 要			0.5 $\mu\text{m}$	1 mm	大気中, 液中
SEM	要	二次電子		3 nm	<5 mm	真空中
STM	要	トンネル電子	0.01 nm	0.1 nm	<1 $\mu\text{m}$	真空中, 大気中, 液中
AFM	不 要	原子間力	0.01 nm	0.15 nm	<1 $\mu\text{m}$	大気中, 液中
PSTM	不 要	トンネリングフォトン	1 nm	<10 nm	<10 $\mu\text{m}$	真空中, 大気中, 液中

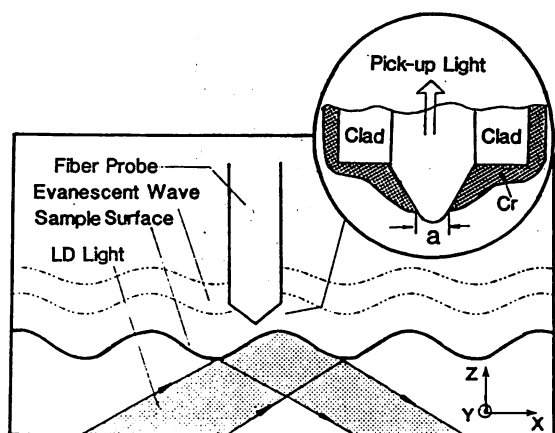


図 1 PSTM の基本原理図<sup>13)</sup>

をもつプローブを用いて、フォトンの位置のスキャンングをすることにより横分解能が決まる。以上を要約すると、PSTM が回折限界を越えた分解能を有する理由はエバネッセント光、微小開口、近視野測定、を採用していることである。

このように、フォトンのトンネル効果の原理を利用した顕微鏡と考えられるので、フォトン走査トンネル顕微鏡と名づけられている。しかし、同時に近視野での光学的測定技術を使うので、近視野顕微鏡 (near field microscope: NFM) とも呼ばれる。現在のところ、十分厳密な名称の定義が必ずしも十分ではなく、今後整理されるべきである。

### 3. PSTM のシステムと実験結果

PSTMの基本的手法として、現在まで、微小開口からの光放射法<sup>6,7)</sup>、微小開口による光ピックアップ法<sup>8-10)</sup>などがおもに開発されている。また、フォトンのトンネル効果だけを利用した縦分解能を追求する表面顕微鏡<sup>11,12)</sup>も報告されている。これらの研究で得られた分解能や、精度などをさらに向上させ、また、光源として使われている大形の気体レーザーや、キセノンランプを小形のものに替えて、従来のSTMの特長の一つと同様の小形性

を実現するために、筆者らは半導体レーザーを用いて透過形および反射共振形 PSTM を提案し<sup>13,15)</sup>、分解能を求めるための理論解析と予備的実験を行っている。本節ではこれらの概略をご紹介します。なお、透過形については類似のシステムの提案は他所でもわれわれとほぼ同時期になされている<sup>8)</sup>。ここでご紹介する方法では従来のPSTM用プローブの位置制御に使われているSTMプローブ<sup>7)</sup>も不要であるという利点を有する。

透過形のPSTMはレーザーのもつ特性のうち、高パワー密度、波長可変特性を活用したものであり、試料表面形状の測定はエバネッセント光のパワーを測定することにより行われる。したがって、システム構成は簡単であるが、低パワーのエバネッセント光の測定感度により、分解能が制限されるという問題点を有する。一方、反射共振形はレーザーの高コヒーレンスを利用したものであり、試料表面形状は周波数シフトの測定により求められる。周波数測定はすべての物理量測定のうちで、最も高精度であることは周知のとおりであり、したがって、透過形のもつ感度に関する問題点を解決するものである。すなわち、透過形、反射共振形を光通信システムと対応させると、それぞれ強度変調・直接検波方式、周波数変調・ヘテロダイン検波方式に対応する。透過形では試料表面の高分解能測定だけでなく、局所的な光化学反応を強制的に誘起させて、その結果を測定すること、さらに、局所的な分光分析、組成分析、などが期待できる。一方、反射共振形はより高い分解能をもつ非破壊測定、細胞プロセッシング、さらに、単原子結晶成長のためのマニピュレータなどにも利用可能と考えられる。

#### 3.1 透過形 PSTM

図2に透過形PSTMの基本装置を示す<sup>13)</sup>。半導体レーザーの光をプリズムに全反射角で入射させる。プリズムの上面には試料が付着しているので、試料の表面形状に依存するエバネッセント光が発生する。このエバネッセント光を微小な開口をもつ光ファイバプローブによって検出する。同図中では検出感度向上の一例としてレー

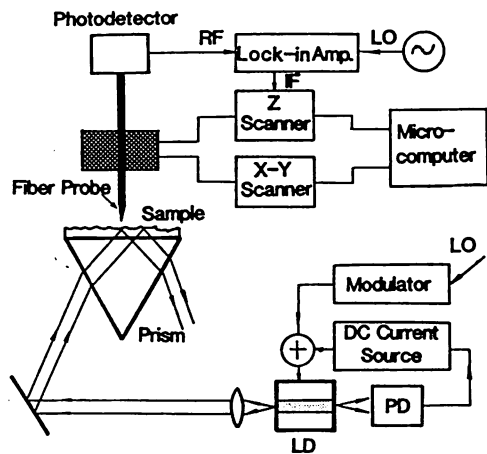


図2. 透過形 PSTM のシステム構成<sup>13)</sup>

ザーパワーの直接変調・位相敏感検波方式が示されているが、このほかに、試料表面での散乱光の影響を除去するためにプローブのz軸方向走査用のPZTを変調して、位相敏感検波する方式、さらに、光子計数法など、種々の方式が可能である。半導体レーザーの直接変調帯域は1GHz以上に及ぶので、他のレーザーに比べ、高速測定の利点を有する。試料表面の三次元形状の測定・表示については従来のSTM等と同様の方法を使う。すなわち、プローブをx-y軸方向に掃引しながら、検出したエバネッセント光パワーが一定となるようプローブのz軸方向位置を制御し、制御ループの誤差信号により、試料表面形状を測定する。すなわち、この信号を計算機により適当な画像処理を施した後、CRTディスプレイ上に三次元形状を表示する。

高い横分解能を得るためには微小開口をもつ光ファイバ・プローブが必要である。このプローブの製作方法は従来いくつか提案されているが<sup>6-9)</sup>、われわれはより高精度な製作方法を試みている。すなわち、単一モード光ファイバ(コア径5μm, クラッド径125μm)の先端をフッ酸を用いた選択エッチングによって尖らせる。次に厚さ100~200nmのクロム薄膜を蒸着し、さらにプラズマエッチングあるいはSTMプローブの先端放電により薄膜を除去して、コア先端に微小開口を形成する。図3に先端を尖らせた後のSEM写真を示す<sup>13)</sup>。図3(b)により、コア先端の曲率半径は約80nmと推定される。クロム薄膜の蒸着、さらに開口形成についてはまだ必ずしも十分な再現性が得られていない。しかし、数十nm以下の開口直径が実現可能であることも指摘されている<sup>9)</sup>。また、STMのプローブ先端放電により金の球面の上の特定位置に直径2nmの穴を開けた結果も報告されている<sup>16)</sup>。

図4(a)に示すようなプリズムの上面の半分に蒸着し

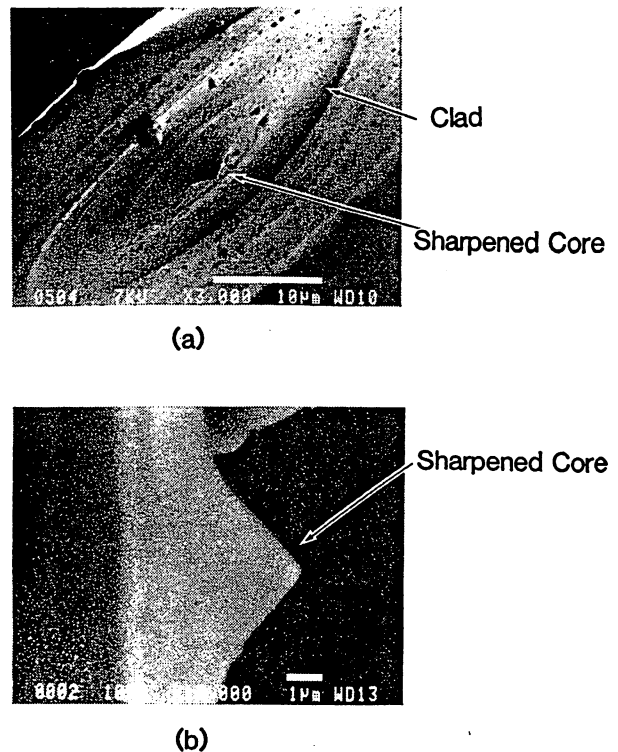


図3 ファイバ・プローブの先端 SEM 写真<sup>13)</sup>  
(a) 先鋭化したコアをもつファイバ先端を斜めから観測したもの。白線のスケールは10μmに相当。(b) 先鋭化したコアを横方向から観測したもの。白線のスケールは1μmに相当。

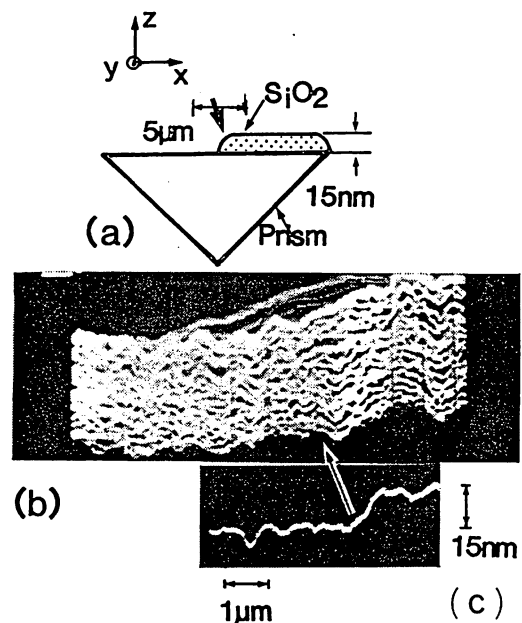


図4 SiO<sub>2</sub> 薄膜の測定結果<sup>14)</sup>  
(a) プリズム上のSiO<sub>2</sub> 薄膜断面の推定図。(b) 三次元形状測定例、紙面内での測定範囲を(a)の矢印で示す。(c) プローブをx軸方向のみに1回掃引したときの結果。

た膜厚 15 nm の SiO<sub>2</sub> 薄膜の形状測定を行った<sup>14)</sup>. その予備実験結果を図 4 (b)に示す. プローブは図 3 に示したものをを用いたが, この段階では, クロム薄膜蒸着および開口形成は行わずに使用した. 図 4 (c)にはプローブを  $x$  軸方向のみに掃引した結果を示す. 信号の  $S/N$  比より, 縦分解能は約 2 nm であると推定されている. ただし, この値は位相敏感検波方式における測定時定数  $\tau$  が 1 ms の場合の結果である. この時定数値は従来の STM などのそれに比べ小さい. これは LD が高速変調可能であることを利用したものであり, 高速測定の特長を示している. システムの雑音は白色雑音と仮定すると, 縦分解能は  $\tau^{-1/2}$  に比例する. したがって,  $\tau$  を大きくすれば, さらに高い縦分解能が期待される.

また, 横分解能は図 2 のプローブ先端形状より推定すると, 100 nm 以内であることは確実であり, 数十 nm 以内と概算されている.

3.2 反射共振形

われわれが提案し, ここでご紹介する反射共振形 PSTM は波長より小さい径をもつ開口から漏れ出るエバネッセント光により生じた位相差を共振法により高感度測定するものである. なお, 類似の考え方に基づく初歩的な干渉形マイクロ波走査トンネル顕微鏡もごく最近提案されていることを付記しておく<sup>17)</sup>.

図 5 に反射共振形 PSTM の基本構成を示す<sup>26)</sup>. レーザー光を導波路形共振器に入射させ, レーザー周波数が共振器の共振周波数に一致するよう制御しておく. 共振器の二つの端面のうち, 試料に面した端面には微小開口を設け, 共振器を試料に接近させる. このとき, 開口からのエバネッセント光が近接する試料表面によって, 摂動を受ける. その結果, 共振器端面の複素反射率が試料の表面形状によって変調され, 共振周波数がシフトする. これにより上記のレーザーの周波数もシフトするので, これを参照用レーザーあるいは他の共振器とのヘテ

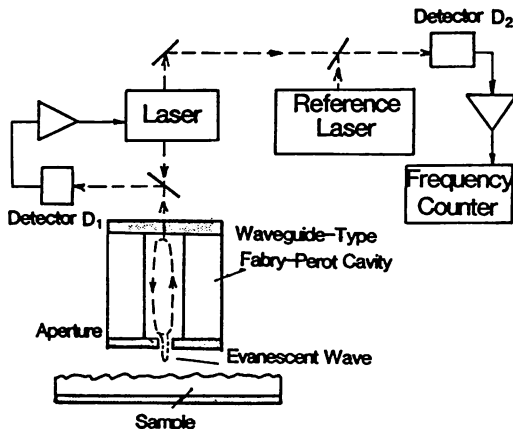


図 5 反射共振形 PSTM の基本構成<sup>26)</sup>

ロダイン信号周波数シフト測定などにより求める.

まず, このシステムの分解能を推定するために, フーリエ変換法<sup>18,19)</sup>を用いて共振周波数シフト  $\Delta f$  の数値解析を行った. 試料表面は平面と仮定した. 図 6 の実線は  $\Delta f/FSR$  の  $a/\lambda$  依存性を示す<sup>14)</sup>. ここで, FSR は共振器の自由スペクトル幅であり, 共振器はコア径 5  $\mu\text{m}$  の単一モードファイバを用いて製作すると仮定している. また,  $z/a$  はおのおの  $1.0 \times 10^{-3}$ ,  $1.0 \times 10^{-2}$  である. 図中の直線 A~D は共振器のフィネス  $F$ , 図 5 の光検出器  $D_1$  への入射パワー  $P$  の値に依存して発生するショット雑音により制限されるレーザー周波数の共振器共振周波数への追従限界を示す. すなわち, これらは  $\Delta f$  の測定精度のショット雑音限界に相当する. たとえば,  $F=1 \times 10^2$ ,  $P=10 \text{ mW}$  のとき, ショット雑音限界は  $a/\lambda=8.5 \times 10^{-3}$  に対応する.  $\lambda=800 \text{ nm}$  とすると,  $a=6.8 \text{ nm}$  であるので, 横分解能のショット雑音限界は約 6.8 nm となる. このとき, もし  $FSR=100 \text{ GHz}$  の共振器を使うとすると, このショット雑音限界に対応する周波数シフトは 14 Hz である. したがって, 反射共振形 PSTM を実現するための要素技術として高フィネスの短共振器や, 高コヒーレンス半導体レーザー, 光位相同期ループが必要である.

高コヒーレンス半導体レーザーとしては筆者らはすでに光・電気 2 重帰還法により線幅 7 Hz の半導体レーザ

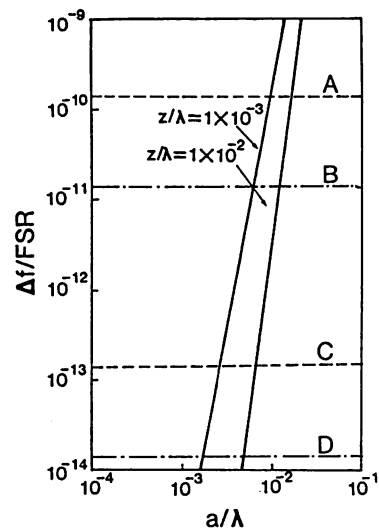


図 6 共振周波数シフト量の開口直径  $a$  依存性の計算結果<sup>14)</sup>  
 $\lambda$ : 光波長,  $z$ : 試料とプローブとの距離,  
 FSR: プローブ用共振器の自由スペクトル域. 直線 A~D は共振器フィネス  $F$ , 図 5 の光検出器  $D_1$  への入射光パワーがおのおの  $10^2$ , 10 mW;  $10^2$ , 1W;  $10^5$ , 10 mW;  $10^5$ , 1W の場合のショット雑音限界を表す.

ーを実現しており<sup>20)</sup>, ヘテロダイン形光位相同期ループの周波数安定度も  $1 \times 10^{-18}$  を実現している<sup>21)</sup>. さらに,  $1 \times 10^{-16}$  のレーザーの周波数安定度も報告されている<sup>22)</sup>. これらの技術を利用すれば上記の 14 Hz の値は十分測定可能であり, 反射共振形 PSTM の実現が期待される. また, 以上のショット雑音限界は  $1/F\sqrt{P}$  に比例するので, 他の任意の  $F, P$  の値についても図5を元に推定できる. また, これらの計算により, 透過形 PSTM の場合と同様に被測定量 (ここでは周波数シフト量  $\Delta f$ ) は  $z$  の増加とともに指数関数的に減少することもわかっており, 高い縦分解能が期待できる.

反射共振形 PSTM の動作確認のための実験を行った. われわれの手許には分解能評価用の微細な標準試料がなかったので, 波長 4.4 cm (周波数 6.8 GHz) のマイクロ波を用いて, シミュレーション実験を行った. 図7(a)に示す断面をもつアルミ板を試料として用い, 共振器を  $x$  軸方向に移動して得られた形状測定結果を図7(b)に示す<sup>14)</sup>. 試料の二つの突起間隔  $b$  が開口径  $a$  より小さいにも係わらず, 図7(b)では二つのピークが明確

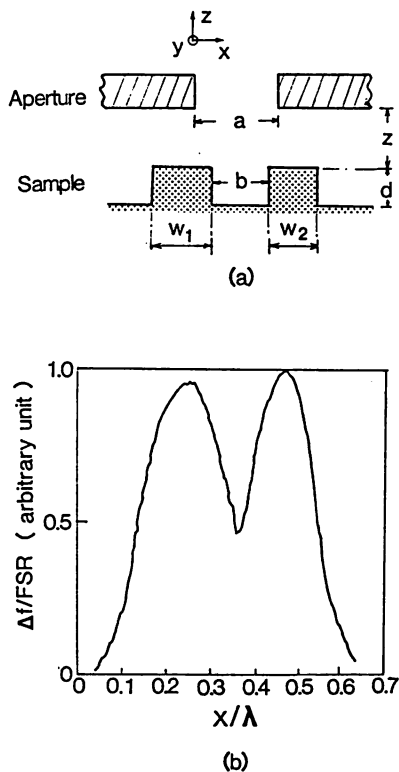


図7 マイクロ波による表面形状の測定結果<sup>14)</sup>  
(a) 試料と開口の断面形状. (b) 共振器を  $x$  軸方向に掃引して得られた測定結果. (a)中の  $a, b, d, w_1, w_2, z$ , さらに測定時定数  $\tau$  は次のとおり:  $a/\lambda = 0.20$ ,  $w_1/\lambda = 0.13$ ,  $w_2/\lambda = 0.11$ ,  $z/\lambda = 0.02$ ,  $d/\lambda = 0.09$ ,  $\tau = 10$  ms.

に現れている. このことから, 開口直径  $a$  と同程度以下の寸法の形状が測定可能な横分解能をもつことが確認された. これはエバネッセント光のパワーが開口中心部に集中しているためと考えられる.

さらに, 測定時定数  $\tau$  や, 図7(a)中の  $a, b, d$  等の値を変化させて, 一連の実験を行った結果, 縦分解能, 横分解能の最良値として, おおの,  $5 \times 10^{-3} \lambda$ ,  $5 \times 10^{-2} \lambda$  が得られている. 今後, 測定条件の改良により, いっそうの分解能向上が期待される.

## 4. 今後の展望

### 4.1 PSTM の性能向上のための課題

PSTM の感度・分解能をいっそう向上させるためにはまず, 近視野波動光学理論の確立が必須である. いままでは近視野波動光学の需要が少なかったため, 近視野波動光学領域での Maxwell 方程式を適切な境界条件で解く近視野波動光学理論は未発達な部分を有する. 原子の大きさ程度の分解能が実現すると, 光に対して物体表面とは何か, 境界条件とは何か, などについての詳細な検討が必要であろう. 最近では超微細加工技術の進歩に伴い, PSTM だけではなく, 微小光学, 微小共振器レーザー<sup>23)</sup>などの実現により近視野波動光学理論の必要性が増し, さらに共振器内量子電気力学 (cavity QED) の研究<sup>24)</sup>の進歩とともに, 上記の理論確立がいっそう重要となっている.

第2の課題は要素作成技術の確立である. 透過形の場合のファイバ研磨, コーティング, 微小開口作成技術の改良により微小開口作成技術の向上が期待される. 反射共振形の場合, 大きな  $F$  および FSR もつ共振器の実現, さらに温度, 振動などによる共振周波数ドリフトの補正法が確立すべき要素技術である. 単一モードファイバを用いて, 誘電体多層膜蒸着により,  $F \geq 200$ ,  $\text{FSR} \geq 100$  GHz (共振器長  $< 2$  mm) の値が報告されている<sup>25)</sup>. また, スーパー共振器では  $F = 120,000$  もすでに実現している<sup>\*1</sup>. 今後さらに, プレーナ技術 (イオン交換, イオン注入) による高安定, 低損失導波路形短共振器の実現が期待できる. また, 共振器の代りに, プロセス技術の進歩により, 半導体レーザーチップのへき開面の特定の場所に, 数十 nm の開口を作り, 半導体レーザーを, 増幅機能を持つ反射共振形プローブとして使うことも期待されている<sup>26,27)</sup>.

このほか, 分解能評価用の標準試料の選定, 用意も今後重要となろう.

\*1 J. Bergquist (NIST, USA) からの私信 (1990年8月)

4.2 可能な応用範囲

現在の PSTM の分解能は光学顕微鏡と電子顕微鏡 (SEM, STM など) との中間の値をとり, かつ視野が比較的広いので非接触・非破壊・実時間形状測定機としての広い応用範囲を有する。まず, 有機超薄膜などの表面形状を広視野で観測しながら, 光源波長を掃引して各部分での局所的な構造解析が可能となろう。さらに結晶表面に吸着した原子, 分子層の評価, 高密度集積回路の評価, などが可能である。さらに, 生命理工学分野では生体細胞膜, DNA, 特に種々のウイルス<sup>28)</sup>などの形状が非破壊で測定可能であろう。また, 複数個のプロープを用いて生体細胞膜中の刺激の伝搬特性の評価, ゲート機構の解明, などに威力を発すると考えられる。

一方, PSTM をたんに測定機として使うのではなく, 加工機としての応用可能性が重要である。すでに STM をキセノンの単一原子の操作に使う試みが報告されている<sup>29)</sup>。一方, PSTM では適当な波長の光源を選べば半導体産業において重要な原子 (シリコン, ゲルマニウム, ヒ素, ガリウム, など) にも適用な加工機となりうる。

その一例として, 筆者らが提案している単一原子操作および結晶成長の手法を以下に概説する<sup>30)</sup>。これは三段階からなる。まず, 第一段階では真空中で気体原子集団にレーザー光を照射し, レーザー冷却および光糖蜜の手法により原子の熱運動の等価原子温度を低下する。現在までに報告されている最低温度は数  $\mu\text{K}$  である<sup>31)</sup>。第二段階として反射共振形 PSTM のプロープをこの冷却原子集団に近づける。冷却原子がプロープから出射するエバネッセント光場に飛び込めば, この原子はエバネッセント光のもつ勾配力によるポテンシャルの井戸に捕獲される。安定な捕獲のためには実際には対向する複数のプロープの対を用いる。捕獲された原子の位置制御には, 原子捕獲の結果互に対向するプロープに生じる共振周波数シフト値が等しくなるような光位相同期ループを施す。また, 捕獲原子数のモニターにはこの共振周波数シフト値を測定する。簡単な計算によるとこれらのシフト値は筆者らの開発した高コヒーレント半導体レーザーおよび光位相同期ループにより十分測定可能であることが確認されている<sup>30)</sup>。以上により, 単一原子をエバネッセント光場中に安定に捕獲できる。

第三段階としてプロープを移動し, 捕獲した原子を冷却結晶基板上に移動する。そして, さらにもう一つの押し出し用プロープを用意しておき, これから光を出射させ, 原子を加速・加熱して押し出し, 結晶基板上に付着・固定させる。ここで, 問題となる点はプロープに入

射させるレーザー光パワーの必要値である。

これを知るためにセシウム原子を例にとって計算した結果を図 8 に示す<sup>30)</sup>。この図中, パラメータは光糖蜜の等価原子温度  $T$  である。この図によると, たとえば原子温度  $T=0.1\text{mK}$  のとき, 開口径  $a/\lambda=1\times 10^{-2}$  なるプロープを用いれば, 必要入射パワーは  $1\text{mW}$  でよいことがわかる。この値は既存の半導体レーザーにより実現可能である。ごく最近, この考え方を支持する関連実験結果が報告された<sup>32,33)</sup>。これは光糖蜜から落下した原子をエバネッセント光により跳ね返し, 原子のトランポリン運動を実現する試みである。ただし, われわれのような微小開口プロープを用いてはいないので, 必要レーザーパワーはわれわれの場合より高く,  $1\text{W}$  以上であった。したがって, 単一原子結晶成長には光糖蜜とともに微小開口プロープが必須要素であるといえよう。

このような極限的結晶成長の類形として, 結晶基板上に原子を一個ずつ積み上げ, 単一原子レベルの細線 (whisker) 形成, さらにこのほかにも超高密度集積回路のトリミング, 局所的レーザー・アニール, 結晶表面上の原子中の  $sp$  混成軌道の斜め方向から光を打ち込んで二次電子を放出させる可能性, などが考えられる。

一方, 細胞プロセッシングの分野では, 従来より使われていたレーザー顕微鏡<sup>34)</sup>の代りに PSTM 用のプロープを使い, 細胞の特定の位置にレーザー光を照射して細胞に穴を開ければ, 細胞への DNA の打ち込み精度が向上するであろう。

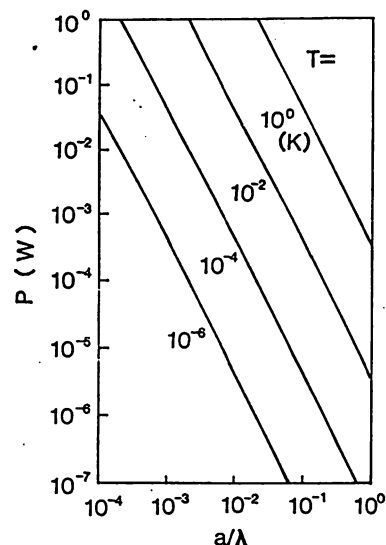


図 8 単一原子の捕獲に必要な入射レーザー光パワー  $P$  の計算値<sup>30)</sup>  
横軸はプロープ開口直径  $a$  を光波長  $\lambda$  で規格化したもの。パラメータ  $T$  は光糖蜜中の等価原子温度。

### 4.3 超高分解能を目指して

PSTM システムの性能は急速に向上しており、とくに反射共振形では STM と同等以上の分解能も期待できる。さらに STM などの性能を追い越し、超高分解能を実現するためにはいくつかの手法が考えられる。まず、マイクロ波周波数帯で採用されている開口合成法の使用可能性である。すでに製作されているマルチコア・ファイバ<sup>35)</sup>、またはプレーナ・プロセス技術を用いれば近接した複数個のプロープをモノリシックに製作することが可能である。このマルチ・プロープにより得られた試料形状測定結果に含まれる各プロープ間の相関を抽出することにより、単一プロープよりも高い分解能が期待される。同様の可能性は従来の STM プロープ先端に原子が複数個ある場合にも得られることがわかっている。この場合、モアレ・パターンに類似の画像が得られるので、計算機処理により STM の分解能はさらに向上しうる。PSTM における上記のマルチ・プロープ法はこれに対応している。

PSTM はヘテロダイン検波法などを採用できるのでショット雑音限界(量子雑音限界)が比較的容易に達成可能である。この意味で PSTM は表1にある各種顕微鏡の内できるとくに量子効果の現れやすいシステム、すなわち quantum microscope (量子顕微鏡)、ということができよう。分解能および感度限界は当面この量子雑音により決まるが、光子数スクイズ状態<sup>36)</sup>の光を利用すれば、この雑音レベルを越える super-quantum microscope の実現可能性も期待できる。

### 5. おわりに

非接触・非破壊の超解像光学顕微鏡として有望なフォトン走査トンネル顕微鏡 (PSTM) について概説した。従来、光が高分解能の顕微鏡システムに利用されている一例として AFM がある。このシステムはすでにヘテロダイン法、光てこ法など、光技術を補助手段として使っている。しかし、PSTM は光を補助手段としてではなく、光の特性を駆使しており、光でなくては実現しない超高性能顕微鏡といえよう。今後、光学の手法は極限技術にますます利用されていくと考えられる。したがって、光の本質をさらに詳しく研究する必要性が増大するであろう。とくに、近視野波動光学は未開発の分野であり、量子光学の手法と組み合わせればさらに新奇な極限光学システムの実現も可能であろう。これらのシステムに必要な要素として、半導体レーザー、光ファイバ、光集積回路、などがあるが、これらの要素の開発のいくつ

かはわが国が世界をリードしている。PSTM および関連する研究分野は若々しく、魅力的であり、広範な科学技術分野への波及効果があるといえよう。

なお、表1については筆者らの調査不足により必ずしも十分公平な値を示していない不安も残る。不備な点をご指摘いただければ幸いである。

研究開始当初に貴重なご助言を賜った計量研究所の山田啓文博士、技術討論をいただいた(株)ニコンの藤井透氏、鈴木正敏氏、大沢日佐雄氏、浅見武史氏、藤倉電線(株)の宮本末広氏、さらに生体動力学に関して指導いただいた本学の猪飼篤教授、システム構成に付いてご議論いただいた中川賢一博士を初めとする筆者らの研究グループ諸氏に感謝します。

### 文 献

- 1) 矢部 明, 谷口彬雄, 増原 宏, 松田宏雄: "有機超薄膜入門" (培風館, 東京, 1989).
- 2) Y. Kuk and P. J. Silverman: "Scanning tunneling microscope instrumentation," *Rev. Sci. Instrum.*, **60**(2) (1989) 165-180.
- 3) D. Rugar and P. Hansma: "Atomic force microscopy," *Phys. Today*, Oct. (1990) 23-30.
- 4) L. J. Cutrona, Emmett N. Leith, L. J. Porcello and W. E. Vivian: "On the application of coherent optical processing techniques to synthetic-aperture radar," *Proc. IEEE*, **54** (1966) 1026.
- 5) E. A. Ash and G. Nichols: "Super resolution aperture scanning microscope," *Nature*, **237** (1972) 510-512.
- 6) U. C. Fischer, U. T. Durig and D. W. Pohl: "Near-field optical scanning microscopy in reflection," *Appl. Phys. Lett.*, **52** (1988) 249-251.
- 7) U. Durig, D. W. Pohl and F. Rohner: "Near-field optical-scanning microscopy," *J. Appl. Phys.*, **59** (1986) 3318-3324.
- 8) R. C. Reddick, R. J. Warmack and T. L. Ferrell: "New form of scanning optical microscopy," *Phys. Rev. B*, **39** (1989) 767-770.
- 9) E. Betzig, M. Isaacson and A. Lewis: "Collection mode near-field scanning optical microscopy," *Appl. Phys. Lett.*, **51** (1987) 2088-2090.
- 10) D. Courjon and J. M. Vigoureux: "External and internal reflection near field microscopy: experiments and results," *Appl. Opt.*, **29** (1990) 3734-3740.
- 11) J. M. Guerra: "Photon tunneling microscopy," *Appl. Opt.*, **29** (1990) 3741-3752.
- 12) 岡本隆之, 山口一郎: "表面プラズモン顕微鏡," *光学*, **19** (1990) 682-686.
- 13) 蔭 曙東, 富田直幸, 中川賢一, 大津元一: "フォトン STM—設計と解析", 平成1年秋応物予稿集, 30 p-ZE-4/III (1989) p. 949.
- 14) 富田直幸, 蔭 曙東, 中川賢一, 大津元一: "フォトン STM (III) (IV)", 平成2年秋応物予稿集, 28 p-B-7/II, 28 p-B-8/II (1990) p. 420.
- 15) 蔭 曙東, 富田直幸, 中川賢一, 大津元一: "半導体レーザーを用いたフォトン STM の基礎研究", 第4回光波センシング技術研究会講演論文集 (1989) pp. 53-59.

- 16) P. F. Marella and R. F. Pease: "Comment on" writing nanometer-scale symbols in gold using the scanning tunneling microscope," *Appl. Phys. Lett.*, **55** (1989) 2366-2367.
- 17) M. Fee, S. Chu and T. W. Hansch: "Scanning electro magnetic transmission line microscope with sub-wavelength resolution," *Opt. Commun.*, **69** (1989) 219-224.
- 18) J. W. Goodman: *Introduction to Fourier Optics*, 1st ed. (Mcgraw-Hill, New York, 1968) Chap. 2.
- 19) O. Bryngdahl: "Evanescent waves in optical imaging," *Progress in Optics*, ed. E. Wolf, Vol. XI (Elsevier Scientific Publ., 1973) pp. 169-184.
- 20) C. H. Shin and M. Ohtsu: "Stable semiconductor laser with a 7-Hz linewidth by an optical-electrical double-feedback technique," *Opt. Lett.*, **15** (1990) 1455-1457.
- 21) C. H. Shin and M. Ohtsu: "Heterodyne optical phase-locked loop by confocal Fabry-Perot cavity coupled AlGaAs laser," *Photon. Technol. Lett.*, **2** (1990) 297-300.
- 22) D. Hils and J. L. Hall: "Ultra-stable cavity-stabilized lasers with subhertz linewidth," *Proc. of Frequency Standards and Metrology*, ed. A. De Machi (1988) pp. 162-173.
- 23) J. L. Jewell, A. Scherer, S. L. McCall and Y. H. Lee: "Low threshold electrically-pumped vertical-cavity surface-emitting micro-laser," *Electron. Lett.*, **25** (1989) 1123-1124.
- 24) F. De Martini, G. Innocenti, G. R. Jacobovitz and P. Mataloni: "Anomalous spontaneous emission time in a microscopic optical cavity," *Phys. Rev. Lett.*, **59** (1987) 2955-2958.
- 25) J. Stone and L. W. Stulz: "Pigtailed high-finesse tunable fiber Fabry-Perot interferometers with large, medium and small free spectral ranges," *Electron. Lett.*, **23** (1987) 781-782.
- 26) S. Jiang and N. Tomita: "Proposal of super-sensitive reflection-mode phase locked PSTM by diode laser," OEC '90, Tech. Dig., Makuhari Messe Japan, 12D1-3 (1990).
- 27) M. Ohtsu, K. Nakagawa, S. Jiang and N. Tomita: "Super-resolution photon scanning tunneling microscope," OEC '90, Tech. Dig., Makuhari Messe Japan, 12D1-1 (1990).
- 28) K. Tanaka, A. Ikai and K. Kameyama: "Proteasomes (multi-protease-complexes) as 20 S ring-shaped particles in a variety of eukaryotic cells," *J. Biol. Chem.*, **263** (1988) 16209-16217.
- 29) D. M. Eigler and E. K. Schweizer: "Positioning single atoms with a scanning tunneling microscope," *Nature*, **344** (1990) 525-526.
- 30) 大津元一, 蔣曙東, 富田直幸, 中川賢一, 藤江嘉彦: "フォトン STM(v)一岸一原子レベル結晶成長", 平成2年秋応物予稿集, 27a-L-9/III (1990) p. 800.
- 31) D. Sesko, C. G. Fan and C. E. Wiemar: "Production of a cold atomic vapor using diode-laser cooling," *J. Opt. Soc. Am., B*, **5** (1988) 1225-1227.
- 32) A. Aspect and E. Arimondo: "Lasercooling below the one-photon recoil energy by velocity-selective coherent population trapping," *Phys. Rev. Lett.*, **61** (1988) 826-829.
- 33) M. A. Kasevich, D. Weiss and S. Chu: "Normal-incidence reflection of slow atoms from an optical evanescent wave," *Opt. Lett.*, **15** (1990) pp. 607-609.
- 34) 粕谷敬宏, 塚越幹郎: "レーザーによる細胞プロセッシング", *応用物理*, **57** (1988) 1035-1040.
- 35) M. Fukuma, I. Ogasawara, A. Nishimura and S. Suzuki: "Characterization of cross-talk in four-core graded-index multicore fiber," *OFC/IOOC '87/WEDNESDAY AFTERNOON* (1987) w17, p. 172.
- 36) 矢島達夫: "光の量子効果", *量子力学と新技術*, 第9章 (日本物理学会, 東京, 1987) pp. 182-202.

# 特集:STMの新しい展開—ハード面より—

## フォトン走査トンネル顕微鏡とその展開

東京工業大学 総合理工学研究科\*

大津 元一

### 1. まえがき

半導体工学, 光エレクトロニクス, バイオエレクトロニクスなどの分野で, 高い分解能をもち, かつ非接触, 非破壊, 実時間測定可能, 大気または溶液中で測定可能な顕微鏡の需要が最近急速に高まっている。フォトン走査トンネル顕微鏡 (Photon Scanning Tunneling Microscopy: PSTM) はそのような需要に応え得るシステムとして最近注目されている。これは光学顕微鏡のもつ広視野・非接触・非破壊の特長と走査トンネル顕微鏡 (STM) のもつ高分解能とを組み合わせたものである。本稿ではこのPSTMの原理, 研究の現状, 今後の研究展望について筆者の研究内容<sup>1)~7)</sup>などをもとにご紹介し, さらに, 今後の装置改良により, 単原子レベルでの結晶成長や加工などにも使用可能であることを指摘する。なお, 頁数の制限のため記述不足部分の詳細については筆者らによる同様の解説記事を参照されたい<sup>8), 9)</sup>。

### 2. PSTMの原理

光学顕微鏡の分解能は回折限界により制限され, 波長 $\lambda$ と同程度の値になることは周知のとおりである。しかし, エバネッセント光と微小開口をもつプローブとを利用すれば, 回折限界を越える光学顕微鏡が可能である。この考え方に基づいて構成されたシステムがPSTMである。図1(a)にPSTMの基本原理を示す<sup>9)</sup>。試料表面内に沿

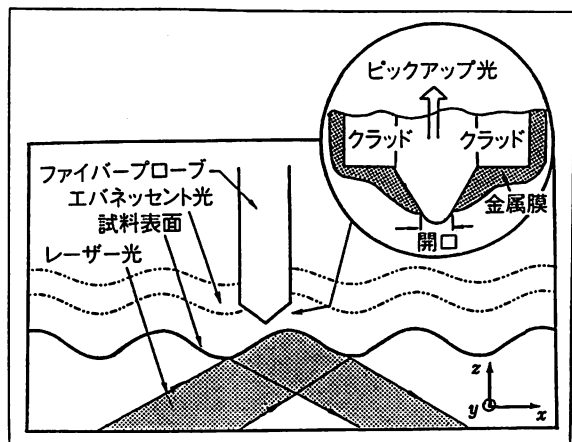
って,  $x, y$  軸をとり, 境界面に垂直方向に  $z$  軸をとる。全反射条件下では, 試料表面上の法線方向  $z < \lambda$  なる近視野で考えると, エバネッセント光が発生しており, そのパワーは  $z$  軸方向に指数関数的に減少する。この光を  $a < \lambda$  なる直径  $a$  をもつ開口でピックアップする。

光をフォトンと見なしてこのピックアップの原理を説明すると, 開口径, 開口・試料間隔, 試料屈折率, などによって決まるフォトン閉じ込めのポテンシャル障壁の高さに依存して, フォトンがトンネル効果により試料からしみだし開口を通り抜けると考えられる。トンネリング・フォトンの存在確率は開口・試料間隔の増加とともに指数関数的に減少するため, 高い縦分解能が得られる。ここで, エバネッセント光の場合は  $a < \lambda$  なる開口をもつプローブにより破壊測定されるので, フォトンの運動量の測定誤差 (これは光の波長の測定誤差  $\Delta\lambda/\lambda (= \lambda/a)$  に比例) は  $\Delta p = \hbar k \cdot \Delta\lambda/\lambda = h/a$  となる。ここで,  $\hbar$  は  $h/2\pi$ ,  $h$  はプランク定数,  $k$  は光の波数である。ハイゼンベルグの不確定性原理 ( $\Delta p \cdot \Delta x \geq \hbar$ ) によると, この誤差により開口で検出されるフォトンの位置測定の最小不確定性は  $\Delta x = a/2\pi$  となり, 開口直径  $a$  で決まる高い横分解能が得られる。つまり, ここでは  $a < \lambda$  なる微小開口をもつプローブを用いることにより波動としての光の特性を測定することを捨て, フォトンの位置を高精度に測定している。すなわちフォトンの位置のスケーリングをすることにより高い横分解能が得られる。要するに, PSTM はエバネッセント光を近視野測定することにより

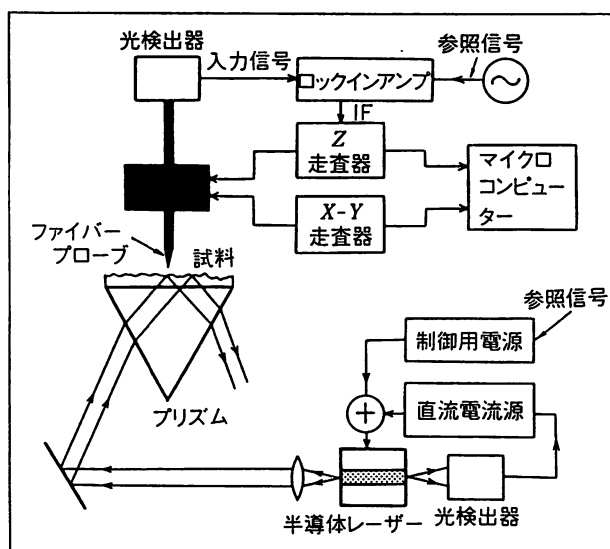
\*〒227 神奈川県横浜市緑区長津田町4259

☎045-922-1111





(a) 透過形 PSTM の基本原理図<sup>9)</sup>



(b) システム図<sup>9), 9)</sup>

図 1

縦分解能を、微小開口を用いて近視野測定することにより横分解能を向上させている。これにより回折限界を越えた分解能が実現する。

PSTM では光の波動および光子としての二重性を活用している。すなわち、システム制御には揺らぎの少ない滑らかな光波の特性を使い、情報抽出には光子の特性を利用している。このように、情報抽出には光子のトンネル効果を利用するので、光子走査トンネル顕微鏡と名づけられている。しかし、同時にシステム制御には光波としての性質も使うので、近視野顕微鏡 (Near Field Microscope: NFM) とも呼ばれる。現在のところ、十分厳密な名称の定義が必ずしも十分ではなく、今後整理されるべきである。

図 1 (b) にシステム全体の概念図を示す<sup>9), 9)</sup>。ここではファイバーの先端に作られた微小開口を測定用プローブとして用いる。試料表面の 3 次元形状の測定・表示については従来の STM と同様の方法を使う。すなわち、プローブを  $x$ - $y$  軸方向に掃引しながら、検出したエバネッセント光パワーが一定となるようプローブの  $z$  軸方向位置を制御し、制御ループの誤差信号強度により、試料表面形状を測定し、計算機により適当な画像処理を施した後、CRT ディスプレイ上に表示する。

### 3. PSTM のシステムと実験結果

PSTM の基本的手法として、現在まで、微小開口からの光放射法<sup>10), 11)</sup>、微小開口による光ピックアップ法<sup>12)~14)</sup>などが開発されている。また、フォトンのトンネル効果だけを利用し、高い縦分解能を追求する表面顕微鏡<sup>15), 16)</sup>も報告されている。しかし、これらの研究では横分解能が必ずしも十分高いとは言えない。また、大型の気体レーザーや、キセノンランプを光源として使っており、従来の STM の特徴の 1 つである小形性に対抗する特長が発揮されていない。さらに、PSTM 用プローブの位置制御に STM プローブが不可欠なシステムも存在している<sup>11)</sup>。また、従来の研究ではシステム性能評価のための理論解析が不足している。そこで、筆者らはこれらの問題点を解決するために、半導体レーザーを用いた透過形および反射共振形 PSTM を提案している<sup>11)~17)</sup>。なお、透過形 PSTM については類似のシステムの提案は他所でもわれわれとほぼ同時期になされている<sup>12)</sup>。本節では図 1 (b) に示すようなわれわれの透過形 PSTM (T-PSTM) の実験結果をご紹介します。

T-PSTM はレーザー光のパワー密度が高いことを利用したものであり、試料表面形状の測定はエバネッセント光のパワーを測定することにより行われる。したがって、システム構成は簡単であるが、低パワーのエバネッセント光を測定するので感度が低く、分解能が制限される。T-PSTM を光通信システムと対応させると、強度変調一直

## 特集: STMの新しい展開—ハード面より—

接検波方式に対応する。T-PSTM を用いると試料表面の高分解能測定だけでなく、局所的な光化学反応を強制的に誘起させて、その結果を測定すること、さらに、レーザー波長を掃引すれば局所的な分光分析、組成分析、などが期待できる。図1(b)中では検出感度向上の一例としてレーザーパワーの直接変調・位相敏感検波方式が示されているが、このほかに、プローブのz軸方向走査用のピエゾアクチュエーターを変調し、位相敏感検波する方式、さらに、光子計数法など、種々の方式が可能である。半導体レーザーの直接変調帯域は1GHz以上に及ぶので、他のシステムに比べ、高速測定可能の利点を有する。

高い横分解能を得るために微小開口をもつ光ファイバー・プローブを使っている。このファイバー先端の微小開口の製作方法は従来いくつか提案されているが(ラテックス球による方法<sup>10)</sup>、石英棒の先端を尖らす方法<sup>11)</sup>、ピペット法<sup>12)</sup>、など)、いまだ加工精度と再現性が低い。一方、われわれの製作方法としてはまず、単一モード光ファイバーのコア先端を弗酸を用いた選択エッチングによって尖らせる。次にクロムおよび金の薄膜を蒸着し、さらにプラズマエッチングあるいはSTMプローブの先端との放電によりコア先端の一部を露出させ、微小開口とする。写真1には先端を尖らせ、金属薄膜を蒸着した後のSEM写真を示す。ファイバー・コア先端の曲率半径は約80nm以内と推定される。金属薄膜の蒸着、さらに開口形成についてはまだ必ずしも十分な再現性が得られていないが、数10nm以下の開口径が可能であることも指摘されている<sup>12)</sup>。

図2にプローブと試料マウント用プリズム面との間隔と、エバネッセント光のパワーとの関係の測定結果を示す。光源にはAlGaAsレーザーを用いており、試料入射時のパワーは数mWである。測定されたエバネッセント光パワーは間隔の増加と共に指数関数的に減少している。この図では光パワーは約1pW以下であるが、光軸調整の精密化などにより最近では10pW以上の値も得られている。さらに開口周囲の金属蒸着膜からの表面ブ

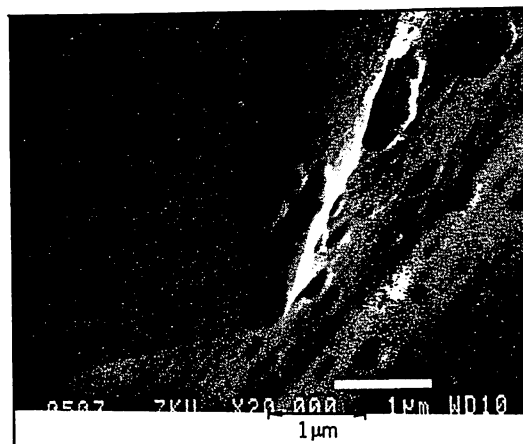


写真1 先端を尖らせ、金属薄膜を蒸着したファイバー端面のSEM写真

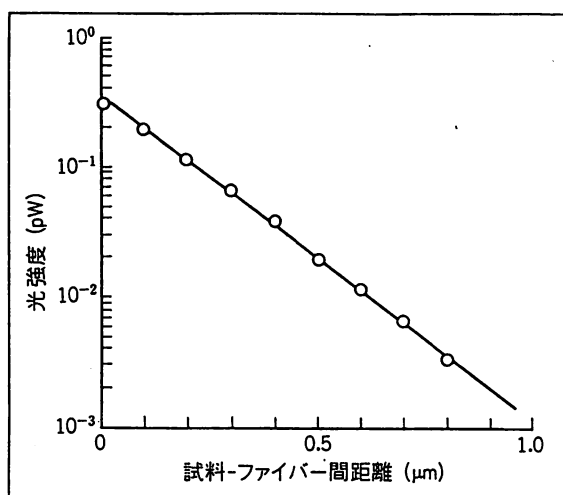
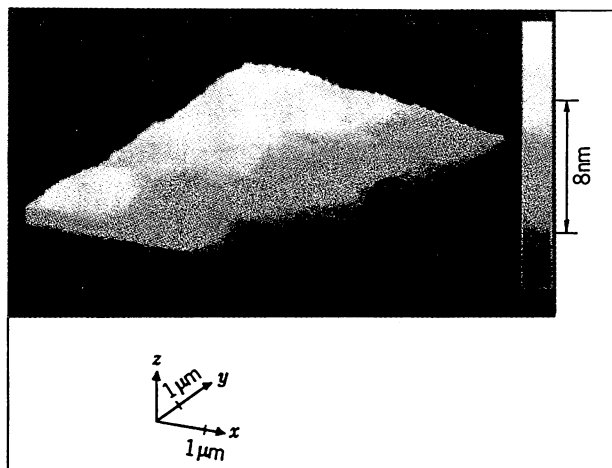


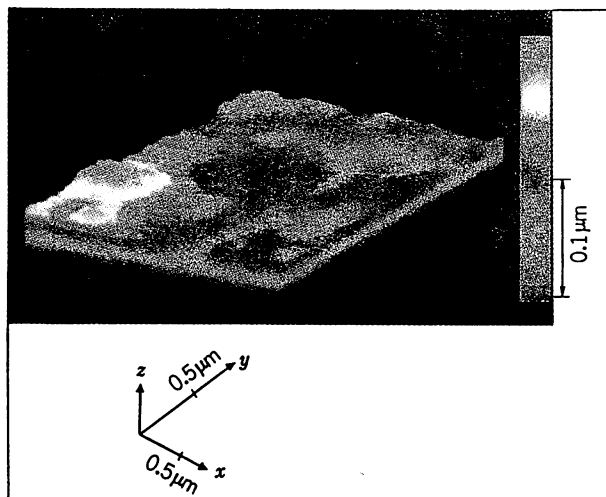
図2 プローブ・試料間隔と測定されたエバネッセント光パワーとの関係

ラズモンを使えばさらに高い光パワーが得られることが確認されている<sup>17),18)</sup>。この場合、横分解能が低下する恐れがあるが、測定感度が向上するので、さらに小さな開口を使うことが可能となり、むしろ分解能向上が期待できると考えられる。

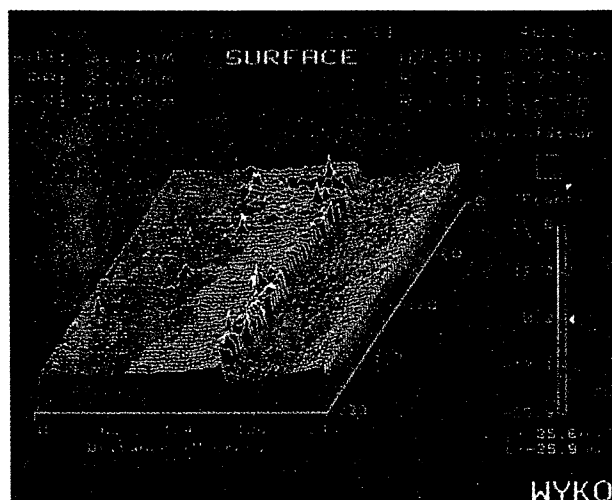
図1(b)のプリズムの上面の半分に蒸着した厚さ15nmのSiO<sub>2</sub>薄膜の端部(すなわち蒸着部と非蒸着部との境目)の形状測定を行った。その実験結果を写真2(a)に示す。写真2(b)は同じ試料の形状をレーザー干渉顕微鏡により測定した結果を示す。また、写真3(a)には深さ約80nm、直径約300nmのピットを有するMoth Eye光ディスク表面形状の測定結果を示す。このディスク表面には厚さ12nmのプラチナ膜が蒸着されて



(a) プリズム面の半分に蒸着された厚さ15nmのSiO<sub>2</sub>薄膜の端部の形状測定結果

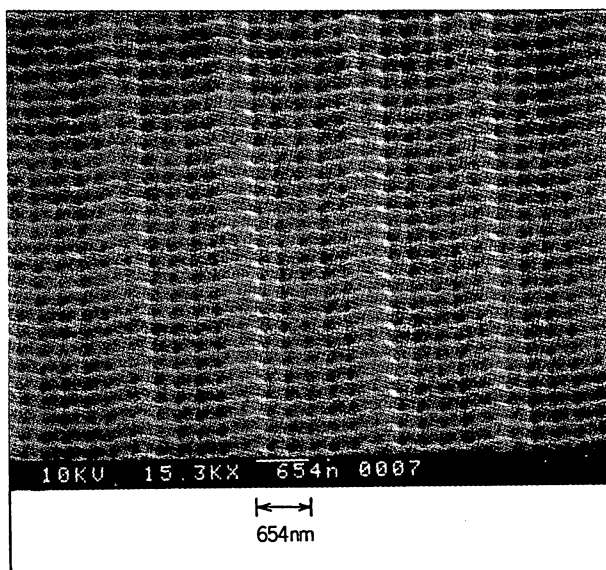


(a) 深さ約80nm, 直径約300nmのピットを有するMoth Eye光ディスク表面形状の測定結果



(b) レーザ干渉頭微鏡による測定結果. 像の一边は約240μm

写真2



(b) SEMによる測定結果. ピットが多数並んでいる  
写真3

いるがほぼ透明である。写真3(b)は同じ試料形状のSEM写真である。写真2(a), (b)の比較, および写真3(a), (b)の比較から本システムが高い横分解能を有することが確認される。これらの測定時の誤差信号のS/N値より, 縦分解能は約2nm, 横分解能は約20nm以内と推定されている。ただし, これらの値は位相敏感検波方式における測定時定数 $\tau$ が1msの場合の結果である。この時定数値は従来のSTMなどのそれに比べ小さい。これはLDが高速変調可能であることを利用したものであり, 高速測定の特長を示している。システムの雑音の基本要因は光検出時のショット雑音,

すなわち白色雑音なので, S/N値は $\tau^{-1/2}$ に比例する。したがって,  $\tau$ を大きくすれば, さらに高い分解能が期待される。

#### 4. 今後の展望

##### 4.1 性能向上のための課題

T-PSTMは簡単なシステムであるが, 微小な光パワーを測定するので, 感度が低く, したがって分解能も制限される。この問題を解決するためにわれわれは反射共振形PSTM(RR-PSTM)を提案している<sup>(4), (8)</sup>。図3にRR-PSTMの基本

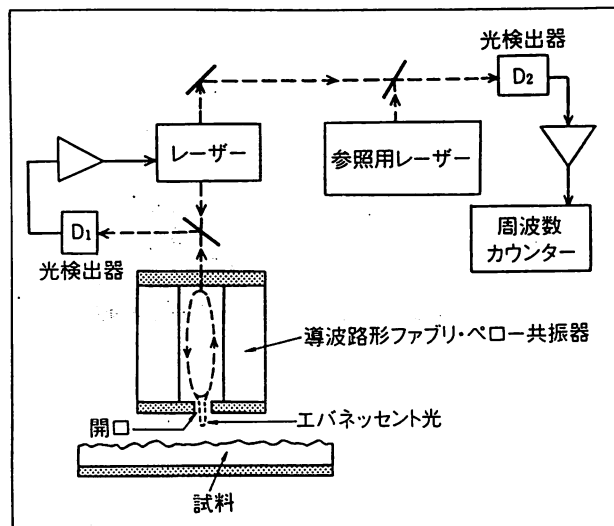


図3 反射共振形 PSTM の基本構成図<sup>4), 9), 10)</sup>

構成を示す<sup>4), 9), 10)</sup>。レーザー光を導波路形共振器に入射させ、レーザー周波数が共振器の共振周波数に一致するようレーザーを制御しておく。共振器の2つの端面のうち、試料に面した端面には微小開口を設け、これをプローブとして用いる。共振器を試料に接近させると、開口からのエバネッセント光が近接試料表面によって摂動をうける。その結果、共振器端面の複素反射率が試料の表面形状によって変化し、共振周波数がシフトする。これにより上記のレーザーの周波数もシフトするので、これを参照用レーザーあるいは他の共振器とのヘテロダイン信号周波数シフト測定により求める。すなわち、RR-PSTMはレーザーの高コヒーレンス特性を活用したものであり、試料形状は周波数シフトの測定により求められる。周波数測定はすべての物理量測定のうちで最高精度であることは周知の通りであるので、これはT-PSTMのもつ感度に関する問題点を解決するものである。すなわち、これは周波数変調—ヘテロダイン検波方式を採用したコヒーレント光通信システムに相当する。RR-PSTMにより、さらに高い分解能をもつ非破壊測定が可能と考えられる。ショット雑音限界では分解能はT-PSTMよりも1桁以上よいことが推定されているが<sup>4)</sup>、これを実現するには約10Hzの光周波数シフトを測定しなければならない。したがって、RR-PSTMを実

現するための要素技術として高フィネスの短共振器や、高コヒーレンス半導体レーザー、光位同期ループが必要である。高コヒーレンス半導体レーザーとしては筆者らはすでに光・電気2重帰還法により線幅7Hzの半導体レーザーを実現しており<sup>19)</sup>、ヘテロダイン形光位同期ループの周波数安定度も $1 \times 10^{-18}$ を実現している<sup>20)</sup>。さらに、 $1 \times 10^{-16}$ のレーザー周波数安定度も報告されている<sup>21)</sup>。これらの技術を利用すれば上記の光周波数シフト値は十分測定可能である。マイクロ波を用いた予備的なシミュレーション実験でもすでにおおの、 $5 \times 10^{-3} \lambda$ ,  $5 \times 10^{-2} \lambda$ の縦、横分解能が得られている<sup>4)</sup>。これらの値はT-PSTMに比べ、すでに優れており、今後測定条件の改良により、一層の分解能向上が期待される。

この他、性能向上には次のような課題の克服が必要と考えられる。

#### 4.1.1 近視野波動光学理論の確立

近視野領域でのマクスウェル方程式を適切な境界条件で解く近視野波動光学理論はまだ十分発達していない。原子の大きさ程度の分解能が実現すると、光に対して物体表面とは何か、境界条件とは何か、などについての詳細な検討により感度、縦分解能、横分解能の相互関係を明らかにする必要がある。

#### 4.1.2 要素作成技術の確立

再現性のある微小開口作成として、エレクトロン・エッチング法<sup>22)</sup>、電界蒸発法<sup>23)</sup>、などの技術を利用するとともに、ファイバー先端をより先鋭化する加工法の開発が必要である。また、半導体プレーナ加工技術を利用して平板上に微小開口を作り、プローブとして使うことも可能であろう。RR-PSTMの場合、高フィネスの短共振器が必要である。現在までに単一モードファイバーを用いて、誘電体多層膜蒸着により、共振器長2mm以下、フィネス200以上の値が報告されている<sup>24)</sup>。また、スーパー共振器では $F=120000$ も実現している<sup>25)</sup>。今後さらに、プレーナ技術(イオン交換、イオン注入)による高安定、低損失導波路形短共振器の実現が期待できる。図3の共振器の代

## 特集：STMの新しい展開—ハード面より—

わりに半導体レーザーの端面に微小開口を作ったものを使えば、これは光増幅機能も備えたプローブとなる<sup>4),9),18)</sup>。

### 4.1.3 新しい測定方式の探索

(a)開口合成法の使用可能性の探求；すでに製作されているマルチコア・ファイバー<sup>26)</sup>，またはプレーナ・プロセス技術を用い，近接した複数個のプローブをモノリシックに製作し，マルチ・プローブとして用いる。これにより得られた試料形状測定結果に含まれる各プローブ間の相関を抽出することにより，単一プローブよりも高い分解能が期待される。同様の可能性は従来のSTMプローブ先端に原子が複数個ある場合にも得られることが分かっている。この場合，モアレ・パターンに類似の画像が得られるので，計算機処理によりSTMの分解能はさらに向上し得る。

(b)量子雑音限界の打破；PSTMはヘテロダイン検波法などを採用できるのでショット雑音限界（量子雑音限界）が比較的容易に達成可能である。この意味でPSTMは量子効果の現れやすいシステム，すなわち quantum microscope（量子顕微鏡），ということができよう。分解能および感度限界は当面この量子雑音により決まるが，光子数スクイズド状態，位相スクイズド状態<sup>27)</sup>の光を利用すれば，それぞれ T-PSTM, RR-PSTMはこの雑音レベルを越える super-quantum microscope になり得る。

### 4.2 可能な応用範囲

現在のPSTMの分解能は光学顕微鏡と電子顕微鏡（SEM, STMなど）との中間の値をとり，かつ視野が比較的広いので非接触・非破壊・実時間の形状測定機として有用である。さらに加工機としても機能し得るので，以下のような広い分野での応用可能性を有する。

(1)有機エレクトロニクス分野：有機超薄膜などの表面形状の広視野観測，かつ光源波長を掃引して各部分での局所的な構造解析。

(2)生命理工学分野：生体細胞膜，DNA，特に種類のヴィールス<sup>28)</sup>などの形状の非破壊測定。ま

た，複数個のプローブを用いた生体細胞膜中の刺激の伝搬特性の評価，ゲート機構の解明。細胞プロセッシング（例えば，従来使われていたレーザー顕微鏡<sup>29)</sup>の代わりにPSTM用のプローブを使い，細胞の特定の位置にレーザー光を照射して細胞に穴を開け，細胞へのDNAの打ち込み精度を向上させる）。

(3)半導体工学分野：結晶表面に吸着した原子，分子層の評価，単原子層結晶成長制御，超高密度集積回路（ULSI）の評価およびトリミング，局所的レーザーアニール，結晶表面上の原子中の  $sp^3$  混成軌道の斜め方向からの光の打ち込みによる2次電子放出。

ここで(3)に関連して，筆者らが提案している単一原子操作および結晶成長の手法を以下に概説する<sup>7)</sup>。すでにSTMをキセノンの単一原子の操作に使う試みが報告されているが<sup>30)</sup>，PSTMでは適当な波長の光源を選べば半導体産業において重要な原子（シリコン，ゲルマニウム，ヒ素，ガリウム，など）にも適用可能な加工機となり得る。これは3段階からなる。まず，第1段階では真空中で気体原子集団にレーザー光を照射し，レーザー冷却および光糖蜜の手法により原子の熱運動の等価原子温度を低下させる<sup>31)</sup>。第2段階としてRR-PSTMのプローブをこの冷却原子集団に近づける。冷却原子がプローブから出射するエバネッセント光場に飛び込んだとき，この原子をエバネッセント光のもつ勾配力によるポテンシャルの井戸に捕獲する。安定な捕獲のためには実際には対向する複数のプローブの対を用いる。第3段階としてプローブを移動し，捕獲した原子を冷却結晶基板上に移動する。そして，さらにもう1つの押出し用プローブを用意しておき，これから光を出射させ，原子を加速・加熱して押し出し，結晶基板上に付着・固定させる。ここで，問題となる点はプローブに入射させるレーザー光パワーの必要値である。これを知るためにセシウム原子を例にとって計算した結果，光糖蜜中の原子温度  $T=0.1\text{mK}$  のとき，開口径  $a/\lambda=1\times 10^{-2}$  なるプローブを用いれば，必要入射パワーは約  $1\text{mW}$  でよい

## 特集:STMの新しい展開—ハード面より—

ことが分かった<sup>7)</sup>。この値は既存の半導体レーザーにより実現可能である。ごく最近、この考え方を支持する関連実験結果が報告された<sup>32)</sup>。ただし、われわれのような微小開口プローブを用いてはいないので、必要レーザーパワーはわれわれの場合より高く、1W以上であった。したがって、単一原子結晶成長には光糖蜜とともに微小開口プローブが必須要素であるといえよう。この方法の類形として、結晶基板上に原子を1個ずつ積み上げ、単一原子レベルの細線 (Atomic Tower, Whisker) や Quantum Dot の形成、などが考えられる。

### 5. おわりに

非接触・非破壊の超解像光学顕微鏡として有望な PSTM について概説した。従来、光技術を補助手段として使っている高分解能の顕微鏡システムに利用されている一例として原子間力顕微鏡 (AFM) がある。これに対し、PSTM は光を主手段として使い、光でなくては実現しない超高性能顕微鏡を実現しているといえよう。今後、光学の手法は極限技術にますます利用されていくと考えられる。特に、近視野波動光学は未開発の分野であり、量子光学の手法と組み合わせればさらに新奇な極限光学システムの実現も可能であろう。これらのシステムに必要な要素として、半導体レーザー、光ファイバー、光集積回路、などがあるが、これらの要素の開発のいくつかはわが国が世界をリードしていることを考慮すると、PSTM はわが国が先頭にたって研究すべき課題であるといえる。PSTM および関連する研究分野は広範な科学技術分野への波及効果を秘めている。

なお、4.2 の記述内容に不正確な点があるとすればそれは筆者の調査不足によるものであり、ご指摘いただければ幸いです。

### 謝辞

研究開始当初に貴重なご助言を賜った計量研究所の山田啓文博士をはじめとする国内外の研究者諸氏、さらに生体動力学に関しご指導いただいた

本学の猪飼篤教授、研究遂行の努力をされた中川賢一博士および蔣曙東氏、富田直幸氏をはじめとする本学大学院生諸氏に感謝します。

### 参考文献

- 1) 蔣 曙東, 富田直幸, 中川賢一, 大津元一:「フォトンSTM—設計と解析」, 第50回応用物理学会学術講演会, 30pZE4/III (1989年9月)
- 2) 蔣 曙東, 富田直幸, 中川賢一, 大津元一:「半導体レーザーを用いたフォトンSTMの基礎研究」, 第4回光波センシング技術研究会講演論文集, pp. 53~59 (1989年12月)
- 3) M. Ohtsu, K. Nakagawa, S. Jiang, and N. Tomita: "Super-resolution photon scanning tunneling microscope", Proc. of the 3rd Optoelectronics Conference, Makuhari Messe, Japan, paper No. 12D1-1 (July, 1990)
- 4) S. Jiang and N. Tomita: "Proposal of super-sensitive reflection-mode phase locked PSTM by diode laser", Proc. of the 3rd Optoelectronics Conference, Makuhari Messe, Japan, paper No. 12D1-3 (July, 1990)
- 5) 富田直幸, 蔣 曙東, 中川賢一, 大津元一:「フォトンSTM (III)」, 第51回応用物理学会学術講演会, 28pB7/II (1990年9月)
- 6) 富田直幸, 蔣 曙東, 中川賢一, 大津元一:「フォトンSTM (IV)」, 第51回応用物理学会学術講演会, 28pB8/II (1990年9月)
- 7) 大津元一, 蔣 曙東, 富田直幸, 中川賢一, 藤江嘉彦:「フォトンSTM (V) —単一原子レベル結晶成長」, 第51回応用物理学会学術講演会, 27aL9/III (1990年9月)
- 8) 大津元一:「フォトン走査トンネル顕微鏡」, 触媒, 32巻, 8号, pp. 548~550 (1990)
- 9) 蔣 曙東, 富田直幸, 大津元一:「フォトン走査トンネル顕微鏡」, 光学, 第20巻, 第3号, pp. 134~141 (1991)
- 10) U. C. Fischer, U. T. Durig and D. W. Pohl: "Near-field optical scanning microscopy in reflection", Appl. Phys. Lett., Vol. 52, No. 4, pp.249~251 (1988)
- 11) U. Durig, D. W. Pohl, and F. Rohner: "Near-field optical-scanning microscopy", J. Appl. Phys., Vol. 59, No. 10, pp. 3318~3324 (1986)
- 12) R. C. Reddick, R. J. Warmack, and T. L. Ferrell: "New form of scanning optical microscopy", Phys. Rev. B, Vol. 39, No. 1, pp. 767~770 (1989)
- 13) E. Betzig, M. Isaacson, and A. Lewis: "Collection mode near-field scanning optical microscopy", Appl. Phys. Lett., Vol. 51, No. 25, pp. 2088~2090 (1987)
- 14) D. Courjon and J. M. Vigoureux: "External and internal reflection near field microscopy: experiments and results", Appl. Opt., Vol. 29, No. 26, pp. 3734~3740 (1990)

## 特集：STMの新しい展開—ハード面より—

- 15) J. M. Guerra: "Photon tunneling microscopy", *Appl. Opt.*, Vol. 29, No. 26, pp. 3741~3752 (1990)
- 16) 岡本隆之, 山口一郎: 「表面プラズモン顕微鏡」, *光学*, 19巻, 10号, pp. 682~686 (1990)
- 17) 富田直幸, 蔣曙東, 藤江嘉彦, 中川賢一, 大津元一, 大澤日佐雄: 「フォトンSTM (IV)」, 第38回応用物理学関係連合講演会, 30pQ2/II (1991年3月)
- 18) S. Jiang, N. Tomita, K. Nakagawa, and M. Ohtsu: "Super-Resolution, Photon Scanning Tunneling Microscope (PSTM) Using Diode Lasers", Conference on Lasers and Electro-Optics, Baltimore, MA, paper No. CThO5 (May, 1991)
- 19) C. H. Shin and M. Ohtsu: "Stable semiconductor laser with a 7-Hz linewidth by an optical-electrical double-feedback technique", *Opt. Lett.*, Vol. 15, No. 24, pp. 1455~1457 (1990)
- 20) C. H. Shin and M. Ohtsu: "Heterodyne optical phase-locked loop by confocal Fabry-Perot cavity coupled AlGaAs laser", *IEEE Photon. Technol. Lett.*, Vol. 2, No. 4, pp. 297~330 (1990)
- 21) D. Hils and J. L. Hall: "Ultra-stable cavity-stabilized lasers with subhertz linewidth", *Proc. of Frequency standards and metrology*, ed. by A. De Marchi, Springer-Verlag, Berlin, pp. 162~173 (1988)
- 22) P. F. Marella and R. F. Pease: "Comment on 'writing nanometer-scale symbols in gold using the scanning tunneling microscope'", pp. 2366~2367 (1989)
- 23) 西川 治: 「FEM・FIM・アトムプローブによる異金属表面の研究」, *応用物理*, 50巻, 8号, pp. 807~817 (1981)
- 24) J. Stone and L. W. Sultz, "Pigtailed high-finesse tunable fiber Fabry-Perot interferometers with large, medium and small free spectral ranges", *Electron. Lett.*, Vol. 23, No. 15, pp. 781~782 (1987)
- 25) J. Bergquist, NIST, USA, 私信 (1990)
- 26) M. Fukuma, I. Ogasawara, A. Nishimura, and S. Suzuki: "Characterization of cross-talk in four-core graded-index multicore fiber", *Proc. of the 6th International Conf. on Integrated Opt. and Opt. Fiber Commun.*, Reno, Nevada, paper No. WI7 (January, 1987)
- 27) 矢島達夫: 「光の量子効果」, (「量子力学と新技術」, 第9章), 日本物理学会, 培風館, pp. 182~202 (1987)
- 28) K. Tanaka, A. Ikai, and K. Kameyama: "Proteasomes (multi-protease-complexes) as 20 S ring-shaped particles in a variety of eukaryotic cells", *J. Bio. Chem.*, Vol. 263, No. 31, pp. 16209~16217 (1988)
- 29) 粕谷敬宏, 塚越幹郎: 「レーザーによる細胞プロセッシング」, *応用物理*, 57巻, 7号, pp. 1035~1040 (1988)
- 30) D. M. Eigler and E. K. Schweizer: "Positioning single atoms with a scanning tunneling microscope", *Nature*, Vol. 344, No. 6266, pp. 525~526 (1990)
- 31) D. Sesko, C. G. Fan, and C. E. Wieman: "Production of a cold atomic vapor using diode-laser cooling", *J. Opt. Soc. Am. B*, Vol. 5, No. 6, pp. 1225~1227 (1988)
- 32) M. A. Kasevich, D. Weiss, and S. Chu: "Normal-incidence reflection of slow atoms from an optical evanescent wave", *Opt. Lett.*, Vol. 15, No. 11, pp. 607~609 (1990)

4:15 pm

**CThO5 Super-resolution photon scanning tunneling microscope using diode lasers**

S. Jiang, N. Tomita, K. Nakagawa, and M. Ohtsu

*Graduate School at Nagatsuta, Tokyo Institute of Technology, 4259 Nagatsuta, Midori-ku, Yokohama, Japan*

In this paper, we report the experimental results of transmission type Photon Scanning Tunneling Microscope (T-PSTM), and propose for the first time a novel reflection-resonance type PSTM (RR-PSTM), with higher sensitivity and higher resolution. The diode lasers which can be directly high-speed modulated make the system compact with high performance.

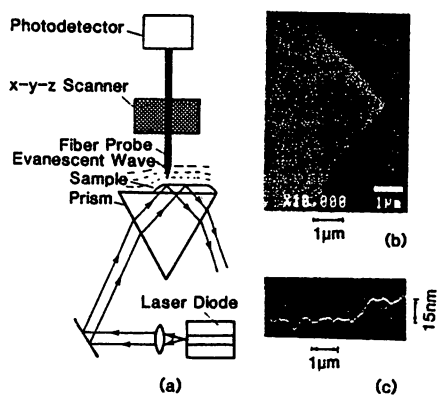
Figure 1(a) shows the T-PSTM system. The evanescent field tunneled photon (depending on the topography of the sample) is picked up by a probe on which the sub-wavelength aperture is fabricated. The top of a fiber probe was sharpened by HF selective etching to achieve 80 nm radius of curvature (Fig. 1(b)). Figure 1(c) shows the two-dimensional profile of 15 nm thick SiO<sub>2</sub> film measured by the phase sensitive detection with the time constant  $\tau$  of 1 ms. The normal resolution is estimated as 2 nm from the noise magnitude of the signal in Fig. 1(c). Because the detected noise magnitude is proportional to  $\tau^{-1/2}$ , higher normal resolution is expected by increasing  $\tau$ . The lateral resolution which is determined by the aperture diameter in the near field region is estimated as 80 nm.

For solving the problem that the low power picked up in T-PSTM which limits the measurement sensitivity, a RR-PSTM is proposed (Fig. 2(a)). A waveguide-type short Fabry-Perot cavity is used as a probe which has a sub-wavelength aperture on one facet. The incident laser frequency is locked to the cavity resonance frequency. The evanescent field is generated at the aperture and is perturbed by the sample. This perturbation varies the effective complex reflectance of the resonator facet, and thus the resonance frequency shifts depending on the topography of the sample. Performance of this system is analyzed theoretically for the plane sample. The exponential decrease of the resonance frequency shift, as in the case of the transmission type, assure the high normal resolution in the RR-PSTM. The relationship between the frequency shift and the aperture diameter is shown by A, B in Fig. 2(b). Lines C ~ F show the shot-noise limit for several values of cavity finesse  $F$  and detected laser power  $P$ . Since super-cavity with high finesse up to  $1 \times 10^5$  and the diode laser with the power up to 1 W are available, shot-noise limited lateral resolution up to  $1.0 \times 10^{-3} \lambda$  can be expected, which corresponds to the frequency shift of 0.1 mHz for the cavity free-spectral range (FSR) of 100 GHz.

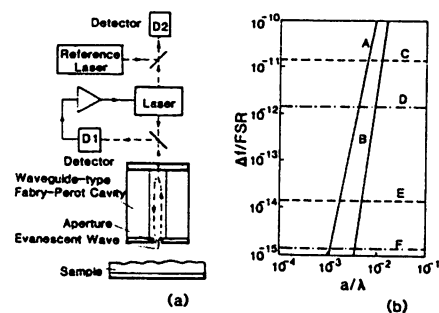
The realization of the heterodyne optical phase-locked loop with the frequency stability of  $1 \times 10^{-18}$ ,<sup>1</sup> can guarantee this shift detection. To confirm our proposal, a simulative measurement using 4.4 cm wavelength microwave is carried out. The result is shown in Fig. 3. Two peaks clearly seen in this figure imply that a lateral resolution higher than the aperture diameter is achieved, because the evanescent field power is concentrated around the aperture center. By a series of measurements for various parameters in Fig. 3, the highest normal and lateral resolution were  $5 \times 10^{-3} \lambda$ ,  $5 \times 10^{-2} \lambda$  respectively. These preliminary resolutions are already high enough to confirm the validity of the present proposal.

1. C. H. Shin and M. Ohtsu, *Photon. Technol. Lett.* 2, 297 (1990).

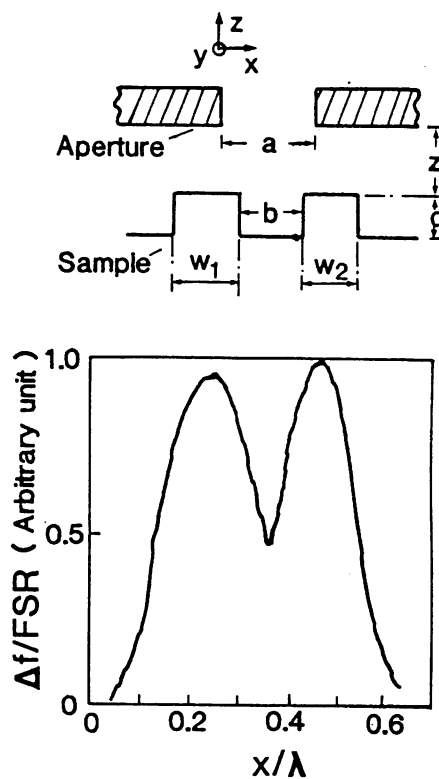




CThO5 Fig. 1. (a) The system of T-type PSTM. (b) Sharpened fiber probe. (c) Measured two-dimensional profile of SiO<sub>2</sub> film with the thickness of 15 nm.



CThO5 Fig. 2. (a) Basic setup and calculation results of RR-PSTM. (b) The relationship between the frequency shift and the aperture diameter. Where  $\lambda$  is the wavelength,  $z$  is the sample-aperture separation, FSR is the free spectral range of the cavity. Lines A, B correspond to the frequency shift where  $z/\lambda = 1 \times 10^{-3}$ ,  $z/\lambda = 1 \times 10^{-2}$  respectively. Lines C ~ F correspond to the shot-noise limits depending on finesse  $F$  of the cavity, and the power  $P$  which is detected by a photo-detector D1 in Fig. 2(a). C:  $F = 1 \times 10^5$ ,  $P = 10$  mW; D:  $F = 1 \times 10^5$ ,  $P = 1$  W; E:  $F = 1 \times 10^5$ ,  $P = 1$  mW; and F:  $F = 1 \times 10^5$ ,  $P = 1$  W, respectively.



CThO5 Fig. 3. The result of the simulative measurement by microwave, where  $a/\lambda = 0.2$ ,  $b/\lambda = 0.13$ ,  $w_1/\lambda = 0.13$ ,  $w_2/\lambda = 0.11$ ,  $z/\lambda = 0.02$ ,  $d/\lambda = 0.09$ , and  $\tau = 10$  ms.